How to Design Hydrogen Storage Materials? Fundamentals, Synthesis, and Storage Tanks

Qiwen Lai, Yahui Sun, Ting Wang, Poojan Modi, Claudio Cazorla, Umit B Demirci, Jose Ramon Ares Fernandez, Fabrice Leardini, Kondo-françois Aguey-zinsou

ADVANCED SUSTAINABLE SYSTEMS
www.advsustainsys.com

How to Design Hydrogen Storage Materials? Fundamentals, Synthesis, and Storage Tanks

*Qiwen Lai, Yahui Sun, Ting Wang, Poojan Modi, Claudio Cazorla, Umit B. Demirci, Jose Ramon Ares Fernandez, Fabrice Leardini, and Kondo-François Aguey-Zinsou**

As the world shifts toward renewable energy, the need for an effective energy carrier is pressing. Hydrogen has often been touted as a universal clean energy vector and the fuel of the future. Unfortunately, mass adoption of the hydrogen economy is slow due to a lack of incentives and technical difficulties in storing hydrogen. Better materials capable of reversible hydrogen uptake/release with hydrogen capacity surpassing 5 mass% at the ambient must emerge. So far, finding such materials has been elusive; alloys capable of ambient hydrogen uptake/release have a low storage capacity while high capacity hydrides have a very high hydrogen release temperature. From metal alloys to complex hydrides, a better understanding of the behavior of hydrogen in hydrides is essential to fine-tune their properties toward application. Herein, the latest approaches to design hydrogen storage materials based on known hydrides are reviewed with the aim to facilitate the emergence of alternative thinking toward the design of better hydrogen storage materials. Synthetic methods and conceptual approaches to achieve particular hydrogen thermodynamics and kinetics are discussed. These include metallurgical alloying, mechanochemical modification, chemical destabilization, the nanosizing approach, and theoretical modeling and machine learning techniques to guide experimental work.

1. Introduction

1.1. Hydrogen in Broader Context

The fate of human kind, is at a cross-road with significant challenges threatening several concepts that were taken for granted, e.g., technological progress will enable us to defeat the general laws of nature and grow economic wealth beyond the capability of our planet.[1] Indeed, we have learnt through the greatest minds to master the use of fire to drive machines to do work for us. We are at the corner of taking these machines closer to artificial intelligence capability—the so called 4.0 Industry. But the idea that such technological advances can lead to further wealth and equal rights across the planet remains a debate and most likely utopia.[2] To date, despite all these progress, we are still failing to recognize the limits of our current enterprise in terms of the amount of natural resources available to us and we are brutally lacking imagination and leadership to reinvent our societal organization and models to cope with the changes ahead (**Figure 1**a). Some call for a "degrowth" economy[3] and a reorganization of economic models; however, this is only one aspect of the solution.

Current energy consumption is projected to double to support the economic growth of the emerging economies. Enabling readily access to large amounts of energy is thus a paramount. Indeed, the viability of our economic models and quality of life are directly related to our ability to access energy.[4] However, the majority of the energy produced is at present consumed by a very small fraction of the world population (Figure 1b). Bringing energy fairness cannot be done through the use of fossil fuels, but via renewable energy that is widely available across the planet. For example, current photovoltaic technology could easily support the energy needs of a population of ten billion.[5] Nonetheless, the large scale deployment of

Dr. Q. Lai, Dr. Y. Sun, T. Wang, P. Modi, Prof. K.-F. Aguey-Zinsou
MERLin
School of Chemical Engineering
The University of New South Wales
Sydney, NSW 2052, Australia
E-mail: f.aguey@unsw.edu.au
C. Cazorla
Material Sciences and Engineering
The University of New South Wales
Sydney, NSW 2052, Australia
Prof. U. B. Demirci
Institut Européen des Membranes
IEM – UMR 5635
CNRS
ENSCM
Univ Montpellier
Montpellier 34000, France
Dr. J. R. Ares Fernandez, Dr. F. Leardini
Laboratorio de Materiales de Interés Energético
Universidad Autonoma de Madrid
Cantoblanco 28049 Madrid, Spain
The ORCID identification number(s) for the author(s) of this article can be found under https://doi.org/10.1002/adsu.201900043.

DOI: 10.1002/adsu.201900043

renewables is still conditioned to the development of an effective energy carrier. Renewable sources are intermittent and our current societies rely on 24/7 dispatchable energy ready for use. This could be achieved through the local production of synthetic hydrocarbons from renewable energy. However, the overall efficiency remains low[6] and in the context of a decarbonized economy, the use of hydrogen as the alternative energy carrier is a more viable option. Hydrogen has three times the gravimetric energy density of gasoline. It is abundant in the form of water and can be used to generate electricity with a fuel cell, mechanical work in combustion engines, or heat through catalytic combustion (**Figure 2**). The idea of substituting current fossil fuels with hydrogen is not new[7] but this has been the subject of many stop and go policies that have left the impression that the technology is not mature.

Kondo-François Aguey-Zinsou completed a Ph.D. in heterogeneous catalysis at the University Pierre et Marie Curie (Paris) in 2001. He carried out postdoctoral research at The University of Queensland in bio-electrochemistry. He later moved to the research center Helmholtz Zentrum Geesthacht in Germany, Queen Mary University London, and University College London where he supervised research projects on hydrogen storage, biofuel cells, and biomaterials. Since 2009, Francois is leading MERLin at UNSW. His research focuses on the development of advanced materials for hydrogen technologies.

1.2. The Hydrogen Economy: Quo Vadis?

The drawback in the use of hydrogen as an energy carrier is often associated with the lack of methods to effectively store it. Hydrogen has a very low volumetric energy density (0.7 kJ L^{-1} at 25 °C and atmospheric pressure), and the current mature storage technology is through hydrogen compression at 70 MPa. This leads to a volumetric energy density of ≈3 MJ L^{-1} at the system level by using composite tanks.[8] These high pressure hydrogen tanks are already finding applications within the first hydrogen

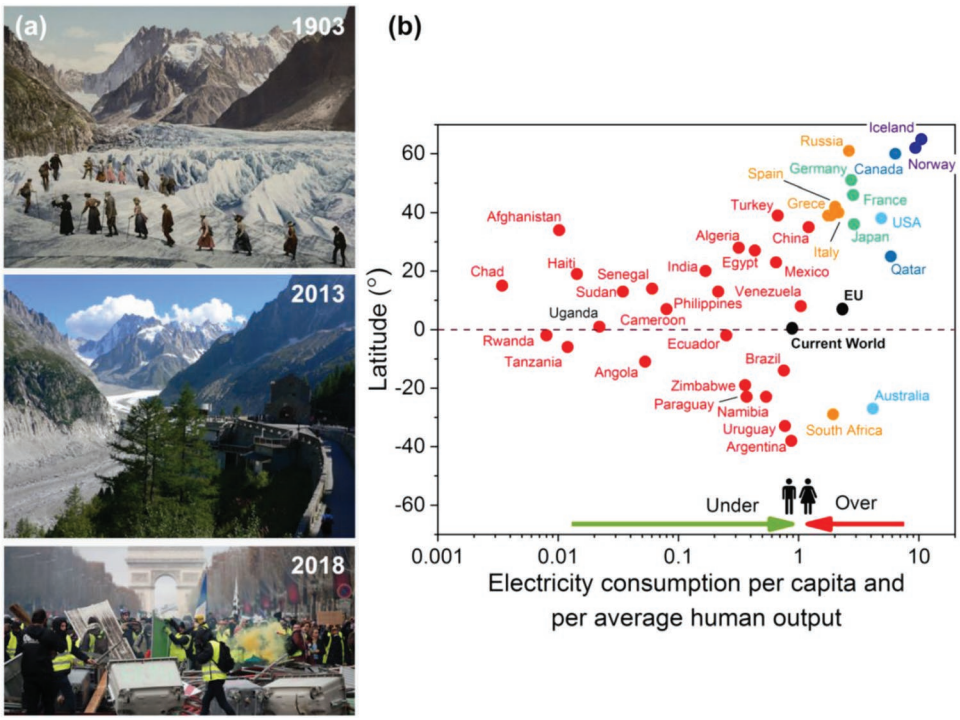

Figure 1. Current energy related challenges facing society. a) Evolution of largest glacier in France "La Mer de Glace." In 1903, the touristic attraction was to walk over the glacier, which was at the level of the Montenvers station (2013 picture). In 2013, the ice was not visible anymore. Subjected to the effects of global warming, the glacier has moved far back. The tension between economic development and the need for new models is emerging across many rich countries as demonstrated by the riots in France in November 2018 (image bottom left); b) electricity consumption normalized per capita and the average human output of 300 W as function of the latitude. Electricity consumptions were sourced from The World Factbook 2016–17 (Washington, DC: Central Intelligence Agency, 2016). A value of 1, a country is consuming the energy that can be produced by a single man or woman. The world current electricity consumption is almost equal to 1, i.e., the earth population, but many countries do not have access to their share of electricity to ensure economic growth. The over consumption in the rich countries is an average that is not reflecting social gaps in access to energy.

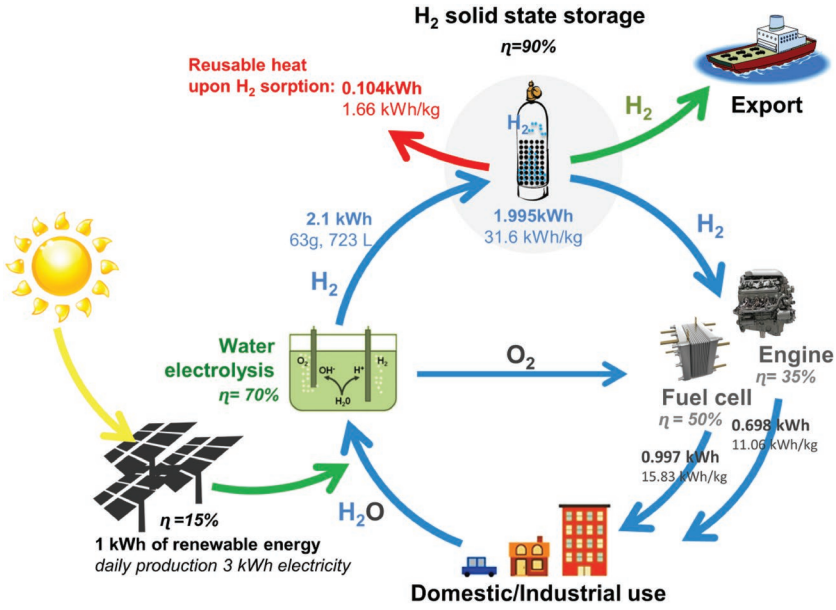

Figure 2. The hydrogen economy. Illustration of the hydrogen renewable energy chain. The difficulty of solid state hydrogen storage remains in the finding of better materials meeting competing requirements. $LaNi_5$ as a hydrogen storage material (1.28 mass% H_2, and 123 g H_2 L^{-1}) was taken as the reference material. Upon hydrogen absorption heat is released owing to the exothermic nature of the reaction of hydrogen with the metal alloy. The storage materials must meet targets of cost, temperature and pressure for hydrogen absorption and release as well as high energy density, both volumetric and gravimetric. The current cost of hydrogen produced from renewables is estimated at ≈AUD $100-270 per MWh.[568]

vehicles being commercialized. However, when considering stationary applications the use of compressed tanks is not the best option owing to their high cost (≈AUD $685 per kg H_2 at the system level[9]—**Figure 3**). Metal hydrides and in particular those based on the early alloys developed, e.g., $LaNi_5$ and TiFe and more recently Ti BCC alloys,[10] provide new and significant opportunities to effectively store renewable energy with a high volumetric density at scale (>10 MJ L^{-1})[11] and in a cost effective manner. These metals store hydrogen via the simple reaction (1) and thus provide a means to safely store hydrogen within their structure at low hydrogen pressures.

$$M + \frac{x}{2}H_2 \leftrightarrow MH_x + \text{heat} \quad (1)$$

For a long time, further research along these alloys has been discouraged in favor of the development of new materials to meet the targets of sole vehicle application. However, with the uptake of renewable energy at levels over 20% in some countries, the emergence of alternative energy storage solutions has become critical. Intermittent renewable energy like wind and solar have fluctuations in their output which require grid integration with energy storage

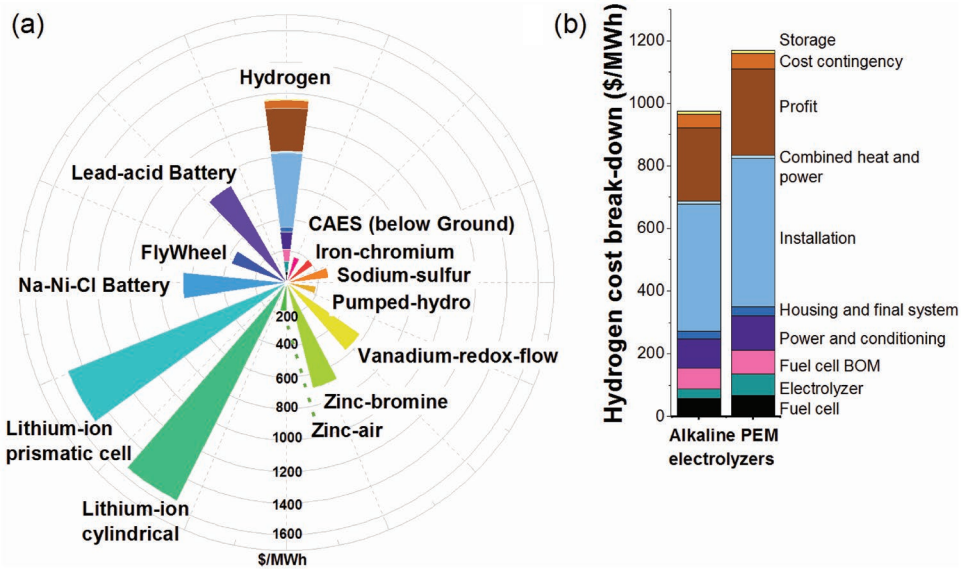

Figure 3. Competitiveness of hydrogen technology for the storage of electricity. a) Cost of electricity per storage technology and b) breakdown cost of hydrogen for stationary energy storage applications using solid state hydrogen storage given. All costs are in AUD/MWh and the following conversion rates were used: 1 USD to 1.36 AUD and 1 EUR to 1.60 AUD. The cost of all the storage technologies besides hydrogen were obtained from the DOE/EPRI report.[569] Prices of individual components of the fuel cell system were obtained from the NREL report[13b] and were adjusted to include the metal hydride prices and production cost of hydrogen from renewable energy technologies. For this calculation, $TiMn_{1.95}$ was used as the metal hydride for the solid state storage of hydrogen. High pressure hydrogen storage tanks for vehicles application cost: AUD $550 per kg H_2, which corresponds to a system cost of AUD $685 per kg H_2,[9] while DOE cost target is AUD $456 per kg H_2 for storage system cost.

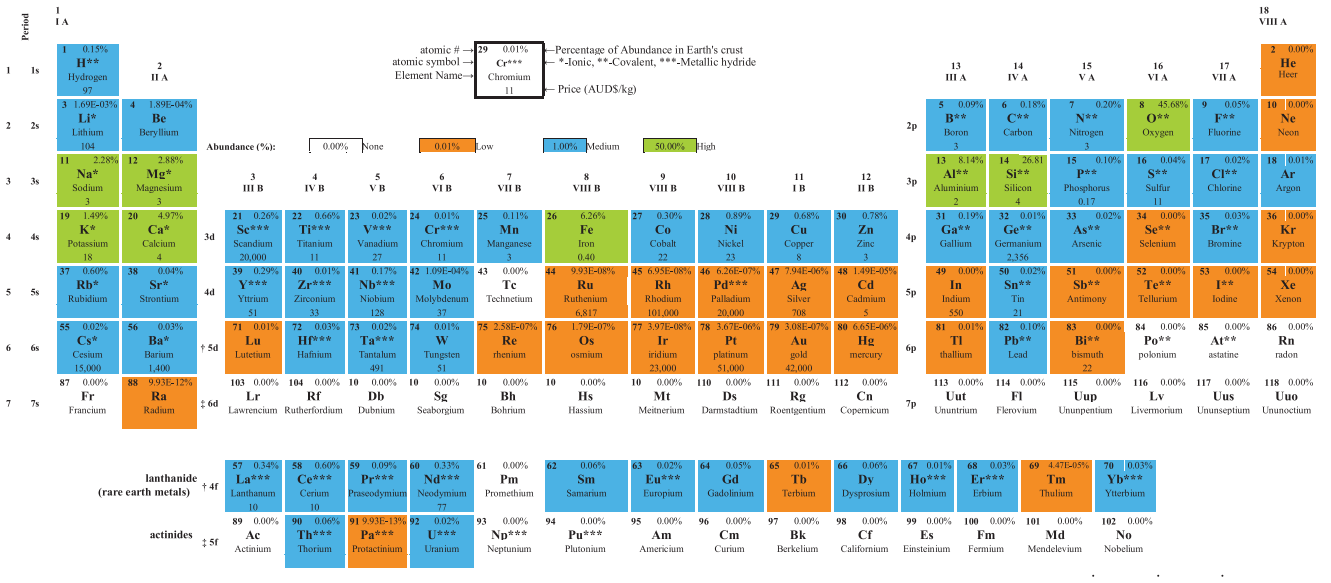

Figure 4. Price and abundance of elements for designing hydrogen storage materials. Periodic table summarizing the elements forming hydrides, their market price (AUD $ per kg), and abundance. Discrepancies arise when multiple processes are involved in extracting the pure elements, and upon additional market variations. This summary indicates that Na, Mg, K, Ca, Fe, Al, Si and O are the most common elements found in the earth's crust. Fortunately, metal hydrides such as $NaBH_4$, MgH_2, and AlH_3 with high hydrogen storage capacities can be formed using such elements.[11]

materials to provide the required energy supply (Figure 2).[12] In the case of stationary applications, hydrogen storage technologies provide solutions through the integration of three technologies: water electrolysis, hydrogen storage, and fuel cells for electricity generation. Once stored, the hydrogen can then be transported to the point of use or even exported. Many feasibility studies and demonstration sites have been showcased to validate the benefits of hydrogen technologies for on-site energy storage and generation in stationary applications.[13] However, the understanding of the potential of hydrogen as an energy carrier remains limited. Thus to date, the current technology considered is that of battery with the hope that more mature battery chemistry will be capable of "high density energy storage" at relatively low costs.

Detailed cost analysis of hydrogen technologies integrating electrolyzers, solid state storage, and fuel cells systems reveals that these integrated hydrogen technologies are already extremely cost competitive (Figure 3). In particular, when considering that currently no large scale manufacturing capability exists along the hydrogen chain, the potential for the technology to become readily accessible as cost goes down is immense. Through this analysis it is apparent that the main cost remains at the level of the electrolyzer and fuel cell. The cost of the storage technology is minimal in comparison. As a first approximate, the cost ($CO_{A_xB_y}$) of the raw hydrogen storage material (A_xB_y) can be determined from

$$CO_{A_xB_y} = \frac{CO_A \times \frac{x}{x+y} \times N_A + CO_B \times \frac{y}{x+y} \times N_B}{\frac{x}{x+y} \times N_A + \frac{y}{x+y} \times N_B} \quad (2)$$

where CO_A, CO_B correspond to the cost of the elements A and B ($ per kg), x and y are the respective amount of the elements A and B, and N_A and N_B their respective molar mass (g mol^{-1}).

By using the tabulated cost of single elements in **Figure 4**, the cost of binary to higher quinary alloys with (non)-stoichiometric compositions, can be determined from Equation (2). The cost of typical hydrogen storage alloys is summarized in **Table 1**. With the cost of room temperature (RT) hydride ≈AUD$10 kg^{-1}, the cost per kg of hydrogen stored in a typical hydride with a storage capacity of 2 mass% H_2 would be around AUD$500, which is comparable to the cost of hydrogen compressed at 70 MPa. However, owing to the lower pressures involved, solid state hydrogen storage is safer and offers much higher volumetric densities. In the context of competitive markets, the awareness of the potential of solid state hydrogen storage must be raised and practical guidelines must be developed for matching operating hydrogen pressures, flow, and temperatures to facilitate the integration of these hydrides with electrolyzers and fuel cells. At the fundamental level strategies, which this review aims to summarize, the design and operation of hydrogen storage materials must be established to consolidate and strengthen the existing knowledge and facilitate the market penetration of hydrides. The advantages of existing low temperature solid-state hydrogen materials lie in their long cycle life, improved safety compared to compressed hydrogen, and full discharge capability with "no memory" drawbacks. Research is needed for the optimization of their operation, large scale production, safety, maintenance, and recycling.

1.3. Beyond Current Materials

Current hydrogen storage alloys with capability to store hydrogen at the ambient have only a low hydrogen storage capacity (typically <2 mass% H_2). The challenge in enabling a

Table 1. Common metal alloys (AUD$ kg^{-1} of material) based on the current market price of individual elements (not including the manufacturing cost of the alloy).

Metal alloys		Price of the alloys
AB_2	$TiMn_{1.95}$	5.61
	$TiMn_{1.25}Cr_{0.25}$	6.95
	$Ti_{0.9}Zr_{0.1}Mn_{1.4}Cr_{0.45}Fe_{0.15}$	8.04
	TiCrMn	8.42
	$Ti_{1.2}CrMn$	8.59
	$Ti_{0.9}Zr_{0.2}Mn_{1.8}V_{0.2}Fe_{0.2}$	9.19
AB_5	$La_{0.8}Nd_{0.2}Ni_5$	23.29
	$La_{0.8}Y_{0.2}Ni_5$	20.76
	$LaNi_5$	18.83
	$LaNi_{4.55}Al_{0.45}$	18.67
AB	$TiFe_{0.7}Mn_{0.2}$	6.05
	$TiFe_{0.88}$	5.80
SS	$Ti_{24}V_{0.45}Cr_{31}Mn_{10}$	10.11
	$V_{0.37}Ti_{0.33}Mn_{.3}$	14.44
	$V_{0.855}Cr_{0.145}$	24.70
Common hydrides		
	NaH	43[445]
	LiH	237[445]
	CaH_2	142[446]
	MgH_2	–
	AlH_3	87
Common complex hydrides		
	$NaAlH_4$	45[447]
	$LiAlH_4$	355
	$NaBH_4$	140[446]
	$2LiBH_4+MgH_2$	818[445]

wider uptake of hydrogen is in the design of better materials with much higher energy densities (>5 mass% H_2) to effectively displace fossil fuels and enable the transport and distribution of renewable energy in a very compact form including vehicles application. Nonmetals like carbon microporous materials and highly porous structures like metal–organic frameworks (MOFs), covalent–organic framework (COFs) can also be used to store molecular hydrogen via physisorption with rapid kinetics (**Figure 5**b).[14] However, in this case the adsorption capacity is often too low, typically ≈0.24 mass% H_2 for carbons[15] and <2 mass% H_2 for MOFs;[16] although Morris et al. recently claimed a reversible excess sorption of 10.5 mass% H_2 at the ambient in a manganese-based MOF.[17] Liquid organic carriers such as those based on NH_3 and cycloalkanes are also potential alternatives and their potential as hydrogen carrier has been summarized in several excellent reviews.[18] However, processes based on organic carriers are often energy intensive and should be improved in terms of catalyst stability, activity, and reversible hydrogen storage capacity. This review does not cover recent progress on materials for hydrogen physisorption or liquid organic carriers, but rather focuses on materials where hydrogen is stored via chemisorption in the form of hydrides. Various elements can effectively form hydrides of extremely high hydrogen densities (Figures 4 and 5),[19] and thus have the potential to deliver a solution to store hydrogen beyond current capabilities. For example, light alkali and alkaline earth metals form ionic hydrides such as LiH and NaH,[20] where hydrogen exists as a hydride (H^-). Compounds including $LiNH_2$ and NH_3[21] form high hydrogen capacity covalent hydrides, where the hydrogen is partially charged positively ($H^{\delta+}$). In contrast, in complex hydrides such as $NaAlH_4$ and $LiBH_4$, the hydrogen exists, again with high density, as a negatively charged $H^{\delta-}$ (**Table 2**). In metals such as Pd and Ti forming interstitial hydrides, the hydrogen bonding is considered to be metallic and these elements in addition to their hydrogen storage properties can provide a solution for hydrogen catalysis in the high hydrogen density hydrides. The variety of existing hydrogen bonds can be viewed as an opportunity of finding ways to modify the properties of existing hydrides toward specific hydrogen storage applications. For example, the combination of $H^{\delta+}$ and $H^{\delta-}$ is a means to facilitate the release of hydrogen from mixed compounds involving hydride and protide owing to the more favorable thermodynamics.[22]

To date, most of these high capacity hydrides are not suitable in their "raw" form for hydrogen storage because they only release hydrogen at temperatures way above the ambient (Table 2); and often the hydrogen release is not reversible. Furthermore, the release or uptake of hydrogen in these hydrides can lead to significant volume changes, which does not simplify their integration into real systems. For example, in a typical metal hydride, hydrogen desorption/absorption can lead to a significant volume expansion owing to the (de)insertion of the hydrogen atoms in the crystalline lattice and structural reorganization of the atomic order.[8] In particular, in intermetallic compounds these volume changes are about 1–3 cm^3 mol^{-1} H.[23] In saline hydrides like Mg/MgH_2 the expansion is of 30%. This can be overcome by leaving some space in the tank for expansion/contraction but it affects the overall hydrogen storage capacity at the system level. Complex hydrides also undergo various decomposition pathways and changes in volume, which depend upon the type of the reaction and the extent of melting/foaming of the material. For example, H_3BNH_3 foams upon thermal heating as the result of the large amount of gases released in addition to hydrogen.[24] $NaAlH_4$ decomposes into Na_3AlH_6 and Al with 30.3% contraction in the first stage of hydrogen release, but in the second decomposition stage of Na_3AlH_6 into NaH and Al a 13.8% expansion is observed.[25]

The current challenge in the use of high hydrogen capacity hydrides is thus in the conception of novel fundamental approaches to effectively control their properties and to simplify their behavior upon hydrogen uptake/release for facile hydrogen sorption near the ambient. This also involves taking into account important parameters including: i) the ease of activation of the material for the initial hydrogen uptake/release, ii) the rate of hydrogen uptake/release, iii) the heat of formation of the hydride and the management of that heat, iv) the hydrogen cycling stability of the material, v) the resistance of the hydride to hydrogen gas impurities, vi) the safety associated with the use of the hydride, and vii) the final cost of the material.[26]

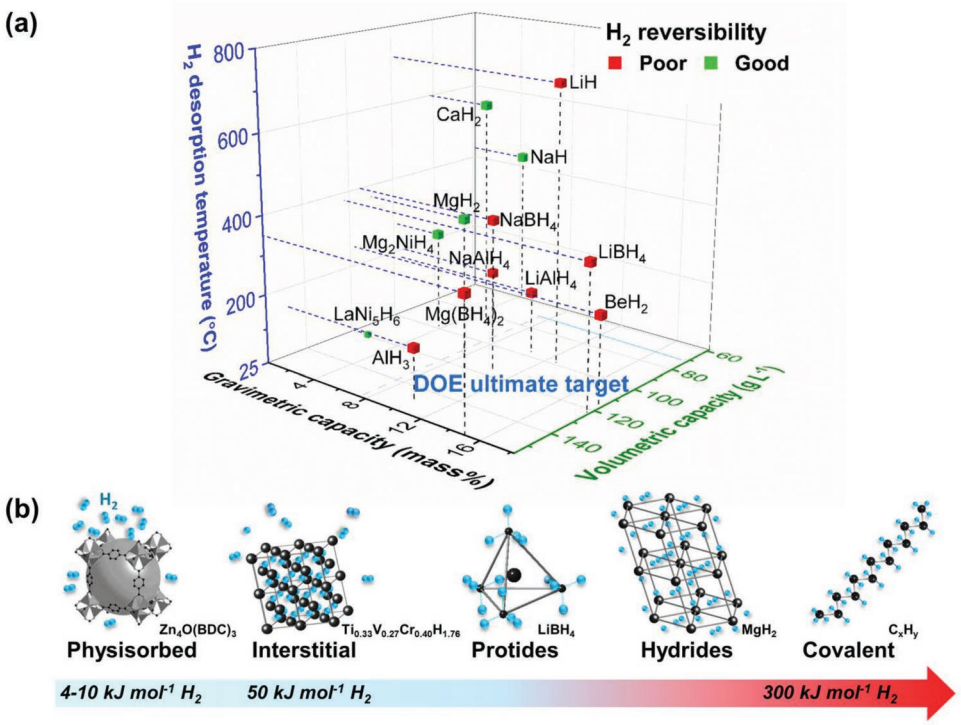

Figure 5. Current potential solid states hydrogen storage materials. a) Energy density and hydrogen desorption temperature of selected hydrogen storage materials versus the US Department of Energy (DOE) targets;[570] and b) typical methods to store hydrogen and associated hydrogen binding strength. For practical applications a relatively weak hydrogen bonding strength is needed to reversibly store hydrogen with a minimum energy input.

Herein, we review current state-of-the-art in the design of hydrogen storage materials and the fundamental understanding of hydrogen sorption in these materials with the aim of facilitating a rationalization of current approaches. A particular emphasis is made on current fundamental understanding of hydrogen behavior in hydrides across materials types, from metal alloys to complex hydrides; across length scales, from several micrometers to the nanoscale; and across phases from nanostructured to amorphous as well as methods to load/unload hydrogen from these materials. Synthesis approaches to reach certain hydrogen storage properties are also reviewed as well as methodologies for modeling guidance and machine learning techniques for materials' discovery and prediction. Additional details of these methodologies can be found in books and a range of excellent previous review articles.[8,27] The difficulties with the engineering steps associated with the insertion and hydrogen cycling of hydrides in tanks and strategies to overcome these difficulties are also discussed. In particular, the importance of integrating engineering aspects at the very early stages of hydride materials synthesis and design is highlighted. The performances of solid state hydrogen tanks are directly related to the initial hydrogen storage material design.

2. How is Hydrogen Practically Loaded into and Released from Materials?

Due to the nature of the reaction involving hydrogen uptake and release in materials (reaction (1)), the most common method to drive hydrogen in and out of materials has been by tuning temperature and pressure (**Figure 6**a). Hence at a given temperature, by applying a hydrogen pressure above the equilibrium pressure P^{eq} of the hydride phase (see Section 3.2), hydrogen can be loaded in materials. In contrast, by applying a pressure below that of P^{eq}, hydrogen is released from the material. One of the drawbacks of such an approach is that under operating conditions of hydrogen absorption/desorption, P^{eq}, which determines the pressure at which hydrogen is released or absorbed by the material, is never at a constant value of pressure but is always increasing/decreasing because of the heat generated by the reaction of hydrogen with the sorption material. Accordingly without appropriate heat management, hydrogen cannot simply be delivered at a given rate. In this case, the hydride must be heated to notably raise P^{eq}, or a hydrogen pressure significantly lower than P^{eq} must be applied, to sustain a constant flow of hydrogen and compensate for the heat consumed by the release of hydrogen from the hydride. The reverse applies for the uptake of hydrogen and in this case, heat must be removed from the hydride bed to facilitate a rapid hydrogen uptake despite the exothermic nature of hydrides formation.

For investigating the hydrogen sorption properties of small samples (≈mg to g) this is not a major issue; however, for large scale systems involving kg of hydrides, heat management becomes critical and external systems to drive heat out or in must be added to the hydride storage tank (see Section 10). This not only adds further complications in terms of system design but also significantly impedes the practical hydrogen storage capacity at the system level. However, because of its simplicity, the use of temperature and pressure as external control of the

Table 2. Summary of the hydrogen gravimetric density, temperature of decomposition (T_{dec}), enthalpy of formation ($\Delta H°_f$), enthalpy of decomposition ($-\Delta H_{dec}$) and entropy (ΔS) of selected hydrides. The hydrides are classified as a function of the type of hydrogen bonding.

	H_2 density [mass%]	T_{dec} [°C]	$\Delta H°_f$ [kJ mol^{-1}]	$-\Delta H_{dec}$ [kJ mol^{-1} H_2]	ΔS [J K^{-1} mol^{-1} H_2] or *[J K^{-1} mol^{-1}]
Protides					
$LiBH_4$	18.5	380[448]	−146,[449] −177[450] −184.7,[451] −190.46[452] −194.44[118a,450,453]	−95.8[22]	*75.9,[450] *128.7[454]
$NaBH_4$	10.7	400[455]	−182~ −188[449] −183.3,[454] −191[118a]	−94.3[22]	*101.3, *126.2[454]
KBH_4	7.5	500[455]	−229,[118a] −228[449] −242.3[454]	−120[454]	*106, *162[454]
$Mg(BH_4)_2$	14.9	323[22]	−99[449]	−24.8[449]	*91.3,[456] *128[457]
$Ca(BH_4)_2$	11.6	360, 260	−151[449]	−37.8[449]	158[458]
$Be(BH_4)_2$	20.5	25[22]	27[118a]	7	–
$Al(BH_4)_3$	16.9	150[459]	−301.8[454]	−50.3[454]	*289[454]
$Zn(BH_4)_3$	8.5	85[22]	−16,[22] −18[449]	−4[22]	–
$Ti(BH_4)_3$	13.1	25[22]	–	–	–
$Zr(BH_4)_4$	10.7	250[22]	–	−10.9[449]	–
H_3BNH_3	19.6	100, 150, 500[460]	−21[461]	−7[461]	–
$LiAlH_4$	10.5	180[22]	–	45.4[22]	*78.8[462]
Li_3AlH_6	11.2	220[22]	–	−76[22]	*102.6[462]
$NaAlH_4$	7.4	247[22]	–	−120[22] −40[463]	*89.7[462]
Na_3AlH_6	5.9	268[22]	–	−178[22]	*161.5[462]
$KAlH_4$	5.7	300[22]	–	−207.4[22]	–
K_3AlH_6	4.0	330[22]	–	−270.8[22]	–
Hydrides					
$LiNH_2$	8.7	380	−186.3[464]	−186.3[464]	–
$NaNH_2$	5.1	400[465]	−118.8	−118.8	*76.9
$Mg(NH_2)_2$	7.1	350	−374[464]	−187[464]	*52[464]
Ionic hydrides					
LiH	12.5	720[22]	−116.3[22]	−232.6[22]	−134[27m]
NaH	4.2	425[22]	−56.5[22]	−113[22]	−162[27m]
KH	2.5	417[22]	−57.7[22]	−115.4[22]	−168[27m]
MgH_2	7.6	327[22]	−75.3[22]	−75.3[22]	−134[27m]
CaH_2	4.8	600[22]	−181.5[22]	−181.5[22]	−140[27m]
RbH	1.2	170[22]	−52.3[22]	−104.6[22]	−170[27m]
CsH	0.75	170[22]	−54.2[22]	−108.4[22]	−170[27m]
SrH_2	2.2	675[22]	−180.3[22]	−180.3[22]	−156[27m]
BaH_2	1.4	–	−177[22]	−177[22]	−144[27m]
Covalent hydrides					
B_2H_6	21.7	40[22]	36.4[22]	12.1[22]	–
GaH_3	4.1	−15[22]	118[22]	25[22] 78.7[22]	–
BiH_3	1.4	−40[22]	217.6[22]	32,[22] 144.6[22]	–
Metallic hydrides					
LaH_2	1.4	600[27m]	−210[27m]	−210[27m]	−152[27m]
YH_2	3.2	600[27m]	–	−225[27m]	−144[27m]
TiH_2	4	380[22]	−126[27m]	−126[27m]	−100[27m]
VH_2	3.8	35[22]	−54[27m]	10.8,[22] −54	−108[27m]
$PdH_{0.5}$	0.47	−78[27m]	–	−40[27m]	−84[27m]

Table 2. Continued.

	H_2 density [mass%]	T_{dec} [°C]	$\Delta H°_f$ [kJ mol^{-1}]	$-\Delta H_{dec}$ [kJ mol^{-1} H_2]	ΔS [J K^{-1} mol^{-1} H_2] or *[J K^{-1} mol^{-1}]
Intermediate					
AlH_3	10	150[22] 25[27m]	−46[22]	−30.6[22] −8[27m]	–
BeH_2	18.2	250[22]	–	−18.9[22]	–
ZnH_2	3	90[22]	–	−5.4[22]	–
CdH_2	1.75	−20[22]	–	26.4[22]	–
Unknown					
TlH_3	1.4	−95[22]	245[22]	164[22]	–
$CoH_{0.5}$	0.84	25	–	0[27m] 30	–
HgH_2	1	−125[22]	–	55.4[22]	–
$NiH_{0.5}$	0.85	20[27m]	–	−6[27m] −58	−116[27m]
FeH	1.76	–	–	14[27m]	–
MnH	1.79	450–730[27m]	–	−9[27m] −22	−116[27m]
PtH	0.5	–	–	26[27m]	–
Intermetallics					
$CaNi_5$	0.99	43[26]	–	31.9[26]	101[26]
$LaNi_5$	1.28	12[26]	–	30.8[26]	108[26]
$TiMn_{1.5}$	1.15	−21[26]	–	28.7[26]	114[26]
TiFe	1.5	−8[26]	–	28.1[26]	106[26]
$MmNi_5$	1.24	−56[26]	–	21.1[26]	97[26]
Mg_2Ni	3.3	255[26]	–	−64.5[26]	−122[26]
$(V_{0.9}Ti_{0.1})_{0.95}Fe_{0.05}$	1.8	36[26]	–	−43[26]	−140[26]

hydrogen reaction with hydrides is still currently the dominant approach.

The possibility of using other means to drive the release/uptake from solid state hydrogen materials has been investigated, but apart from the electrochemical methods, all the other approaches (e.g., microwave, laser, and ultrasound irradiation) also involve the direct or indirect generation of heat (Figure 6a). For example, the use of microwave radiation has been investigated by several groups because it has the potential to provide rapid, energy-efficient heating. Heating by microwave involves electromagnetic radiations in the frequency range of 300 MHz to 300 GHz.[28] The interaction of charged particles within dielectric materials with the electric field component of electromagnetic radiations causes the materials to heat up due to the Maxwell–Wagner effect.[29] Several results have been reported on the possibility of using microwave to drive hydrogen desorption from metal hydrides and complex hydrides.[30] For example, hydrogen could be released from TiH_2 by microwave irradiation but the release was incomplete because of low penetration depth of the microwave irradiation in the TiH_2 particles.[30a] Transition metal hydrides, such as $VH_{0.81}$, ZrH_2, and $LaH_{2.48}$, also showed a rapid temperature increase upon microwave irradiation with some hydrogen release.[30c]

By using ultrasonic irradiation, it is also possible to generate shock waves and localized heating by acoustic cavitation. Ares et al. reported the possibility of releasing hydrogen from MgH_2 through this principle.[31] The idea of using a laser was also tested. For example, starting with Ti in hydrogen atmosphere, the formation of TiH_2 was reported upon laser irradiation at 4 J cm^{-2}.[32] Investigations of laser heating of MgH_2 and Mg_2NiH_4 + MgH_2 were also conducted by Plasma Kinetics Corporation. It was reported that ≈80 continuous watts were needed to release about 4.5 kg of hydrogen from 119 kg of MgH_2 at rates of ≈0.9 kg h^{-1}.[33] A temperature of 390 °C was reached within 1 ms to enable the decomposition of the hydride.

Exposure of hydride materials to UV radiation was also proposed decades ago as a means to release hydrogen from hydrides, including MgH_2,[34] $LiAlH_4$,[35] and AlH_3,[36] but this led to little amounts of hydrogen. For example, upon UV irradiation with an intensity of 280 mW cm^{-2}, 100 mg of MgH_2 powder released 0.008 mass% H_2, at room temperature.[37] The mechanism for hydrogen release was proposed to be associated with an electronic charge and/or energy transfer process involving the creation of doubly excited sites.[34b] Based on the similar idea of using light to drive hydrogen absorption/release, Sun et al. recently proposed an alternative method, by using the plasmonic effect of Au nanoparticles to generate local heat at the surface of hydride particles and thus locally trigger hydrogen absorption/desorption.[38] It is expected that by such an approach, the localized generation

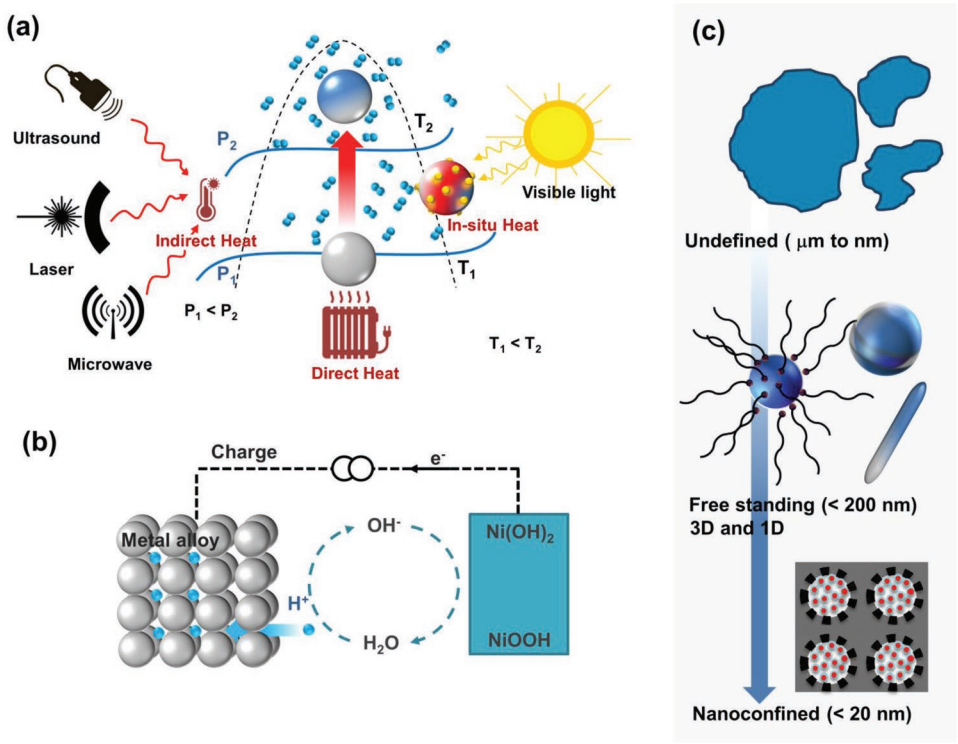

Figure 6. Principles of methods to store hydrogen. a) Illustration of existing methods to facilitate the loading and unloading of hydrogen in materials; b) principles of electrochemical hydrogen storage; and c) the various morphologies of hydrogen storage materials. P_1 and P_2 correspond to the equilibrium plateau pressure (P^{eq}) at the temperature T_1 and T_2. Materials are usually heated to raise P^{eq} and facilitate the release of hydrogen above atmospheric pressure to feed a fuel cell, for example.

of heat can help to minimize the need of additional external heat management systems. This is highly desirable because it can lead to practical systems of much higher hydrogen storage capacity than currently feasible. However, to date there are very few investigations on this topic[39] and many concern the use of plasmonic effect toward the design of hydrogen sensors.[40]

Electrochemical charging/discharging of hydrides is another approach, but this is mainly applicable to hydrides with high resistance to alkaline corrosion. Accordingly, the application of this concept to hydrides of high hydrogen storage capacity such as Mg/MgH_2 has been limited.[41] Electrochemical charging/discharging relies on the oxidation and reduction of a strong alkaline electrolyte to generate H atoms that are directly absorbed by a metal alloy (M) forming a hydride (MH) (Figure 6b). The charging process follows the general reaction

$$M + nH_2O + ne^- \leftrightarrow MH_n + nOH^- \quad (3)$$

and the reverse reaction applies during discharging. During this process, a nickel counter electrode swinging between its oxide hydroxide and hydroxide is used to balance (4)

$$Ni(OH)_2 + nOH^- \leftrightarrow NiOOH + nH_2O + ne^- \quad (4)$$

It should be noted that reaction (3) is equivalent to the reaction observed upon direct use of temperature and pressure (1). Accordingly both processes are comparable and the gas equilibrium pressure P^{eq} and electrochemical equilibrium potential E^{eq} are linked by the relationship[42]

$$E^{eq} = \frac{RT}{nF} \ln P^{eq} \quad (5)$$

where n corresponds to the number of electrons involved, R is the universal gas constant (8.314 J mol^{-1} K^{-1}), and F is the Faraday constant (96 500 C mol^{-1}).

However, P^{eq} in excess of 0.1 MPa is not desirable to avoid a significant self-discharge of the metal alloy at the ambient and the excess formation of hydrogen through the secondary reaction

$$H_2O + e^- \rightarrow OH^- + 1/2H_2 \quad (6)$$

A P^{eq} comprised between 0.001 and 0.1 MPa at 25 °C is considered as optimal. In the case of the archetypical $LaNi_5$ alloy at the basis of Ni–MH commercial battery, this means that its initial P^{eq} of 0.23 MPa at 25 °C had to be modified through the substitution of A and B.[42b] For a one electron process, the electrochemical charging capacity (C_{el} in mAh g^{-1}) is also linked to the solid–gas charging capacity (C_{gs}, i.e., the amount of hydrogen absorbed per mol of metal alloy) by

$$C_{el} = \frac{C_{gs}F}{3.6M} \quad (7)$$

where M is the molecular weight of the alloy.

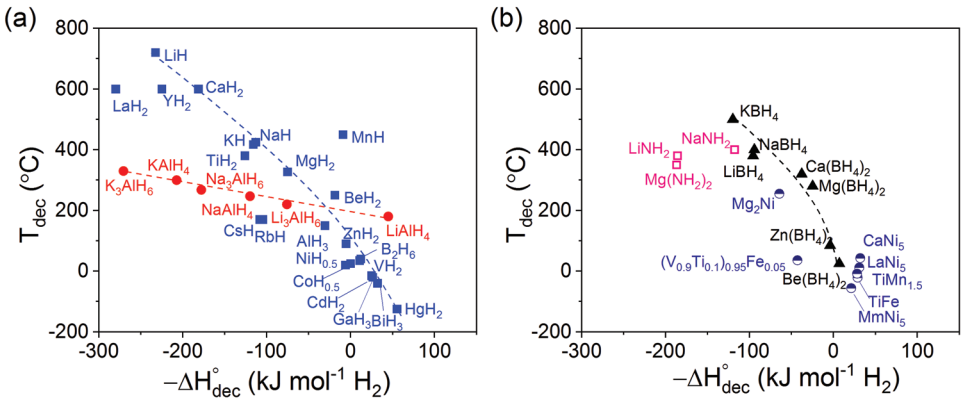

Figure 7. Thermodynamic of a range selected hydrides. Evolution of the enthalpy of decomposition ($-\Delta H^{\circ}_{dec}$) of a) common metal hydrides and alanates, and b) selected borohydrides, amines and intermetallics as a function of their decomposition temperature (T_{dec}) for hydrogen release. The hydrides with a reasonable hydrogen storage capacity decompose at high temperatures.

It should also be noted that the effectiveness of the method used to load/unload hydrogen in hydrides depends on the particle morphology and the initial state of the hydride particle surface (Figure 6c).

3. Hydrogen Storage Properties of Materials: Fundamental Principles

Today, most of the hydride materials of high hydrogen gravimetric density, e.g., MgH_2, LiH, $LiAlH_4$, $LiBH_4$, and H_3BNH_3, have hydrogen storage properties unsuitable for application, i.e., temperatures and/or pressures too high for hydrogen absorption/desorption cycling with often very poor hydrogen rates of uptake and release to meet the regimes of an electrolyzer or a fuel cell (Table 2 and **Figures** 5 and 7). Enabling hydrogen storage under moderate conditions of hydrogen pressure and temperature requires the modification of the heat of reaction of these materials with hydrogen as well as their rate of reaction. This necessitates a better understanding of the interaction of hydrogen with hydride forming elements and a weakening of M−H bonds and intrahydrogen pairing (H−M−H) in these elements to improve the thermodynamics of the reaction as well as the energy barriers controlling the rate of the hydrogen uptake/release. In the context of stationary applications, additional development of such knowledge, along existing low temperature hydrides, e.g., FeTi, Ti BCC (Table 2), has also become critical. In addition to a better understanding of the interaction of hydrogen with alloys, the effects of compositional adjustment on the ease of their activation and operating conditions must be progressed to effectively facilitate their application in the field.

3.1. Current Understanding of the Basic Rules Guiding the Rate of Hydrogen Uptake/Release

The rate of reaction of hydrogen with absorbing materials first of all depends upon the probability of collision of hydrogen molecules in the gas phase with the material's surface (**Figure 8**a). In the gas phase, hydrogen molecules have an average thermal velocity of ≈1775 m s^{-1} at 26 °C.[20b] Part of the initial kinetic energy is released upon interaction with the surface of the absorbing material and at speed of ≈18 Å ps^{-1}, the van der Waals (vdW) interaction comes into play to physisorb hydrogen (Figure 8a).[20b] The initial rate of reaction thus depends upon the material's available surface area and any additional activation barriers for the chemisorption of hydrogen. In particular, a high surface area is important when considering the storage of hydrogen through physisorption processes on mesoporous carbons or MOFs, for example.[15,43] Usually the physisorption of hydrogen involves a low energy barrier of ≈1–10 kJ mol^{-1} and thus is readily achievable at low temperatures.[27e,44] For example, hydrogen physisorption is observed in many porous materials including silicas, aluminas, zeolites, graphites, activated carbons, and carbon nanofibers at −196 °C.[45] For materials such as Mg absorbing hydrogen, a high surface area is also very important as a higher number of available surface sites help to improve the rate of hydrogen chemisorption and thus the overall reaction. For example for Mg, which is notorious for the high hydrogen dissociation barrier (≈432 kJ mol^{-1} H_2)[44] at its surface, a reduction of the overall activation energy (E_a) from 156 to 120 kJ mol^{-1} has been reported upon a tenfold increase in the specific surface area of Mg particles.[46] The absorption of hydrogen until the formation of the hydride phase is also controlled by many additional barriers involving the penetration of hydrogen into the subsurface and then further diffusion through the material (Figure 8).[27e] Indeed, assuming the formation of an hydride layer at the surface of the material upon the absorption of the first hydrogen molecules, the diffusion of hydrogen through the hydride phase becomes slower (e.g., 1.5×10^{-16} m^2 s^{-1} in MgH_2, instead of 1×10^{-8} m^2 s^{-1} in Mg at 350 °C).[44,47]

The rate (k) of the hydrogenation/dehydrogenation reactions depends on the activation energy barrier (E_a) following the Arrhenius equation

$$k(T) = Ae^{\frac{-E_a}{RT}} \quad (8)$$

In this equation, A is a pre-exponential factor. For a given reaction, the reaction rate k at a given temperature depends on

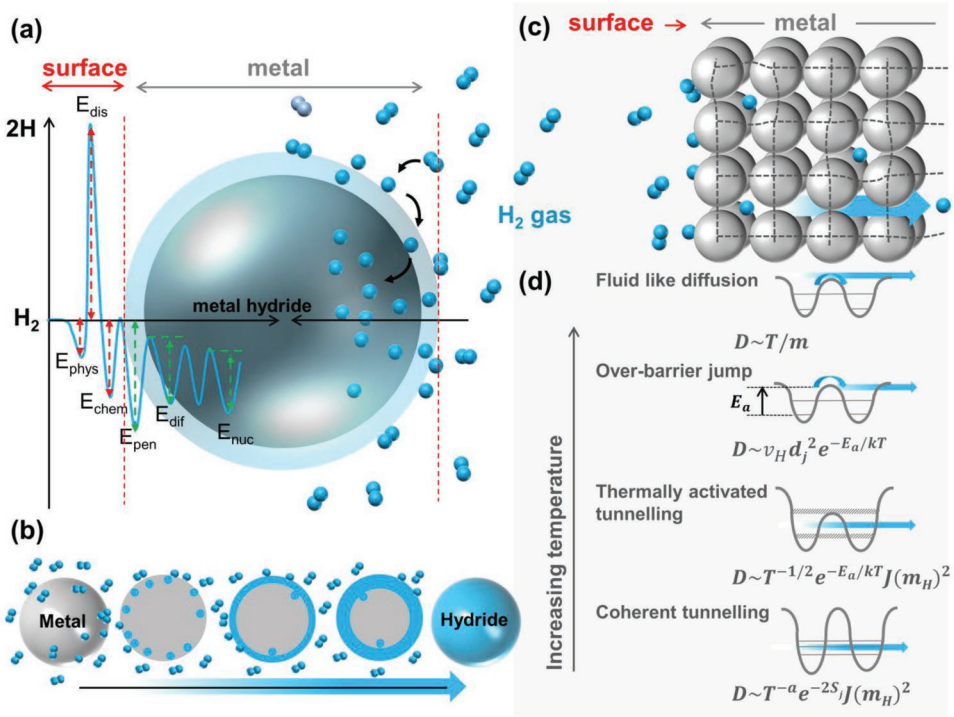

Figure 8. Illustration of the hydrogen absorption/desorption principles in metals. a) Lennard-Jones potential diagram corresponding to the successive energy barriers encountered by hydrogen during absorption/desorption in a metal. E_{phys}: energy for hydrogen physisorption, E_{dis}: energy for hydrogen dissociation, E_{chem}: energy for hydrogen chemisorption, E_{pen}: energy for hydrogen penetration in the subsurface, E_{dif}: energy for hydrogen diffusion in the bulk, and E_{nuc}: energy for the nucleation and growth of the hydride; b) growth of the hydride phase upon hydrogen absorption through a shrinking core; c) hydrogen diffusion in metal leading to an expansion of the lattice structure; and d) examples of models relevant to hydrogen diffusion in metals. D is the diffusion coefficient, a the lattice parameter, S_j the elementary jump distance, d_j is the jump distance, $J(m)$ is the tunneling-matrix element, m_H the mass of hydrogen, E_a the activation energy, and ν_H the vibration frequency of an hydrogen atom ($\nu_H \sim m_H^{-1/2}$). For $S_j > 0$, the hopping is incoherent. The thermally activated tunneling is considered to be non-adiabatic; which is the case for most hydrides. Reproduced with permission.[27m] Copyright 2005, Springer.

both the pre-exponential factor (A) and the E_a of the reaction process, i.e., a higher pre-exponential factor (A) and a lower value of E_a favor faster reaction rates.

The physical meaning of A remains elusive.[48] Although $A = e^{\frac{\Delta S}{R}}$ was proposed by Wert and Zener in 1949 for diffusion processes,[49] this was found to be inconsistent with many numerical results. A is more often regarded as an empirical factor that can be affected by the reactant states, e.g., particle size and defective sites, and the reaction conditions, e.g., microwave aid.[50] The Meyer–Neldel rule, which describes the compensation correlation between thermodynamics or kinetics factors,[48] has also been used to explain the relationship between A and E_a, and their compensation effects observed both experimentally and computationally.[50b,51] Nevertheless, predictions based on the Meyer–Neldel rule were found to lack sufficient levels of accuracy to enable the reliable determination of the pre-exponential factor from the activation energy.[48] It is noteworthy that in the case of hydrogen storage materials, such a correlation has barely been explored owing to the difficulty of separating individual energy barriers (Figure 8a). Typical efforts have mainly focused on lowering the overall energy barrier (E_a) by facilitating the uptake and release of hydrogen along what is believed to be the slowest reaction step. For example, in the case of the Mg/MgH_2 system, Mg is often doped with Pd, Nb, or V[27e,52] to recombine/split hydrogen atoms at the metallic surface of the storage material, because this is believed to be the slowest step. It is possible that defects and grain boundaries introduced in hydride materials are positive factors enhancing the pre-exponential factor for their reaction with hydrogen.[53] However, the interaction of hydrogen with solid materials includes several barriers that may become the rate-limiting steps as the reaction progresses.

Various models including the Jander[54] and Johnson–Mehl–Avrami–Kolmogorov (JMAK)[55] models have been used to better understand the rate-limiting steps involved in hydrogen sorption,[56] with the assumption that individual particles are of similar size, shape, surface reactivity, and undergo similar growth regimes (e.g., are defect free). These models summarized in **Figure 9** include the "shrinking core" models which assume that the decomposition starts from the surface and proceeds inward,[57] and the "nucleation and growth" models based on the assumption of random nucleation and growth process within the bulk of the material.[55d] However, it should be noted that the interpretations based on these models are highly subjective to the quality of the fit. Accordingly, these models are often not conclusive owing to the dynamic multistep reaction paths of hydrogen in materials. For example in the case of Mg/MgH_2, Liang et al. concluded on a 2D growth model as the best fit for the rate-limiting step at 300 °C for MgH_2 doped with transition metals.[58] In contrast, Hanada et al. proposed that the

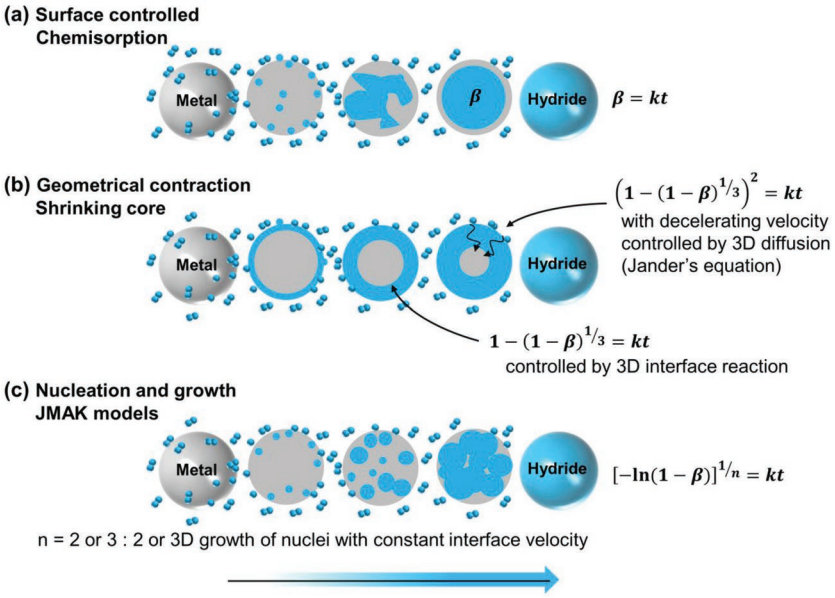

Figure 9. Classical rate-limiting step models. Despite their "simplicity" these models have been found to be useful in understanding the rate-limiting steps of hydrogen sorption in metals and complex hydrides.

hydrogen desorption reaction from Ni catalyzed MgH_2 is of first order.[59] In another example, Pourabdoli et al. showed that for MgH_2-10 wt% (9Ni–2Mg–Y) the difference in the fit correlation of the hydrogen desorption rate between the 2D and 3D JMAK model is about 1%.[60]

The hydrogen kinetics of complex hydrides are somewhat more complicated because of the multidecomposition steps and reaction intermediates involved, the disproportionation of the initial complex hydride upon hydrogen release, and the resulting phase segregation (**Figure 10**).[61] In this case, the rate-limiting step of each individual reaction step is often modeled by using the classical models summarized in Figure 9.[62] However, in addition to the rate-limiting steps associated with the adsorption and diffusion of hydrogen within the material, mass transfer leading to elemental dissociation or recombination upon hydrogen absorption must also be considered. An archetypical example of such complexity is the Ti-doped $NaAlH_4$ system for which the exact reaction paths and rate-limiting steps upon Ti doping remain unclear. Considering the rehydrogenation from NaH and Al particles (Figure 10a), Na_3AlH_6 as the intermediate must first be formed at the interface of NaH and Al particles, where hydrogen molecules from the gas must be "activated" (reaction (7)). The Na_3AlH_6 intermediate must then be further reacted with Al and H_2 to lead to the regeneration of $NaAlH_4$

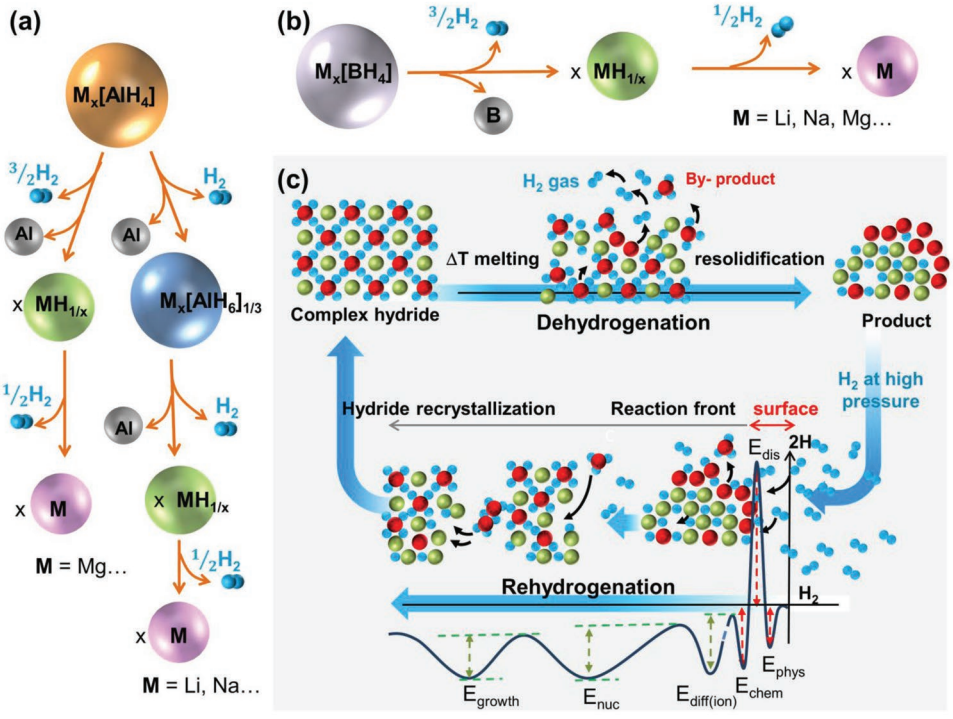

Figure 10. Illustration of the hydrogen desorption/absorption principles in complex hydrides. General decomposition path of a) alanates and b) borohydrides; c) hypothetic mechanisms for hydrogen release and uptake in complex hydrides and associated Lennard-Jones potential diagram corresponding to the successive energy barriers encountered by hydrogen during absorption. E_{phys}: energy for hydrogen physisorption, E_{dis}: energy for hydrogen dissociation, E_{chem}: energy for hydrogen chemisorption, E_{pen}: energy for hydrogen penetration in the subsurface, $E_{diff(ion)}$: energy for ionic diffusion, and E_{nuc} and E_{growth}: energy for the nucleation and growth of the hydride. In complex hydrides, the reaction is believed to occur at the interface of segregated elements.

$$Na_3AlH_6 \leftrightarrow 3NaH + Al + 1.5H_2 \quad (1.8\ \text{mass\%}\ H_2) \tag{9}$$

$$3NaAlH_4 \leftrightarrow Na_3AlH_6 + 2Al + 3H_2 \quad (3.7\ \text{mass\%}\ H_2) \tag{10}$$

If some Al particles remain trapped within the forming Na_3AlH_6 phase, and transport of Al is limited, then additional Al must be added to the system to reach the full regeneration.[63] Since Ti is a transition metal, it has been claimed from H_2/D_2 scrambling experiments[64] that Ti facilitates the recombination/dissociation of hydrogen molecules at the material/hydrogen gas interface. But this is not sufficient to explain the increase in reaction rate observed because the rate of H_2/D_2 scrambling is much faster than the rate of hydrogen release and uptake of Ti–$NaAlH_4$. It has thus been suggested that additional Ti dispersed within the material must help with the significant mass transfer involved in this reaction,[63,65] and thus the dissociation/recombination of coexisting NaH and Al phases.[66] In this context, vacancies have also been claimed to play a role.[67] It is noteworthy that despite the significant mass transfer involved, the dehydrogenation of $NaAlH_4$ and the Ti-doped counterpart have been found to follow a simple Arrhenius law (Equation (6)) and lead to a modification of both the activation energy and the pre-exponential factor (A).[68] At Ti additions >0.9 mol%, the E_a was found to remain constant while A increased and was thus solely responsible for the additional improvement in dehydrogenation rate observed.

A key factor for improving the kinetics is also in the understanding of the hydrogen diffusion behavior in materials. For example, it is generally admitted that as the hydrogen molecule dissociates at the surface of metals into individual atoms, these have to diffuse through the metal lattice by occupying interstitial sites within the metal lattice (Figure 8c). This results in elastic interactions between the interstitial atoms, phase transitions, lattice strains, and a modification of the electronic and magnetic properties as hydrogen migrates from one interstitial site to another upon formation of the hydride phase. To diffuse through the metallic lattice, the hydrogen atoms have to overcome the energy barrier generated from the compression of the surrounding atoms, as a consequence the diffusion coefficient D follows the Arrhenius law[11,27m,69]

$$D = D_0 e^{-\frac{E_a}{k_B T}} \tag{11}$$

where E_a is the activation energy related to the elasticity of the lattice and the size of the atoms, k_B is the Boltzmann constant, T is the temperature, and D_0 is the probability of diffusion, which depends upon the frequency of the thermal vibration (ω_0) of the interstitial atoms of mass (m).

Once in metals the diffusion of hydrogen atoms is relatively fast (e.g., at a rate of 2×10^{12} H jumps per second at room temperature in vanadium)[70] as compared to complex salts (e.g., 5×10^3 jumps per second at −223 °C in $NaAlH_4$—which is equivalent to a relaxation frequency of 10^{11} s^{-1} at room temperature).[71] For example, diffusion coefficient of H in $Ti_{1.2}Mn_{1.8}$ is $\approx 10^{-7}$ cm^2 s^{-1} at 25 °C,[72] while for $NaMgH_3$, a diffusion coefficient of $\approx 10^{-22}$ to 10^{-23} cm^2 s^{-1} has been determined for the negatively charged $H^{\delta-}$ and associated vacancies.[73] Quantum effects can also be observed because of the small size of the diffusing hydrogen atoms and this may influence the diffusion process.[27j] The migration of hydrogen atoms in metals is believed to occur via different mechanisms depending on the temperature (Figure 8d). At low temperatures where the phonon contribution is minimal, hydrogen diffuses through coherent tunneling. As the temperature is increased the diffusion evolves to incoherent hopping and then with the increasing number of phonons available, the resulting lattice vibration further facilitates the diffusion of hydrogen (Figure 8d). At higher temperatures hydrogen atoms may be regarded as classical particles jumping over barriers via thermal excitations and if the temperature is further increased the hydrogen atoms are free to move as in the gas phase and do not remain within the potential wells of interstitial sites (Figure 8d).

The diffusion of hydrogen in metals can be improved by minimizing the interactions of H atoms with each other's and the metallic atoms of the host material. At low hydrogen concentration in metals, it is believed that the hydrogen occupies octahedral sites in fcc metals, e.g., Cu,[74] Ag,[75] Pd,[76] Pt,[77] Al,[78] and Ni.[79] In this case, the two nearest octahedral sites are separated by a gap of ≈2.5–2.9 Å. In bcc metals, e.g., Fe,[80] V,[81] Nb,[82] Ta,[81a] Mo,[83] and W,[84] when the hydrogen concentration does not exceed the solid–solution phase, hydrogen occupies tetrahedral sites with a separation of 1.01–1.17 Å. Due to short distances, significant hydrogen tunneling is observed and this plays a role in the diffusion coefficient and thus results in a lower activation barrier for diffusion in bcc metals as compared to fcc metals.[27j,69,72,85] Similar to bcc metals, hydrogen occupies tetrahedral sites in hexagonal metals like Ti,[86] Zr,[87] Sc,[88] Y,[89] and La alloys;[90] however, due to the degree of high concentration range of solid solutions especially in rare earth metals ≈20% for La and Y at room temperature, the next-nearest neighboring pairs of hydrogen condense strongly to form a bridging metal atom (in c-axis direction).[27j] In general hydrogen diffusion is not the rate-limiting step in metal hydrides. However, considering the Mg/MgH_2 systems, theoretical calculations have predicted that the diffusion of hydrogen in MgH_2 can be locally limited by the presence of impurities including doping elements such as Ti, Fe, and Mn often used as catalysts.[91] In contrast, applying external strain has been postulated to enhance hydrogen diffusion within the MgH_2 lattice.[92] Diffusion in amorphous phase/grain boundary is often faster,[93] owing to the broad distribution of site energies. The diffusion of interstitial hydrogen in amorphous materials can be determined from the equation[94]

$$D = D_0^{\circ} e^{\left(\frac{-Q^{\circ}}{RT}\right)} \frac{\partial}{\partial c}\left\{(1-c)^2 e^{\left(\frac{\mu}{RT}\right)}\right\} \tag{12}$$

where c is the hydrogen concentration for a distribution of site energies, D_0° is a prefactor, and Q° is the average activation energy which is the difference between the constant saddle point energy and the average value of the site energy, R is the universal gas constant, and μ is the chemical potential of hydrogen.

In ionic hydrides, the models above are not valid and the release or uptake of hydrogen is often driven by initial and significant mass transport of hydride ionic species and not

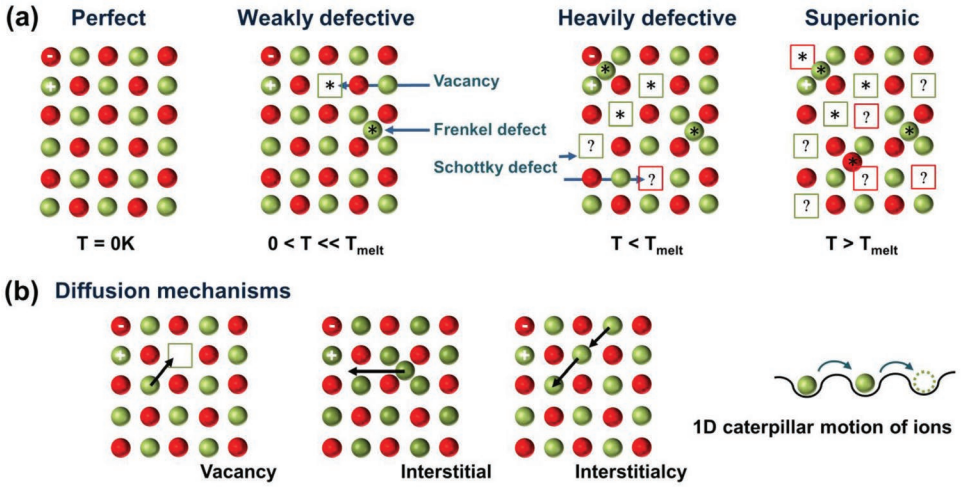

Figure 11. Illustration of ionic diffusion in complex hydrides. a) Progressive evolution of crystal with zero defects up to a superionic conductor; and b) models of ionic diffusion.[571] In complex hydrides superionic conduction is expected to occur after the melting of the hydride.

hydrogen itself (**Figures** 10c and **11**). For example, in the case of $NaAlH_4$, the diffusion of AlH_4^- and/or AlH_3[67b] and their recombination at the surface of the $NaAlH_4$ particles into Al and H_2 is believed to control the desorption rate.[67a,95] Similarly, in the case of borohydrides, translational diffusion of BH_4^- was found to be dominant upon hydrogen release.[96] As a consequence, improving the hydrogen sorption kinetics of ionic hydrides strongly depends upon means to improve ionic conduction. As discussed above, diffusion of mobile species in a crystalline solid needs to overcome energetic barriers across two local energy minima. For ionic solids, the ionic conductivity (σ) can be expressed as[97]

$$\sigma = N(\mathrm{Ze})\mu_{\mathrm{M}} \tag{13}$$

where N is the concentration of mobile ions (cationic or anionic), Ze is the ionic charge, and μ_{M} is the rate of diffusion of the mobile ion per unit of electric field, i.e., the ion mobility. Both the ion mobility and concentration of the charge carriers are temperature dependent following

$$N = N_0 \exp(-E_{\mathrm{f}}/k_{\mathrm{B}}T) \tag{14}$$

$$\mu_{\mathrm{M}} = \mu_0 \exp(-E_{\mathrm{m}}/k_{\mathrm{B}}T) \tag{15}$$

where N_0 and μ_0 are the pre-exponential factors, and E_{f} and E_{m} the energies of formation and migration of the mobile charge carriers, respectively. The activation energy E_{a} for the diffusion of ions in solids is thus the sum of E_{f} and E_{m}.

Improving diffusion in ionic compounds depends highly upon the amount of interstitials, vacancies and partially occupied lattice sites (Figure 11a), as these provide minimum energy diffusion pathways.[98] Interstitials and vacancies sites can be created by aliovalent substitution of cations/anions. However, this approach often reaches a maximum diffusion at the optimum aliovalent substitution. Beyond this optimum, the strong lattice distortion induced by the excessive aliovalent concentration induces a slower ionic diffusion. For example, Ca aliovalent doping in $LiBH_4$ showed an increase in Li-ion conductivity up to a maximum of 4 mol% $Ca(BH_4)_2$ doping, then the conductivity decreases.[99]

Both ion valency and size can influence ionic conductivity.[100] Indeed, a decrease in ionic diffusion can be observed when electrostatic interaction between the mobile ionic specie and the ion forming the structural skeleton is increased. Similarly, increasing the valence of the mobile ionic species as well as ionic size reduces mobility. **Figure 12** aims to summarize these effects for borohydrides, although the trends are less obvious than those observed for solid-state battery electrolytes[100] owing to the limited number of available data. If the diffusing ion is too small it may remain trapped within large electrostatic wells of the larger ions forming the skeleton. On the other hand, if the diffusing ionic species are too large, they will experience large bottlenecks when diffusing between the smaller skeleton ions. Therefore, achieving fast hydrogen kinetics in ionic hydrides requires a careful balance of often diverging requirements.

A hopping mechanism is generally used to describe the diffusion of ionic species (Figure 11). In this mechanism, ions can jump from one site to a neighboring site through vacancies such as Schottky defects or via interstitial defects (Frenkel defects) as described in Figure 11b. However, it should be noted that diffusion mechanisms may take additional forms depending upon the material structure and the temperature. For example, in the superionic state a caterpillar mechanism (Figure 11b), whereby the mobile ion can jump to a neighboring site even if occupied, may take place as well as continuous diffusion at high temperatures.[101]

Diffusion coefficients of 5×10^{-16} m^2 s^{-1} at 75 °C and 7×10^{-14} m^2 s^{-1} at 200 °C have been reported for the BH_4^- and AlH_4^- anions, respectively.[102] Li^+ conductivity in $LiAlH_4$ was found to be of 2.9×10^{-6} S cm^{-1} at 107 °C.[102] At room temperature the tetrahedral BH_4^- unit reorients at a fast rate,[103] and a slow Li^+ hopping motion has been suggested to occur.[104] At higher temperatures (>120 °C), upon the structural phase transition of $LiBH_4$ from orthorhombic to hexagonal the diffusion of Li^+ is very fast,[104,105] and this is accompanied with a rapid reorientational motion of the BH_4^- ions (at a rate of

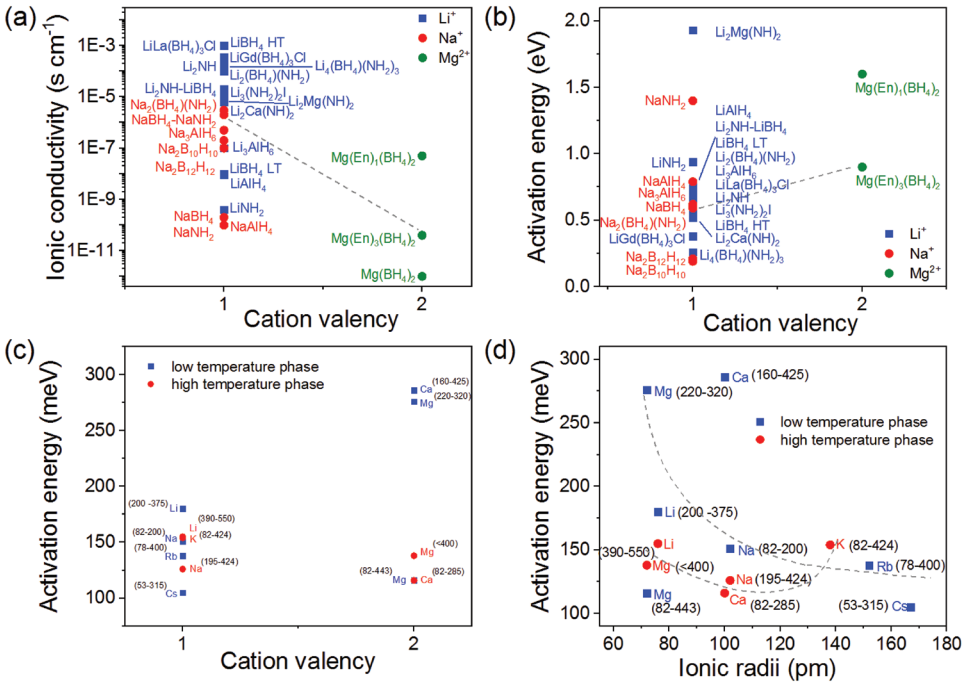

Figure 12. Ionic diffusion in complex hydrides. Summary of reported values of a) ionic conductivity of Li^+, Na^+, and Mg^{2+} in respective borohydrides, and b) the associated activation energy for diffusion as function of the cation valency at 25 °C. Activation energy for the ionic diffusion of BH_4^- as function of c) the cation valency and d) the cation radii of borohydrides. The ions should not be too small or too large.

$\approx 10^{13}$ s^{-1})[106] suggesting that the fast rotation of the anion is facilitating the translational diffusion of Li^+. Upon melting of $LiBH_4$ at 450 °C (before hydrogen release), both translational diffusion of BH_4^- (with a diffusion coefficient of 10^{-9} m^2 s^{-1})[96] and Li^+ is believed to occur. The fast diffusion of Li observed in $LiBH_4$ and its wide electrochemical window has triggered significant work toward the use of borohydrides as solid state ionic conductors for batteries.[107] For example, a partial substitution of the BH_4^- ion with I^- has shown to lead to a Li^+ conductivity of $\approx 10^{-4}$ S cm^{-1} at 60 °C.[108] Similarly, lithium amide-borohydrides showed Li^+ conductivity of 10^{-4} to 10^{-3} S cm^{-1} at room temperature.[109] Similar improvements in conductivity have been reported for $NaBH_4$-based electrolytes, and in particular $NaCB_9H_{10}$ showed Na^+ conductivity of $\approx 10^{-2}$ S cm^{-1} at the ambient.[107f] However, it should be noted that the improvements of Li^+ or Na^+ conductivity did not effectively translate into better overall hydrogen storage properties of complex hydrides, because ionic diffusion is only one parameter among the multi-interrelated factors controlling the storage mechanism of hydrogen in complex hydrides.

3.2. Current Understanding of the Basic Thermodynamics Rules Controlling the Temperature for Hydrogen Sorption

The Gibbs free energy difference between products and reactants (ΔG) is the driving force of a reaction and it has to be negative for the reaction to occur (**Figure 13**d). Therefore, controlling ΔG is crucial for the thermodynamics of the reaction hydrogen with sorption materials. The definition of Gibbs free energy is $G = H - TS$. At a fixed temperature (T)

$$\Delta G = \Delta H - T\Delta S \tag{16}$$

where ΔH is the enthalpy change of the reaction, while ΔS is the entropy change of the system. In the case of hydrogen/metal systems, ΔS mainly results from the entropy (ΔS_{gas}) of the hydrogen gas which is lost upon hydrogen absorption in the material. Other entropy effects (ΔS_e) as summarized below are relatively small in comparison to ΔS_{gas}[23]

$$\Delta S_e = \Delta S_H^{vib} + \Delta S_{host}^{vib} + \Delta S^{el} + \Delta S^{conf} \tag{17}$$

where ΔS_H^{vib} corresponds to the vibrational entropy of the hydrogen atoms in the hydrides, ΔS_{host}^{vib} is related to the vibrational spectrum of the host material, ΔS^{el} is due to the difference in the electronic heat capacity between the materials and its hydrided state, and ΔS^{conf} corresponds to configurational entropy of the vacancies in the hydride

Under reference state (25 °C, $P°$)

$$\Delta G° = \Delta H° - T\Delta S° \tag{18}$$

also

$$\Delta G° = -RT \ln K_{eq} \tag{19}$$

and for a reaction

$$\Delta G = \Delta G° + RT \ln Q_r \tag{20}$$

where K_{eq} is the equilibrium constant and Q_r the reaction quotient.

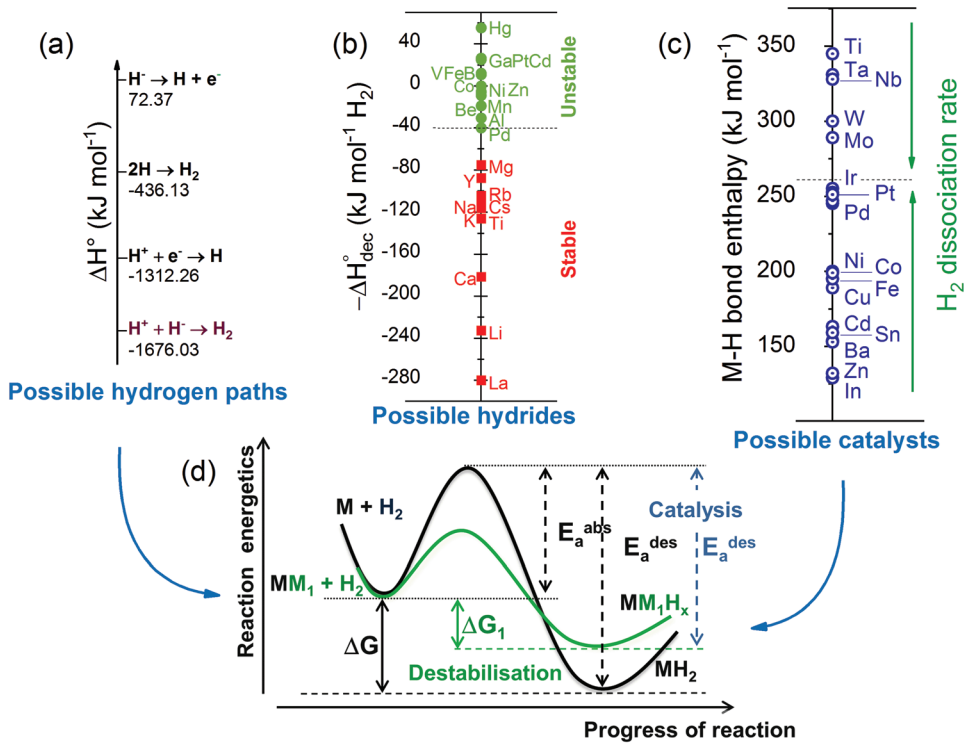

Figure 13. Basic tool box for designing hydrogen storage materials. a) Ease of reaction path via H^-, H, or H^+ for the generation of hydrogen,[22] b) enthalpy of formation of various metal hydrides; c) metal hydrogen bond strength of potential catalysts; and d) general principles for adjusting the properties of hydrides. Both thermodynamic and kinetics should be improved at the same time. The hydride path is potentially better to release hydrogen,[22] although it may lead to irreversibility. Combining unstable and stable hydrides can lead to intermediate enthalpies of reaction with hydrogen.

For a hydriding reaction, assuming that the rest of the reactants are solids (which is the case for most metal hydrides and complex hydrides), the pressure of hydrogen is the only factor that needs to be taken into account and thus K_{eq} and Q_r take the form

$$K_{eq} = \frac{P^\circ}{P^{eq}} \tag{21}$$

$$Q_r = \frac{P^\circ}{P_{op}} \tag{22}$$

where P_{op} is the operating pressure.

Therefore, the Van't Hoff plot for the reaction can be derived from (17)–(19) as

$$\ln\frac{P^{eq}}{P^\circ} = \frac{\Delta H^\circ}{RT} - \frac{\Delta S^\circ}{R} \tag{23}$$

and by associating (19)–(22), the Gibbs free energy of the hydriding reaction is

$$\Delta G = RT\ln\frac{P^{eq}}{P_{op}} \tag{24}$$

where P^{eq} is the equilibrium pressure. Therefore, when $P_{op} > P^{eq}$, $\Delta G < 0$, the hydriding reaction is thermodynamically favored; and the reverse applies for the dehydriding reaction.

The relation between the equilibrium pressure and operating temperature is represented by the pressure composition temperature (PCT) curves as shown in **Figure 14**a. A hysteresis is often observed experimentally between the equilibrium pressure of absorption P^{eq}_{abs} and desorption P^{eq}_{des} in metallic systems (Figure 14a) and this can be expressed as an energy difference following

$$\Delta G_{hyst} = RT\ln\left(P^{eq}_{abs}/P^{eq}_{des}\right) \tag{25}$$

The hysteresis observed in metallic systems is often explained by the occurrence of irreversible plastic deformations upon hydrogen absorption and was initially observed in the Pd–H system.[110] In some compounds, such as the AB_5, the hysteresis may decrease after a few cycles, owing to a reduction of P^{eq}_{abs} and this has been attributed to the introduction of defects as a result of the significant lattice expansion experienced by the alloy upon hydrogen insertion.[111] In complex hydrides similar hysteresis have also been observed, e.g., in $LiBH_4 + MgH_2$,[112] and $NaBH_4 + MgH_2$ systems.[113] It should be noted that sloppy equilibrium plateaux are often assigned to inhomogeneity in the alloy composition.[114] However, this can also be observed in pure metals and thus the hypothesis is that the slope is the result of constraints generated during the insertion/deinsertion of the hydrogen atoms in the metal.[115] In nanosized metal hydrides, similar sloppy plateau pressures have been interpreted along a broader particle size distribution, a structural heterogeneity of the nanoparticle, or interfacial

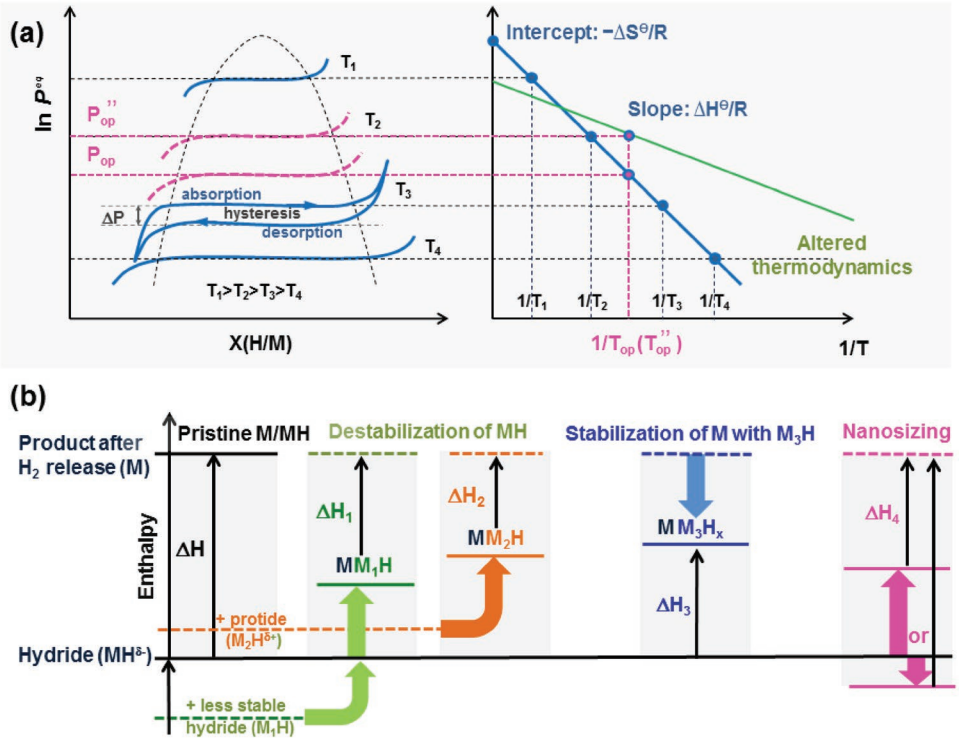

Figure 14. Current approaches for adjusting the thermodynamics of hydrides. a) Pressure composition temperature (PCT) plot (left) and the corresponding van't Hoff plot (right) for hydrogen storage reactions in metals and complex hydrides; b) generalized enthalpy diagram illustrating the destabilization of hydrides through: a) alloy formation with less stable hydrides, e.g., Fe, Ni (green); reaction of a hydride, e.g., LiH, MgH_2, $NaBH_4$, $NaAlH_4$, with a corresponding protide, e.g., $LiNH_2$, NH_3 (orange); stabilization of the decomposition products (blue); and nanosizing (pink). To enable room temperature hydrogen storage, ΔH should be brought down while ΔS remains constant.

stress at the stabilizer/nanoparticle interface.[116] Such a sloppy plateau complicates the utilization of hydrides in real systems because of the inherent variation of the hydrogen released pressure In addition, the strong stress (≈several GPa) undergone by the alloys absorbing hydrogen results in a decrepitation and thus a pulverization of the alloy particles.[117]

From the equilibrium plateau pressure measured at different temperatures, a corresponding van't Hoff plot can be generated based on the PCT (Figure 14a). At a given operating pressure (P_{op}), there is a corresponding temperature (T_{op}) for hydriding and dehydriding reactions. The operating conditions (P''_{op} and T''_{op}) can be tuned by altering the thermodynamics, i.e., the enthalpy and entropy of the reactions, which are related by the Gibbs free energy (24). In equilibrium, ΔG equals to zero, and the decomposition temperature (T_{dec}) at 0.1 MPa can be expressed as

$$T_{dec} = \frac{\Delta H^{\circ}_{dec}}{\Delta S^{\circ}_{dec}} \tag{26}$$

Some of the desorbing temperatures of common hydrides are tabulated in several references[26,118] and the most interesting ones, of high hydrogen capacity, require high temperatures for releasing hydrogen (Table 2). Ideally, high capacity hydrides should be capable of absorbing and releasing hydrogen at near ambient temperature. Assuming a constant ΔS (130.7 J mol^{-1} K^{-1} of H_2, for most metal hydrides),[26] the enthalpy of decomposition and thus the strength of the metal–hydrogen (M−H) bond is the main indicator of the thermal stability of the hydrides. If the enthalpy is high, a low equilibrium pressure and high decomposition temperature are expected (Figure 13). To achieve an equilibrium pressure of 0.1 MPa and room temperature, the enthalpy of decomposition should be close to 19.6 kJ mol^{-1}. One approach to achieve this is through the combination of elements with opposite bonding strength to hydrogen (Figures 13b and 14b). For example, the combination of $3/2MgH_2 + 1/2MgCu_2$[119] and MgH_2/Al[120] has been shown to lead to some improvement in the thermodynamics, e.g., a decreasing in the enthalpy of reaction from 75 kJ mol^{-1} H_2 for pristine Mg/MgH_2 to 70 kJ mol^{-1} H_2 once Mg is milled with Al.[121] However, this occurs with a concomitant decrease in hydrogen storage capacity.

One framework to understand the strength of the M−H bonds is by considering the standard enthalpy of formation (ΔH°_f), which is related to the enthalpy of atomization of the M (ΔH°_{atom}), enthalpy of ionization of M (ΔH°_{ioniz}), the crystal or lattice energy (ΔH°_{cryst}), and thus according to the Born–Haber cycle[22]

$$\Delta H^{\circ}_f = \Delta H^{\circ}_{atom} + \Delta H^{\circ}_{ioniz} + n(1.51\,\text{eV}) - \Delta H^{\circ}_{cryst} \tag{27}$$

where n corresponds to the stoichiometry of the hydride (MH_n).

From this equation it can be deduced that only stable hydrides are formed for (ΔH°_{cryst}) significantly larger than $\Delta H^{\circ}_{atom} + \Delta H^{\circ}_{ioniz}$, which is the case for ionic hydrides of relatively low melting point.

Since ΔH°_{atom} and ΔH°_{ioniz} are correlated to the standard redox potential (E°) of hydrides and a correlation exists between the decomposition temperature (T_{dec}) of hydrides and the standard redox potential of binary hydrides, Grochala and Edwards proposed the use of such a correlation to predict T_{dec} of ternary hydrides.[22] Accordingly, in a similar manner ΔH can be used to design hydride materials of targeted T_{dec} (Figure 7), through an appropriate choice and combination of elements forming hydrides with intermediate E°. However, the experimental hydrogen behavior of the ternary hydrides predicted by this assumption is often difficult to control owing to the multiple decomposition paths of hydrides and their reaction intermediates.[122] As compared to binary metal hydrides, controlling the thermodynamics of complex hydrides is much more difficult due to their dehydrogenation along multistep paths with additional side reactions generating byproducts.[123] The most common complex hydrides of interest for high capacity hydrogen storage are alanates ($[AlH_4]^{-1}$), borohydrides ($[BH_4]^{-1}$) and amides ($[NH_2]^{-1}$). The full decomposition of alanates is a two or three-step process depending on the metallic cation involved. For example (Figure 10a), the decomposition of $LiAlH_4$ and $NaAlH_4$ involve the intermediate phase $[AlH_6]^{3-}$, while $Mg(AlH_4)_2$ decomposes directly to MgH_2 and Al.[124] Similarly, the decomposition of borohydrides can be assumed to be a two-step reaction, including the formation of the corresponding metal hydride and boron in the first instance and then further decomposition of metal hydride (Figure 10b).

As for amides, the decomposition process is even more intricate.[125] The direct decomposition of amides alone does not lead to the release of hydrogen, but ammonia or nitrogen instead.[16a,125,126] Hydrogen released from amides requires the aid of metal hydrides[118a]

$$LiNH_2 + 2LiH \leftrightarrow Li_2NH + LiH + H_2 \quad (28)$$

$$Li_2NH + LiH \leftrightarrow Li_3N + H_2 \quad (29)$$

Mixture of amide and metal hydride of different metals may also result in different reaction paths, and thus complexity further escalates. Hence to date, it is very difficult to translate an successful approach from one hydride to the others.

It is often assumed that the hydrogen sorption behavior of complex hydrides mainly depends upon the ΔH of the reaction although significant changes in ΔS may also occur, in addition to the related changes in ΔS associated with the transition of hydrogen from the gas phase to the hydride phases. In fact, the entropy of complex hydrides strongly varies during hydrogen desorption/cycling and is a function of the decomposition path as highlighted below[127]

$$LiBH_4 \rightarrow Li + B + 2H_2 \quad \Delta S = 219\ J mol^{-1} K^{-1} H_2 \quad (30)$$

$$LiBH_4 \rightarrow LiH + B + 3/2H_2 \quad \Delta S = 150\ J\ mol^{-1} K^{-1} H_2 \quad (31)$$

It has thus become crucial to develop tools not only to control ΔH but also the ΔS of the hydrogen reaction with sorption materials (see Section 8.1.3).

3.3. General Principles to Design Hydrogen Storage Materials

By taking into account the above considerations, Figure 13 summarizes the basic "tool box" to design hydrogen storage materials. First of all, a form of hydrogen, i.e., as atomic (H), hydride (H^-), protide (H^+), or a combination (Figures 13a and 14) believed to lead to a low reversible energy path is chosen. This choice is further dictated by the requirement of high gravimetric and volumetric hydrogen density of the hydride material, and this not only further limits the list of potential candidates but also brings an additional level of complexity in achieving low hydrogen release and uptake temperatures. Indeed, as discussed above, the elements capable of binding large amounts of hydrogen often form stable hydrides and thus release their hydrogen at high temperatures (Figures 4 and 7). To overcome such a drawback, the common strategy is then to adjust the enthalpy of the reaction by combining the chosen hydride with elements forming unstable hydrides (Figure 13b). If the rate of hydrogen release and uptake is not adequate, the search for a catalyst begins by assessing the potential of various transition metals that may help the dissociative absorption and/or recombination of hydrogen during desorption. Figure 13c summarizes some potential catalysts. The hydrogen dissociation rate of the catalyst should be high enough and its binding strength to hydrogen relatively low to facilitate hydrogen release/uptake from the hydride material. Hence, the difficulty in adjusting the properties of hydrogen storage materials is in the requirement of combining strategies for improving both thermodynamics and kinetics simultaneously (Figure 13d), without "losing" the hydrogen storage capacity. Surprisingly, these basic principles/concepts, developed in the very early stages of the field of hydrogen storage research, for the design of hydrogen storage materials still continue to form the basis of the more advanced and recent approaches further discussed below.

4. Metallurgical Synthetic Approaches to form Metal Alloys and Alternative Phases to Store Hydrogen

With the discovery of hydrogen sorption in Pd[128] and the early alloys to effectively store hydrogen at the ambient, initial research efforts have focused on metallurgical approaches to design better hydrogen storage alloys. Hence, a vast majority of the early research efforts has been devoted toward a fundamental understanding of the behavior of hydrogen in metals. To date, this knowledge is more than relevant as alloys such as those based on $LaNi_5$, TiFe and Ti BCC have potential to open new applications in the storage of renewable energy. This section is thus reviewing current understanding along the modification of the hydrogen storage properties of metal alloys as well as conventional methods to prepare such alloys.

4.1. Modifying the Thermodynamics of Metal Hydrides

Many metals are known to form hydrides (Figure 4), hence by an alloying approach several metal alloy families have been found to effectively store hydrogen with altered properties as compared to

pure metals. These alloys include intermetallics, e.g., AB, AB_2, AB_5, A_2B, and solid solutions.[26] Solid solutions are formed by dissolving one or more minor elements (solutes) into a hydrogen absorbing primary element (solvent). Examples of solid solutions include Ti and V-based solid solution hydrides such as Ti–V–Fe ($Ti_{43.5}V_{49.0}Fe_{7.5}$),[118b] V–Ti–Cr,[129] and V–Ti–Ni,[130] and unlike stoichiometric or near-stoichiometric intermetallic compounds, solid solutions can also have nonstoichiometric arrangements.

Intermetallic compounds correspond to an intermediate phase between A and B. Alloying two elements increases the degrees of freedom in the final materials and leads to various structural defects including vacancies and antiphase boundaries that may benefit the overall hydrogen storage properties. In these families, A is a transition metal or a rare earth with a strong affinity for hydrogen and thus of high thermal stability, e.g., YH_2, LaH_2, TiH_2, and ZrH_2. B corresponds to transition metals forming unstable hydrides, e.g., Cr, Mn, Fe, Co, and Ni absorbing hydrogen at very high hydrogen pressures only (Figures 4 and 13). Intermetallics synthesized through the association of A and B usually form alloys with intermediate hydrogen sorption properties. This is typically the case for a range of intermetallics including TiFe, ZrV_2, and alloys of the type $CaCu_5$. For example, $LaNi_5$ has an enthalpy of −32 kJ mol^{-1} H_2,[131] while La forms a stable hydride (LaH_2) with $\Delta H = -208$ kJ mol^{-1} H_2 and Ni forms an unstable hydride with $\Delta H = -6$ kJ mol^{-1} H_2.[11]

Table 2 lists elemental hydrides with their respective heat of formation, entropy values and decomposition temperature values. Using this list, one can calculate the enthalpy of formation (ΔH_f) of ternary hydrides ($A_nB_mH_{x+y}$) by using the semiempirical model proposed by Miedema et al.[132a]

$$\Delta H_f\left(A_xB_yH_{m+n}\right) = \Delta H\left(A_xH_n\right) + \Delta H\left(B_yH_m\right) - \Delta H\left(A_xB_y\right) \quad (32)$$

where $\Delta H(A_xH_n)$ and $\Delta H(B_yH_m)$ are the heats of formation of hydride A and B and $\Delta H(A_xB_y)$ is the heat of formation of A_xB_y alloy. This model known as Miedema's rule of reverse stability was found to work well for ternary hydrides where A (with a strong affinity for hydrogen) is the minor phase as compared to B (with a low hydrogen affinity).

A more accurate model to determine the enthalpy of formation (ΔH_f) of ternary hydrides is the semiempirical band-structure model of Griessen and Driessen[133]

$$\Delta H_f\left(A_{\gamma A}B_{\gamma B}H_n\right) = \alpha\left(\frac{\gamma_A\Delta E_A^* + \gamma_B\Delta E_B^*}{\gamma_A + \gamma_B}\right) + \beta \quad (33)$$

where γi is related to the stoichiometric amount of the metal i in the ternary alloy ($A_{\gamma A}B_{\gamma B}H_n$), ΔE_i^* corresponds to the band structure energy parameter of the scaled density of state of the metal i after alloying, and α = 29.62 kJ eV^{-1} mol^{-1} H, $\beta = -135.0$ kJ mol^{-1} H.

When both metals have the same d-band width but different density of states at the Fermi energy, (33) can be simplified as

$$\Delta H^\circ\left(A_{1-\gamma}B_\gamma H_n\right) = (1-\gamma)\,\Delta\tilde{H}^\circ(AH_n) + \gamma\Delta\tilde{H}^\circ(BH_n) - \alpha n\gamma(1-\gamma)(\varnothing_A - \varnothing_B)(n_A - n_B)\frac{1}{(1-\gamma)n_A + \gamma n_B} \quad (34)$$

where $\Delta\tilde{H}^\circ(iH_n)$ is the integral enthalpy of formation for one mole of binary metal hydride i, i.e., $\Delta H^\circ(MH_n) = \Delta\tilde{H}^\circ(iH_n)/n$, $\varnothing_i$ is the work function and n_i the value of density of states at the Fermi energy of the metal i.

It should however be noted that as compared to the Miedema's model, which was designed to describe a wide class of alloys, the band-structure model is limited to metal hydrides where all hydrogen atoms are surrounded by a fraction of A and B atoms. Therefore this model does not apply to disordered alloys or intermetallic compounds such as AB_2 Laves phases which can contain several types of interstitial sites including A_2B_2, AB_3, and B_4 sites. More recent approaches building on data mining and machine learning techniques (see Section 9.2.3), e.g., artificial neural network and principal component analysis, have also emerged with the aim of providing more accurate methods for the prediction of the enthalpy of AB intermetallics.[134]

4.2. Tuning the Hydrogen Thermodynamics of Alloys by Partial Elemental Substitution

Partial substitution provides a means to adjust the thermodynamic properties of hydrides, and the approach has been widely used to design hydrides with capability for hydrogen storage at the ambient and with capacity beyond the hydrogen storage capacity of $LaNi_5$ and FeTi, i.e., >1.2–1.9 mass% H_2.[135] For example, Reilly and Wiswall[136] reported in 1968 that alloying nickel with magnesium decreased the enthalpy of reaction with hydrogen to −64.5 kJ mol^{-1} H_2 instead of the −75 kJ mol^{-1} H_2 of the Mg/MgH_2 system. This meant a temperature of absorption of ≈ 240 instead of 400 °C.[46a] However, this was at the expense of the hydrogen storage capacity, i.e., it was reduced from 7.6 to 3.6 mass% H_2. By further tuning of the thermodynamics via the addition of Ca, the $(Mg_{1-x}Ca_x)_2Ni$ alloy displayed an enthalpy of −37 kJ mol^{-1} H_2 and thus hydrogen desorption at room temperature but with a storage capacity of 1.2 mass% H_2.[137] This demonstrates the potential of the approach but also highlights the difficulty of modifying the properties of hydrogen materials by a simple partial substitution.

For some hydrides, a correlation between elemental substitution and P^{eq} has been evidenced and this may help to some extent with the adjustment of the thermodynamic properties. Taking $LaNi_5$ as an example, a partial substitution of the Ni leads to a decrease of P^{eq} and a reduction of the storage capacity. When Ni is partially substituted with Al, this leads to a 50% loss of hydrogen storage capacity owing to the larger size of the Al atoms (**Figure 15**b). Partial substitution with Co (>0.25%) can lead to two P^{eq} as the result of the formation of an intermediate γ phase.[138] The evolution of P^{eq} has also been shown to be linearly correlated to the composition of the alloy and thus the evolution of cell volume upon partial substitution of La or Ni (Figure 15d).[42a] From this variation, one can thus tune P^{eq} to the desired value.

Contrary to MgH_2 and $LaNi_5$, a small amount of substitution of Mn in $TiMn_{1.5}$ was found to cause no loss of capacity with a notable shift in the plateau pressure.[139] For $TiMn_{1.5}$, P^{eq} was shifted up by substituting Mn with Cu, Fe, and Co; while V and Ni led to a reduction of P^{eq}. The potential of partial substitution

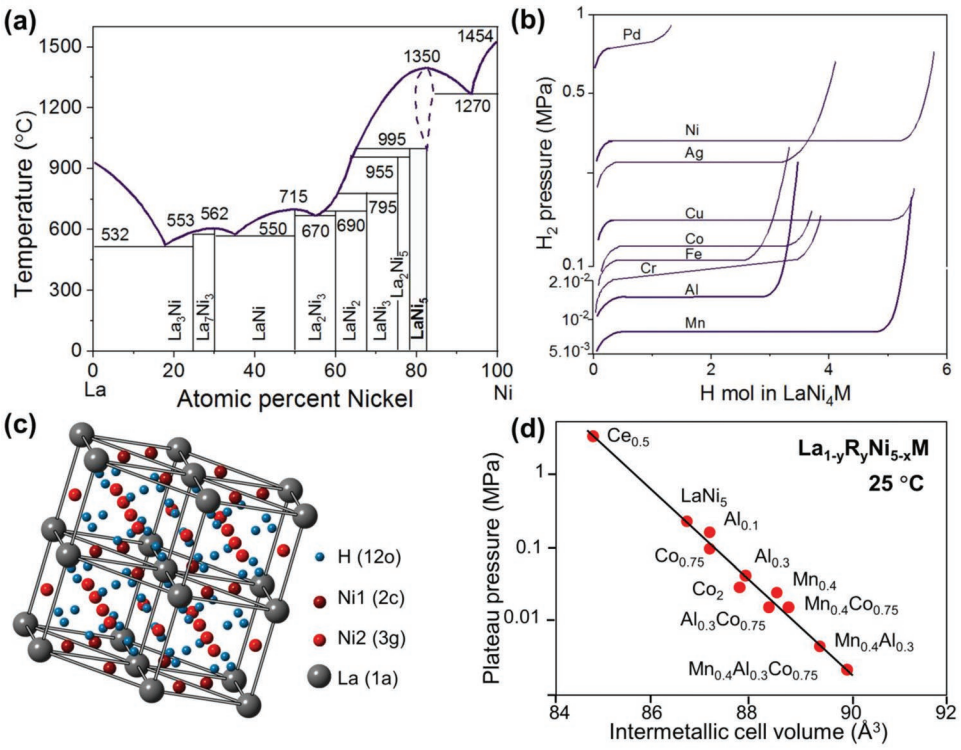

Figure 15. Tuning the thermodynamic of intermetallics with $LaNi_5$ as an example. a) Phase diagram of the La-Ni system; b) evolution of the equilibrium plateau pressure of $LaNi_5$ upon partial alloying with various elements; c) crystalline structure of $LaNi_5$ structure showing the position of the hydrogen atoms (the *c*-axis has been doubled in length for clarity); and d) linear dependence of the equilibrium plateau pressure of $LaNi_5$ as function of the evolution of the cell volume upon a partial substitution of La by R or Ni by M in $LaNi_5$. Reproduced with permission.[42a] Copyright 2001, Springer-Verlag.

may thus be an effective means to adjust the plateau pressure of hydrides. However, this may also pose problems during large scale manufacturing, as a small amount of impurities (0.1 by stoichiometric composition) can cause shifts in plateau pressure outside the desired range.

4.3. Methods for Making Hydrogen Storage Alloys and Intermetallics

The first step to make an alloy of a given composition is to check the phase diagram of the elements to be alloyed in order to determine possible miscibility issues, phase formations, and ultimately determine the synthetic conditions, i.e., temperature, pressure, and heat treatment. For binary alloys the phase diagrams are relatively well known.[140] However, the phase diagram of ternary or higher intermetallic compounds are scarce.[141] Therefore in this case, a trial and error approach is the only option to achieve the targeted composition and phase. The phase diagram of La–Ni is shown on Figure 15a, as an example. The La atom can be substituted by many elements, e.g., 4f elements such as Ce, Nd, and Pr owing to the existence of many AB_5 compounds.[142] The possibilities to substitute Ni are more complicated. Ni can be fully substituted by Cu, Co, or Pt, but it is also possible to substitute Ni in $LaNi_5$ with low levels of Al,[143] Mn,[144] or Fe,[145] for example.

The level of substitution varies strongly depending on preparation method and the duration and temperature of the heat treatment process. For example, in $LaNi_{5-x}Mn_x$, x can be 0.99 if the alloy is annealed at 1175 °C and 2 for annealing at 800 °C.[144,146] The solidification of the alloy phase can occur congruently; however, this is not always the case (e.g., FeTi exhibits a peritectic solidification). It should be noted that depending on the level of deviation from the stoichiometric composition, the amount of impurities (e.g., C, N, O), and the volatility of the melted elements, additional vacancies and structural defects may be created within the alloy lattice. With $LaNi_5$ this was not observed. However, in FeTi, an excess of one of the atoms (Fe or Ti) was found to lead to a substitution on the deficient sublattice.[147]

The common procedure to prepare alloys is through melting methods including radiofrequency induction and arc melting. Once a homogenous melt is formed, the cooling rate of the melt should be carefully controlled to avoid any phase segregation. For a small sample size this can be achieved by quenching the melt (e.g., at a cooling rate >10 °C s^{-1}) to limit any shift in elemental concentration across the alloy. When the solidification of the melt is peritectic, additional annealing in high vacuum or an inert atmosphere (to avoid oxidation) is often required to facilitate the homogenization of the alloy and remove any microsegregation and structural defects. Homogenization is beneficial for the hydrogen sorption properties because it often leads to a "flat" equilibrium plateau pressure without significant hysteresis.[26]

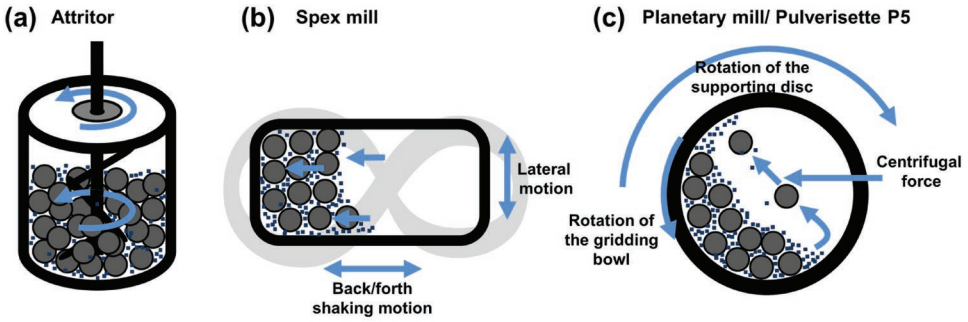

	(a) Attritor	(b) Spex mill	(c) Planetary mill/ Pulverisette P5
Velocity of the ball (m/s)	0-0.8	< 3.9	2.5-4.0
Kinetic energy (10^{-3} J/hit)	< 10	< 120	10-400
Shock frequency (Hz)	> 1000	200	~ 100
Power (W/g/ball)	< 0.001	< 0.24	0.01-0.8

Figure 16. Illustration of mechanical milling tools. Summary of milling conditions for a) attritor mill; b) spex mill; and c) planetary mill.

5. Mechanical Milling for Making New Hydrogen Storage Materials

Following the development of mechanical alloying by high energy ball milling technique around 1966 at the Paul D. Mercia Research laboratory to produce nickel-based superalloys for gas turbines,[148] mechanical milling/alloying emerged in the late 1980s as an approach for the synthesis of hydride materials. In particular, Ivanov et al. were among the first to report the synthesis of Mg-based alloys with Ni, Fe, Co, or Ce for hydrogen storage.[149] The nanostructuration by ball milling of Mg_2Ni[150] and then MgH_2[151] both leading to significantly enhanced hydrogen kinetics further established mechanical milling as a significant tool for the modification of the properties of hydride materials.[152] Mechanical milling involves a very simple experimental setup and operating conditions, and the possibility of producing large quantities of solvent free material further contributed to the widespread uptake of this technique across research laboratories.[153] Various terminologies are commonly used to describe the different type of processes that can be achieved through mechanical milling: i) mechanical alloying describes the processing of mixtures of metallic powders to form alloys,[154] ii) mechanical milling refers to the refinement of powder, iii) mechanochemical synthesis is related to the acceleration of solid state synthetic reactions upon milling between chemical powders, iv) cryomilling refers to milling carried out at liquid nitrogen temperature—usually to facilitate powder refinement and further reduction in particle size, v) reactive milling involves the milling of powders in the presence of chemically reactive solids, liquids, or gases (e.g., hydrogen, oxygen, nitrogen, air, etc.)—for example, the milling of Mg under hydrogen atmosphere to produce MgH_2.[155]

During the milling process, the material is subjected to different stresses including compression, deformation, attrition, shear, and impact resulting from the milling tools (**Figures 16** and **17**).[153,156] This generates new surfaces and cracks but also defects and dislocations resulting in a reduction of crystallite sizes, a higher number of grain boundaries, and a high surface area. All these are supposed to facilitate the kinetics of hydrogen release/uptake and diffusion in hydrides.[118b,157] Depending on the ductility of the powder, agglomeration of particles may also occur upon ball impact by cold-welding, mechanical interlocking resulting from rough surfaces or chemical reactions between particles.

5.1. Fundamentals of the Mechanical Milling Process

The process of mechanical milling is simple and conducted by placing the powder(s) to be refined, alloyed, or reacted in a milling vial with balls that are free to impact the powder.[157a,158] The vial and/or balls are shaken by various means (Figure 16) and the powder is milled upon repeated and intermittent impact of the balls until a steady state between cold-welding and fracturing is achieved. Instead of balls, cubes, rods, ballpebs, and cylpebs have been tried, but the spherical shape of the milling balls offers a higher gridding surface area and favors lower wear.[159] Several theoretical models have been proposed in an attempt to describe the milling process;[160] however, in a first approximation, the intensity involved in the milling process can be simplified as the product of the kinetic energy (ΔE) released in a single impact of a ball and the total number of impacts per unit of time (N_i)

$$I = \varepsilon \Delta E N_i \tag{35}$$

where ε is a factor comprised between 0 (elastic collision—no energy transferred) and 1 (perfect inelastic collision), and $\Delta E = 1/2 m_b v_b^2$, with m_b and v_b corresponding to the mass of the ball and its velocity. Accordingly, the overall specific energy (W_s) involved in milling the material is given by[161]

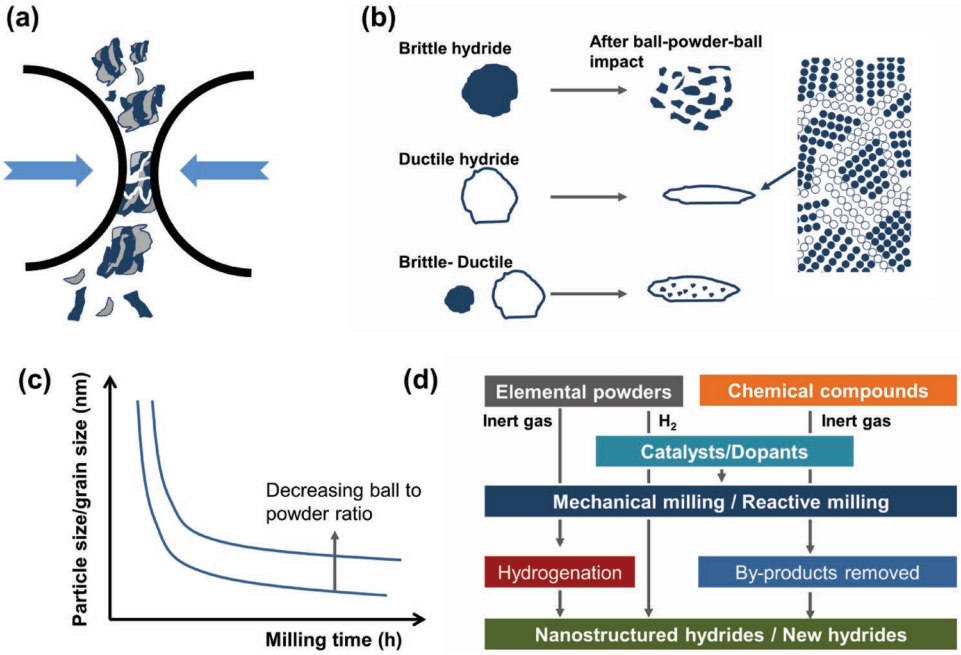

Figure 17. Principles of the mechanical milling process. a) Particle fracturing upon ball-powder-ball collision; b) deformation characteristics of ductile and brittle hydride materials upon mechanical milling; c) evolution of particle/grain size for brittle materials; and d) flow chart showing the different paths for using mechanical milling for preparing hydrides.

$$W_s = \frac{1}{M} It \tag{36}$$

where M is the mass of material milled and $t = (t_b/t_{imp})\tau$. t_b corresponds to the ball impulse duration, t_{imp} the impulse period and τ the grinding duration.

It can thus be concluded from the equation above that W_s depends only on intrinsic parameters of the milling process including the mass of the grinding balls, the rotation frequency of the vials, the ball-to-powder ratio, and the milling time.

The initial particle size of the starting material does not matter because upon milling the particle size is rapidly reduced to a few µm within the first few minutes of milling as it follows an exponential decay (Figure 17c).[162] However, the ductility or brittleness of the powder to be milled will significantly affect the end results. Upon milling, ductile particles will tend to be flattened and cold welded and thus no particle size reduction occurs but some alloying at the atomic level may happen (Figure 17b). In contrast, brittle particles are extensively fragmented; however, at very small particle sizes cold-welding occurs because the particles then behave in a ductile manner. A mixture of ductile–brittle leads to the embedment of the brittle particles within the ductile matrix.

The main types of high energy mills found in many laboratories are summarized in Figure 16 as well as the velocity of the balls, kinetic energy per impact, shock frequency and power involved. Spex mills are much more energetic than attritor mills. Hence, for the same end result much shorter milling times are required with a high energy shaker mill. However, a higher energy of milling also involves an increase in the milling vial temperature owing to the impact of the balls. It has been estimated that only 5–15% of the energy is effectively used toward milling, while the remaining energy is dissipated as heat.[163] Higher temperatures may facilitate atomic/ionic diffusion and thus lead to a better homogenization of the final product; but these may also trigger the premature decomposition of the milled powder and thus be detrimental.

The overall increase in macroscopic temperatures of the mill has been found to be moderate, e.g., ≈50 °C for a Spex mill,[164] but at the microscopic level upon ball-to-ball or ball-to-wall collision temperatures have been predicted to be as high as 350 °C.[164b,165] However, by observing the phase transformation occurring on some materials during milling, it was estimated that the temperature locally raised to at least 1000 °C during the processing of γ-AlO(OH) on a planetary mill, for example.[166] To minimize this, mechanical milling can be carried out with the aid of a cooling medium including air, water, or liquid nitrogen.[167] However, in practice, long milling runs are often divided into shorter milling periods paused with cooling breaks to dissipate any excessive heat. This is particularly important when milling complex hydrides with low decomposition temperatures (**Tables** 2 and **3**).[122,168]

Various grinding materials can also be used and the most common milling tools are made of hardened steel, chromium steel, tungsten carbide, agate, silicon nitride, and sintered corundum. However, the density of the milling balls should be high enough to create sufficient impact on the powder to be milled. Furthermore, when possible the milling tools should be made of the same material as the powder to avoid cross contamination otherwise the milling tools should be harder than the powder to mill to avoid excessive cross-contamination. Indeed, a drawback of mechanical milling is the contamination emerging from the milling tools. In particular, using stainless steel in a high energy shaker mill can introduce a large amount

Table 3. Summary of selected hydrides modified or synthesized by mechanical milling. Notations are as follow: Reactant melting point (R_{mp}), hydrogen pressure (P_H) used during milling, total milling time (M_t), milling speed (M_s), ball to-powder weight ratio (B:P), ball diameter (B_d), and process control agent (PCA).

Compounds		Device	Reactants	R_{mp} [°C]	P_H [MPa]	M_t [h]	M_s [rpm]	B:P	B_d [mm]	PCA	Side product	Ref.
Binary hydride	MgH_2	planetary	Mg	650	0.066	3	–	–	3	–	–	[466]
	MgH_2	Planetary	Mg	650	2.4	47.5	–	–	12	–	–	[467]
	MgH_2	Fritsch P6	Mg	650	1–9	18	500	10:1	10	–	–	[468]
	MgH_2	Fritsch P4	Mg	650	8	4	400, 800	60:1	12	–	–	[155]
	MgH_2	Spex 8000	Mg	650	1	3	–	2:1	–	–	–	[469]
	MgH_2	Fritsch P4	Mg	650	7	4	400, 800	60:1	12	–	–	[470]
	MgH_2	Planetary	Mg	650	Ar	35	250	20:1	10	Steric acid, toluene	–	[471]
	MgH_2	Uni ball mill II	Mg	650	0.5	50	196	44:1	–	Graphite	MgO	[472]
	MgH_2	Spex 8000	MgH_2	327	Ar	10	–	8:1	–	$MgCl_2$	MgO	[473]
	MgH_2	Fritsch P5	MgH_2	327	Ar	100	–	10:1	10	MgO	–	[174a]
	MgH_2	Spex 8000	MgH_2	327	Ar(0.6)	10	–	10:1	–	Nb_2O_5	$Mg_xNb_yO_z$, MgO	[474]
	$TiH_{1.9}$	Planetary	Ti	1668	2.4	5.5	–	–	12	–	–	[467]
	$TiH_{1.8}$	Spex 8000	Ti	1668	0.2	3	–	–	–	–	–	[475]
	TiH_2	Fritsch P4	Ti	1668	8	0.16	400, 800	60:1	12	–	–	[155]
	TiH_2	Fritsch P4	Ti	1668	30	20	400	50:1	15	–	–	[476]
	TiH_2	Fritsch P4	Ti	1668	7	4	400, 800	37.5:1	12	–	–	[470]
	TiH_2	Fritsch P5	Ti	1668	–	10	300	10:1	10	Toluene	TiH_x	[477]
	VH_x	Fritsch P5	V	1910	1	0.17	400	30:1	7	–	–	[478]
Ternary hydride	$ZrNiH_3$	Fritsch P5	ZrNi	–	2	3	–	30:1	10	–	–	[220]
	ZrNiH	Fritsch P7	ZrNi	–	0.1	0.08	400	30:1	7	–	–	[479]
	$TiNiH_3$	Rod-mill	Ti+Ni	1668, 1445	0.1	200	–	30:1	10	–	–	[480]
	$TiVH_{2.8}$	Fritsch P5	TiV or Ti+V	1668, 1910	0.4	100	–	20:1	10	–	–	[481]
	$LaNi_5H_{0.15}$	Fritsch P7	$LaNi_5$	480	1	0.08	400	30:1	7	–	–	[482]
	Mg_2FeH_6	Fritsch P5	2Mg+Fe	650, 1538	1	20	325	4:1	10	–	MgH_2,Fe	[483]
	Mg_2FeH_6	Spex 8000	$2MgH_2$+Fe	327, 1538	0.1	60	–	10:1	10	–	Mg,MgO,Fe	[484]
	Mg_2CoH_5	BX254E	$2MgH_2$+Co	327, 1495	0.1	10	–	8:1	4	–	–	[485]
	Mg_2CoH_5	Fritsch P6	$2MgH_2$+Co	327, 1495	0.5	5	400	80:1	–	–	–	[486]
	Mg_2NiH_4	–	$2MgH_2$+Ni	327, 1445	–	60	–	–	–	Graphite	–	[487]
	Mg_2NiH_4	Fritsch P5	$2MgH_2$+Ni	327, 1445	0.5	22	325	4:1	10	–	Mg,MgH_2,Ni	[488]
	Mg_2NiH_4	Fritsch P4	$2MgH_2$+Ni	327, 1445	7.5	12	400	60:1	12	–	MgO	[489]
	$Mg_2NiH_{1.8}$	Fritsch P7	Mg_2Ni	–	1	80	400	30:1	7		–	[490]
	$Mg_{0.8}Ti_{0.2}$	Spex 8000	Mg, Ti	327, 1668	Ar	16	–	–	–	Graphite	–	[491]
	$Mg_{0.75}Ti_{0.25}$	Spex 8000	Mg, Ti	327, 1668	Ar	12	–	–	–	Stearic acid	–	[491]
	Al_3Mg_2	Planetary	Al, Mg	660, 327	Ar	10	–	–	15	Stearic acid	Al, Mg	[492]
	γ-$Mg_{17}Al_{12}$	Retsch PM400	Mg, Al	327, 660	Ar	40	300	10:1	–	Methanol	MgH_2, MgO,$Mg_{28}Al_{45}$	[493]
	Al_3Zr	Fritsch P4	Al, Zr	660, 1855	Ar	5	300	20:1	10	Ethanol	Al, ZrH_2,Zr,ZrC	[494]
	Ti_3Al	–	Ti, Al	1668, 660	Ar	300	–	–	–	Methanol, benzene	–	[495]
	Ti_xAl_{1-x}	Planetary	Ti, Al	1668, 660	Ar	100	–	10:1	10	Hexane	TiC,TiH_2, $A1_2Ti_4C_2$	[496]
	Sr_2AlH_7	Fritsch P5	SrH_2, Al	1050, 660	Ar	10	150	20:1	10	Stearic acid	Sr_8Al_7, Sr	[497]
Quaternary hydride	$(Mg_{0.8}Ti_{0.2})_{0.95}Ni_{0.05}$	Spex 8000	Mg, Ti, Ni	327, 1668, 1445	Ar	24	–	–	–	Graphite	–	[491]
	$(Mg_{0.65}Ti_{0.35})_{0.95}Ni_{0.05}$	Spex 8000	Mg, Ti, Ni	327, 1668, 1445	Ar	28	–	–	–	Stearic acid	–	[491]
	$Mg_{1.9}Al_{0.1}Ni$	Spex 8000	Mg, Al, Ni	327, 660, 1445	Ar	40	–	10:1	12	CCl_4	–	[498]

Table 3. Continued.

Compounds		Device	Reactants	R_{mp} [°C]	P_H [MPa]	M_t [h]	M_s [rpm]	B:P	B_d [mm]	PCA	Side product	Ref.
	$Mg_{88.5}Ni_xLa_y$	Planetary	Mg, Ni, La	327, 1445, 920	Ar(0.1)	10	200	30:1	–	Graphite	Mg, MgH_2, $Mg_2NiH_{0.3}$, Mg_2NiH_4,LaH_2	[499]
	$(TiNi)_{0.7}Mg_{0.3}$	Planetary	$Ti_{50}Ni_{50}$, Mg	–, 327	Ar	40	400	4.4:1	20	Ethanol	Fe_2TiO_4	[500]
Alanate	$LiAlH_4$	Fritsch P5	LiH+Al	692, 660	1	24	400	–	9.5	–	Li_3AlH_6	[501]
	Li_3AlH_6	–	$2LiH+LiAlH_4$	692, 150	–	5	–	30:1-42:1	–	–	–	[296b]
	$LiMg(AlH_4)_3$	Retsch	$3LiAlH_4+MgCl_2$	150, 714	–	3	–	11.3:1	–	–	LiCl	[502]
	$NaAlH_4$	Fritsch P7	NaH+Al	300, 660	8.3	4	500	50:1	–	–	NaCl,Al	[503]
	$NaAlH_4$	Fritsch P5	NaH+Al	300, 660	0.6	120	350	50:1	10	–	Na_3AlH_6,NaH,Al	[504]
	$NaAlH_4$	Fritsch P5	NaH+Al	300, 660	1.2	240	230	10:1	10	–	NaCl,Al	[504]
	$NaAlH_4$	Planetary	NaH+Al	300, 660	3	60	350	30:1	8	–	Na_3AlH_6,Al	[505]
	Na_3AlH_6	Planetary	NaH+Al	300, 660	0.5	30	350	30:1	8	–	Al	[505]
	Na_3AlH_6	Fritsch P4	3NaH+Al	300, 660	10	8	400	90:1	15	–	NaCl,NaH,Al	[225c]
	Na_3AlH_6	Spex 8000	$2NaH+NaAlH_4$	300, 183	0.2	20	–	10:1	12.7,14.3	–	Al	[506]
	Na_2LiAlH_6	Spex 8000	$NaH+LiH+NaAlH_4$	300, 692, 183	0.2	20	–	10:1	12.7,14.3	–	Al	[506]
	Na_2LiAlH_6	Fritsch P4	2NaH+LiH+Al	300, 692, 660	10	4	400	90:1	15	–	NaCl	[225c]
	$NaLi_2AlH_6$	Fritsch P4	NaH+2LiH+Al	300, 692, 660	10	4	400	90:1	15	–	NaCl,$NaAlH_4$,Al	[225c]
	$KAlH_4$	Fritsch P7	KH+Al	417, 660	10	10	400	–	–	–	KH,Al	[502]
	$KAlH_4$	Fritsch P7	KH+Al	417, 660	>17.5	0.5	–	–	10,5	–	Al	[507]
	K_2LiAlH_6	SPEX8000	$2KH+LiAlH_4$	417, 150	–	0.5	–	27:1	–	–	–	[225a]
	K_2NaAlH_6	Fritsch P4	$2KH+NaAlH_4$	417, 183	1	25	150	40:1	–	–	–	[508]
	$Mg(AlH_4)_2$	Magneto	$2NaAlH_4+MgCl_2$	183, 714	0.6(Ar)	40	225	40:1	–	–	NaCl,Al	[509]
	$Mg(AlH_4)_2$	Fritsch P7	$2AlH_3+ MgH_2$	150, 327	0.1	4	400	175:1	10	–	AlH_3,MgH_2,Al	[510]
	$Mg(AlH_4)_2$	Spex 8000	$2NaAlH_4+MgCl_2$	183, 714	–	1	–	35:1	7.9	–	NaCl	[511]
	$Mg(AlH_4)_2$	Planetary	$2NaAlH_4+MgCl_2$	183, 714	–	3	500	60:1		–	NaCl	[512]
	$Ca(AlH_4)_2$	Planetary	$2NaAlH_4+CaCl_2$	183, 772	1	48	200	40:1	–	–	CaH_2,Al,NaCl	[513]
	$CaAlH_5$	Fritsch P7	CaH_2+AlH_3	816, 150	0.1	3	400	80:1	10	–	CaH_2,Al	[510]
Borohydride	KBH_4	Fritsch P7	$2MgH_2+KBO_2$	327, 947	–	2	490	–	13	–	MgO	[514]
	$NaBH_4$	–	$4MgH_2+Na_2B_4O_7$	327, 743	–	2	2750	–	13	–	MgO	[515]
	$NaBH_4$	QM-3C	$2MgH_2+NaBO_2$	327, 966	–	4	–	20:1	–	–	MgO	[393]
	$Mg(BH_4)_2$	Fritsch P7	$5MgCl_2+4NaBH_4$	714, ≈500	0.1(Ar)	2	–	–	7	–	NaCl	[516]
	$Zn(BH_4)_2$	Spex 8000	$ZnCl_2+2NaBH_4$	290, ≈500	–	0.5	–	35:1	7.9	–	NaCl	[517]
	$Mn(BH_4)_2$	Planetary	$3LiBH_4+MnCl_2$	275, 654	–	6	175	32:1	12	–	LiCl	[518]
	$Ca(BH_4)_2$	Spex 8000	CaH_2+MgB_2	816, 830	–	1.5	–	10:1	–	–	MgH_2	[262a]
	$K_2Mn(BH_4)_4$	Planetary	$2KBH_4+MnCl_2$	585, 654	–	6	175	32:1	14	–	KMnCl3	[231a]
	$LiZn_2(BH_4)_5$	–	$2LiBH_4+ZnCl_2$	275, 290	Ar	2	–	–	–	–	LiCl	[229]
	$NaZn_2(BH_4)_5$	–	$3NaBH_4+ZnCl_2$	≈500, 290	Ar	2	–	–	–	–	NaCl	[229]
	$NaZn(BH_4)_3$	–	$4NaBH_4+ZnCl_2$	≈500, 290	Ar	2	–	–	–	–	NaCl	[229]
	$Mg_xMn_{(1-x)}(BH_4)_2$	Fritsch P7	$LiBH_4$,$MgCl_2$,$MnCl_2$	275, 714, 354	–	5.83	600	25:1	15	–	LiCl,Li_2MgCl_4	[519]
	$Li_3MgZn_5(BH_4)_{15}$	Fritsch P7	$LiBH_4$,$MgCl_2$,$ZnCl_2$	275, 714, 290	Ar	5.83	600	25:1	15,12,10	–	Li_2MgCl_4	[230]
	$Li_3MnZn_5(BH_4)_{15}$	Fritsch P7	$LiBH_4$,$MnCl_2$,$ZnCl_2$	275, 654, 290	Ar	3	600	25:1	15,12,10	–	Li_2MnCl_4	[230]
Amide	$LiNH_2$	Fritsch P7	LiH	692	0.4(NH_3)	2	400	–	–	–	–	[520]
	$NaNH_2$	Fritsch P7	NaH	300	0.4(NH_3)	1	400	–	–	–	–	[520]
	$Mg(NH_2)_2$	Fritsch P7	MgH_2	327	0.4(NH_3)	13	400	–	–	–	–	[520]
	$Ca(NH_2)_2$	RM-10	CaH_2	816	0.5(NH_3)	18	–	–	7	–	CaH_2	[521]
	$Ca(NH_2)_2$	Planetary	Ca	842	–	24	–	30:1	–	–	–	[522]

Table 3. Continued.

Compounds		Device	Reactants	R_{mp} [°C]	P_H [MPa]	M_t [h]	M_s [rpm]	B:P	B_d [mm]	PCA	Side product	Ref.
Imide	Li_2NH	Fritsch P7	$LiNH_2$+LiH	390, 692	1	2	400	–	7	–	–	[221c]
	CaNH	Fritsch P7	$Ca(NH_2)_2 + 3CaH_2$	–,816	1	2	400	–	7	–	CaH_2	[521]
	Ca_2NH	–	Ca_3N_2+CaH_2	–,816	–	–	–	–	–	–	–	[283]
	MgNH	–	$Mg(NH_2)_2$+MgH_2	–,714	–	72	–	26:1	10	–	–	[523]
	$Li_2Ca(NH_2)_2$	Fritsch P7	$2LiNH_2$+CaH_2	390, 816	–	1	400	–	–	–	–	[524]
	$Li_2Mg(NH_2)_2$	Planetary	$LiNH_2$+$2MgH_2$	390, 714	Ar	36	–	–	–	–	–	[525]
Metal amidoborane	$LiNH_2BH_3$	Fritsch P7	LiH+NH_3BH_3	692, 104	–	2	200	40:1	10	–	–	[526]
	$NaNH_2BH_3$	Planetary	NaH+NH_3BH_3	300, 104	–	–	200	–	–	–	–	[236]
	$Ca(NH_2BH_3)_2$	Fritsch P7	CaH_2+$2NH_3BH_3$	816, 104	0.1 (He)	1	200	–	–	–	–	[527]
	$LiNa(NH_2BH_3)_2$	–	LiH+NaH+$2NH_3BH_3$	692, 300, 104	–	–	–	–	–	–	–	[237]
	$Na_2Mg(NH_2BH_3)_2$	–	NaH,MgH_2,NH_3BH_3	300, 714, 104	–	–	–	–	–	–	–	[234a]
	$KAl(NH_2BH_3)_4$	Fritsch P6	$KAlH_4$+ NH_3BH_3	–,104	12	12	–	30:1	10	–	$KAlH_4$,NH_3BH_3	[235e]

of Fe contamination (>5 wt%) into the milled material.[164a] Using less energetic milling machines or "softer milling" tools can help reduce the level of contamination from the milling tools. For example, Ares et al. reported a significant reduction of contamination by ball milling MgH_2 on a planetary mill with zirconia milling tools (Zr contamination ≈0.5 mass%) instead of stainless steel vials and balls (Fe contamination ≈ 4 mass%).[169]

Contamination is also influenced by the length of the milling process—longer milling times leading to higher levels of contamination—and the size of the balls used and remaining empty space in the vial. If the size of individual balls is too large as compared to the capacity of the milling vial, then the interaction between ball/powder is going to be low and this leads to a low milling efficiency. Similarly, the vial should contain sufficient powder so there is enough ball/powder interaction. If the vial is overfilled, then there is not enough space for the balls to move. As a rule of thumb the vial should be filled at 50% to enable an appropriate milling of the powder and minimize direct ball to ball/wall impact leading to some partial fragmentation of the milling tools and a lower milling efficiency. In this configuration, the ball to powder mass ratio is often taken as 10:1 in vials of small capacity (≈50 mL). A larger ball to powder mass ratio of 50:1 or 100:1 may be used in a large capacity attritor mill. The ball to powder mass ratio has a significant effect on the milling time. The higher this ratio the shorter the time (Figure 17c).[170]

To limit cold-welding and facilitate further powder refinement, a process control agent can also be added during milling. This process control agent can be a solid, liquid or gas and it is believed to reduce the surface energy created at freshly made surfaces, hence limiting particle agglomeration and thus cold-welding upon impact. Several process control agents in the form of hydrocarbons, surfactants, and carbon materials have been used in the range of 1–5 mass% of the total powder charge (Table 3).[171] However, these compounds may decompose during milling and bring oxygen and/or carbon to the milled powders resulting in the formation of oxides and carbides. Hence the choice of the process control agent depends upon the acceptable purity of the final material. In the case of materials for hydrogen storage, this choice is critical since this may lead to serious deterioration of material's properties. Excessive surface contamination of the hydride powder may delay the hydrogen release/uptake at the core of the particles. In this case, hydrogen cycling at high temperatures is required to overcome the oxide or carbon layers. For example, in the case of MgH_2,[172] the formation of an oxide passivation layer of ≈4 nm delays the hydrogen release by ≈50 °C. Using carbon materials may also facilitate the refinement of MgH_2 particles but in this case this will lead to the release of CO (a poison for PEM fuel cells) and C–H contaminants in the hydrogen stream.[173] We reported several years ago the use of oxides and in particular MgO as effective process control agents leading to very fast hydrogen sorption kinetics comparable to the best catalysts reported so far with pure hydrogen release only.[174] It should be noted that no universal process control agent exists and this intrinsically depends upon the chemical nature of the material to be milled. Figure 17d summarizes the main steps toward the synthesis/modification of materials for hydrogen storage. Furthermore, in the case of hydrogen storage materials, mechanical milling must be carried out under a very well controlled atmosphere (inert argon or hydrogen) to minimize the formation of oxide or nitrides.

5.2. Modification of the Properties of Hydrides via Mechanical Milling

By using mechanical milling on materials for hydrogen storage, one of the aims is to reduce the hydrogen-metal bond strength by making new alloys, nanostructures and/or creating fresh surfaces and a large amount of grain boundaries to improve the hydrogen kinetics.[157a] An underlying assumption is that mechanical alloying can also lead to the formation of metastable phases, i.e., a nonequilibrium state resulting from the "energizing and rapid quenching of the nonequilibrium phase"

upon repeated and severe plastic deformations (Figure 17b).[175] With the reports on the drastic improvements of the hydrogen kinetics of the Mg/MgH_2 systems[150,151b,176] and the demonstrated hydrogen reversibility in $NaAlH_4$ with Ti doping,[63,65a,177] mechanical milling has also been revealed to be an effective technique to finely disperse/react transition metals and other elements or alloys that are believed to act as catalysts or for the synthesis of novel hydride materials.[46c,52a,151a,178]

5.2.1. Nanostructured Hydrides

Nanocrystalline materials, characterized by a crystal size <100 nm, can be formed by techniques including vapor condensation,[179] sputtering,[180] thermal decomposition,[181] chemical precipitation,[182] and so on.[183] But the advantage of mechanical milling is in the possibility of producing bulk quantities of material. However, from a commercial perspective, mechanical milling remains an expensive production method and alternatives in the forms of high pressure torsions, equal channel angular pressing, and cold rolling have been proposed.[184]

Nanocrystalline materials are typically described by a mixture of nanodomains composed of lattice atoms with some long range order and boundary atoms with a random interatomic arrangement separating individual nanograins. In nanocrystalline materials, the number of nanocrystalline domain/grain boundaries interfaces can be as large as 6×10^{25} m^{-3} for grain sizes of 10 nm, and by assuming that the grains are spherical or cubic, the volume fraction of nanocrystalline material (C) can be determined as[185]

$$C = 3\delta/d \tag{37}$$

where δ and d correspond to the average grain thickness and diameter, respectively.

This means that the volume fraction of atoms in the grains boundary can be as high as 50% for 5 nm grains. Such an evolution in crystallinity can be determined directly by transmission electron microscopy imaging or indirectly from the broadening of the diffraction peaks width as observed by X-ray diffraction analysis. Assuming appropriate correction from instrumental and strain effects, the average grain size can also be calculated with the Scherrer equation from the diffraction pattern.[186]

The severe plastic deformation occurring during high energy milling generally leads to the formation of nanocrystalline structures. This has been observed in many materials (e.g., metals, intermetallics, and alloys), and thus can be considered as a general trend. The exact mechanism leading to nanostructuration remains unclear, but it is expected that the disintegration of the coarse grains is the result of an increase in the density of dislocations, vacancies and stacking faults within the heavily strained regions formed under severe plastic deformation.[187] As these relax along the shear bands, nanocrystalline grains randomly oriented and free form dislocations are formed. The energy transferred from the mechanical milling process to the material can then be considered to be stored in the form of atomic disorder and/or grain boundaries and follow

$$\Delta G\left(\text{milling}\right) = \Delta G\left(\text{disorder}\right) + \Delta G\left(\text{grain boundaries}\right) \tag{38}$$

It should be noted that the formation of nanostructures has mainly been observed in metallic hydrides. For complex hydrides such a nanostructuration has not been observed owing to the low hardness/ductility of the powder (**Table 4**).[188] During the process, many parameters can influence the properties of the final products including the milling temperature, milling time, grinding ball diameter, ball-to-powder ratio, and process control agent. Therefore, the determination of the achievable grain size is not straightforward.[153,189] However, Li et al. found that in most of the cases, the rate of refinement of the grain size roughly shows a power–law relationship with milling processing time (Figure 17c)[190]

$$d = Kt^{-2/3} \tag{39}$$

where d is the grain size, t is the milling time, and K is a constant.

Mohamed also proposed a dislocation model whereby the minimum achievable grain size can be related to the hardness, melting temperature, and stacking fault energy of the material to be milled.[191] The minimum grain size achievable was found to scale with the inverse of the melting temperature of fcc metals including Al, Ag, Cu, and Ni. However, no similar trend was found for fcc metals with a high melting point and bcc, hcp metals.[192] Nanocrystalline materials display higher mechanical strength, hardness, and extremely high diffusion rates as compared to their microcrystalline counterparts,[164b,185,193] and these are believed to lead to unique physical, mechanical, and magnetic properties. In the case of metals for hydrogen storage, the lower atomic packing density at the grain boundaries can facilitate the hydrogen solubility[194] and diffusion,[27m] and thus provides additional hydrogen "paths" for the rapid hydrogenation of materials. This is particularly the case for Pd, Ni, and MgH_2.[151a,195] It is, however, important to mention that upon the first hydrogen cycling, the nanocrystalline structure will undergo a rapid restructuration and crystalline growth owing to the annihilation of defects,[46c,174a,196] the crystalline structure evolution upon hydrogen uptake and release (e.g., 30% expansion/contraction upon Mg/MgH_2 conversion), and the driving force to reduce interfacial energy at grain boundaries. The latter is proportional to the grain boundary area and thus is relatively high in nanocrystalline materials, i.e., ≈4 J m^{-2} instead of the 1 J m^{-2} observed in polycrystalline materials.[197]

Typically, upon mechanical milling crystallite sizes can be reduced from several μm to ≈10–50 nm.[46c,157a,174] This crystallite size will increase back to >80 nm upon hydrogen cycling,[198] and this can affect the hydrogen kinetics of hydrides. For example, upon hydrogen cycling, nanocrystalline MgH_2 shows kinetics in the order of 30 and 120 min for hydrogen release and uptake, respectively.[151a,174a,199] However, as the grain size grows from 9 to >100 nm, hydrogen kinetics have been observed to slow down by a factor 2 to 5 after 100 cycles.[200]

Strategies to maintain the nanocrystalline structure of metal hydrides remains unclear, although it has been claimed that the addition of particles in the form of TiH_2,[155,201] MgO,[174] or Nb_2O_5[202] may reduce crystalline growth upon hydrogen cycling. Hence in addition to catalytic activity, reduced forms of Nb_2O_5 embedded within the MgH_2/Mg domains may also limit the restructuration of grain boundaries.[202c] In contrast, MgO cannot catalyze the

Table 4. Summary of the hardness of selected elements/compounds relevant for the synthesis of hydrides.

Elements/compounds: hardness [Mohs][a)]			
Al: 2.2–2.9[529]	Al_2O_3: 8–9[530]	N: –	NH_4Cl: 2[531]
Ag: 2.7[529]	AgCl: 2.5[531]	Na: 0.5[532]	NaF: 2–2.5[531]
Au: 2.5[529]	–		NaCl: 2[531]
C: 0.5–10[528,533]	Graphite: 0.5–1[533a]	Nb: 6[534]	Nb_2O_5: 5–6[535]
Ce: 2.5[532]	CeO_2: 6[536]	Ni: 3.5–5[529]	NiO: 5.5[531]
Ca: 1.75[532]	CaF_2: 4[531]	Os: 7[529]	–
Cd: 2[529]	–	Pb: 1.5[529]	–
Cu: 3[529]	CuO: 3.5[530]	Pd: 4.5–5[537]	–
–	Cu_2O: 3.5–4[529]	Pt: 4–4.5[537]	–
Co: 5[529]	–	Ta: 7[529]	–
Cr: 4.5–8[529]	Cr_2O_3: 9[531]	Ti: 6[529]	TiH_2: 7.8[533a]
Fe: 3.5–4.5[529]	Fe_2O_3: 6[531]		TiO_2 (anatase): 5.5–6[538]
	Fe_3O_4: 6[531]		TiB: 9[531]
	$FeTiO_3$: 5–6[539]		TiC: 8–9[529]
	$FeAl_2O_4$: 7.5–8[531]	Sb: 3[532]	–
K: 0.4[532]	KCl: 2[540]	Si: 7[529]	SiO_2:6.5–7[531]
La: 2.5[541]	$LaNi_5$: 3.5[541]		SiC: 9[542]
	La_2O_3:8[536]	Sn: 2[529]	SnO_2:6–7[531]
	$LaNi_{3.5}CoAl_{0.5}$: 5–6[543a)]	Sr: 1.5[532]	$SrTiO_3$: 6–6.5[544]
	$LaNi_{4.5}Al_{0.5}$: ≈6[543a)]	V: 7[532]	V_2C_3: 8[529]
	$LaNi_4Co$: ≈6[543]		VC:9–10[529]
Li: 0.6[532]	LiH:3.5[545]	W: 7[529]	WC: 8–9[531]
	$LiNH_2$: ≈6.5[546]	Zn: 2.5[529]	ZnO: 4[547]
Mg: 2.5[529]	MgH_2: 4[198b]	Zr: 7–7.5[548]	$ZrFe_2$: ≈8.3[546]
			ZrO_2: 8–8.5[549]
			$Zr_{0.2}La_{0.8}Ni_{4.5}Al_{0.5}$: 5.56[543a)]
	MgO: 6[529]		
	$MgSiO_3$: 5–6[531]		
Mn: 7[529]	MnO_2: 6–6.5[531]	Mischmetal	$MmNi_{4.6}Mn_{0.4}$: 5–5.5[550a)]
	Mn_2O_3: 6.5[529]		$MmNi_{4.6}Mn_{0.8}$: ≈5.5[550a)]
	Mn_3O_4:5–5.5[531]	–	–

a)Converted to Mohs hardness value.[528]

dissociation/recombination of hydrogen at the H_2/Mg/MgH_2 interfaces and thus its role is purely limited to that of grain boundaries stabilization. As observed in several metallic nanocrystalline structures,[203] the activation energy for the grain growth is comparable to the activation energy associated with lattice diffusion and isothermal grain growth can be modeled following the equation

$$d^g - d_0^g = Kt \tag{40}$$

where d_0 is the initial grain size and d is the grain size at time t, and at a constant temperature, K is a constant, and g (value varying from 2 to 10)[185] the grain growth exponent.

It is also noteworthy that nanostructuration does not seem to affect the thermodynamic properties of metal hydrides.[196] Considering the high excess energy at grain boundaries, a reduction of enthalpy greater than 30% should be possible assuming Mg particles smaller than 5 nm.[27e] However, this has not been observed experimentally because of recrystallization occurring upon hydrogen cycling. It has also been proposed that an excess in vibrational and configurational entropy at grain boundary could prevent grain growth,[197] but this has not been observed in hydride systems.

The structure inside the grain is often assumed to be the same as that of the initial micrometer-sized material, although it may contain defects such as dislocations, twin boundaries and stacking faults.[204] The structure of the grain boundaries has been the subject of many hypotheses in particular to support the enhanced hydrogen kinetics observed in the Mg/MgH_2 systems and alloys. For example, it is often assumed that the atomic structure in grain boundaries is more random without long range order,[205] and this would support models predicting faster hydrogen diffusion.[27m] However, it remains unclear if the structure of grain boundaries in nanocrystalline materials significantly differs from that of coarse-grained materials.[206]

5.2.2. Catalysts Dispersion for Improved Hydrogen Sorption Kinetics

Assuming the right hardness of the powders involved, mechanical milling is a very effective method for the refinement of powders and thus the dispersion of catalytic phases at the surface of hydride materials. This is particularly the case with MgH_2 which upon milling not only undergoes nanostructuration, but also can be "decorated" with various catalysts including transition metals (e.g., Ni, Ti, Fe, Nb, V),[52b,58–59,178b,207] their oxides,[202a,208] or intermetallics (e.g., FeTi, $LaNi_5$).[209] Typically a few at% of catalyst is sufficient. However, it should be noted that depending on the respective hardness of the powders to be milled and the conditions of milling, the catalyst may not only end up at the surface of the hydride but also be fully embedded within the hydride particles.[202c,207a,210] The embedded catalyst is believed to provide additional paths for hydrogen diffusion within the nanocrystalline structure.[202c,211] Other archetypical examples are complex hydrides and in particular $NaAlH_4$ for which ball milling has been revealed to be very effective for the dispersion of Ti-based[212] and other additives (e.g., Ce, Pr, Mn, Sc, Pr, Zr and Carbons)[213] that are believed to act as catalysts. However, in this case, not only the catalyst is finely "confined" within the hydride phase but it is also partially or fully reacted owing to the strong reducing character of complex hydrides.

For example, upon milling $TiCl_3$ with $NaAlH_4$, a metathesis reaction occurs

$$(1-x)\,NaAlH_4 + x\,TiCl_3 \rightarrow (1-4x)\,NaAlH_4 + 3x\,NaCl + x\,Ti + 3x\,Al + 6x\,H_2 \quad (41)$$

Two hypotheses have been suggested concerning the chemical state of Ti species when used as catalyst in alanates: i) Ti° is formed during ball milling and the active catalyst is a Ti/Al alloy, and ii) Ti is substituted within the lattice of the bulk hydride.[177,214] Leon et al. identified the reduction of $TiCl_3$ to Ti° by ball milling $NaAlH_4$ with $TiCl_3$ and Ti was in a distorted state.[214,215] Balde et al. found that the majority (≈70%) of Ti occupied interstitial sites in $NaAlH_4$ and the rest of the Ti remained at the surface of Al.[216] $TiAl_3$ clusters were also observed by Weidenthaler et al. upon heating at 225 °C a mixture of Ti-doped $NaAlH_4$.[216,217] To date, the mechanism for the substitution of Na by Ti within the lattice of hydride remains unclear, but Weidenthaler et al. assumed that the replacement of Al atoms seems more plausible since the radius of the Ti^+ cation is smaller than that of Na^+.[217] The exact role of Ti in facilitating the release and uptake of hydrogen in $NaAlH_4$ is also controversial. First-principles calculations suggest that the dehydrogenation of Ti-doped $NaAlH_4$ is rate limited by the diffusion of AlH_4^- and AlH_3 vacancies and Ti has been suggested to facilitate the release of hydrogen from these diffusing species.[67a] Ti may also facilitate: i) the catalytic scission of the H_2 bond at the surface, ii) the catalytic breaking of H-AlH_3 bonds, and/or iii) the nucleation of the Al phase resulting from strong Ti-Al bonds and the formation of a coherent $TiAl_3$ phase.[67b,218]

5.2.3. Synthesis of Novel Hydrides

Mechanical milling has traditionally been used to prepare alloys and intermetallic compounds of the desired nanostructure and phase.[150,219] Early investigations also explored the formation of hydrides under low hydrogen pressures.[27i,149a,220] The development of advanced milling tools including high pressure vials equipped with pressure and temperature sensors has facilitated the emergence of new approaches to mechanochemically synthesize hydride materials, including amides, alanates, borohydrides, and reactive composite hydrides.[189a]

Metal amides, such as KNH_2, $LiNH_2$, $NaNH_2$, $Mg(NH_2)_2$, and $Ca(NH_2)_2$ can be prepared by ball milling alkaline earth metal hydrides in gaseous ammonia to form the corresponding amides, following the general reaction path[189a,221]

$$MH_n + n\,NH_3 \rightarrow M(NH_2)_n + n\,H_2 \quad (42)$$

As a common practice, NH_3 is loaded at ≈0.4–0.5 MPa in the milling vials containing the desired metal hydride and the vials are refilled approximately every 2 h to ensure the progression of the reaction. An unavoidable problem with the practical application of metal amides for hydrogen storage is the simultaneous release of NH_3 and H_2.[213b,222] To limit this, metal amides are usually milled with the corresponding metal hydride to form imides or nitrides,[213b,222,223] and this ultimately modifies the thermodynamic path for hydrogen release through H^+ (amides) and H^- (hydrides) intereactions.[224]

The important family of alanates (e.g., $LiAlH_4$, $NaAlH_4$, Na_3AlH_6, $KAlH_4$, $Mg(AlH_4)_2$, $CaAlH_5$ and Ba_2AlH_7) can also be synthesized by ball milling metal hydrides with Al or AlH_3 under hydrogen pressure.[152] Li_3AlH_6 and Na_3AlH_6 have also been prepared by milling LiH/NaH with $LiAlH_4$/$NaAlH_4$ under hydrogen (Table 3). A few examples on the synthesis of bimetallic alanates have also been reported. These include Na_2LiAlH_6, $NaLi_2AlH_6$, K_2LiAlH_6, K_2NaAlH_6, and $LiMg(AlH_4)_3$.[225] For example, Na_2LiAlH_6 and $NaLi_2AlH_6$ were prepared by directly milling NaH, LiH, and Al or $NaAlH_4$ under hydrogen pressure (Table 3). Similarly, K_2LiAlH_6, K_2NaAlH_6 were synthesized from KH with $LiAlH_4$ and $NaAlH_4$, respectively (Table 3). In contrast, the synthesis of $LiMg(AlH_4)_3$ was only achieved by an indirect route involving the ball milling of $Mg(AlH_4)_2$ with LiCl.[225a,226]

The direct synthesis of borohydrides from their elements by ball milling is difficult to achieve owing to the high hydrogen pressure needed and the difficulty of breaking the B—B or B—metal bond in favor of the formation B—H. $LiBH_4$ and $NaBH_4$ have been successfully obtained by ball milling Li, B, or Na, B under 15 MPa hydrogen pressure (Table 3).[227] By using diborane (B_2H_6) as the starting reactant the synthetic route is easier and quantitative[228]

$$MH_n + n/2B_2H_6 \rightarrow M(BH_4)_n \quad (43)$$

where M is the metal and n is the valence.

This approach has been effective for the synthesis of $LiBH_4$, $NaBH_4$, $Ca(BH_4)_2$, $Mg(BH_4)_2$, and $Y(BH_4)_3$.[227b,228] However, it is not generally applicable, since the formation of the borohydride phase competes with the formation of the corresponding boride. For example, in the case of TiH_2 ball milled with B_2H_6, the final solid product is not $Ti(BH_4)_2$ but TiB_2, which is thermodynamically more stable.[227a] Bimetallic borohydrides have also been prepared by ball milling metal borohydrides with alkali metal chlorides or other borohydrides (Table 3). For example, Ravnsbæk et al. reported the synthesis of $LiZn_2(BH_4)_5$, $NaZn_2(BH_4)_5$, $NaZn(BH_4)_3$ by ball milling different ratios of $LiBH_4$, $NaBH_4$ with $ZnCl_2$, respectively. These new bimetallic borohydrides revealed remarkable structural diversity and low decomposition temperatures.[229] Similarly, the trimetallic borohydride $Li_3MZn_5(BH_4)_{15}$ (M = Mg, Mn) was synthesized by ball milling a $LiBH_4$, $M(BH_4)_2$ and $ZnCl_2$ mixture.[230]

A metathesis reaction approach is a common way to synthesize metal borohydrides and alanates by mechanochemical reaction. Usually an n-valent metal chloride or fluoride (NX_n) is reacted with alkaline metal borohydrides ($M(BH_4)$) or alanates ($M(AlH_4)$) to produce a new complex metal borohydride or alanates.[231] The reaction can be simplified as

$$NX_n + n\,M(BH_4)/n\,M(AlH_4) \rightarrow N(BH_4)_n/N(AlH_4)_n + n\,MX \quad (44)$$

The advantage of performing such a synthesis by ball milling is that the reaction is done at the solid state and thus does not involve solvents that may form intermediate complexes. However, a purification step involving some solvents may be

required at the end of the process to remove the halide and intermediate products.

Mixed hydrides, e.g., metal borohydrides/alanates/amides have also been synthesized mechanochemically. By tuning the ratio in the initial mixtures, different borohydride amides or alanate amides can be formed (Table 3). For example, Noritake et al. reported the synthesis of $Li_2(BH_4)NH_2$ and $Li_4(BH_4)(NH_2)_3$ by varying the ratio of $LiNH_2$:$LiBH_4$ from 1:1 to 3:1.[232] Chua et al. found that $LiAlN_2H_2$ and Li_2AlNH_2 were formed by the interaction of $LiAlH_4$ with $2NaNH_2$ and $2LiAlH_4$ with $NaNH_2$, respectively.[233]

Compositional alteration of ammonia borane (AB) by mechanochemical milling with metal hydrides to form metal amidoboranes has also been investigated by mechanochemical synthesis, with the aim of partially substituting its protic $H^{\delta+}$ with a more electropositive metal[234]

$$M_1H_n + nNH_3BH_3 \rightarrow M_1(NH_2BH_3)_n + nH_2 \quad (45)$$

$$M_1H_n + M_2H_m + (m+n)NH_3BH_3 \rightarrow M_1M_2(NH_2BH_3)_{m+n} + 2(m+n)H_2 \quad (46)$$

where n and m are the valence states of M_1 and M_2, respectively. M_1 can be Li, Na, K, Ca, and Sr. In this case, M_1M_2 is LiNa, KAl, and Na_2Mg.[235]

Xiong et al. synthesized $LiNH_2BH_3$ and $NaNH_2BH_3$ by ball milling stoichiometric amounts of AB with LiH and NaH, respectively.[236] The synthesized $LiNH_2BH_3$ and $NaNH_2BH_3$ released ≈11 and ≈7.4 mass% H_2 at ≈91 °C, respectively. Unlike AB, which releases borazine with H_2 at the same time, there was no emission of borazine found from $LiNH_2BH_3$ and $NaNH_2BH_3$.[236] $Na[Li(NH_2BH_3)_2]$ was found to decompose exothermally between 75 and 110 °C with ammonia as a byproduct.[237] A similar approach was also successfully applied to hydrazine borane $N_2H_4BH_3$, a derivative of AB,[238] to synthesize alkali hydrazinidoboranes of formulae $MN_2H_3BH_3$ (with M = Li, Na, K).[239] The latter hydrazinidoborane derivatives were found to have much better dehydrogenation properties in terms of H_2 purity, onset temperatures of dehydrogenation and safety. $LiNH_2BH_3 \cdot NH_3BH_3$ as an AB derivative has also been synthesized by ball milling under H_2 pressure. It showed better dehydrogenation kinetics over $LiNH_2BH_3$ and AB alone. The first-principles study showed that the enhanced dehydrogenation property was via the combination of hydridic $H^{\delta-}$(B) from $LiNH_2BH_3$ and protonic $H^{\delta+}$(N) from the adjacent AB.[240]

5.2.4. Formation of Other Novel Phases by Mechanical Milling

The intense plastic deformation induced in high energy milling can sometimes result in the introduction of disorder to the extent of forming an amorphous structure.[164] The mechanism for amorphization is similar to the solid state amorphization reaction proposed by Schwarz and Johnson.[241] It is therefore often observed that upon mechanical milling partial or complete amorphization of hydride materials can occur. For example, Wang et al. synthesized amorphous Mg–$FeTi_{1.2}$ with enhanced hydrogen absorption kinetics.[242] An amorphization can also be observed for complex hydrides. For example, ball milling MgB under 10 MPa hydrogen pressure led to amorphous $Mg(BH_4)_2$.[243] Its decomposition behavior was similar to crystalline $Mg(BH_4)_2$. The possibility of rapid energization and quenching during the milling process upon ball to powder impact can potentially also lead to the formation of metastable phases,[164a] i.e., phases which have a higher free energy than the equilibrium phase thermodynamically stable. For example, the high pressure metastable γ-MgH_2 phase is commonly obtained in a low amount (≈2–6%) by ball milling MgH_2.[46a,52b,174a] Xiao et al. reported a higher amount (≈18%) of γ-MgH_2 by milling MgH_2 with LiCl.[244] γ-MgH_2 is believed to lead to improved hydrogen diffusions and better thermodynamic properties and thus a lower temperature at which hydrogen can be released. However, the rapid restructuration of ball milled MgH_2 upon the first hydrogen cycling has never enabled the characterization of its hydrogen properties. Recently, we reported the electrochemical synthesis of a γ/β-MgH_2 mixture with ≈30% γ-MgH_2, which enabled for the first time the experimental determination of the hydrogen properties of γ-MgH_2.[245] γ-MgH_2 was found to display a reduced enthalpy of 57.7 ± 5.3 kJ mol^{-1} H_2 instead of the 75 kJ mol^{-1} H_2 of β-MgH_2; and thus was amenable to fully release hydrogen at 200 °C.

It should also be noted that mechanical milling has also shown some potential toward the formation of solid solutions[246] and the alloying of immiscible systems. For example, the solubility of Ti in Mg is very small (<0.1 at%). By mechanical alloying, under nonequilibrium conditions,[246a] this solubility can be extended to 12.5 at% due to a favorable size factor (9%) and an isomorphous structure.[247]

The dissolution of the alloying atom through mechanical milling can also modify the lattice parameters of the host materials. For example, Cd, In, Li, Al, Zn, Ag, Ga, Ti, and Sn have been found to reduce the Mg lattice parameters by forming a solid solution. In contrast, Sc and Pd were found to expand the lattice of Mg.[247,248] The formation of Mg-based solid solutions can enhance its hydrogenation and dehydrogenation. For example, the bcc solid solution $(Nb, Mg)H_x$ ($x < 2$) was predicted to lead to lower hydrogen desorption temperatures (300 instead of 400 °C) as compared to pristine MgH_2.[249] In contrast, the formation of Mg(Li) solid solution did not lead to any improvement in the hydrogen properties of Mg because of the formation of the segregated and stable LiH phase upon hydrogenation.[248]

6. Metastable and Amorphous Phases: Storing Hydrogen through Thermodynamic Instability

A metastable state is a thermodynamically stable state with a local free energy minimum which does not correspond to the thermodynamic equilibrium state. Metastable phases can be crystalline and amorphous and are formed by various synthetic techniques including melt spinning,[250] atomization process,[251] ball milling,[44] and high pressure torsion.[252] For hydrogen storage materials, it is expected that metastable hydrides can display lower hydrogen desorption temperatures owing to their thermodynamic instability. For example,

nanocrystalline TiFe when ball milled with 4 wt% Ti was reported to lead to the formation of the nanocrystalline $Fe_{46}Ti_{54}$ metastable phase.[151b,253] This not only decreased P^{eq} but also flattened the plateau.

Some weakly bound chemical hydrides, e.g., AlH_3, NH_3BH_3, and $LiAlH_4$, are also considered as metastable or kinetically stabilized hydrides.[254] These compounds have a P^{eq} above 0.1 MPa at the ambient and thus only decompose very slowly at room temperature due to kinetic limitations. However, for these compounds hydrogen reversibility only occurs under harsh conditions of temperature and pressure, for example, 8.9×10^3 MPa hydrogen pressure and 600 °C are required to recombine hydrogen with Al.[255] We found that after nanosizing these materials, some hydrogen reversibility was possible. Hence, for $LiAlH_4$ nanoconfined in a mesoporous carbon, hydrogen uptake and release was achieved at 300 °C and under 7 MPa hydrogen pressure.[256] Similarly, upon nanosizing NH_3BH_3, hydrogen reversibility was achieved at 200 °C and under 6 MPa hydrogen pressure.[24c]

Amorphous alloys such as TiCu and Ti_2Cu may display larger hydrogen storage capacity compared to their crystalline counterparts.[257] For example, TiCu amorphous alloys were reported to absorb about 35% more hydrogen than crystalline TiCu.[257] This is because in the crystalline structure, the number of interstitial sites within the lattice limit the introduction of hydrogen.[258] However, no evidence of a plateau pressure exists for amorphous hydrides owing to the large distribution of interstitial site energies (i.e., a large variation of sites with different coordination numbers and geometrical configurations) available for hydrogen.[27m] The lack of equilibrium plateau is a drawback for application, since hydrogen cannot be delivered at a constant pressure from the amorphous alloy. In some cases, the absorption of hydrogen can also result in an amorphization of the alloy, e.g., Zr–Rh systems, and hydrogen induced amorphization has been observed on many intermetallic compounds.[259] The empirical rule of Aoki et al. can be used to determine if an alloy can undergo hydrogen amorphization. For a Goldschmidt radii $R_A/R_B > 1.37$ (with R corresponding to the ionic radius of A and B), the alloy AB should undergo hydrogen amorphization as a result of its low crystal lattice stability.[260] Most amorphous alloys are formed by rapid quenching (cooling rate of the melt $\approx 10^4$ °C s^{-1}). By mechanical milling, an amorphous phase can also be generated and in the case of nanocrystalline materials, it is believed that the structure at grain boundaries is amorphous – hence, the higher hydrogen solubility and the faster hydrogen kinetics,[151] assuming that the temperature of hydrogenation does not exceed the recrystallization temperature of the metal hydride.

7. Improving the Hydrogen Properties of Light Hydrides via Chemical Destabilization

Light metal hydrides such as LiH and MgH_2, and light metal complex hydrides such as amides (e.g., $LiNH_2$), alanates (e.g., $NaAlH_4$), and borohydrides (e.g., $LiBH_4$), have been at the center of many investigations owing to their high volumetric and gravimetric hydrogen storage capacities. The challenges remain their high thermodynamic barrier and sluggish kinetics. The chemical bonding in light metal hydrides is predominately covalent, ionic, or a mixture. This means that light hydrides are thermodynamically stable in comparison to transition metal hydrides having a delocalized metallic bonding within their structures. Covalent, or ionic bonds also result in large activation barriers for atomic motion, and this results in slow hydrogen sorption kinetics which further restricts the hydrogen reversibility. Following the early examples of thermodynamic destabilization of metal hydrides (Figure 14b),[119,136] similar ideas have emerged to improve the thermodynamics of complex hydrides but this often assumes that the entropy of reaction for these hydrides remains constant which is not the case.[261]

7.1. The Approach of Reactive Hydride Composites (RHC)

Vajo et al.[112,261] were among the first to demonstrate the concept of RHC based on the idea that the reactions between two or more hydrides (MH_n and M_1H_m) can lead to the formation of an unstable hydride phase and/or a more stable product (MM_1) during dehydrogenation and thus facilitate the release of hydrogen (Figure 14b)

$$MH_n + M_1H_m \leftrightarrow MM_1 + \frac{n+m}{2}H_2 \tag{47}$$

The enthalpy of formation of composite hydrides is usually exothermic, and this leads to an overall reduction of the dehydrogenation enthalpy for the composite hydride, while a high hydrogen storage capacity is maintained. The dehydrogenation enthalpy (ΔH°_{deh}) in this case is equal to the difference in the standard enthalpy of formation between the products and starting hydrides

$$\Delta H^{\circ}_{deh} = \frac{2}{n+m}\left(\Delta_f H^{\circ}_{MM_1} - \Delta_f H^{\circ}_{MH_n} - \Delta_f H^{\circ}_{M_1H_m}\right) \tag{48}$$

Similarly, the entropy of dehydrogenation (ΔS°_{deh}) is given by the difference between standard entropy of the products and starting hydrides

$$\Delta S^{\circ}_{deh} = \Delta S^{\circ}_{H_2} + \frac{2}{n+m}\left(\Delta S^{\circ}_{MM_1} - \Delta S^{\circ}_{MH_n} - \Delta S^{\circ}_{M_1H_m}\right) \tag{49}$$

The enthalpy of formation and entropy of the decomposition reaction of some common hydrides that can be used for synthesizing RHC systems are summarized in Table 2.

The $LiBH_4$ and MgH_2 mixture is an archetypical example of RHC that has been widely investigated owing to the high hydrogen capacity of both hydrides, i.e., 18.5 and 7.6 mass% H_2, respectively. The composite $LiBH_4/MgH_2$ is effectively less stable than the individual hydrides (**Figure 18**a) and follows the decomposition paths

$$LiBH_4 + 1/2MgH_2 \leftrightarrow LiH + 1/2MgB_2 + 2H_2 \tag{50}$$

$$LiH + 1/2MgB_2 \leftrightarrow Li + 1/2MgB_2 + 1/2H_2 \tag{51}$$

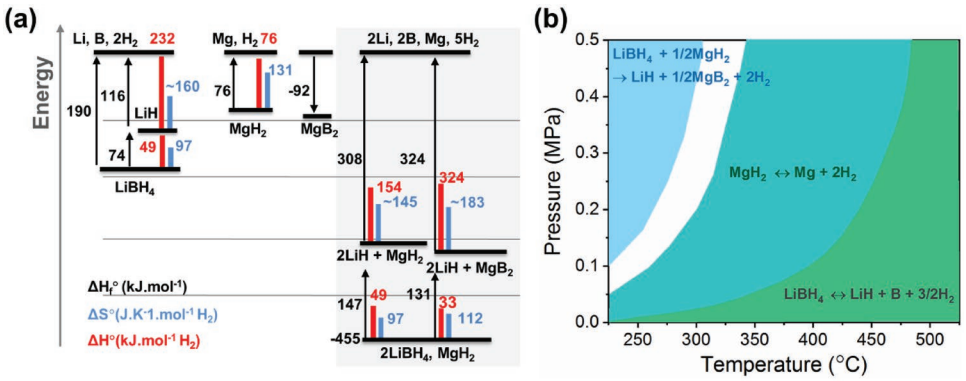

Figure 18. Thermodynamics of RHC systems with $LiBH_4/MgH_2$ as an example. a) Evolution of the ΔH and ΔS as function of the reaction path; and b) phase boundary diagram of $LiBH_4 + 1/2MgH_2$ determined from theoretical calculations based on the enthalpy and entropy obtained by Vajo et al.[112] ΔH and ΔS were determined by using the NIST Chemistry WebBook and NIST-JANAF thermochemical tables. The calculated values of ΔS reported here do not correspond to the experimental values reported in equations (30) and (31).

For Figure 18a, it can be seen that the desorption enthalpy of (50), 33 kJ mol^{-1} H_2, is reduced as compared to that of pristine $LiBH_4$ (49 kJ mol^{-1} H_2). In contrast, the entropy of (50), 112 J K^{-1} mol^{-1} H_2, was found to be higher than that of pristine $LiBH_4$ (97 J K^{-1} mol^{-1} H_2) but lower than the entropy for MgH_2 (131 J $K^{-1}$$mol^{-1}$ H_2). Achieving hydrogen reversibly for borohydrides was also found to be easier under this approach. Indeed, direct rehydrogenation of mixtures of MgB_2 and the binary hydrides (LiH, NaH, or CaH) led to the formation of $LiBH_4$, $NaBH_4$, and $Ca(BH_4)_2$.[262] The kinetic barrier for the hydrogenation reaction starting from MgB_2 is believed to be much lower than that starting from elemental boron.[262b] Additionally, the reactivity of boron in MgB_2 is much higher than elemental boron, possibly due to: a) the different strength of boron bonding (B—B = 297 ± 21 kJ mol^{-1}, B—H = 340 kJ mol^{-1}),[263] b) the different bond lengths (1.77–1.83 Å for icosahedra of elemental boron,[264] and 1.78 Å for B—B and 2.5 Å for Mg—B of MgB_2[265]) and c) the different coordination numbers in B—B, B—H, Mg—B—H.

However, as compared to the alloying of metals, reactive hydride mixtures involving complex hydrides are much more difficult to control owing to the possibility of multiple decomposition paths. These further depend upon the reaction conditions and the ratio between the two hydrides,[243] and such a complexity can lead to very different destabilization effects. For example, it was found that the $2LiBH_4/MgH_2$ mixture led to production of MgB_2 (reaction (50)) under hydrogen atmosphere according to the boundary diagram (Figure 18b), and this facilitates the destabilization of $LiBH_4$ while stabilizing the dehydrogenated state. Through this mixture, the enthalpy of the reaction was reduced by 25 kJ mol^{-1} H_2, as compared to pure $LiBH_4$,[112] and the dehydrogenation temperature was reduced to 225 °C at a hydrogen equilibrium pressure of 0.1 MPa. This is significantly lower than the decomposition temperature of the single hydrides (Table 2).[112] In contrast, the same $2LiBH_4/MgH_2$ mixture decomposed under vacuum led to formation of elemental Mg and B following (50)

$$LiBH_4 + 1/2MgH_2 \leftrightarrow Li + 1/2Mg + B + 5/2H_2 \quad (52)$$

Additionally, enriching MgH_2 (up to a mass ratio of 1:4) in the $LiBH_4/MgH_2$ system was found to result in the formation of Li–Mg alloys, e.g., the $Mg_{0.816}Li_{0.184}$ and the $Mg_{0.70}Li_{0.30}$ alloys, following the reaction paths (53) and (54)[266]

$$0.3LiBH_4 + MgH_2 \rightarrow 0.3LiBH_4 + Mg + H_2 \quad (53)$$

$$0.3LiBH_4 + Mg + H_2 \rightarrow 0.78Mg_{0.816}Li_{0.184} + 0.52Mg_{0.70}Li_{0.30} + 0.3B + 1.60H_2 \quad (54)$$

This also resulted in partial hydrogen reversibility of the system under 10 MPa hydrogen pressure and at 400 °C.[266] Hence, the formation of MgB_2 is not necessary for enabling hydrogen reversibility.

The most favorable conditions for hydrogen reversibility can be determined from the phase boundary diagram of the $LiBH_4$ + $1/2MgH_2$ system (Figure 18b). Under sufficient hydrogen back pressure, direct decomposition of $LiBH_4$ leading to formation of elemental boron can be avoided, and thus it is possible to alter the reaction path by adjusting the hydrogen pressure upon the decomposition of the hydride mixture.[267]

Although the concept of RHC can lead to some enhancement in the dehydrogenation reaction, this does not address the kinetic issues which significantly limit hydrogen reversibility under moderate conditions owing to slow ionic diffusion even at high temperatures.[268] Hydrogen absorption in a metal involves multiple steps: physisorption, dissociation, chemisorption, diffusion, phase transition, hydride formation of nucleation and growth (Figure 8a). The reverse processes occur during the dehydrogenation reaction and the rate of hydrogen sorption is governed by the slowest reaction step. Understanding hydrogen or ionic diffusion in complex hydrides involves very different mechanisms that may evolve during the hydrogen uptake/release because of the changes in crystalline and amorphous structures occurring in reactive hydride mixtures. In this case, fast hydrogen desorption kinetics also requires both the mobility of hydrogen carrying species (e.g., the BH_4^- unit)[269] and the metal counter ions. The finite hydrogen flux ($j_{H,i}$) in the material is thus limited by the gradient in chemical potential ($\nabla\mu_{H,i}$) for the ions (i) across the different hydride phases as follows[270]

$$j_{H,i} = -L_i \nabla \mu_{H,i} \quad (55)$$

where L_i is the parameter related to the transport mechanism within the material, such as the concentration of the hydrogen gas and temperature.[271]

For borohydrides, the chemical potential ($\mu_{H,i}$) is proportional to $\ln(P)$. Thus the diffusion of hydrogen is linearly correlated to $\ln\left(\frac{P}{P^{eq}}\right)$ at the reaction interface.[272] In contrast, hydrogen desorption from MgH_2 varies linearly with $(P - P^{eq})^a$, with $0.5 < a < 1$, assuming that hydrogen diffusion through the MgH_2 particles is the main limiting step.[178b] Hence, owing to the variations in hydrogen desorption regimes, different decomposition steps corresponding to the decomposition of MgH_2 first and then of $LiBH_4$ can lead to a single or double plateau pressure.

Experimentally, the E_a for the dehydrogenation of the $LiBH_4/MgH_2$ system determined by the Kissinger method was found to be of 221 ± 5 and 306 ± 10 kJ mol^{-1} for the successive dehydrogenation of MgH_2 and $LiBH_4$, respectively.[273] These values are higher than the E_a reported for pristine MgH_2 (156 kJ mol^{-1})[270] and $LiBH_4$ (59 ± 2 kJ mol^{-1}),[274] alone. Accordingly, kinetic enhancement through the RHC system approach can be limited. A similar observation was made for the $NaBH_4/MgH_2$ composite. In this case, E_a was found to be of 100 ± 4 and 133 ± 13 kJ mol^{-1}, for the decomposition of MgH_2 and pristine $NaBD_4$, respectively.[270]

The kinetics of RHC systems is controlled by various activation barriers and also the microstructure of the system and the particles/particles interactions as illustrated in Figure 10.[275] Modeling the reactions kinetics through the Johnson–Mehl–Avrami (JMA) approach revealed that the absorption and desorption reactions both follow a 3D growth of contracting volume with a constant and decreasing interface velocity.[55b-d] This means that during the de/rehydrogenation process, the growth of new phases starts from the surface and propagates inward toward the particles' center. Therefore under this assumption, the nucleation of MgB_2 can be a major impediment for the progress of the reactions in the case of the $LiBH_4/MgH_2$ system, for example.[268] Indeed, experimentally an incubation period is often observed after the decomposition of MgH_2 into metallic Mg, before the start of the second step, i.e., decomposition of $LiBH_4$.[270] Therefore, parameters including phase distribution, particles/particles interaction, grain boundaries, and crystallite size should be properly controlled to maximize the mobility of atoms/ions and promote the reactivity of the complex hydrides. For hydrogen absorption, the mobility of Mg, B and Li, as well as hydrogen diffusion upon the decomposition of MgB_2 and LiH govern the regeneration of the initial borohydride/hydride mixture. It has been claimed that hydrogen reaction at the MgB_2 interface is the rate-limiting step during absorption, rather than the diffusion of hydrogen and ions participating in the regeneration of $LiBH_4$ and MgH_2.[268] This again suggests that the microstructure of MgB_2 is important for the rehydrogenation process.

Addition of so called "catalysts" including transition metal halides, is a popular approach to further enhance the desorption kinetics of RHC, leading in some cases to improved hydrogen reversibility.[275a] For instance, it has been claimed that addition of Ti additives can act as nucleation seeds and provide effective growth sites for the MgB_2.[276] The kinetics of RHC can be further improved via nanoconfinement (Figure 6c). For example, $2LiBH_4$–MgH_2 confined within a resorcinol formaldehyde carbon aerogel scaffold showed a reduced E_a of 89 ± 2 and 279 ± 5 kJ mol^{-1} for the MgH_2 and $LiBH_4$ dehydrogenations, respectively.[273] This is attributed to the reduced diffusion distance for hydrogen.

7.2. Metathesis Reaction and Partial Substitution to Trigger Low Temperature Desorption

Reducing the energetic barriers to allow the decomposition of hydrides under milder conditions involves weakening of M—H bonds and intrahydrogen pairing (H—M—H). An alternative method to enhance the dehydrogenation and reversibility of complex hydrides is through the addition of a second metal to partially substitute for the central metal cation (M^+) in the complex hydride.[277]

$$\left(1+m/n\right)M(BH_4)_n + M_1X_m\,(X = Cl,Br,I,\text{etc.}) \rightarrow M_1M(BH_4)_{n+m} + m/nMX_n \quad (56)$$

This can be achieved by taking advantage of significant electronegativity differences between hydrides forming elements and thus the partial substitution of M by a more electronegative element M_1 (Figure 14b). Archetypical examples of such an approach are based on borohydrides for which a correlation between the metal electronegativity and the hydrogen decomposition temperature has been established (**Figure 19**).[252b] In this case, the modification of the hydride and the partial substitution of M are usually performed via mechanical milling with the desired metal halide (see section 5.2.3). Examples of this include bimetallic borohydrides incorporating Sc and Zn within the Group I metal borohydrides (Figure 19a), because $Sc(BH_4)_3$ and $Zn(BH_4)_2$ are thermodynamically unstable.[278] By ball milling of $LiBH_4$ and $ScCl_3$, $LiSc(BH_4)_4$ with a hydrogen storage capacity of 14.5 mass% was easily prepared.[279] This new compound showed low temperature hydrogen release; however, no reversibility was achieved at 250 °C under 12 MPa hydrogen pressure.[279d] The release of hydrogen from $LiSc(BH_4)_4$ was found to follow multiple decomposition paths (57)–(60) and this does not facilitate hydrogen reversibility[279a]

$$LiSc(BH_4)_4 \rightarrow 2/5LiBH_4 + 3/10Li_2B_{12}H_{12} + ScH_2 + 22/5H_2 \quad -128\,^{\circ}C \quad (57)$$

$$\rightarrow LiBH_4 + 1/10Li_2B_{12}H_{12} + ScB_2 + 29/5H_2 \quad -147\,^{\circ}C \quad (58)$$

$$\rightarrow Li_2B_{12}H_{12} + 2/3LiH + ScB_2 + 20/3H_2 \quad 170\,^{\circ}C \quad (59)$$

$$\rightarrow LiH + 4/5ScB_2 + 1/5ScB_{12} + 15H_2 \rightarrow 553\,^{\circ}C \quad (60)$$

In addition the reaction leads to the release of gaseous B_2H_6, and the formation of the thermodynamically more stable intermediates $Li_2B_{12}H_{12}$ and LiH.

Mixed-cation borohydrides are of great interest due to: i) their high hydrogen content, ii) the facility to tune their hydrogen

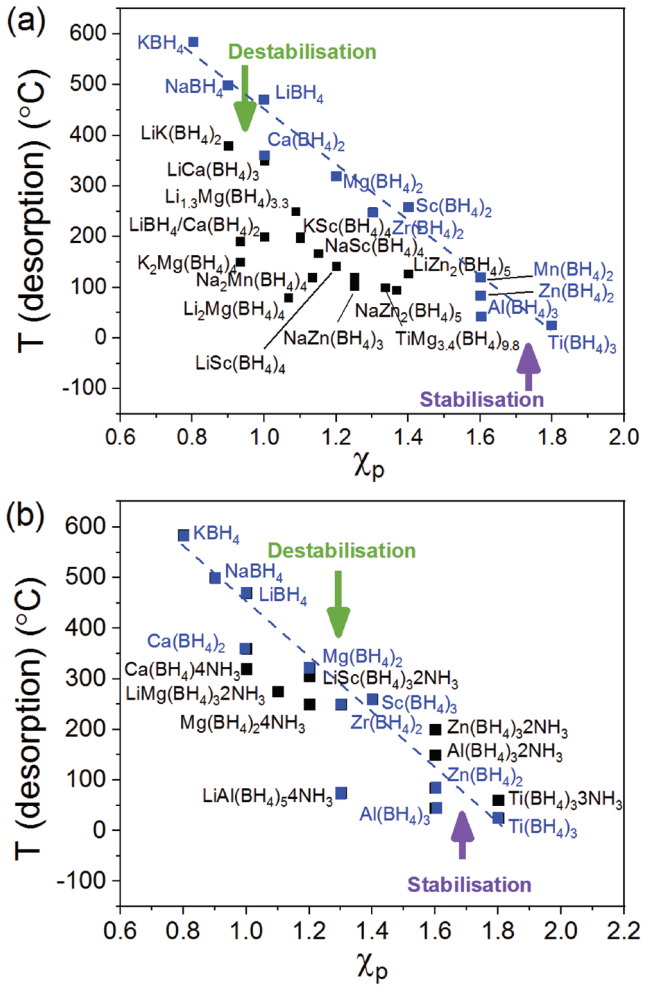

Figure 19. Adjusting the thermodynamics of complex hydrides. Experimentally observed decomposition temperatures for selected a) metal borohydrides and bimetallic metal borohydrides; and b) metal borohydrides and ammine borohydrides plotted as a function of the electronegativity, χ_p, of the metal cation. The blue dashed line represents the linear relationship between the decomposition temperatures and electronegativity of metal cation borohydrides.

sorption properties by adjusting the molar ratios between the two reactants, and iii) the variety of crystalline structures that can be obtained.[229] However, this approach has several drawbacks: a) most dual-borohydride cations still release hydrogen above 100 °C, b) the synthesis of mixed-cation borohydrides often leads to undesired halide byproducts, which reduces the available hydrogen content, and c) their instability results in the formation of unwanted byproducts (e.g., B_2H_6) and thermodynamically stable products, e.g., dodecaborate ($[B_{12}H_{12}]^{2-}$) and transition metal borides during thermal decomposition.[279d] This limits the conditions for rehydrogenation.[278] Nanoconfinement can provide an approach to overcome some of these problems owing to the shorter diffusion paths and the likelihood of minimizing the number of side reactions. For instance, nanoconfined eutectic composites of borohydrides have shown great improvements on the hydrogen release temperature,[280] with the possibility of modification of the decomposition path.[281] This is often reflected by the suppression of the formation of volatile gases, i.e., B_2H_6, upon nanoconfinement, which may further improve the reversibility of the materials.

7.3. Destabilization of Hydrides through H^+/H^- Interaction

Metal hydrides can be classified into three categories, based on the bonding between the metal and hydrogen: i) ionic, e.g., LiH where the hydrogen existed as a H^- ion, ii) covalent, and iii) metallic hydrides (Figure 4). In complex hydrides, such as $LiBH_4$, the hydrogen exists as a partially negatively charged $H^{\delta-}$. In contrast, hydrogen exist as partially positively charged $H^{\delta+}$ in covalent hydrides, such as $LiNH_2$.[282] A strategy to facilitate the release of hydrogen from hydrides is thus through the combination of ionic and covalent hydrides, which is equivalent to a Lewis acid/base reaction with $H^{\delta-}$ acting as an electron donor, while $H^{\delta+}$ acts as an electron acceptor with[282]

$$\delta H^- + H^{\delta+} \rightarrow (1+\delta)H_2 \quad (61)$$

$$H^- + H^- \rightarrow H_2 + 2e^- \quad (62)$$

$$H^{\delta+} + H^{\delta+} + 2\delta e^- \rightarrow H_2 \quad (63)$$

Reaction (61) is easier as compared to the reaction paths (62) and (63), which require high temperatures due to the repulsive potential between the two positively or negatively charged hydrogen ions and the additional need of electron transfer.

One of the first demonstrations of the H^+/H^- concept was with the $LiNH_2/LiH$ system.[283] By combining $H^{\delta+}$ in $LiNH_2$ and H^- in LiH a dehydrogenation temperature as low as 150 °C was achieved along the decomposition paths[284]

$$LiNH_2 + LiH \rightarrow Li_2NH + H_2 \quad 150\,^\circ C \quad 6.5\,\text{mass\%}\ H_2 \quad (64)$$

$$LiNH_2 + 2LiH \rightarrow Li_3N + 2H_2 \quad 320\,^\circ C \quad 9.6\,\text{mass\%}\ H_2 \quad (65)$$

Further investigation by Hu and Ruckenstein[285] and Ichikawa et al.[221c] claimed the formation of intermediates (i.e., NH_3). Therefore, the destabilization effect could be from the interaction between $H^{\delta+}$ in ammonia and H^- in LiH according to

$$2LiNH_2 \rightarrow Li_2NH + NH_3 \quad 374\,^\circ C \quad 9.6\,\text{mass\%}\ H_2 \quad (66)$$

$$LiH + NH_3 \rightarrow LiNH_2 + H_2 \quad 100\,^\circ C \quad 8.1\,\text{mass\%}\ H_2 \quad (67)$$

These initial results further inspired the exploration of mixing metal amides/imides with hydrides to achieve high capacity hydrogen storage materials. For example, the decomposition of $2LiNH_2/MgH_2$ resulted in the formation of the $Li_2Mg(NH)_2$ intermediate, with a 4.2 mass% H_2 reversibility at 200 °C and 3 MPa hydrogen pressure.[286] It is noteworthy that $Mg(NH_2)_2$ and LiH mixtures with various ratios of amide to hydride can lead to formation of different products as following[287]

$$Mg(NH_2)_2 + nLiH \leftrightarrow Li_2Mg(NH)_2 + (n-2)LiH + 2H_2 \quad 140-250\,^{\circ}C \quad 5.6\ \text{mass\%}\ H_2 \tag{68}$$

$$Mg(NH_2)_2 + 8/3LiH \leftrightarrow 1/3Mg_3N_2 + 4/3Li_2NH + 8/3H_2 \quad 140-280\,^{\circ}C \quad 7\ \text{mass\%}\ H_2 \tag{69}$$

$$Mg(NH_2)_2 + 4LiH \leftrightarrow 1/3Mg_3N_2 + 4/3Li_3N + 4H_2 \quad 140-520\,^{\circ}C \quad 9.1\ \text{mass\%}\ H_2 \tag{70}$$

This concept of H^+/H^- interaction has also been expanded to a large range of hydrides with the use of ball milling as the main technique to favor the intimate mixing between both hydrides. For example, different ratios between $LiBH_4$ and $LiNH_2$ led to quaternary hydride $Li_3BN_2H_8$,[288] and $Li_4BN_3H_{10}$.[289] $Li_3BN_2H_8$ has a theoretical hydrogen capacity of 11.9 mass% and this compound released 10 mass% H_2 with only a small amount of ammonia (2–3 mol%) above 250 °C. In this case, the destabilization effect was further evidenced by first-principles calculations, where the dehydrogenation enthalpy of the $LiBH_4/2LiNH_2$ mixture was reduced from 75 kJ mol^{-1} H_2 for pure $LiBH_4$ to 23 kJ mol^{-1} H_2. The same concept was also investigated for $NaBH_4$,[290] $Mg(BH_4)_2$,[291] and $Ca(BH_4)_2$,[292] and similar reaction mechanisms were observed. More recent investigations used $CO(NH_2)_2$—an organic carbonyl diamide—to modify $LiBH_4$ and produce $LiBH_4 \cdot CO(NH_2)_2$. This new system was able to release 8.13 mass% H_2 exothermically at temperatures below 250 °C.[293]

Mixing $LiAlH_4$ and $LiNH_2$ can also lead to the formation of Li–Al–N intermediates to release hydrogen at reduced temperatures. But once again, the reaction paths significantly depend upon the $LiNH_2$ to $LiAlH_4$ ratios[294]

$$2LiNH_2 + LiAlH_4 \leftrightarrow Li_3AlN_2 + 4H_2 \quad 25-600\,^{\circ}C \quad 9.6\ \text{mass\%}\ H_2 \tag{71}$$

$$2LiNH_2 + 2LiAlH_4 \leftrightarrow 2Li_2AlNH + 5H_2 \quad 50->700\,^{\circ}C \quad \sim 8.2\ \text{mass\%}\ H_2 \tag{72}$$

$$LiNH_2 + 2LiAlH_4 \leftrightarrow 2Al + Li_2NH + LiH + 4H_2 \quad 85-320\,^{\circ}C \quad 8.1\ \text{mass\%}\ H_2 \tag{73}$$

To date, the problem with such an approach remains the low hydrogen reversibility. Only 3.5–4.0 mass% H_2 is usually reabsorbed in $LiNH_2/LiAlH_4$ mixtures at temperatures ≈380 °C and under 20 MPa hydrogen pressure. An additional drawback is the formation of the more stable Li_3AlH_6 as an intermediate, and because the rehydrogenation of Li_3AlH_6 to $LiAlH_4$ requires extreme conditions this further impedes hydrogen reversibility.[295] The decomposition of these systems toward LiH is thus a more thermodynamically favorable path.[296] The alternative is to directly mix $LiNH_2$ with Li_3AlH_6. In this case, a higher reversible hydrogen content of 7 mass% was observed at moderate conditions (300 °C, 10 MPa).[297]

An additional example of protic–hydridic-based hydrogen storage materials is ammonia borane (NH_3BH_3, AB). AB has a very high hydrogen content of 19.6 mass%. The existence of dihydrogen bonding in AB between protic (N—H) and hydridic (B—H) hydrogens is believed to lead not only to enormously high volumetric and gravimetric density but also to aid the low temperature hydrogen release, e.g., 6.5 mass% of H_2 at 100 °C.[298] However, the use of AB as a hydrogen storage material is not without major drawbacks. The thermal decomposition of AB not only leads to the formation of various polymers, e.g., polyaminoborane ($(NH_2BH_2)_n$) and polyiminoborane ($(NHBH)_n$), but also volatile gases including ammonia (NH_3), diborane (B_2H_6), and borazine ($B_3N_3H_6$). Moreover, the full decomposition of AB only occurs at a temperature above 1000 °C, with formation of the thermodynamically stable boron nitride. This means that achieving full reversibility of AB is out of reach. Recent investigations focused on modifying the properties of AB via its confinement within a wide range of nanoscaffolds such as SBA-15,[299] carbons,[300] MOFs,[301] boron nitride,[302] and polypyrrole nanotubes.[303] We recently showed the possibility of achieving reversibility with a nanosized AB/Ni matrix at 200 °C and 6 MPa.[24c] This demonstrates that some paths may enable the use of AB derived compounds as reversible hydrogen storage materials.

Following the example of AB, attempts have also been made to synthesize novel compounds incorporating both hydridic and protic hydrogens, through the reaction of NH_3 with borohydrides, for example. The possibility to synthesize ammine borohydride was reported many decades ago.[304] As illustrated by Figure 19b, this strategy leads to a destabilization of borohydrides involving metals of high electronegativity. In contrast, borohydrides with metallic cations of low electronegativity were found to be more stable. Borohydrides combined with NH_3 have shown hydrogen capacities reaching 17.8 mass%, with in some cases the protic and hydridic hydrogen enabling hydrogen release at near room temperature. For example, 8.9 mass% of hydrogen was released from $Zn(BH_4)_2 \cdot 2NH_3$ and 16.8 mass% of hydrogen was released from $Al(BH_4)_3 \cdot 5NH_3$.[305] However, some studies suggested that the thermal decomposition of ammine borohydrides causes a loss of ammonia during the hydrogen release and this contributes to the irreversibility of these systems. For example, $LiBH_4 \cdot NH_3$[306] and $Ca(BH_4)_2 \cdot nNH_3$ ($n = 1$, 2, and 4)[306d,307] mainly release ammonia rather than hydrogen below 300 °C under dynamic vacuum. Furthermore, combinations of different amine borohydrides with borohydrides, such as $Al(BH_4)_3 \cdot 4NH_3/2LiBH_4$,[305] $LiMg(BH_4)_3(NH_3)/LiBH_4$,[308] $Ca(BH_4)_2 \cdot 2NH_3/LiBH_4$,[306d] and $Ca(BH_4)_2 \cdot 4NH_3/Mg(BH_4)_2$[307a] can significantly increase the available amount of hydrogen while improving the issue of hydrogen purity.

8. The Nanosizing Approach

To enhance the effects of the basic concepts discussed above, intensive experimental work has been carried out in recent years on the hydrogen sorption properties of various hydride materials upon nanosizing, i.e., a reduction of the hydride particle size to a few nm (Figure 6c).[309] Upon nanosizing, improved thermodynamics, e.g., ΔH decreasing from 74.5 to 44.5–66 kJ mol^{-1} H_2 was reported for Mg/MgH_2,[309a-d,310] faster hydrogen kinetics, e.g., E_A decreasing from 116 to 58 kJ mol^{-1} H_2 for $NaAlH_4$ nanoparticles of 2–10 nm,[183,309q,311] and reduced hydrogen desorption temperatures[309f,312] were observed. For

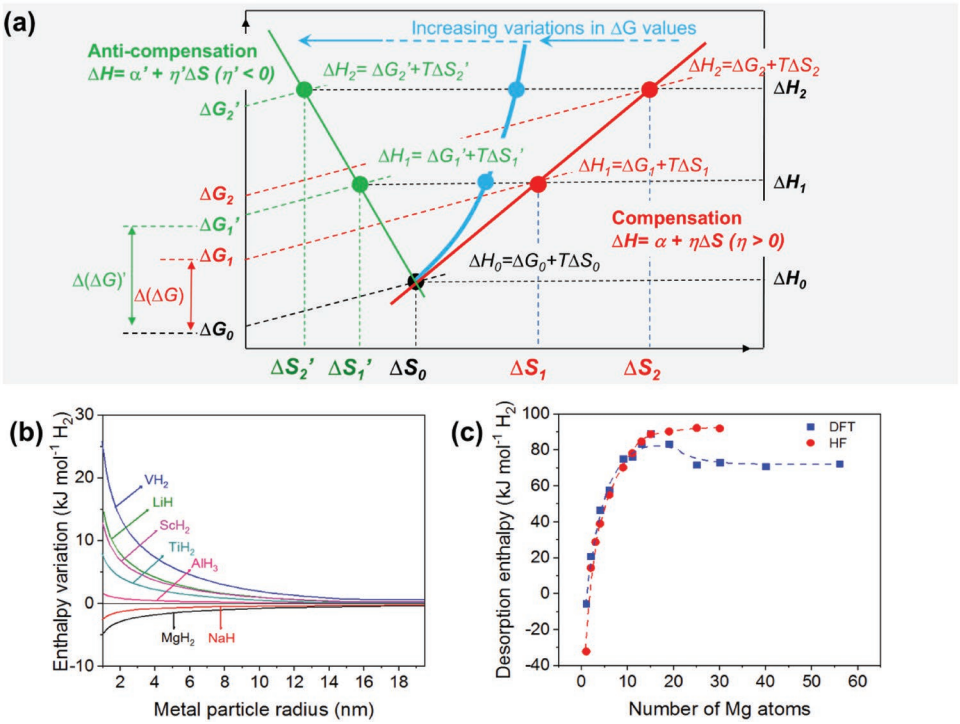

Figure 20. Thermodynamics of metal hydrides at the nanoscale a) Schematic correlation between ΔH and ΔS of nanosized hydrides and the role of ΔG variation ($\Delta(\Delta G)$). The correlation between ΔH and ΔS depends upon the variations of ΔG as compared to the variation ($\Delta(\Delta H)$). If ($\Delta(\Delta G)$) < ($\Delta(\Delta H)$) a compensation effect is observed and an anticompensation effect is reached for the reverse, i.e., for ($\Delta(\Delta G)'$) > ($\Delta(\Delta H)$); b) theoretically calculated evolution of ΔH for various metal/metal hydrides systems at the nanoscale;[322] c) theoretically evaluated desorption enthalpy for MgH_2 clusters with both HF and DFT methods as a function of the numbers of Mg atoms.[323c]

example, LiH confined high surface area graphite released hydrogen at 350 °C instead of 680 °C.[309f] Mg nanoparticles with the size of 4 nm incorporated in CMK3 showed a remarkable decrease in hydrogen desorption temperature of 253 °C.[309b] Milder temperatures and pressures for achieving hydrogen reversibility[313] have also been reported for some complex hydrides and this was attributed to an alteration of reaction pathways upon nanosizing.[309i,314] For example, carbon nanotubes confined $LiBH_4$ showed a single decomposition at 140 °C, much lower than the temperatures required for bulk $LiBH_4$ (>400 °C) and some hydrogen reversibility.[313a,314b] Similarly, the hydrogen desorption temperature was found to be much lower for nanoconfined $NaBH_4$ (150 °C),[313a] $LiAlH_4$ (120 °C),[315] $NaAlH_4$ (≈180 °C)[309s] compared to their bulk counterparts.

8.1. Nanosizing for Better Thermodynamics

It is widely accepted that particles at the nanoscale display different physical/chemical properties as compared to their bulk counterparts as a result of their higher surface energy.[186,316] In this case, when considering a reaction with nanoscale materials, the Gibbs free energy (ΔG_{nano}) can be expressed as

$$\Delta G_{nano} = \Delta G_{bulk} + \Delta G_{surf} \quad (74)$$

where ΔG_{bulk} is the reaction Gibbs free energy of the bulk material (i.e., the core of the nanoparticle) and ΔG_{surf} corresponds to the excess of surface energy owing to the nanodimension of the material and the excess energy arising from unsatisfied surface atoms bonds.[27e,316] When considering a hydrogenation reaction, the basic thermodynamic laws described above (section 3.2) still apply and

$$\Delta G_{nano} = RT \ln \frac{P^{eq}_{nano}}{P} \quad (75)$$

where P^{eq}_{nano} is the equilibrium pressure of the nanosized hydride.

Hence, by associating (74) and (75),

$$\ln \frac{P^{eq}_{nano}}{P^{eq}_{bulk}} = \frac{\Delta G_{surf}}{RT} \quad (76)$$

Thus at a given temperature and assuming sufficient excess of surface energy, the equilibrium pressure for the hydriding reaction of nanoparticles will be higher than that for the bulk material. Hence in principle, the thermodynamics of the hydrogen absorption and desorption reactions could be tailored by adjusting the surface energy of nanosized hydrides (**Figures** 14a and **20**). Further considering Equations (21) and (74), the van't Hoff equation for the hydrogen storage reactions at nanoscale takes the form

$$\ln \frac{P^{eq}_{nano}}{P^{\circ}} = \frac{\Delta H^{\circ}}{RT} - \frac{\Delta S^{\circ}}{R} + \frac{\Delta G_{surf}}{RT} \quad (77)$$

In this equation, the surface Gibbs free energy (ΔG_{surf}) is a function of temperature[317] as observed experimentally[318]

$$\Delta G_{surf} = \Delta H_{surf} - T\Delta S_{surf} \quad (78)$$

Combining (77) and (78) leads to a new van't Hoff equation for nanoscale materials

$$\ln \frac{P^{eq}_{nano}}{P^{\circ}} = \frac{\Delta H^{\circ} + \Delta H_{surf}}{RT} - \frac{\Delta S^{\circ} + \Delta S_{surf}}{R} \quad (79)$$

Hence through nanosizing, additional factors could affect both the ΔH and ΔS of the hydriding reaction. Indeed, for individual particles both ΔH and ΔS have been observed to vary at the nanoscale.[319]

In the context of hydride materials, it is difficult to predict a general trend for ΔH and ΔS as function of particle size, since this is highly subjective to the particle size and the nature of the reactants and products. An additional factor to consider is the long-standing empirically proposed "enthalpy–entropy compensation effect" which has been observed for some hydrides;[320] although it has been proposed that it may be a phantom phenomenon.[27d,321]

8.1.1. Thermodynamics of Nanosized Metal Hydride Systems

By taking into consideration the above, the thermodynamics of nanosized hydrides could potentially be controlled by an additional surface free energy term expressed as[27e,316]

$$\Delta G_{surf} = \frac{3V_M}{r}\left[\gamma_{MH_2}(r)\left(\frac{V_{MH_2}}{V_M}\right)^{\frac{2}{3}} - \gamma_M(r)\right] + E_{ads} \quad (80)$$

where V_M is the molar volume, r is the particle radius and γ the surface free energy per surface unit. The additional energy term (E_{ads}) is the result of the difference in surface energy between the nonhydrided and hydrided nanoparticle upon hydrogen binding.[27e,316]

Therefore, ΔG_{surf} depends upon the particle size, its nanostructure, and the surface properties of the nanosized hydride as well as E_{ads}. The latter is hard to predict. If ΔG_{surf} displays a positive value, the system will be destabilized. Otherwise, the hydride phase will be stabilized.

Theoretical calculations regarding the evolution of ΔH have been carried out for various hydrides using the Wulff construction.[322] As shown in Figure 20b, the enthalpy variation introduced by nanosizing effects differs significantly for different M/MH systems and depending on the M/MH system a destabilization or stabilization may occur. However, according to these calculations, these effects only occur at extremely small particle sizes. Similar conclusions have been suggested by additional theoretical calculation on Mg/MgH_2 (Figure 20c).[323]

Although theoretical calculations suggest that the particle size needs to be very small (<5 nm) for any observable thermodynamic alteration (Figure 20b,c),[322] or even smaller for Mg/MgH_2 (<1 nm),[323a,c,d] reduction of enthalpy has been commonly reported experimentally for relatively large particles (10–50 nm).[182a,309a,d,g,324] The divergence between experimental observations and theoretical calculations is possibly explained by the fact that theoretical simulations are often simplified and performed in vacuum without consideration of the chemical/physical environment that exists experimentally. Furthermore, the experimentally determined thermodynamic parameters are significantly affected by measurement methods and the experimental conditions used[126b] – hence, the significant disparities in experimental observations. It is noteworthy that particle size alone is not a determining factor for the reduction of ΔH observed (**Figure 21**a). The experimentally determined ΔH is greatly affected by the synthesis method which conditions the nanoparticle surface state, structure, and the atomic arrangements at the nanoparticle core.[126b] In an attempt to exclude parameters associated with synthetic variations, we investigated the evolution of thermodynamics as a function of the particle size reduction of the Mg/MgH_2 and $LaNi_5/LaNi_5H_6$ systems.[182a,309g] In both cases, the correlation of enthalpy and entropy was found to follow the linear "enthalpy–entropy compensation" effect as previously described for other chemical systems (Figure 21c,d). A similar trend was reported for Pd nanoparticles[325] and other hydrides.[309g,326] Such a compensation effect has also been observed experimentally for several chemical systems.[320]

Evolution of the entropy during hydrogen uptake and release mainly occurs through the conversion of hydrogen from the gaseous phase to its chemisorbed state in the hydride phase. This entropic value is often considered to be constant and equal to 130 J mol^{-1} K^{-1} for many hydrides.[27e] However, for nanomaterials, besides the dominant contribution of hydrogen, additional effects due to the higher degree of disorder in both the starting and final hydride material cannot be neglected and thus the effect of the additional ΔS_{surf} factor in the van't Hoff Equation (79) must be considered.[316]

Owing to the complexity of determining entropic evolution by theoretical modeling, there have not been reports on possible enthalpy–entropy compensation effects by theoretical calculations. However, assuming that the experimentally observed "enthalpy–entropy compensation" effects are real, this does not favor lower hydrogen desorption temperatures $\left(T_{1bar} = \frac{\Delta H}{\Delta S}\right)$ because any targeted reduction in temperature induced by ΔH will lead to a similar reduction in ΔS. This in turn limits the increase in the equilibrium pressure. This correlation of ΔH and ΔS could be reversed through a distinct alteration of ΔG as further discussed below (Figure 20a); however, strategies to do so have not been found yet.

8.1.2. Thermodynamics of Nanosized Complex Hydrides

The hydrogen absorption and desorption processes of complex hydrides are more complicated as compared to metal hydrides systems, since complex hydrides generally involve multistep reactions with additional side reactions generating byproducts.[123] Accordingly, it is very difficult to predict any thermodynamic evolution of the hydrogen properties of complex hydrides at the nanoscale.[16a] In addition, during hydrogen release, complex hydrides undergo significant entropic

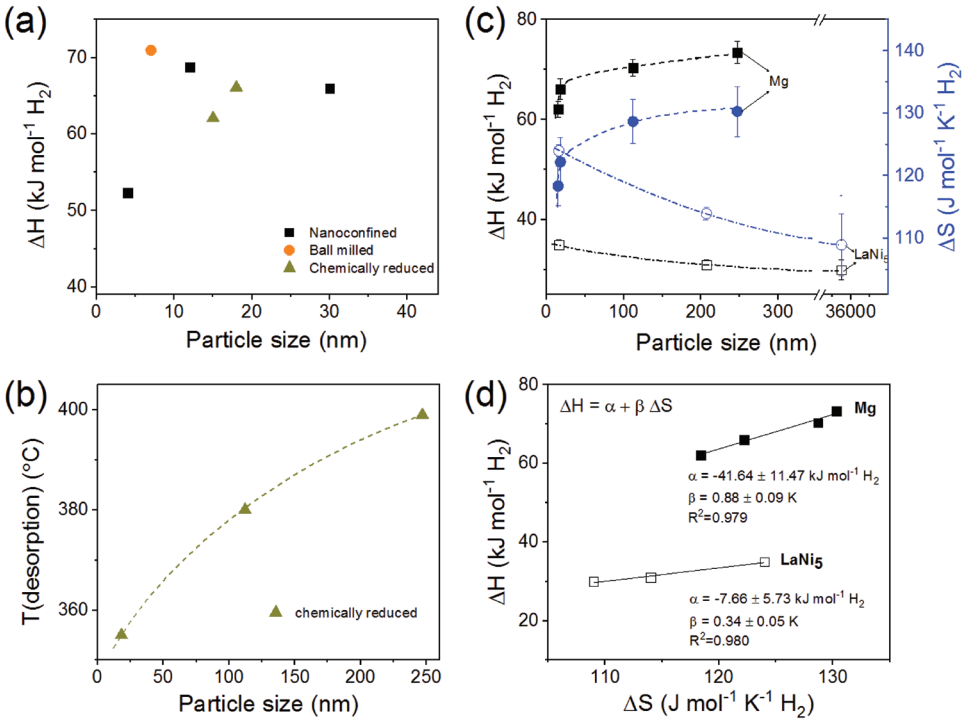

Figure 21. Thermodynamic properties of metal hydrides at the nanoscale. a) Summary of reported values[182a,309a,b,d,326b] of ΔH for nanosized Mg/MgH_2 as function of Mg particle size; b) particle size dependent hydrogen desorption temperature of MgH_2 particles synthesized by chemical reduction;[182a] c) particle size dependence of ΔH and ΔS for Mg[182a] and $LaNi_5$[309g] when synthesized using the same method and similar conditions; d) correlation of ΔH and ΔS for Mg[182a] and $LaNi_5$.[309g]

evolution owing to the number of products formed. Another typical characteristic of complex hydrides is their melting upon decomposition, e.g., $LiAlH_4$ melts at 150–175 °C and this does not simplify the behavior of such hydrides at the nanoscale.

There are various models that have been proposed to predict the melting temperature (T_{nano}) of nanoparticles.[327] For example, for spherical nanoparticles, Qi proposed that[328]

$$T_{nano} = T_{bulk}\left(1 - \frac{2d}{D}\right) \quad (81)$$

where T_{bulk} is the melting temperature of the bulk material, d is the diameter of the atom and D is the diameter of the nanoparticle.

Therefore, the melting point for nanoparticles is lower than that of the corresponding bulk material. For free standing complex hydride nanoparticles, this means that they would melt at lower temperatures and if this occurs before the release of hydrogen, the molten nanosized hydrides will simply behave like their bulk counterparts. One strategy to minimize this effect is to confine the nanoparticles within a stable inorganic scaffold.[186,329] By doing so, the diffusion of the decomposition products upon hydrogen release is further restricted and this facilitates hydrogen reversibility. Another approach is to suppress the melting behavior of complex hydrides through elemental doping.[330]

Assuming that the initial hydride nanoparticles retain their nanofeatures, the thermodynamics and kinetics of the hydrogen absorption and desorption reactions of nanosized complex hydrides should deviate from the behavior of their bulk counterparts. In this case, the trends described above should apply to each reaction step involved in the dehydrogenation or re-hydrogenation process. Therefore, for individual reaction step at a given temperature a shift of the equilibrium pressure should be observed depending on the evolution of the nanoparticles and their disproportionation upon hydrogen release or uptake.

With $NaAlH_4$ as an example, it has been suggested from experimental observations that a shift of the equilibrium pressure occurs upon nanosizing and this leads to a destabilization of the hydride and the disappearance of the two step decomposition mechanism in favor of a single step (**Figure 22**a,b).[331] The theoretically calculated phase diagram and reaction map as function of particle size and temperature suggest similar assumptions.[332] In this case, the intermediate decomposition phase, Na_3AlH_6, would be destabilized upon nanosizing and this would result in a positive ΔG_{surf} value for the first decomposition step ($NaAlH_4 \rightarrow 1/3Na_3AlH_6 + 2/3Al + H_2$) but a negative ΔG_{surf} value for the second step ($1/3Na_3AlH_6 \rightarrow NaH + Al + 1/2H_2$)[331] leading to a single step decomposition from $NaAlH_4$ to NaH. The actual decomposition process of nanosized $NaAlH_4$ is probably more complex than this simplified assumption.[332a]

Similar thermodynamic alterations were observed for $LiAlH_4$ and $LiBH_4$ confined in carbon nanotubes (diameter 2 nm) with a single broad hydrogen release peak instead of multiple peaks corresponding to the multiple decomposition steps of the bulk materials.[314b] $LiAlH_4$ nanoparticles (2–16 nm) synthesized by

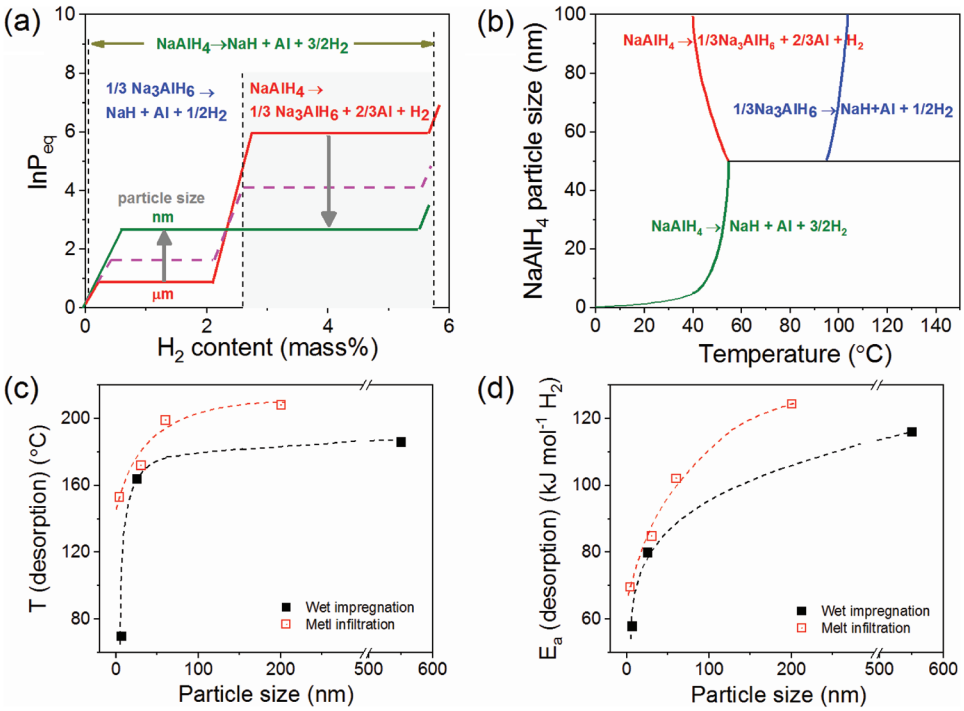

Figure 22. Thermodynamics and kinetics of complex hydrides at the nanoscale. a) Diagram of equilibrium plateau pressure shift observed for $NaAlH_4$ upon nanosizing. Adapted with permission.[331] Copyright 2010, Elsevier; b) reaction map indicating the thermodynamically favored decomposition paths for nanosized $NaAlH_4$ as a function of the particle size and the temperature. Adapted with permission.[332a] Copyright 2010, ACS; evolution of c) the hydrogen desorption temperature and d) the activation energy (E_a) of nanoconfined $NaAlH_4$ through pore impregnation[309q] and melt infiltration.[572]

solvent evaporation with Ti doping also decomposed to LiH, Al and H_2 directly via a single step ($LiAlH_4 \rightarrow LiH + Al + \frac{3}{2}H_2$).[315] However, a single step decomposition is not an inevitable outcome of nanosizing. For instance, high surface area graphite (HSAG) supported $LiAlH_4$ nanoparticles with the size ranging from 3–15 nm still followed the three decomposition steps of bulk $LiAlH_4$.[256] Once again, the thermodynamic evolution upon particle size reduction is affected by the chemical/physical environment of the nanoparticles. But if such a concept could be controlled, nanosizing could potentially lead to a one step decomposition of the complex hydrides at low decomposition temperatures. Another benefit of the nanosizing approach is the suppression of side products. For example, the elimination of diborane (B_2H_6) release upon borohydride or ammonia borane nanoconfinement has been reported.[309i,333]

Evolutions of ΔH and ΔS for complex hydrides upon nanosizing are barely reported in the literature due to the difficulty of measuring the full equilibrium plateau pressure at varying temperatures and the poor stability of nanoconfined complex hydrides upon hydrogen cycling. Therefore, the reported thermodynamic alterations are often embodied in the better reversibility and changed pathways. Hence, the reversible hydrogen storage reported for various complex hydrides, e.g., $LiAlH_4$, $LiBH_4$, $NaBH_4$, Mg $(BH_4)_2$, Ca $(BH_4)_2$,[256,313] upon nanosizing assumes an alternation of their thermodynamics.

It should be noted again that the main approach to nanosize complex hydrides is through the use of a inorganic porous host, and thus the reversible hydrogen capacity of these nanoconfined hydride is often too low for application (<1 mass%). This means that better approaches to stabilize and confine the nanoparticles need to be developed. One possible strategy is via a core–shell method.[186] For example, a remarkable reversible capacity of 5 mass% was achieved for $NaBH_4$–Ni core shell structure.[334]

8.1.3. The Enthalpy–Entropy Compensation Effect

Enthalpy–entropy compensation effect is a phenomenon observed for homologous reactions with ΔH and ΔS evolution following the same trend along the proposed linear correlation[320a,335]

$$\Delta H = \alpha + \eta \Delta S \tag{82}$$

where α and η are constants. As discussed above, similar compensation effects have been observed for metal hydrides (Figure 21d) and understanding this phenomenon is critical to achieve any significant improvement in the hydrogen sorption thermodynamics of nanosized hydrides.

Different hypotheses have been advanced to explain the enthalpy/entropy compensation effect observed in chemical systems involving solvents or variations in surfactant chain length, for example.[320b-d,321a,336] But one approach to better describe the observations made to date is by considering the interrelation between ΔH, ΔS, and ΔG.[320a] Hence, according to Pan et al. by comparing (16) and (82), it can be proposed that α and η should have the same dimension as that of ΔG and T,

respectively.[320a] Under these conditions, ΔG and T should have distinct values and be constant.

Following this principle, by varying a parameter experimentally (e.g., the particle size of the absorbing hydrogen material), the observation of small differences in ΔG at a constant temperature upon particle size variation, should then lead to a positive slope (η) corresponding to a compensation effect. The intercept (α) would correspond to the average of all the small variations in ΔG values (Figure 20a). However, if the variations in ΔG are large, i.e., very dissimilar values of ΔG are obtained at a constant temperature for different particle sizes; a nonlinear or curved correlation will be observed (Figure 20a). At larger variations of ΔG in comparison to ΔH this would result in an anticompensation effect (Figure 20a).

Observation of such enthalpy/entropy anticompensation effects has been reported for molecular pairs in solutions and the complexation of metal ions,[337] so these are not uncommon. Applying this concept to nanoscale hydrides, this means that variations of ΔG should be related in the first instance to variations in ΔG_{surf} and the correlation between ΔH and ΔS upon nanosizing. Achieving anticompensation effects for nanosized hydrides is highly desirable because it would lead to a significant improvement in the thermodynamics upon hydrogen cycling, but to date, methods to achieve this are unknown.

8.2. Nanosizing for Better Hydrogen Sorption Kinetics

While the scenario for nanosizing induced thermodynamics evolution is complicated, the kinetics has been universally reported to be improved for both metal hydrides[311a,338] and complex hydrides[309j,v,316,339] upon nanosizing. Often, the lower desorption temperatures reported for nanosized hydrides are claimed to be the results of kinetic enhancements. However, it should also be noted that the experimental hydrogen desorption temperatures determined by thermal gravimetric methods coupled with mass spectrometry are the result of combined effects of thermodynamic and kinetic evolutions and thus not conclusive.

Nanosizing has the potential to lead to a reduction of kinetic barriers by facilitating the dissociation/recombination of hydrogen at the surface and the diffusion of hydrogen (Figures 8 and 10c). Through nanosizing, the surface-to-volume ratio of the material is remarkably increased, which means that more atoms are exposed to the surface, and this results in an increased number of adsorption and dissociation sites, in the form of steps, kinks, corners and edge atoms.[27e,126b] As for the penetration and diffusion process, the easiness for hydrogen atoms or ionic species to diffuse in the material depends upon the nature of the atomic organization within the nanoparticle core but assuming very small particles a significant reduction of diffusion lengths should improve hydrogen kinetics.[195a,338b] For relatively small particles, the number of nucleation points for the growth of the hydride phase should be limited and thus this should also contribute to faster kinetics since the likelihood of forming a blocking MH/M layer through which the reactive phases have to diffuse is reduced (Figure 8b). Hence, if all these barriers are removed, the kinetics of the reaction should be solely controlled by the nucleation and growth of the hydride or dehydrogenated phase. This last step mainly depends upon the material structure and composition as well as the temperature and pressure conditions used to drive the hydrogen absorption/desorption process.[44] In complex hydrides, this assumes that during hydrogen cycling the decomposition products are easily recombined and thus "active" toward hydrogen and ionic mobility as well as tightly confined and restricted from diffusing away.

Similar to enthalpy evolution for thermodynamics, the kinetics improvement is not strictly determined by the particle size and often the experimentally obtained E_a values may significantly vary depending on the synthesis methods and experimental conditions (**Figure 23**a). However, when the chemical/physical environment of the nanoparticles is controlled and restricted, E_A appears to depend upon particle size reduction, i.e., smaller particles display a lower E_A that favors faster reaction rates and lower temperatures (Figure 22c,d). More remarkably, this seems to hold for both metal hydrides and complex hydrides (Figures 22d and 23a).

However, it should be noted that this correlation may be affected by the pre-exponential factor (A) (from the Arrhenius equation $k(T) = Ae^{\frac{-E_a}{RT}}$) that may vary for different materials. The correlation between the pre-exponential factor (A) and E_a for hydrogen storage reactions is barely evaluated in literature. With Mg as an example, Figure 23b,c summarizes selected experimental results from the literature and existing discrepancies. Accordingly the validity of a pre-exponential factor-activation energy compensation effect is still to be determined.

8.3. Looking Beyond the Particle Size Reduction to Enable Practical Hydrogen Storage

There is now much evidence suggesting that nanosizing is an approach that could potentially lead to the design of practical hydrogen storage materials with high hydrogen capacity and cycling capability near the ambient. These observed improvements in hydrogen properties are not the direct consequence of particle size reduction, but the result of interrelated parameters including: i) the nanosized hydride surface/host interaction, ii) the structural and atomic order/disorder of the nanosized hydride core and surface, and iii) the nanostructure/hydrogen properties relationships including atomic coordination states, hydrogen bonding sites, and diffusion mechanisms. Many of these factors are currently not very well understood, including the interaction of hydrogen with nanosized materials and this constitutes an important barrier for progress. An obvious limitation is also in the effective achievable hydrogen storage capacity through the nanosizing approach,[309c,311a,313a,324,340] and alternative approaches must emerge to enable the synthesis of nanosized hydrides via optimum stabilization methods, where weight, volume, heat convection, diffusions paths and distances are appropriately managed. Reactant residuals, surfactants or stabilizers, as well as the scaffold or support materials for nanoconfinement are a dead mass to the hydride material and this leads to a decrease of the effective hydrogen storage capacity. The additional sensitivity of hydrides to oxidation and exacerbated reactivity at the nanoscale is also a challenge, not only in the synthesis of the nanosized hydrides but also upon material handling and

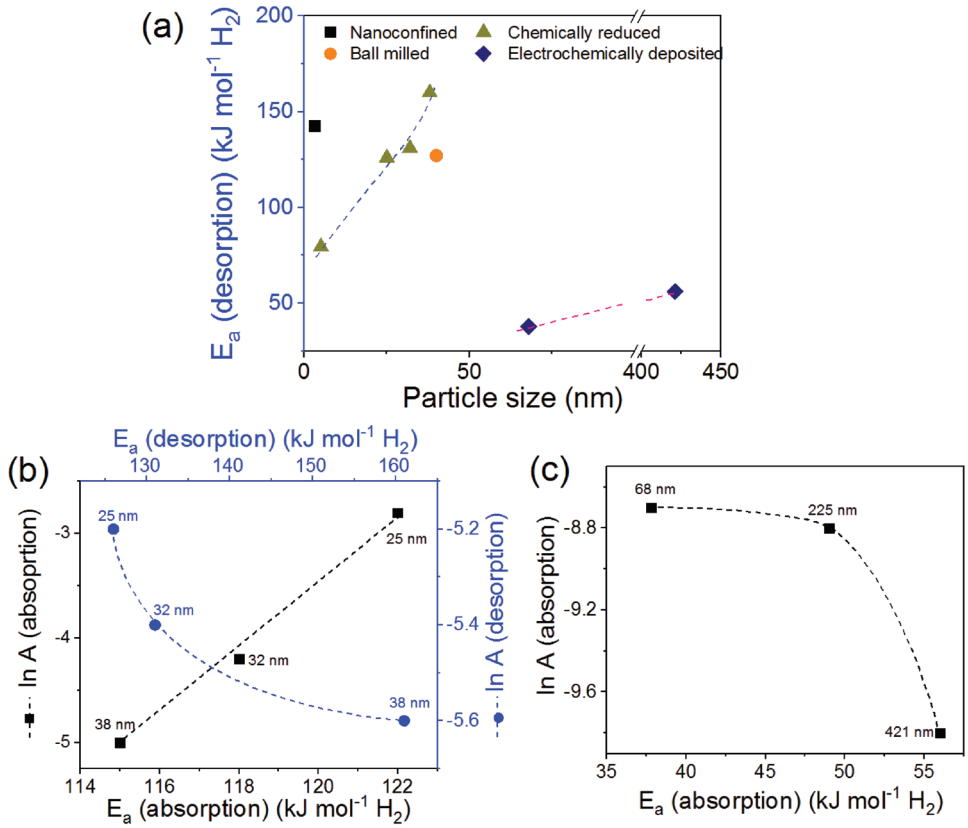

Figure 23. Activation energy (E_a) and pre-exponential factor (A) of Mg at the nanoscale. a) Size dependence E_a for Mg synthesized by chemical reduction[53a,311a] and electrochemical deposition;[183] b) correlation between A and E_a for Mg nanoparticles. Values were extracted from the literature.[53a,183]

hydrogen cycling. For example, the reversible hydrogen storage capacity demonstrated for some complex hydrides through nanosizing tends to decrease with cycling because of the side reactions of the hydrides with the host material and/or a loss of nanoconfinement. Ideally, the method of confinement should retain the nanosized features of the hydride upon hydrogen uptake and release, and protect it from any "aggressive" environment. Synthetic paths to achieve this have been reviewed elsewhere.[126b,186] Along this, a narrowing of the equilibrium plateau pressure has also been observed owing to the lower number of hydrogen binding sites in metal hydride nanoparticles,[309g,325] and this would mean that nanosized hydrides could potentially display low hydrogen storage capacities because of the small "bulk" volume of nanoparticles. Such behavior has not currently been observed with complex hydrides, and may be overcome by designing nanostructures that can accept more hydrogen atoms per site than their bulk counterparts.

9. Designing Novel Hydrogen Storage Materials with Modeling Guidance

The outcomes of computer simulations may also contribute greatly to the design of hydrogen-storage materials. Computer simulations can be used to rationalize the causes behind unresolved observations as the systems and processes of interest can be accessed at the atomic scale under controlled conditions. Indeed, key properties for the design of hydrogen-storage materials, which may be difficult to measure in practice, e.g., molecular absorption/adsorption energies and kinetic energy barriers, can often be estimated accurately with theory. In addition, from a resource point of view, computer simulations are inexpensive. For instance, by using open-source software with a standard office computer, one can already simulate complex gas-adsorption phenomena and assess the thermodynamic stability of energetically competitive crystal polymorphs – provided that fine interaction models are in use. Consequently, modeling of materials can be done systematically and ahead of the experiments in order to provide useful analytical guidance.

The reliability of computer simulations in mimicking real systems, however, strongly relies on the simplifications made in the adopted methods and structural models. In materials modeling there is a trade-off between structural model reliability and computational method accuracy and this is due to practical limitations. Hence, if the approach is to employ accurate first-principles methods (see next sections) then the simulations are likely to be performed at zero temperature and by considering perfectly ordered atomic/molecular systems, which may result in unrealistic conditions as compared to the experimental conditions. Likewise, to study gas-absorption phenomena at high temperatures on systems containing large concentrations of crystalline defects, the calculations will be preferentially performed with classical interatomic potentials, which may suffer from critical transferability issues and in general low predictive

power. Fortunately, there are ways of achieving a suitable balance between computational accuracy and model reliability and it is the responsibility of the modeler to balance these requirements in order to provide meaningful guidance. In the next section, some relevant quantities that can be estimated efficiently with computer simulation methods in order to boost and further rationalize the design of hydrogen-storage materials are discussed. Then, the energy-force methods that can be used to calculate such quantities are briefly reviewed by emphasizing some of their advantages and limitations.

9.1. Modeling Key Physical and Chemical Properties of Hydrides

9.1.1. Hydrogen Bonding Strength

The strength of hydrogen molecule binding to a material serves as a measure of its potential for hydrogen storage applications. The hydrogen binding energy is defined as

$$E_{\text{bind}}(\text{H}_2) = E_{\text{el}}(\text{M}) + n/2E_{\text{el}}(\text{H}_2) - E_{\text{el}}(\text{MH}_n) \tag{83}$$

where $E_{\text{el}}(X)$ represents the energy of system X calculated by considering all atoms perfectly still at their equilibrium positions, M the material under study, and MH_n the same material but with n adsorbed hydrogen atoms.

The more (less) positive E_{bind} is, the stronger (weaker) hydrogen is bound to M. In order to meet the target of low temperatures for hydrogen release and uptake, the hydrogen binding energy of a material should lie within the interval $0.7 > E_{\text{bind}} > 0.2$ eV/H_2.[341] Such a binding energy interval, from which thermal effects are explicitly excluded, holds both for hydrogen absorption and hydrogen adsorption.

Adsorption of hydrogen molecules (that is, H_2 binding to the surface of a material) also can be simulated directly at finite temperatures with Monte Carlo (MC) methods.[342] In MC simulations random Markovian moves are used to sample a particular statistical mechanical ensemble in order to provide averaged quantities (e.g., equilibrium gas uptake and enthalpies). Adsorption isotherms, for instance, can be estimated in grand canonical MC simulations as the average number of uptake molecules, where the temperature and volume of the system are maintained fixed while its chemical potential is allowed to equilibrate with a gas phase that is not explicitly simulated. MC simulations, however, involve the use of large simulation cells (≈1000 atoms) and numerous sampling moves (>1 000 000), hence normally they are performed with semiempirical interaction models, e.g., force fields (see next section).

9.1.2. Enthalpy of Hydride Formation

As previously discussed, the enthalpy of hydride formation indirectly determines the hydrogen absorption/desorption temperatures and kinetics (assuming a constant entropy). The simplest way of hydrogenating a metal (M) is through direct dissociative chemisorption (Figure 8a).

The enthalpy of formation ΔH_{f} of the resulting metal hydride (MH_n) then can be expressed as

$$\Delta H_{\text{f}} = (E + pV)_{\text{MH}_n} - (E + pV)_{\text{M}} - \frac{n}{2}(E + pV)_{\text{H}_2} \tag{84}$$

where the dependence on temperature is implicitly introduced via the pV terms.

Since the molar volumes of the metal hydride and metal in general are small as compared to that of the gas, the expression above can be approximated as[343]

$$\Delta H_{\text{f}} \approx \Delta H_{\text{el}} + \Delta H_{\text{ZPE}} + \delta\Delta H_{\text{T}} \tag{85}$$

where

$$\Delta H_{\text{el}} = E_{\text{el}}(\text{MH}_n) - E_{\text{el}}(\text{M}) - \frac{n}{2}E_{\text{el}}(\text{H}_2) \tag{86}$$

$$\Delta H_{\text{ZPE}} = E_{\text{ZPE}}(\text{MH}_n) - E_{\text{ZPE}}(\text{M}) - \frac{n}{2}E_{\text{ZPE}}(\text{H}_2) \tag{87}$$

$$\delta\Delta H_{\text{T}} = E_{\text{vib}}(\text{MH}_n) - E_{\text{vib}}(\text{M}) - \frac{n}{2}\left[\frac{7}{2}k_{\text{B}}T + E_{\text{vib}}(\text{H}_2)\right] \tag{88}$$

E_{el} represents the energy of the system calculated by considering the atoms perfectly still at their equilibrium positions; E_{ZPE} and E_{vib} are respectively the zero-point and vibrational energies of the material, which are estimated as

$$E_{\text{ZPE}} = \frac{1}{N_q}\sum_{q,s}\frac{1}{2}\hbar\omega_{qs} \quad E_{\text{vib}} = \frac{1}{N_q}\sum_{q,s}\frac{\hbar\omega_{qs}}{e^{\frac{\hbar\omega}{k_{\text{B}}T}} - 1} \tag{89}$$

where the summations run over wave vectors q and phonon branches s, N_q is the total number of wave vectors used for integration within the first Brillouin zone, and ω_{qs} are the phonon frequencies of the system.

By following Equations (85)–(89) and using first-principles methods for the calculation of zero-temperature energies and phonon frequencies (see Section 8.2.), it is possible to estimate the formation enthalpy of metal hydrides with reasonable accuracy (**Figure 24**). We note, however, that in this case the level of agreement with the experiments may depend somewhat on the approximation used for the exchange-correlation energy. This effect is explicitly shown for alkaline earth metal hydrides in Figure 24, where the enthalpy values obtained with the LDA and GGA approximations tend to bound the experimental data either by below or above.[343]

9.1.3. Thermodynamic Stability of Polymorphs

The calculation of phonon frequencies also may provide some valuable information on the thermodynamic and vibrational stability of crystal polymorphs. Phonon frequencies and vibrational modes can be calculated efficiently with several techniques, including linear response theory[344] and the small displacement method.[345] For a crystal to be vibrationally stable all the phonon frequencies at any arbitrary wave vector belonging to its Brillouin zone must be real, i.e., nonimaginary. Once the phonon frequencies of a given system are known, one

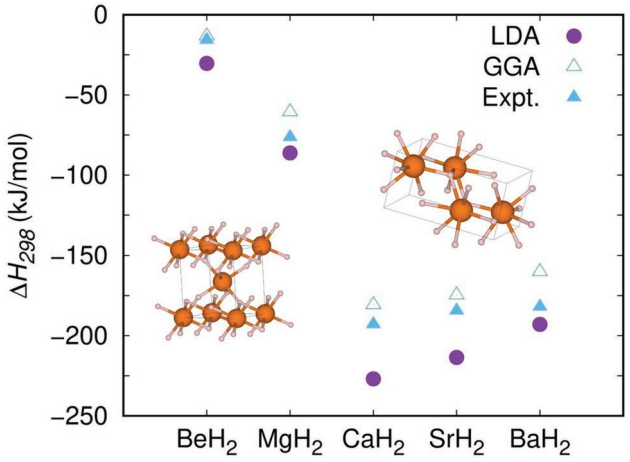

Figure 24. Enthalpy of formation of several alkaline earth metal hydrides at room temperature. LDA and GGA points refer to first-principles results obtained with local and semi-local density functional theory techniques, respectively. The sketched atomic configurations correspond to the rutile (left) and contunnite (right) structures rendered by the stable phases of small-radius and large-radius metal atom hydrides, respectively. Hydrogen (metal) atoms are represented with small (large) spheres. Reproduced with permission.[343] Copyright 2008, IOP Publishing Ltd.

can use the quasi-harmonic approximation to estimate the corresponding Gibbs free energy

$$G = F_{hz} + pV = H - TS \tag{90}$$

where F_{hz} represents the Helmholtz free energy.

In the quasi-harmonic approximation it can be assumed that the potential energy of a crystal can be estimated as a quadratic atomic-displacement expansion around the equilibrium configuration.[346] The system is then mapped onto a collection of noninteracting harmonic oscillators with frequencies ω_{qs} and energy levels $E^{N}_{qs} = (1/2 + n)\cdot\omega_{qs}$. The Helmholtz free energy of such a system F_{harm} is analytically known and reads

$$F_{harm} = \frac{1}{N_q} k_B T \sum_{qs} \ln\left[2\sin h\left(\frac{\hbar\omega_{qs}}{2k_B T}\right)\right] \tag{91}$$

By further considering that hydrostatic pressure in a quasi-harmonic crystal can be estimated as

$$p = -\frac{\partial(E_{el} + F_{harm})}{\partial V} \tag{92}$$

the corresponding Gibbs free energy can be determined. Consequently, the thermodynamic stability between different crystal polymorphs can be accurately determined upon calculation and comparison of their *G*s.

The quasi-harmonic approach is particularly well-suited for studying materials with a relatively small number of particles in their unit cells (≈10 atoms) with first-principles simulation methods (see next section). In **Figure 25**, we show quasi-harmonic free-energy results obtained for the hydride $LiBH_4$, a promising hydrogen-storage and ionic conductor material.[347] At ambient pressure, $LiBH_4$ undergoes a first-order phase

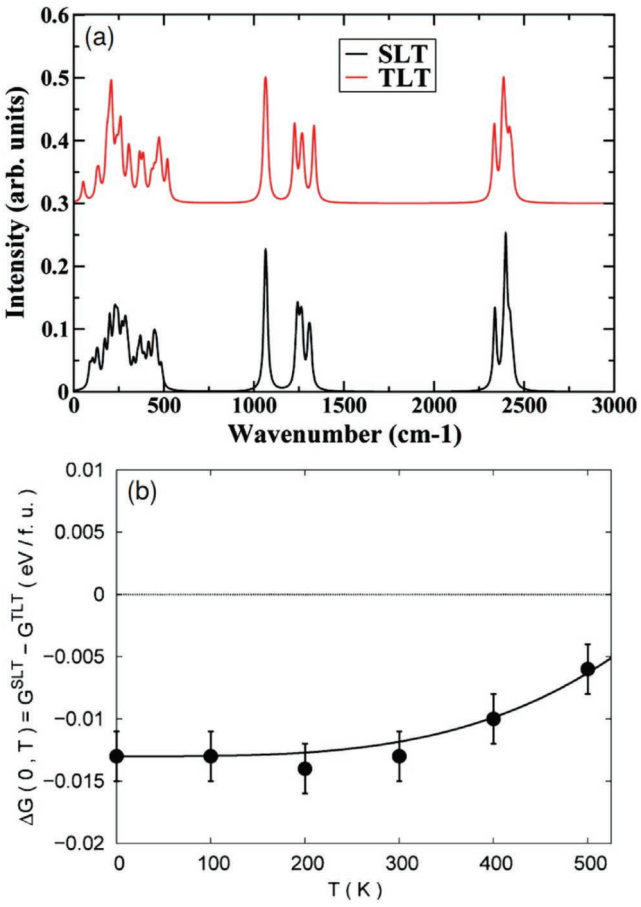

Figure 25. Calculated low temperature and pressure polymorphs stability in $LiBH_4$. a) Density of vibrational states corresponding to the experimentally determined and theoretically predicted low temperature and pressure phases, SLT[348] and TLT[349] respectively; b) Gibbs free-energy difference between the SLT and TLT structures expressed as a function of temperature. The results were obtained within the quasi-harmonic approximation using the small-displacement method.

transition from a low-temperature (LT) phase to a high-temperature (HT) phase around 108 °C;[348] upon further heating, it is possible to liberate 13.1 mass% H_2 via the two-step reaction

$$12LiBH_4 \leftrightarrow Li_2B_{12}H_{12} + 10LiH + 13H_2 \leftrightarrow 12LiH + 12B + 18H_2 \tag{93}$$

The exact crystal structure of the LT and HT phases in $LiBH_4$, however, remain contentious. Experimentally, the LT phase has been ascribed by Soulié et al. to an orthorhombic *Pnma* structure and the HT to an hexagonal $P6_3mc$.[348] Tekin et al. have proposed new candidate structures for the LT and HT phases of $LiBH_4$ based on standard first-principles calculations.[349] At zero temperature, the structures predicted by Tekin et al. are energetically competitive with respect to the ones resolved in the experiments; however, it has been subsequently demonstrated by Shevlin et al. that after considering entropy contributions to the Gibbs free energy, the LT and HT phases are most likely to be the structures proposed by Soulié et al.[348] (Figure 24). This case illustrates the importance of considering thermal effects when assessing the relative stability between

different structures and assigning the correct crystal symmetry to experimentally observed phases.

Another way of assessing the thermodynamic stability of a particular structure or system is to simulate it directly with molecular dynamics (MD) techniques.[350] In MD simulations the trajectories of atoms are determined numerically by solving the corresponding Newton's equations of motion; thermostatting and barostatting techniques can be used along the way in order to reproduce specific thermodynamic constraints, e.g., pressure and temperature. In contrast to quasi-harmonic approaches, anharmonic effects are fully taken into consideration in MD simulations. Nonetheless, large system sizes (≈1000 atoms) and long simulation times (≈1 ns) normally are required in MD simulations so as to obtain well-converged quantities, hence semiempirical interaction models are customarily employed. It is worth noting that Gibbs free energies of crystal polymorphs cannot be accessed directly in MD simulations.

9.1.4. Hydrogen Release and Uptake Kinetics

Besides favorable hydrogen binding energy and thermodynamic stability, it is desirable for hydrogen-storage materials to display quick charge and discharge kinetics. In order to assess such dynamic features, the harmonic transition-state theory[351] can be used to calculate the hydrogen diffusion rate (11). The quantity governing the hydrogen kinetics generally is E_a as it enters Equation (11) via an exponential. The less (more) positive E_a is, the quicker (slower) the uptake/discharge reaction occurs. In practice, E_a is calculated by determining minimum energy reaction pathways. This is commonly done by using the nudged-elastic band (NEB) method,[352] in which a number of intermediate configurations between the initial (e.g., free H_2 molecules and unloaded system) and final (e.g., H_2-loaded system) states are defined and made to interact with their nearest-neighbor images through fictitious harmonic springs. The minimum energy reaction pathway is then determined by minimizing the perpendicular forces along the configuration path. It is relatively easy to perform NEB calculations for materials in which hydrogen molecules are adsorbed since appropriate intermediate configurations can be guessed easily; by contrast, NEB calculations of hydrogen absorption processes involving changes in the stoichiometry of the materials may be convoluted.

9.2. Computational Methods Overview

In materials modeling the interactions between atoms normally are described with energy-force methods that can be classified within two major categories: semiempirical and first-principles. In semiempirical approaches, the forces between particles are modeled via physically inspired analytical functions known as force fields or classical potentials. Force fields contain a number of parameters that are set so as to reproduce a certain amount of experimental data or the results of highly accurate quantum-chemistry calculations. The low computational cost associated with semiempirical approaches makes it possible to address the study of hydrogen-storage materials within ample thermodynamic intervals without sacrificing complexity in the adopted structural models. It is even feasible to reproduce the breaking and forming of bonds during chemical reactions through the use of special reactive force fields.[353] Nevertheless, classical potentials may suffer from impeding transferability issues as due to the impossibility of mimicking the systems of interest at conditions different from those in which the force-field setups were performed. In this context, first-principles methods, also known as ab initio, turn out to be preferable. In first-principles approaches no empirical information is generally assumed on the derivation of the atomic interactions, as those are directly obtained from applying quantum mechanics principles to the electrons and nuclei in the system. Nonetheless, due to their great accuracy, ab initio methods are very demanding in terms of computational expense. Consequently, first-principles calculations generally are restricted to zero-temperature conditions and the involved structural models are highly ideal, i.e., contain a relatively small number of particles ≈100–1000. A third general materials modeling approach exists that is gaining a lot of attention at the moment and which is based on machine learning techniques. Machine learning modeling may combine the best of the first-principles and semiempirical worlds, namely, great accuracy at affordable computational cost. This third approach is entirely mathematically oriented, that is, it employs algorithms and statistical models while leaving aside any chemical intuition. For machine learning techniques to provide reliable information, the constitutive mathematical models need to be built upon extensive "training data" sets usually generated with first-principles methods; how to construct those training sets and generate the desired mathematical models, however, is not always a straightforward and self-contained task. Next, we briefly review the basic ingredients in first-principles, semiempirical, and machine learning modeling of hydrogen-storage materials.[342,354]

9.2.1. First-Principles Methods

The starting point in most first-principles methods is the nonrelativistic Born–Oppenheimer electronic Hamiltonian

$$H_{\mathrm{el}}^{\mathrm{BO}} = -\frac{1}{2}\sum_i \nabla_i^2 - \sum_I \sum_i \frac{Z_I}{|\mathbf{R}_I - \mathbf{r}_i|} + \sum_i \sum_{j\neq i} \frac{1}{|\mathbf{r}_i - \mathbf{r}_j|} \tag{94}$$

where Z_I represent nuclear charges, $\mathbf{r}_i$ the positions of electrons, and $\mathbf{R}_I$ the positions of nuclei (which are considered to be fixed).

By solving the corresponding Schrödinger equation one has access to the many-electron wave function of the system Ψ, and hence to all its static properties. In real materials, however, such a many-electronic wave function is a tremendously complex function that cannot be determined in practice. The mission of any ab initio method is to find out a good approximation for Ψ, or related quantity, that while being accurate still allows for carrying out practical calculations. Examples of first-principles methods include quantum Monte Carlo, Moller–Plesset perturbation theory, coupled clusters with perturbative excitations, and density functional theory. Of these techniques density functional theory (DFT) probably presents the best balance

between accuracy and computational expense. For this reason, the vast majority of computational works done on modeling of hydrogen-storage materials involve DFT methods, which we briefly review next.

In the sixties, Kohn and Sham developed a pioneering theory[355] showing that the exact ground-state energy E_{el} and electronic density $n(\mathbf{r})$ of a system can be determined by solving effective one-electron Schrödinger equations involving the Hamiltonian

$$H_{el}^{eff} = -\frac{1}{2}\nabla_i^2 + \int \frac{n(\mathbf{r}')}{|\mathbf{r}-\mathbf{r}'|} d\mathbf{r}' + V_{xc}(\mathbf{r}) \tag{95}$$

where

$$n(\mathbf{r}) = \sum_{i,\sigma} |\psi_{i\sigma}(\mathbf{r})|^2 \tag{96}$$

and $V_{xc}(\mathbf{r})$ represents the exchange-correlation potential.

The exchange-correlation energy has a genuine quantum origin and, despite representing a small portion of E_{el}, has a crucial role on the bonding between atoms. For most systems V_{xc} is unknown and needs to be approximated: this is the only source of fundamental error in DFT methods.

In local DFT approaches (e.g., LDA), the exchange-correlation energy is approximated as

$$E_{xc}^{l}[n] \approx \int \varepsilon_{xc}^{l}(\mathbf{r}) n(\mathbf{r}) d\mathbf{r} \tag{97}$$

where the adopted exchange-correlation energy functional ε^{L}_{xc} is taken equal to that in a gas of noninteracting electrons at density $n(\mathbf{r})$, which is numerically known from exact quantum Monte Carlo calculations.[356] In semilocal approaches, e.g., GGA, the ε^{L}_{xc} functional is made to depend on the electronic density and also its gradient in order to fulfil a series of analytical constraints known from slowly varying $n(\mathbf{r})$ systems. Both local and semilocal DFT approaches work reasonably well for most bulk systems at equilibrium conditions. However, they cannot reproduce long-range electronic exchange or correlation interactions, e.g., dispersion forces.

Dispersion DFT methods have been recently developed that allow to reproduce satisfactorily long-range correlation effects in materials while still keeping the accompanying computational loads within moderate levels. One illustrative example is the suite of DFT-D techniques,[357] in which an attractive energy term reproducing the asymptotic C_6/r^6 interaction between two particles in a gas is added to H_{el}^{eff} (see Equation (95)). Several improvements have been proposed that go beyond DFT-D, in which the values of the dispersion coefficients C_6 and other higher-order terms are obtained by taking into account the specific environment of the atoms.[358] Other more elaborate and computationally intensive dispersion DFT approaches exist in which many-electron long-range interactions can be estimated seamlessly without the need of introducing ad hoc parameters, e.g., vdW-DF[359] and the random phase approximation.[360]

We should note that the choice of the exchange-correlation approximation in DFT studies of gas-storage materials may have an important effect on the final results.[354a,361] As explained in previous sections, molecular physisorption represents a promising hydrogen-storage route; van der Waal's interactions are critical in this context and thus any DFT work attempting to describe H_2 physisorption should take into account dispersion forces. $Ca^+(H_2)_4$, a system for which several computational benchmark studies have been reported (see, for instance[362]) is an illustrative example of how crucial the choice of the right exchange-correlation approximation may be. It turns out that standard DFT approaches, e.g., LDA and GGA, tend to overestimate the cohesion energy of the system by $\approx$0.1 eV/H_2 as compared to the results obtained with advanced dispersion DFT and quantum chemistry methods. Overall, for arriving at meaningful conclusions on modeling of hydrogen-storage materials the blind use of local and semilocal DFT approaches is not recommended owing to their inherent limitations in describing long-range exchange and correlations in many-electron systems.[354a]

9.2.2. Semiempirical Methods

In semiempirical approaches, the interaction between atoms is normally modeled with simple Lennard–Jones (LJ) plus Coulomb potentials of the form

$$V_{ij}^{FF}(r_{ij}) = 4\epsilon_{ij}\left[\left(\frac{\sigma_{ij}}{r_{ij}}\right)^{12} - \left(\frac{\sigma_{ij}}{r_{ij}}\right)^{6}\right] + \frac{q_i q_j}{r_{ij}^2} \tag{98}$$

where r_{ij} represents the separation between atoms i and j having charges q_i and q_j, and σ_{ij} and ε_{ij} are potential parameters to be determined.

In semiempirical approaches, pairwise additivity normally is assumed when computing total energies and forces. The first term in Equation (98) accounts for the short-ranged atomic repulsion deriving from the overlapping between electron clouds; the second term represents long-ranged atomic attraction due to dispersive van der Waals forces, and the third is the usual Coulomb interaction between atomic point charges. In ionic materials the atomic point charges q_i typically adopt the value of the oxidation state of the ions, whereas in molecular systems they are set to reproduce the polarity of the gas molecules, e.g., H_2 quadrupole moment, and internal electric fields. The value of the LJ potential parameters ε, σ, and q can be obtained from different sources, including the fit to thermodynamic data or highly accurate quantum chemistry calculations. Arithmetic averages such as the Lorentz–Berthelot mixing rules are usually employed to straightforwardly obtain the value of LJ potential parameters corresponding to crossed gas–material interactions. Further and more complex terms can be added to Equation (98) in order to account for higher-order dispersion terms and molecule torsional degrees of freedom.

The low computational expense associated with semiempirical potentials allows explicit consideration of thermal and structural disorder/nanostructuring effects, e.g., slit-like pores, in the simulation of hydrogen-storage materials (see, for instance[342]). Due to the usual light atomic masses and weak intermolecular interactions involved in hydrogen-storage

materials, quantum nuclear effects (QNE) may also significantly affect their gas-uptake capacity at room temperature.[346] This is the case, for instance, of the adsorption and diffusion of hydrogen molecules on the surface of graphene and other related carbon-based nanomaterials.[363] Indeed, by using semiempirical potentials and quantum simulation techniques, e.g., path-integral Monte Carlo methods, it has been possible to assess quantitatively the non-negligible role of QNE on the adsorption of hydrogen and deuterium molecules to the interior of carbon-based nanotubes with varying radii.[364] Likewise, QNE have been shown to be key for understanding the proton dynamics in lithium imide Li_2NH,[365] a promising hydrogen-storage material that is able to liberate more than 5 wt% H_2 through the decomposition reaction

$$Li_2NH + LiH + H_2 \leftrightarrow Li_3N + 2H_2 \quad (99)$$

9.2.3. Machine Learning Techniques

As explained in previous sections, many physical quantities that are relevant to modeling of hydrogen storage materials (e.g., free energy of hydrogen storage/release reactions and materials decomposition processes) can be calculated accurately with first-principles methods. However, in order to determine the most favorable reaction pathways, adsorption sites, chemical structures, and other properties, a number of candidate processes and configurations need to be guessed first. The guessing of such candidate systems relies entirely on chemical intuition hence may be erroneous and/or incomplete depending on the complexity of the problem. To deal with such "open" problems, one would like to have access to theoretical frameworks that automatically, and with acceptable precision, could predict the thermodynamically most favorable reaction paths, states, and configurations by simply providing the overall chemical composition of the system or similar certain information. Machine learning techniques come to fill such a modeler's need, leaving aside any chemical intuition in favor of computational affordability and objectiveness.

In ML, algorithms and statistical models are employed to steadily improve the computational performance on a specific task; in the context of hydrogen-storage materials those tasks can be, for example, the prediction of lowest-energy configurations and decomposition reaction pathways. The analytic approaches that are used to construct ML algorithms and models include permutation invariant polynomials, the modified Shepard method using Taylor expansions, Gaussian processes, interpolating moving least squares, and artificial neural networks.[366] ML models, however, need to be trained on specific and comprehensive sets of data, usually generated with first-principles methods and sometimes difficult to be completed. Theoretical ML-based studies of hydrogen storage materials have started to appear in the literature and we foresee that in the next few years their number will grow steadily due to the great versatility that they offer when it comes to screen vast numbers of different systems and processes. Examples of such ML studies include, the analysis of catalytic activity of the hydrogen evolution reaction on nanoclusters,[367] generation of thousands of new alloy combinations presenting favorable enthalpies of formation for the design of high pressure hydrogen compressor materials,[368] and identification of the performance limits of physical hydrogen storage of 850 000 different nanoporous materials.[369]

10. Design of Hydride Tanks toward Practical Application

Assuming that materials are designed with the right hydrogen storage properties, their practical application relies on their integration at the kg scale into a storage tank meeting practical requirements for the rate of charging and discharging. Depending on the reversibility of the hydrogen release, two types of systems can be designed: i) one shoot tanks containing hydrides that are hydrolyzed to produce hydrogen, and ii) reversible tanks that contain hydrides that can be simply regenerated by applying hydrogen pressure. In both cases, tank design poses several challenges including careful heat management, appropriate choice of the tank material capable of withstanding pressure, stresses and hydrogen embrittlement, and an appropriate management of the slurry (hydrides and water mix) as well as the decomposition products in the case of hydrolysis tanks.

10.1. One Shoot Hydrogen Delivery Tanks

Chemical hydrides like the much-investigated sodium borohydride $NaBH_4$ and ammonia borane NH_3BH_3 are traditionally not considered for reversible hydrogen storage because of the formation of thermodynamically stable residues (i.e., byproducts). Instead, to extract hydrogen from these compounds significant efforts have been devoted to developing methods to control their hydrolysis.[370] As discussed below, prototypes have been developed for hydrolysis of $NaBH_4$, but to our knowledge hydrolysis of NH_3BH_3 has not been scaled up to date. One may, however, cite Keskin et al.'s work that can be seen as a first step toward scaling up.[371] They developed NH_3BH_3 composite pellets (10 mm diameter and 1 mm thickness) and based on their hydrolysis results, they made recommendations for fuel cartridge.

The first prototype using hydrolysis of $NaBH_4$ for on-board H_2 production was developed by the now-bankrupted company Millennium Cell (USA).[372] With an apparently basic design (**Figure 26**), the prototype consisted of a storage tank filled with alkaline aqueous $NaBH_4$; for H_2 generation, the solution had to be pumped onto a tubular catalyst bed.[373] A similar design was later developed by other groups. Kojima et al. worked on a device of 80 kg with a body size of about 200 L (**Figure 27**), mainly made up of a 2 L stainless steel tank for storing aqueous $NaBH_4$ (8.8 mol L^{-1}) and a 4 L stainless steel tank for storing the spent fuel.[374] Using a similar concept, Richardson et al. focused their attention on the performance of a ruthenium-based catalytic reactor.[375] Wang and co-workers' prototype was able to feed a 3000 W fuel cell to power an electric vehicle.[376] Recently, Gang and Kwon adapted this H_2 generator (5.9 L H_2 min^{-1}) for a portable electric power plant with a specific energy density of 211 Wh kg^{-1}.[377] Kim et al. powered a small

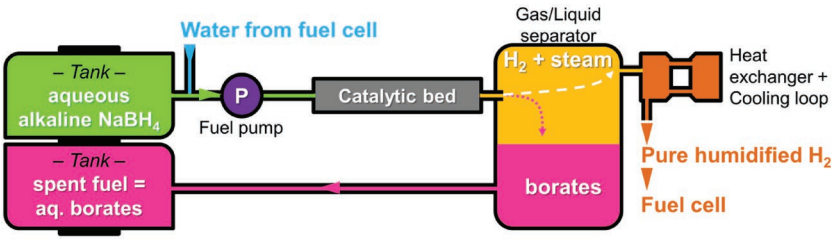

Figure 26. The hydrogen generator developed by Millennium Cell.[372] The generator is based on the use of alkaline aqueous solution of $NaBH_4$ (stored in a tank) that is pumped onto a tubular catalytic bed (ruthenium-based). H_2 generated by hydrolysis is then separated by the spent fuel (aqueous solution of borates) to feed a PEM-type fuel cell. The as-separated spent fuel is stored in another tank. Reproduced with permission.[373a] Copyright 2018, WILEY-VCH.

unmanned aircraft (requiring 80 W for cruising and 300 W for take-off) with 360 g of a 15 wt% $NaBH_4$ solution using a cobalt catalyst.[378] For the same application, Jung et al. reported a $NaBH_4$ hydrogen generator based on a cobalt–phosphorus/nickel foam catalyst. Their system, coupled to a 100 W PEMFC, produced H_2 at a constant rate for 3 h with a conversion efficiency of 97.8% and a maximum power and energy density of 95.96 W and 185.2 Wh kg^{-1}, respectively.[379] Gang and Kwon took the technology further by successfully constructing an integrated hybrid electric power system based on a $NaBH_4$-PEMFC (300 W h^{-1}) system, a solar cell (80 W h^{-1}) and a battery (117 W h^{-1}).[380]

For more compact technologies, miniaturization has also been targeted.[381] For example, Lee and Kim developed a H_2 generator for a 1 W fuel cell to be used in nanosatellites.[382] According to the authors, the specific energy density of their system is three times higher than that of a Li-ion battery. The device is inspired from the aforementioned prototype but it is different by the absence of a spent fuel tank (**Figure 28**). Indeed, for compactness, the borates are stored, upon reaction, in the fuel tank. They confirmed the superiority of the miniaturised $NaBH_4$ cartridges over Li-ion batteries for a specific mission of a small unmanned vehicle, which had to flight more than 5 h with, e.g., a cruise speed of 50 km h^{-1}.[383] The power system based on $NaBH_4$ as H_2 generator coupled to a H_2/air PEMFC (gravimetric power density of 400 W kg^{-1}) showed an endurance of 7 h versus the 4.8 h achievable with a Li-ion battery of 290 Wh kg^{-1} gravimetric energy density. It is worth mentioning that a lithium–sulfur battery (gravimetric energy density of 420 Wh kg^{-1}) was found to be a bit more enduring with 7.1 h. On a larger scale, Rivarolo et al. compared, from thermodynamic and economic standpoints, traditional H_2 storage in pressurized tanks with H_2 storage in the from of $NaBH_4$.[384] The model was based on a plant where H_2 is produced from solar (power peak of 1 MW) coupled with water electrolysis (alkaline electrolyzer of 1 MW delivering hydrogen at 3 MPa). The as-generated H_2 is then used to synthesize $NaBH_4$ (600 °C, 3 MPa H_2; capacity of 171 kg h^{-1}) from its spent fuel $NaBO_2{\cdot}4H_2O$ using Mg as catalyst. In this model, trucks are used to transport $NaBH_4$ to the local usage zone and a ruthenium-catalyzed hydrolysis at 80 °C is considered to regenerate 36 kg H_2 h^{-1}. The spent fuel is recovered and transferred back to the pant. In this cycle of using $NaBH_4$ as the hydrogen carrier, the total cost of the method using $NaBH_4$ was found to be 15.5 € kg^{-1} instead of 22.5 € kg^{-1} for the approach based on compressed H_2. Transportation of $NaBH_4$, which is safer, is one of the positive features of the technology and this makes distribution of hydrogen easy.

Figure 27. The hydrogen generator based on $NaBH_4$ developed by Kojima et al.[374] The two stainless steel tanks used to store the fuel (alkaline aqueous solution of $NaBH_4$, 8.8 mol L^{-1}) and the spent fuel (borates in aqueous solution) are shown. The system has a body size of about 200 L and a weight of 80 kg. With this prototype, the effective hydrogen storage capacities would be at best of 2 mass% H_2 and 15 kg (H_2) m^{-3}, which would be comparable to a compressed H_2 system at 25 MPa. Reproduced with permission.[374] Copyright 2004, Elsevier B.V.

The widespread development of the $NaBH_4$-based H_2 generator discussed above has, however, been hindered by several technical problems. Most of them have recently been summarized in an excellent paper authored by Lapeña-Rey et al. from Boeing R&D Europe who tested the technology with a fuel cell-powered unmanned aerial vehicle (200 W) using an alkaline solution (1 L) of $NaBH_4$ (20 wt%) as a H_2 generator (900 Wh).[385] In this trial, they used the commercial device sold by the company Horizon Energy Systems (Singapore), a device that is comparable to the millennium cell's generator.[386] The main drawbacks were found to be that: i) the catalytic activity unavoidably deteriorates after about 8 h of use; ii) the $NaBH_4$ fuel is irritant; iii) the fuel requires rapid deployment because of spontaneous hydrolysis and H_2 generation; iv) the fuel cost is high; v) precipitation of borates in the piping takes place, resulting in system clogging; vi) the device thus requires water flushing and tedious maintenance after each use to remove the precipitated borate byproducts. Few other problems were reported elsewhere. Kim et al. detected the presence of Na^+ in the water vapor generated because of the exothermicity of the hydrolysis reaction, and such Na^+ deteriorates the performance of the Nafion membrane

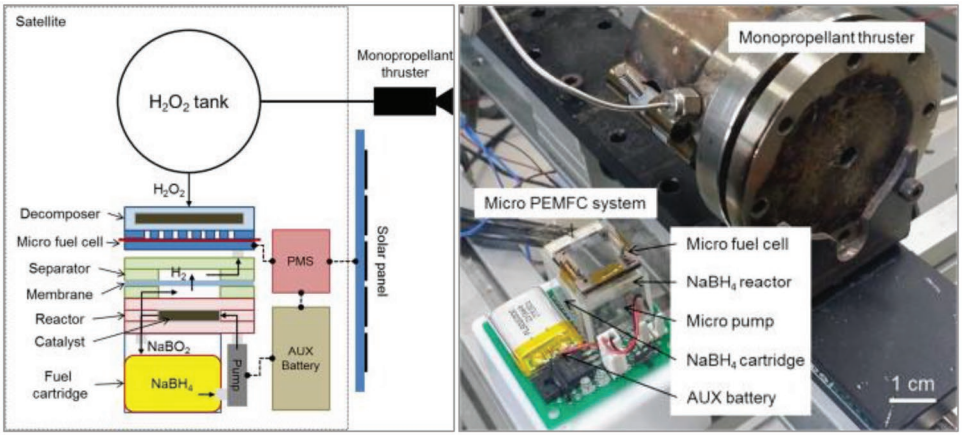

Figure 28. $NaBH_4$-based nanosatellite hydrogen generator. Schematic representation and photography of the power system developed for nanosatellites by Lee and Kim: A membrane is used to separate H_2 from the spent fuel that is finally stored in the cartridge of $NaBH_4$. Reproduced with permission.[382] Copyright 2014, Elsevier Ltd.

of a PEM-type fuel cell.[387] Petit et al. found that the generated H_2 carries borates, and is thus not as pure as what is often claimed.[388] This may explain why Kim and Kim used a third tank (filled with water), called a "wash tank" (**Figure 29**),[389] in which the generated H_2 was bubbled to be cooled down and to favor the precipitation-solubilization of the evolving borates. Taking into account the aforementioned technical issues, there is thus a clear need to mature this technology, as it could be ideal for operation in remote areas while avoiding storage systems based on high pressures.[385]

10.2. Regeneration of Hydrides from One Shoot Tanks

As discussed above, hydrogen can effectively be released from many hydrides through their hydrolysis. However, the drawback of such an approach is that once reacted with water, the hydrides are fully oxidized and thus cannot be simply regenerated. The only option to close the hydrogen cycle is to regenerate the oxides through effective chemical synthetic approaches.[373]

10.2.1. Recycling of Hydrolytic Boron Hydrides

The attractive feature of $NaBH_4$ is its ability to spontaneously hydrolyze at ambient conditions, the process being accelerated and completed with the help of an accelerator like an acid or a metal-based catalyst, following the reaction[390]

$$NaBH_4 + 4H_2O \rightarrow NaB(OH)_4 + 4H_2 \quad (100)$$

The byproduct forming at ambient conditions (<80 °C) is sodium tetramethoxyborate $NaB(OH)_4$, one of the hydrated forms of sodium metaborate $NaBO_2$.[391] Because the B–O bond is as energetic as the C–O bond of CO_2, the formation of B–H bonds from B–O bonds requires harsh conditions and the use of reducing agents. Another issue with $NaB(OH)_4$ and more widely with borates (including $NaBO_2$) is the absence of suitable solvents (besides the protic solvents like water and ethanol into which $NaBH_4$ is not stable). For example, Kojima and Haga showed that the ball milled mixture of $NaBO_2$ and MgH_2 can generate $NaBH_4$ (with a yield of almost 100%) if heated at 550 °C for 2 h under 7 MPa of H_2.[392] With the objective of decreasing the overall cost of the process, further works focused on improvements by using the couple Mg–Si or Mg_3La hydrides instead of MgH_2,[392a,393] ball milling under inert atmosphere,[394] and/or substituting Mg by another element like Al or Ti.[395]

From a commercial point of view, it is preferable to recycle the hydrated form of the borate as this is the species that forms directly upon hydrolysis of $NaBH_4$. Furthermore the formation of $NaBO_2$ by

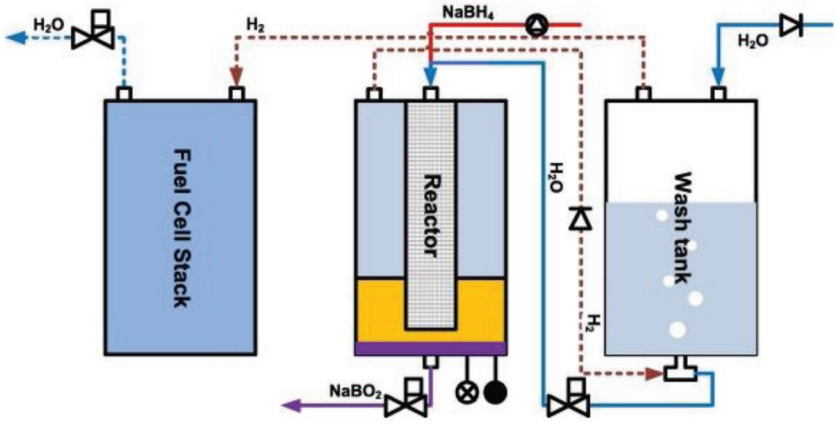

Figure 29. $NaBH_4$-based hydrogen generator developed by Kim and Kim. An additional tank called a "wash tank" is used to bubble the generated H_2 in order to cool the gas stream down and trap the evolving borates (by solubilization in water). Reproduced with permission.[389] Copyright 2010, Elsevier Ltd.

dehydration of $NaB(OH)_4$ requires temperatures higher than 250 °C and is consequently less cost-effective.[396] Adapting Kojima et al.'s approach, Chen et al. showed that $NaB(OH)_4$ can be used instead of $NaBO_2$.[397] It reacts with MgH_2 by ball milling with a yield of almost 90%

$$NaBO_2 \cdot 2H_2O + 4MgH_2 \rightarrow NaBH_4 + 4MgO + 4H_2 \quad (101)$$

Zhong et al. also used $NaB(OH)_4$ that was reacted with Mg_2Si by ball milling at room temperature and under inert atmosphere to regenerate $NaBH_4$.[398] $NaBH_4$ formed with a maximum yield of 74%, and was isolated by dissolution in ethylenediamine. To date, chemical recycling of $NaBO_2$ or $NaB(OH)_4$ using a metallic reducing agent like Mg or MgH_2 has been the most investigated method.[399]

An alternative approach is to use sodium tetramethoxyborate $NaB(OCH_3)_4$. Kemmitt and Gainsford synthesized it by methoxylation of $NaBO_2$.[400] To regenerate $NaBH_4$ (with a yield higher than 80%), $NaB(OCH_3)_4$ was refluxed with $NaAlH_4$ (in diglyme)

$$NaB(OCH_3)_4 + NaAlH_4 \rightarrow NaBH_4 + NaAl(OCH_3)_4 \quad (102)$$

Although the process appears not to be viable because of the high cost of the alanate (Table 3), it can be adapted to the "classical" industrial synthesis path of $NaBH_4$, namely the Brown–Schlesinger process (**Figure 30**).[399a,401] The step 6 of this process could be adapted to use directly $B(OCH_3)_4^-$ and a cheap hydride source (cheaper than the aforementioned $NaAlH_4$), or even better, to use the acidic counterpart $B(OCH_3)_3$ and NaH. Note that the aforementioned recycling processes are all based on solid-phase reactions; an intimate mixture of the borate and of the reducing agent is therefore much important, which can only be done by ball milling.

A last regeneration approach that is worth mentioning is electrochemical reduction[402]

$$B(OH)_4^- + 4H_2O + 8e^- \rightarrow BH_4^- + 8OH^- \quad (103)$$

Similar to the electrochemical reduction of CO_2, this is a high energy-demanding process. The standard potential (E°) of the reaction (103) is +1.24 V.[403] Hence, all the recycling processes developed so far suffer from the need of a significant energy input to regenerate $NaBH_4$, and thus the only viable solution is to use excess electricity from renewable sources.[399a,404]

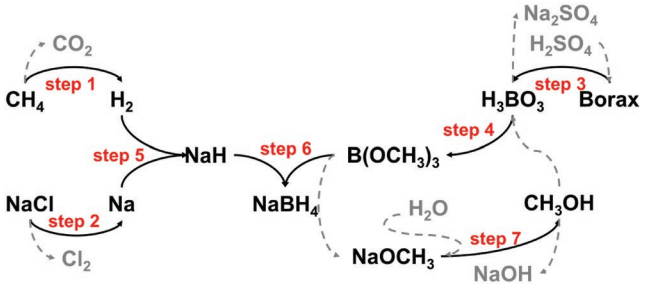

Figure 30. The Brown-Schlesinger process for the stepwise industrial production of $NaBH_4$: from methane CH_4 as hydrogen H_2 source (step 1) and sodium chloride NaCl as metallic sodium Na source (step 2), via the intermediate sodium hydride NaH (step 5); from borax (step 3) and methanol as sources of trimethoxyborate $B(OCH_3)_3$ (step 4). $NaBH_4$ is obtained by reaction of NaH and $B(OCH_3)_3$ (step 6) and the by-product $NaOCH_3$ is recovered to be recycled into CH_3OH (step 7). Reproduced with permission.[401] Copyright 2007, Elsevier B.V.

Like $NaBH_4$, NH_3BH_3 has also been considered as a hydrolytic hydrogen carrier. To our knowledge, the recycling of its hydrolysis byproducts has not been reported so far. Upon hydrolysis, the species $B(OH)_3$ (104) and $B(OH)_4^-$ (105) form if an excess of water is used[405]

$$NH_3BH_3 + 3H_2O \rightarrow NH_3 + B(OH)_3 + 3H_2 \quad (104)$$

$$B(OH)_3 + 2H_2O \leftrightarrow B(OH)_4^- + H_3O^+ \quad (105)$$

Polyborates (B_4^-/B_5^--based compounds) form when water is used in stoichiometric conditions or if the excess of water is extracted.[406] It is preferable to keep the byproducts in aqueous solution, and especially at acidic pH values in order to favor the predominance of $B(OH)_3$. Kemmitt and Gainsford's approach[400] could be adapted in order to methoxylate the byproduct $B(OH)_3$ to form $B(OCH_3)_3$ one of the key reactants of the Brown–Schlesinger process (Figure 30). In other words, the hydrolysis byproducts of NH_3BH_3 could be recycled to form $NaBH_4$, and then NH_3BH_3 since $NaBH_4$ is its precursor.[373]

10.2.2. Recycling of Ammonia Borane's Thermolytic Residue

To release hydrogen for ammonia borane, a thermolysis process whereby ammonia borane is heated up to 200 °C can also be used.[24a,b,300–301,303] In this case, ammonia borane cannot be regenerated by simply applying hydrogen pressure on the thermolysis. To close the hydrogen cycle, it is essential not to totally dehydrogenate the borane into a hydrogen-free residue like boron nitride. To achieve its chemical regeneration, the dehydrogenation of NH_3BH_3 by thermolysis should be conceived so that less than 2.5 equivalents of H_2 are released under heating. Under these conditions, a polymeric residue of complex composition (mixture of polyaminoborane, polyiminoborane, *o*-polyborazylene, and/or graphitic cross-linked polyborazylene) is formed but its exact composition is still unknown.[407]

Regeneration of NH_3BH_3 has thus been investigated while considering only one of the aforementioned polymers.[408] Gordon and co-workers considered polyborazylene as a model residue.[409] The regeneration method they then developed is multistep (**Figure 31**). By using benzenedithiol, polyborazylene is digested and the as-forming reaction intermediate is reduced with Bu_3SnH or Bu_2SnH_2 into NH_3BH_3 with an overall yield of 67%. Although efficient, this multistep method is complex, requires the use of several chemicals, and results in an average yield. All of these are detrimental to the overall cost of the process. Later, the same group reported a much simpler approach (Figure 31),[410] whereby polyborazylene was rehydrogenated with the participation of the reducing agent N_2H_4 in liquid NH_3 through a one-step protocol. In this case, NH_3BH_3 formed with a yield of 100%. By slightly modifying the conditions, the formation of $N_2H_4BH_3$ was even obtained and this is clearly the most efficient regeneration method reported so far.

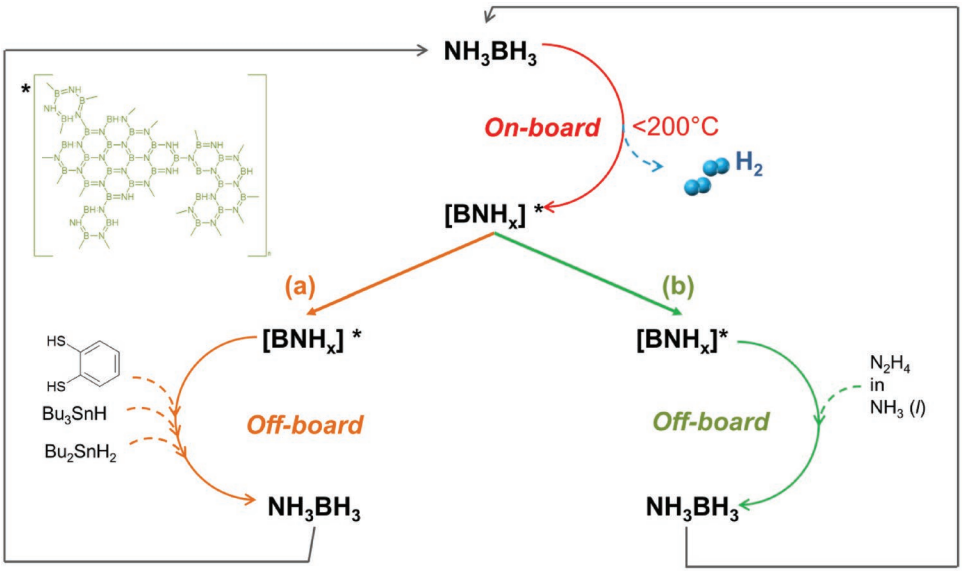

Figure 31. The possible ammonia borane (NH_3BH_3) hydrogen cycle. According to the processes proposed by Gordon and co-workers: a) from ref. [409] and b) from ref. [410]. Both processes use polyborazylene as model residue (denoted [BNH_x] in the scheme, and with the structure associated with the *) of the thermolytic decomposition of NH_3BH_3. Reproduced with permission.[373b] Copyright 2015, WILEY-VCH.

However, the N_2H_4-assisted rehydrogenation can be applied to polyborazylene, only.

This approach was also applied for hydrogenating the thermolysis residues of $LiNH_2BH_3$ and BN-confined NH_3BH_3.[411] For example through this approach, Tang et al. regenerated $LiNH_2BH_3$ from its dehydrogenated counterpart and the conversion back to the targeted borane was found to be of only 63%.[411b] The incomplete conversion is explained by the presence of a fraction of polymers different from the polyborazylene structure.[373] Though targeted, the thermolytic dehydrocoupling of B–N–H compounds does not lead to the selective formation of polyborazylene,[407] and other polymers (e.g., polyaminoborane, polyiminoborane) are formed. With this in mind, Mertens and co-workers developed a generic digestion procedure based on the use of the superacid HCl(4 MPa)/$AlCl_3$/CS_2 solvent system at 80 °C for 12 h.[412] This digestion was successfully applied to borazine, polyaminoborane, and crosslinked polyborazylene. More recently these authors proposed a more effective superacid digestion system based on the trio $AlBr_3$/HBr/CS_2.[413] Linear polyaminoborane was digested at room temperature within 4 h and polyborazylene required a temperature of 80 °C (for >12 h). All of these important achievements demonstrate that B–N–H-based hydrogen compounds can potentially be used as one-shoot hydrogen generation systems and that a new chemical industry could be built to support their commercialization and regeneration.

10.3. Reversible Hydrogen Storage Tanks

Typically the design of an appropriate storage tank for reversible hydrides involves choosing appropriate bed geometries, and methods for the simulation of the tank performances to enable its optimization in terms of heat management and hydrogen flows. The absorption of hydrogen in metal hydride tanks is an exothermic process, and the release of hydrogen endothermic. As a result, without proper heat management the driving force toward the progress of the hydrogen uptake or release reaction decreases as P^{eq} is shifting with temperature (Figure 14a). Hence cooling must be provided during hydrogen charging and heating during hydrogen discharging to achieve sufficient rates of hydrogen uptake and release. The latter can be achieved by coupling the low heat generated by a fuel cell to the hydride via a heat transfer media.[414] However, the heat transfer across the hydride/heat transfer media interface must also be optimized in addition to the heat across the hydride bed because of the low thermal conductivity ≈0.1 W m^{-1} K^{-1} of metal–hydride powders.[415] The nonregular shape of the hydride bed particles results in additional thermal resistance (contact resistance).[416] In order to achieve close contact between the hydride bed and the heat transfer fluid, the bed is often compacted with some additional powder material enhancing heat conduction.[415,417] Heat conduction rather than radiation has been identified as the main issue in low temperature hydride (e.g., $LaNi_5$) tanks.[417a] In contrast, heat exchange by radiation plays an important role in tanks based on high temperature hydrides such as Mg-based hydrides.[418] Several strategies can be used to improve heat transfer. This includes inserting solid pieces of metals of high thermal conductivity including aluminum foams.[419] Finally, heat losses can be minimized during hydrogen sorption by insulating the tanks walls.[420] Based on this understanding, prototypes are then built to evaluate the performance of the overall system, i.e., tank and hydrogen storage materials coupled to the desired application, e.g., fuel cells, and validate the simulation work for further optimization.

The bed geometry can be planar or cylindrical (**Figure 32**); however, if the storage tank is to be subjected to extensive hydrogen pressures, only a cylindrical design, which allows a uniform distribution of the stress and heat/mass transfer, is possible. For planar tanks, the geometry can be rectangular[421]

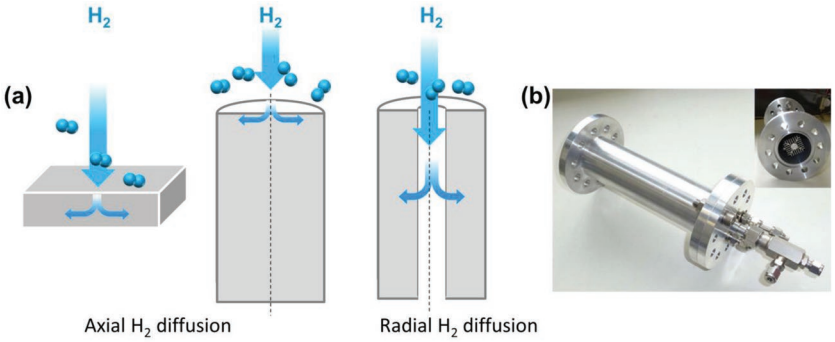

Figure 32. Reversible hydrogen tanks. a) Possible geometry of the hydride tanks (planar/rectangular, cylindrical) and hydrogen diffusion; b) Al-alloy hydrogen tank for $NaAlH_4$. Reproduced with permission.[554] Copyright 2014, Elsevier Ltd.

or that of a disc;[422] however, this comes with the constraint of a low degree of freedom for the integration of a heat exchanger. In contrast, cylindrical shaped reactors, provide more freedom in terms of design and integration of the heat exchanger with the metal hydride powder. Bottle-shaped tanks can also be envisaged. However, this may be restricted to small scale application owing to the difficulty of introducing a heat exchanger within the restricted opening of the bottle neck. The use of toroidal tanks can also be considered, however, such a design has so far been limited to gaseous storage owing to the complexity of the design and the intrinsic difficulty of filling such a tank with hydride powder.[423]

For modeling, several parameters need to be considered. These include: i) hydrogen diffusion through the material's bed, ii) the chemical reaction driving the temperature, pressure and rate of hydrogen release, and iii) the effective transfer of heat across the hydride bed because this is one of the main factors affecting the overall performance of storage tanks.[424] To build the kinetic model, the dehydrogenation/hydrogenation mechanism needs first to be determined. This is often done by evaluating the hydrogen sorption kinetics of materials with a Sievert's apparatus and by fitting the reacted fraction (β) to determine the general equation rate $g(\beta)$ (Figure 9). Then by using the Equation (106) the kinetic model of the storage tank can be determined.[425]

$$d\beta/dt = \left(Ae^{-E_a/RT}\right) \times f\left(p, p_{eq}\right) \times g(\beta) \quad (106)$$

where A is the pre-exponential factor, E_a is the activation energy, R is the universal gas constant and $f(p, p_{eq})$ is usually described as $\ln(p/p_{eq})$.

Using this methodology, various kinetic models have been developed for tanks based on $NaAlH_4$, for example. This includes the optimization of shell, tube, fin-based hydride bed systems, and multitubular reactors equipped with fins.[426] For example, Na Ranong et al. simulated the effect of the storage tank diameter,[427] and scoping models for the evaluation of the tank design were also proposed.[428] Additional models were also proposed to evaluate the heat removal efficiency of a design and couple reaction kinetics with heat and mass transfer across the storage tank.[416d,429] Models were also developed to evaluate the effect of the compaction of the hydride bed including the addition of elements, e.g., expanded natural graphite or metal foams, to improve heat conduction across the bed.[430] 3D models have also been proposed to simulate the effects of pressure drop, heat propagation as well as the evolution of the equilibrium plateau pressure through the sorption process.[431] One difficulty in the simulation of solid state hydrides tanks is the prediction of the behavior of the hydride bed thermal conductivity, because it evolves with many parameters including the packing density, bed porosity, particle size distribution, hydrogen pressure,[432] and hydrogen concentration in the hydride.[433] Based on these simulations, various tank prototypes have been built by utilizing many different types of hydrides such as intermetallics, Mg, and $NaAlH_4$. These are summarized in **Table 5**, and demonstrate that upon appropriate heat management, relatively fast filling can be achieved and good overall hydrogen cycling performances are maintained.

Practically, the outer diameter of solid state store tanks is limited to ensure adequate heat management of the bed, and this results in long tanks with small cross section and aspect ratios larger than 10.[434] Single tanks can then be bundled to reach the required hydrogen storage capacity.[435] The heat exchanger module (spiral coils, tube bundles, heat pipes) can then be embedded in the metal hydride bed within the tank. A phase change material can also be used to collect the heat generated during charging and reuse that heat during discharging.[436] To date, the application of reversible solid-state hydrogen tanks remains limited despite their vast potential in stationary application for long term energy storage or even load levelling. Toshiba has commenced demonstration and operation of the H2One units based on an AB_5 alloy (mischmetal nickel alloy).[437] The potential of the McPhy system based on Mg/MgH_2 has also been demonstrated across several projects, but large scale implementation remains limited.[438] The remnant barriers are in the lack of understanding of the technology by the general community and the misconception around battery storage and its competitiveness as a mature technology.

11. Conclusion and Outlook

Despite being a young area of research as compared to the more traditional fields, e.g., catalysis or battery research, significant progress has been made by many groups on hydrogen storage materials since the early developments in the 1970s. Focus was initially on the interaction of hydrogen with metals and from this, fundamental understanding of hydrogen in metal hydrides has rapidly emerged. However, with the finding of hydrogen reversibility in $NaAlH_4$ significant progress has also been made over the last two decades with complex hydrides.

Today, the "art" of material design for hydrogen storage is still based on this early understanding of the evolution of the hydrogen properties of metal hydrides upon their alloying. Elements are first selected for their capacity to bind large amounts of hydrogen and their properties modified by combining

Table 5. Example of solid state hydrogen storage tanks designed.

Storage material	Weight of storage material [kg]	Design	Capacity of the tank [wt% H_2]	Operation conditions	Kinetics/cycles	Purpose/limitations
Sodium alanate-based tank system						
$NaAlH_4$ doped with 2 mol% ($TiCl_3$-0.3$AlCl_3$) and 5 mol% carbon	8	Tubular reactor with porous sintered metal tube	3.7	Charging at 125 °C and 10 MPa H_2. Discharging at 160–175 °C	80% of the capacity reached in 10 min	Large scale and stationary applications[551]
$NaAlH_4$ doped with 4 mol% $CeCl_3$	0.087	Hydride bed reactor with flow-thru mode	3.9	Charging at 130 °C and 10 MPa H_2. Discharging at 180 °C	–	Investigation on operational principles[552]
$NaAlH_4$ with Al and 10 wt% graphite	4 × 21.5	Modular system of 12 tubular vessels	3.2 in 10 min	Charging at 120–150 °C and 5.52-6.89 MPa H_2.	40 cycles	To be refueled in 10 min and to deliver H_2 up to 2.0 g s^{-1}[430b]
$NaAlH_4$ doped with 4 mol% $TiCl_3$	2.7	Stainless steel tank with double wounded helical coil heat exchanger	2.24	Charging at 135 °C and 10 MPa H_2. Discharging at 120–180 °C	–	To couple with HT-PEM fuel cell. Poor thermal conductivity of the sodium alanate leads to low heat transfer[553]
Na_3AlH_6 doped with 4 mol% $TiCl_3$	0.213	Al-alloy tank with bayonet heat exchanger	1.7	Charging at 2.5 MPa. Discharging at 177–180 °C	10 cycles	To develop and test lightweight Al-alloy storage tank[554]
Na_3AlH_6 doped with 4 mol% $TiCl_3$, 8 mol% Al and 8 mol% activated carbon	1.9	Al-alloy tank with corrugated heat exchanger	2.1	Charging at 160 °C and 2.5 MPa H_2. Discharging at 180 °C	31 cycles	To develop the lightweight Al-tank[555]
$NaAlH_4$ doped with 2 mol% ($TiCl_3$-0.3$AlCl_3$) and 5 mol% expanded graphite	4.4	Ti-alloy tube-and-shell system tank	4	Charging at 124 °C and 10 MPa H_2. Discharging at 120–170 °C	33 cycles	Slow hydrogen sorption because of the large diameter of tank[556]
Metal amide-based tank system						
$Mg(NH_2)_2$–2LiH–0.07KOH with 9 wt% ENG	0.098	–	N/A	Charging at 220 °C and 8 MPa H_2. Discharging at 220 °C	Desorption duration of 79.5 min at 0.6 L H_2 min^{-1}	To investigate influence of graphite content and compaction pressure on the desorption rate.[557]
$LiNH_2$–MgH_2–$LiBH_4$ 3 wt% $ZrCoH_3$ (in annulus) $LaNi_4.3Al0.4Mn0.3$ (in core)	0.6	Tubular reactor with two materials separated by a gas permeable layer	–	Charging: 165–170 °C up to 0.17 MPa; discharging at constant and periodic H_2 mass flow.	10% hydrogen desorption in 30 min and full release in 1 h	To validate a model and study effects of the reactor concept on desorption performance.[558]
$LaNi_5$-based materials						
$LaNi_5$		Concentric triple-tube tank.	–	Hydrogen absorption at 3.5 MPa, and 20 °C. Desorption at 0.8 MPa, and 49 °C	The tank is fully charged with hydrogen after 20 s.	Low-temperature hydrogen storage[559]
Ti-based hydrogen storage material						
Alloy tank based on Ti–Cr–V–Mo	225	Multicylinder hydrogen-absorbing alloy tanks (13 L)	2.5	–	75% of capacity reached in 5 min	For high-pressure hydrogen storage[560]
Alloy tank based on Ti–Cr–Mn	207	Multicylinder alloy tanks	2.5–3	–	60% of storage capacity reached in 5 min	For high-pressure hydrogen storage.[560]
$Ti_{25}Cr_{50}V_{20}Mo_5$	225	Cylindrical tank	2.5	Hydrogen can be supplied at low temperature e.g., –30 °C.	72% of capacity reached in 5 min	For fuel cell vehicles[561]
Mg-based hydrogen storage material						
MgH_2 doped with 5 wt% TiF_4 and activated carbon		Cylindrical tank tightly packed with four beds of MgH_2–TiF_4–AC (≈60.5 g)	4.4	Hydrogen absorption at 250 °C and 1–1.5 MPa H_2. Hydrogen desorption at 300 °C with H_2 pressure of 0.1 MPa.	–	Gravimetric hydrogen capacity decreasing from 4.46 wt to 3.42–3.62 wt% after 15 cycles[562]

Table 5. Continued.

Storage material	Weight of storage material [kg]	Design	Capacity of the tank [wt% H_2]	Operation conditions	Kinetics/cycles	Purpose/limitations
MgH_2	11.7	Cylindrical 316 stainless steel tank	6	Hydrogen absorption: starting from 90 °C with 0.6 MPa H_2. Hydrogen desorption: from 370 °C with H_2 pressure of 0.1–0.3 MPa	50 cycles	For cheap and high hydrogen storage capacity. Needs effective heat management[563]
Other alloy materials						
$Lm_{0.85}Ca_{0.15}Ni_5$ (Lm: La-rich mischmetal)	4,3	Hydrogen tank using four shunted reactors, made of aluminum alloy tubes of 50 mm outer diameter and 3 mm wall thickness	–	Equilibrium pressure controlled in the range of 0.8–1.0 MPa at 25 °C	Full hydrogen release in 120 min	For electric bicycles[564]
$Ti_{0.9}Zr_{0.15}Mn_{1.6}Cr_{0.2}V_{0.2}$	2.9	Hydrogen tank made of an aluminum alloy tube of 60 mm outer diameter and 3:6 mm wall thickness.	2.1	Desorption pressure 0.7 MPa at 25 °C	90% hydrogen released in 60 min	For electric bicycles[564]
$Lm_{1.06}Ni_{4.96}Al_{0.04}$ (Lm: La-rich mischmetal)	15	Horizontal vessel divided into compartments by metal plates	–	–	Refueling time: 2 h with 2 MPa H_2	For hydrogen storage on-board city transit bus[565]
$Fe_{0.9}Mn_{0.1}Ti$	–	Horizontal vessel divided into compartments by metal plates	–	50% loading at 50 °C and 0.75 MPa H_2	90% full in 60 min	For a commercial John Deere Gator utility vehicle[565]
$MmNi_5$ metal hydride alloy	85	Horizontal tank	–	Hydrogen absorption 1.5–2.5 MPa Hydrogen desorption 0.5–1 MPa	Absorption rate of 11.8 NL min^{-1} Desorption rate of 8.1 NL min^{-1}	[566]
Li–Mg–N–H system		Cylindrical tank with heating and cooling jacket	2.45	Hydrogen filling pressure 6.7 MPa. Hydrogen release pressure 0.15 MPa	Maximum filling time 15 min. 70% of hydrogen released at 160 °C in 1 h	Integrated with HT-PEM fuel cell.[567]

additional elements/compounds that may lead to intermediate hydrogen binding strengths toward room temperature sorption. The modification of the lattice parameters of the hydride or the addition of a catalyst are then used to speed-up the rate of hydrogen sorption. This approach has been central to the emergence of Ni–MH batteries,[439] getters, hydrogen sensors,[440] hydrides for hydrogen purification and compressors,[441] and it remains highly relevant in the current context of energy storage for renewable energy. Indeed, many of the room temperature hydrides that have been discovered have the potential to effectively store renewable energy assuming that their properties can be adapted for this application. This includes the development of: i) advanced manufacturing methods to reduce production cost, ii) methods to improve the initial activation for hydrogen cycling, iii) a better understanding of the materials' evolution upon repeated hydrogen cycles to ensure long cycling life (>20 000 cycles), iv) stable hydrogen capacity, resistance to oxidation and hydrogen impurities, and v) facile reactivation upon maintenance of the storage tank and associated valving system. The preparation methods of alloys by metallurgical synthesis, mechanical milling or high pressure torsions and cold rolling[184] can provide new paths to achieve an easy manufacturing process. Better control over the properties of high entropy alloys could also help in the design of alloys with higher hydrogen storage capacities, i.e., >2 mass%.[442]

From this basic understanding of the hydrogen behavior in metals, novel ideas have also appeared toward the design of new hydrogen storage materials mainly based on light elements and complex hydrides. This has been particularly facilitated by the emergence of more comprehensive mechanochemistry tools, the approach of chemical destabilization and more recently nanosizing. Destabilization has the potential to lead to new forms of hydrides with adequate properties, assuming that the adjustment of a particular hydride's hydrogen storage properties is not done at the expense of the storage capacity. This loss of hydrogen storage capacity currently remains the main barrier as the approach has demonstrated its potential on many hydrides and in particular the amide systems.[443] New ideas to achieve chemical destabilization without affecting the final hydrogen storage capacity also need to emerge as well as strategies to maintain a long cycling life and avoid hydrogen uptake/release alongside reaction paths.

Depending on the hydride of interest, a known approach cannot simply be translated to another hydride to improve its hydrogen storage properties, and this remains one of the major difficulties in the field. To date, there are no general rules that can be used to unify the behavior of hydride materials. Even, within a single family, e.g., borohydrides, different hydrogen behaviors are observed. Such diversity significantly hinders the translation of concepts from one system to the other, and this currently limits progress. In particular, light complex hydrides, at the basis of future applications including vehicles, require the development of a new fundamental understanding to grasp this complexity. New thinking along the control of ionic transport in complex hydrides is needed in addition to effective concepts to release/absorb hydrogen along predetermined thermodynamic paths. Understanding of the hydrogen interaction in ionic hydrides and the stabilization of "active" forms of light elements resulting from the decomposition of the complex hydrides is also needed to achieve low temperature hydrogen sorption.

The approach of nanosizing could potentially help to establish general rules since the behavior of hydrides at the nanoscale seems to be more consistent. Through a nanosizing approach both the thermodynamics and kinetics of hydrides can be modified at the same time and this offers new opportunities to effectively design hydrogen storage materials. However, one of the challenges is in the synthesis and accurate characterization of the properties of nanosized hydrides with respect to hydrogen. Current synthetic methods are not well established in particular in the making of nanosized hydrides stable upon successive hydrogen cycles, although some progress has been made over the last few years.[126b,186] Precise control in the synthetic approach is often overlooked, but this is a prerequisite for the exact determination of the behavior of hydrogen in the nanostructures without additional artefacts due to the oxidation, degradation, and partial reaction of the confined hydride within the host material. Beyond this, the effective hydrogen storage capacity achievable by the nanosizing approach is also limited because of the dead mass of the mesoporous host material nanoconfining the hydrides. As discussed above, this is currently a recurring problem that must be tackled through radical concepts. In this respect, theoretical modeling can significantly help but alternative methods to run more complex calculations to determine enthalpy and entropy evolutions across length scales as well as ways to take into account the chemical environment of the hydrides must emerge.

New thinking is also needed in the way hydrogen is loaded and unloaded in materials. Currently, the preferred method relies on variations in hydrogen pressure and temperature to shift the equilibrium plateau to the required pressure. This not only complicates the implementation of materials in tanks but also brings additional engineering challenges for the heat management of the hydride bed to ensure reasonable charging/discharging times. If alternative methods could be developed where the loading/unloading of hydrogen in the hydride bed proceeded without significant heat evolution, tank engineering would be simplified and hydrogen storage capacities at the system level improved. We have started to work on alternatives where the plasmonic effect of Au can be used to locally control the release of hydrogen.[38,444] Although this solution is not viable for large solid state storage tanks, it may provide a path for a simpler design of small, portable and light hydrogen storage devices.

To date, the early vision of a hydrogen economy is more than ever pertinent. Enabling the use of hydrogen as the universal energy vector will be disruptive but also benefit society from multiple perspectives including new means for many to locally access energy. Technologies for water electrolysis and fuel cells are market ready and further reduction in cost will accelerate their uptake. Hydrogen vehicles are now a commercial reality, and this coupled with the sharp price fall of solar panels are undoubtedly the first enablers of a transition to the hydrogen economy. The challenge for the scientific community is to facilitate this transition by accelerating the pace of thinking along the behavior of hydrogen in materials, in particular those composed of light elements, and by unlocking creativity in the design of new strategies and approaches to synthesize, control and engineer hydrogen storage materials.

Acknowledgements

Financial support by UNSW Internal Research Grant program is gratefully acknowledged along with the Office of Naval Research (Award No: ONRG–NICOP–N62909-16-1-2155).

Conflict of Interest

The authors declare no conflict of interest.

Keywords

complex hydrides, hydrogen storage, metal hydrides

Received: March 22, 2019
Revised: May 11, 2019
Published online: June 26, 2019

[1] a) S. Brenner, *Science* **1998**, *282*, 1411; b) S. Şener, E. Sarıdoğan, *Procedia—Soc. Behav. Sci.* **2011**, *24*, 815.
[2] M. F. Perutz, in *Science and Technology Education and Future Human Needs* (Eds: J. L. Lewis, P. J. Kelly), Pergamon, Exeter **1987**, pp. 17–56.
[3] G. Kallis, C. Kerschner, J. Martinez-Alier, *Ecol. Econ.* **2012**, *84*, 172.
[4] Ö. Esen, M. Bayrak, *J. Econ. Financ. Admin. Serv.* **2017**, *22*, 75.
[5] A. Züttel, A. Remhof, A. Borgschulte, O. Friedrichs, *Philos. Trans. R. Soc., A* **2010**, *368*, 3329.
[6] a) I. Ridjan, B. V. Mathiesen, D. Connolly, N. Duic, *Energy* **2013**, *57*, 76; b) S. H. Jensen, P. H. Larsen, M. Mogensen, *Int. J. Hydrogen Energy* **2007**, *32*, 3253.
[7] J. B. S. Haldane, *Daedalus, or, Science and the Future*, Kegan Paul, Trench, Trubner & Co, Cambridge **1923**.
[8] M. Hirscher, *Handbook of Hydrogen Storage: New Materials for Future Energy Storage*, Wiley-VCH Verlag GmbH & Co, Anguilla **2009**.

[9] C. Yang, J. Ogden, *Int. J. Hydrogen Energy* **2007**, *32*, 268.
[10] E. Akiba, H. Iba, *Intermetallics* **1998**, *6*, 461.
[11] D. P. Broom, *Hydrogen Storage Materials: The Characterisation of Their Storage Properties*, Springer Science & Business Media, London **2011**.
[12] a) J. M. Carrasco, L. G. Franquelo, J. T. Bialasiewicz, E. Galván, R. C. PortilloGuisado, M. M. Prats, J. I. León, N. Moreno-Alfonso, *IEEE Trans. Ind. Electron.* **2006**, *53*, 1002; b) T. Zhou, B. François, *IEEE Trans. Ind. Electron.* **2011**, *58*, 95.
[13] a) S. M. Schoenung, W. V. Hassenzahl, *Long-vs. Short-Term Energy Storage Technologies Analysis: A Life-Cycle Cost Study: A study for the DOE Energy Storage Systems Program*, Sandia National Laboratories, Albuquerque and Livermore **2003**; b) B. D. James, D. A. DeSantis, *Manufacturing Cost and Installed Price—Analysis of Stationary Fuel Cell Systems, Strategic Analysis Inc.* Arlington VA **2015**; c) S. Satyapal, J. Petrovic, C. Read, G. Thomas, G. Ordaz, *Catal. Today* **2007**, *120*, 246; d) M. P. de Wit, A. P. C. Faaij, *Int. J. Hydrogen Energy* **2007**, *32*, 4859; e) G. Gahleitner, *Int. J. Hydrogen Energy* **2013**, *38*, 2039; f) C. Darras, M. Muselli, P. Poggi, C. Voyant, J. C. Hoguet, F. Montignac, *Int. J. Hydrogen Energy* **2012**, *37*, 14015; g) C. Ziogou, D. Ipsakis, C. Elmasides, F. Stergiopoulos, S. Papadopoulou, P. Seferlis, S. Voutetakis, *J. Power Sources* **2011**, *196*, 9488; h) L. Ntziachristos, C. Kouridis, Z. Samaras, K. Pattas, *Renewable Energy* **2005**, *30*, 1471.
[14] A. P. Côté, A. I. Benin, N. W. Ockwig, M. O'Keeffe, A. J. Matzger, O. M. Yaghi, *Science* **2005**, *310*, 1166.
[15] K. M. Thomas, *Dalton Trans.* **2009**, *1487*, 1505.
[16] a) Q. Lai, M. Paskevicius, D. A. Sheppard, C. E. Buckley, A. W. Thornton, M. R. Hill, Q. Gu, J. Mao, Z. Huang, H. K. Liu, Z. Guo, A. Banerjee, S. Chakraborty, R. Ahuja, K.-F. Aguey-Zinsou, *ChemSusChem* **2015**, *8*, 2789; b) Y. B. He, F. L. Chen, B. Li, G. D. Qian, W. Zhou, B. L. Chen, *Coord. Chem. Rev.* **2018**, *373*, 167.
[17] L. Morris, J. J. Hales, M. L. Trudeau, P. Georgiev, J. P. Embs, J. Eckert, N. Kaltsoyannis, D. M. Antonelli, *Energy Environ. Sci.* **2019**,*12*, 1580.
[18] a) P. Preuster, C. Papp, P. Wasserscheid, *Acc. Chem. Res.* **2017**, *50*, 74; b) T. He, P. Pachfule, H. Wu, Q. Xu, P. Chen, *Nat. Rev. Mater.* **2016**, *1*, 16059; c) N. Onishi, G. Laurenczy, M. Beller, Y. Himeda, *Coord. Chem. Rev.* **2018**, *373*, 317.
[19] L. Klebanoff, *Hydrogen Storage Technology: Materials and Applications*, CRC Press, Boca Raton **2013**.
[20] a) A. J. Maeland, A. F. Andersen, *J. Chem. Phys.* **1968**, *48*, 4660; b) K. Christmann, *Surf. Sci. Rep.* **1988**, *9*, 1.
[21] D. A. Hutchinson, *Can. J. Chem.* **1966**, *44*, 2711.
[22] W. Grochala, P. P. Edwards, *Chem. Rev.* **2004**, *104*, 1283.
[23] K. H. J. Buschow, P. C. P. Bouten, A. R. Miedema, *Rep. Prog. Phys.* **1982**, *45*, 937.
[24] a) M. G. Hu, R. A. Geanangel, W. W. Wendlandt, *Thermochim. Acta* **1978**, *23*, 249; b) M. Bowden, T. Autrey, I. Brown, M. Ryan, *Curr. Appl. Phys.* **2008**, *8*, 498; c) Q. Lai, A. Rawal, M. Z. Quadir, C. Cazorla, U. B. Demirci, K.-F. Aguey-Zinsou, *Adv. Sustainable Sys.* **2018**, *2*, 1700122.
[25] G. Sandrock, K. Gross, G. Thomas, C. Jensen, D. Meeker, S. Takara, *J. Alloys Compd.* **2002**, *330–332*, 696.
[26] G. Sandrock, *J. Alloys Compd.* **1999**, *293–295*, 877.
[27] a) A. Schneemann, J. L. White, S. Kang, S. Jeong, L. F. Wan, E. S. Cho, T. W. Heo, D. Prendergast, J. J. Urban, B. C. Wood, M. D. Allendorf, V. Stavila, *Chem. Rev.* **2018**, *118*, 10775; b) I. Sreedhar, K. M. Kamani, B. M. Kamani, B. M. Reddy, A. Venugopal, *Renewable Sustainable Energy Rev.* **2018**, *91*, 838; c) S. Garroni, A. Santoru, H. J. Cao, M. Dornheim, T. Klassen, C. Milanese, F. Gennari, C. Pistidda, *Energies* **2018**, *11*, 1027; d) L. Pasquini, *Crystals* **2018**, *8*, 106; e) V. Bérubé, G. Radtke, M. Dresselhaus, G. Chen, *Int. J. Energy Res.* **2007**, *31*, 637; f) A. Pundt, R. Kirchheim, *Annu. Rev. Mater. Res.* **2006**, *36*, 555; g) G. Walker, *Solid-State Hydrogen Storage: Materials and Chemistry*, Elsevier, Cambridge **2008**; h) S. Qiu, H. Chu, Y. Zou, C. Xiang, F. Xu, L. Sun, *J. Mater. Chem. A* **2017**, *5*, 25112; i) R. A. Varin, T. Czujko, Z. S. Wronski, *Nanomaterials for Solid State Hydrogen Storage*, Springer Science & Business Media, New York **2009**; j) H. Wipf, *Hydrogen in Metals III: Properties and Applications*, Springer, Berlin **1997**; k) G. AlefeldJohann, J. Völkl, *Hydrogen in Metals I*, Springer, Berlin **1978**; l) G. Alefeld, J. Völkl, *Hydrogen in Metals II*, Springer-Verlag, Berlin **1978**; m) Y. Fukai, *The Metal-Hydrogen System: Basic Bulk Properties*, 2nd rev. and updated ed., Springer, Berlin **2005**.
[28] J. A. Menéndez, A. Arenillas, B. Fidalgo, Y. Fernández, L. Zubizarreta, E. G. Calvo, J. M. Bermúdez, *Fuel Process. Technol.* **2010**, *91*, 1.
[29] A. Zlotorzynski, *Crit. Rev. Anal. Chem.* **1995**, *25*, 43.
[30] a) Y. Nakamori, S.-I. Orimo, T. Tsutaoka, *Appl. Phys. Lett.* **2006**, *88*, 112104; b) M. Matsuo, Y. Nakamori, K. Yamada, S.-I. Orimo, *Appl. Phys. Lett.* **2007**, *90*, 232907; c) M. Matsuo, Y. Nakamori, K. Yamada, T. Tsutaoka, S. Orimo, *Adv. Mater. Res.* **2008**, *10*, 157.
[31] J. R. Ares, F. Leardini, P. Díaz-Chao, J. Bodega, J. F. Fernández, I. J. Ferrer, C. Sánchez, *Ultrason. Sonochem.* **2009**, *16*, 810.
[32] M. Schwickert, E. Carpene, K. P. Lieb, M. Uhrmacher, P. Schaaf, H. Gibhardt, *Phys. Scr.* **2004**, *T108*, 113.
[33] *Executive Summary of Laser Hydrides-Laser Induced Adsorption of Hydrogen from Magnesium Hydride*, P. K. Corporation, Scottsdale **2008**.
[34] a) J. G. McCaffrey, J. M. Parnis, G. A. Ozin, W. Breckenridge, *J. Phys. Chem.* **1985**, *89*, 4945; b) D. Dougherty, P. J. Herley, *J. Less Common Met.* **1980**, *73*, 97.
[35] P. J. Herley, D. H. Spencer, *J. Phys. Chem.* **1979**, *83*, 1701.
[36] a) P. J. Herley, O. Christofferson, *J. Phys. Chem.* **1981**, *85*, 1887; b) I. E. Gabis, A. P. Voyt, I. A. Chernov, V. G. Kuznetsov, A. P. Baraban, D. I. Elets, M. A. Dobrotvorsky, *Int. J. Hydrogen Energy* **2012**, *37*, 14405; c) P. Herley, O. Christofferson, *J. Phys. Chem.* **1981**, *85*, 1882.
[37] P. Herley, P. Levy, *J. Chem. Phys.* **1967**, *46*, 627.
[38] Y. Sun, K. F. Aguey-Zinsou, *ChemPlusChem* **2018**, *83*, 904.
[39] P. Verma, Y. Kuwahara, K. Mori, H. Yamashita, *Chem. - Eur. J.* **2017**, *23*, 3616.
[40] a) M. Matuschek, D. P. Singh, H.-H. Jeong, M. Nesterov, T. Weiss, P. Fischer, F. Neubrech, N. Liu, *Small* **2018**, *14*, 1702990; b) W. L. Watkins, Y. Borensztein, *Sens. Actuators, B* **2018**, *273*, 527; c) F. A. A. Nugroho, I. Darmadi, V. P. Zhdanov, C. Langhammer, *ACS Nano* **2018**, *12*, 9903.
[41] Y. Zhu, C. Yang, J. Zhu, L. Li, *J. Alloys Compd.* **2011**, *509*, 5309.
[42] a) F. Cuevas, J. M. Joubert, M. Latroche, A. Percheron-Guégan, *Appl. Phys. A: Mater. Sci. Process.* **2001**, *72*, 225; b) J. J. G. Willems, *Philips J. Res.* **1984**, *39*, 1.
[43] a) B. Panella, M. Hirscher, *Adv. Mater.* **2005**, *17*, 538; b) Y. Jia, C. Sun, Y. Peng, W. Fang, X. Yan, D. Yang, J. Zou, S. S. Mao, X. Yao, *J. Mater. Chem. A* **2015**, *3*, 8294.
[44] K.-F. Aguey-Zinsou, J.-R. Ares-Fernandez, *Energy Environ. Sci.* **2010**, *3*, 526.
[45] M. G. Nijkamp, J. Raaymakers, A. J. Van Dillen, K. P. De Jong, *Appl. Phys. A: Mater. Sci. Process.* **2001**, *72*, 619.
[46] a) J. Huot, G. Liang, S. Boily, A. Van Neste, R. Schulz, *J. Alloys Compd.* **1999**, *293–295*, 495; b) K. F. Aguey-Zinsou, J. R. A. Fernandez, T. Klassen, R. Bormann, *Int. J. Hydrogen Energy* **2007**, *32*, 2400; c) K. F. Aguey-Zinsou, J. Ares-Fernandez, T. Klassen, R. Bormann, *Int. J. Hydrogen Energy* **2007**, *32*, 2400.
[47] C. Nishimura, M. Komaki, M. Amano, *J. Alloys Compd.* **1999**, *293–295*, 329.
[48] J. Philibert, *Defect Diffus. Forum* **2006**, *249*, 61.
[49] C. Wert, C. Zener, *Phys. Rev.* **1949**, *76*, 1169.

[50] a) J. G. P. Binner, N. A. Hassine, T. E. Cross, *J. Mater. Sci.* **1995**, *30*, 5389; b) J. Vilčáková, P. Sáha, V. Křesálek, O. Quadrat, *Synth. Met.* **2000**, *113*, 83; c) K. Park, D. Lee, A. Rai, D. Mukherjee, M. R. Zachariah, *J. Phys. Chem. B* **2005**, *109*, 7290.
[51] N. Katada, S. Sota, N. Morishita, K. Okumura, M. Niwa, *Catal. Sci. Technol.* **2015**, *5*, 1864.
[52] a) J. Huot, J. F. Pelletier, L. B. Lurio, M. Sutton, R. Schulz, *J. Alloys Compd.* **2003**, *348*, 319; b) G. Liang, J. Huot, S. Boily, A. Van Neste, R. Schulz, *J. Alloys Compd.* **1999**, *291*, 295.
[53] a) N. S. Norberg, T. S. Arthur, S. J. Fredrick, A. L. Prieto, *J. Am. Chem. Soc.* **2011**, *133*, 10679; b) P. Heitjans, S. Indris, *J. Mater. Sci.* **2004**, *39*, 5091; c) S. D. Benedetto, M. Carewska, C. Cento, P. Gislon, M. Pasquali, S. Scaccia, P. P. Prosini, *Thermochim. Acta* **2006**, *441*, 184.
[54] J. Wilhelm, *Z. Anorg. Allg. Chem.* **1927**, *163*, 1.
[55] a) W. A. Johnson, R. F. Mehl, *Trans. Metall. Soc. AIME* **1939**, *135*, 396; b) M. Avrami, *J. Chem. Phys.* **1940**, *8*, 212; c) M. Avrami, *J. Chem. Phys.* **1941**, *9*, 177; d) M. Avrami, *J. Chem. Phys.* **1939**, *7*, 1103.
[56] a) K.-C. Chou, Q. Li, Q. Lin, L.-J. Jiang, K.-D. Xu, *Int. J. Hydrogen Energy* **2005**, *30*, 301; b) M. Martin, C. Gommel, C. Borkhart, E. Fromm, *J. Alloys Compd.* **1996**, *238*, 193; c) Y. Pang, Q. Li, *Int. J. Hydrogen Energy* **2016**, *41*, 18072; d) G. Stepura, V. Rosenband, A. Gany, *J. Alloys Compd.* **2012**, *513*, 159.
[57] a) F. J. Castro, G. Meyer, *J. Alloys Compd.* **2002**, *330–332*, 59; b) E. A. Evard, I. E. Gabis, A. P. Voyt, *J. Alloys Compd.* **2005**, *404–406*, 335.
[58] G. Liang, J. Huot, S. Boily, A. Van Neste, R. Schulz, *J. Alloys Compd.* **1999**, *292*, 247.
[59] N. Hanada, T. Ichikawa, H. Fujii, *J. Phys. Chem. B* **2005**, *109*, 7188.
[60] M. Pourabdoli, S. Raygan, H. Abdizadeh, D. Uner, *Int. J. Hydrogen Energy* **2013**, *38*, 11910.
[61] a) A. Borgschulte, M. O. Jones, E. Callini, B. Probst, S. Kato, A. Zuttel, W. I. F. David, S. Orimo, *Energy Environ. Sci.* **2012**, *5*, 6823; b) S. Nayebossadri, K. F. Aguey-Zinsou, *Phys. Chem. Chem. Phys.* **2011**, *13*, 17683.
[62] a) L. L. Shaw, W. Osborn, T. Markmaitree, X. Wan, *J. Power Sources* **2008**, *177*, 500; b) G. Amica, F. Cova, P. Arneodo Larochette, F. C. Gennari, *Int. J. Hydrogen Energy* **2017**, *42*, 6127.
[63] B. Bogdanović, M. Felderhoff, S. Kaskel, A. Pommerin, K. Schlichte, F. Schüth, *Adv. Mater.* **2003**, *15*, 1012.
[64] J. M. Bellosta von Colbe, W. Schmidt, M. Felderhoff, B. Bogdanović, F. Schüth, *Angew. Chem., Int. Ed.* **2006**, *45*, 3663.
[65] a) B. Bogdanović, R. A. Brand, A. Marjanović, M. Schwickardi, J. Tölle, *J. Alloys Compd.* **2000**, *302*, 36; b) G. J. Thomas, K. J. Gross, N. Y. C. Yang, C. Jensen, *J. Alloys Compd.* **2002**, *330–332*, 702; c) M. Felderhoff, K. Klementiev, W. Grunert, B. Spliethoff, B. Tesche, J. M. Bellosta von Colbe, B. Bogdanovic, M. Hartel, A. Pommerin, F. Schuth, C. Weidenthaler, *Phys. Chem. Chem. Phys.* **2004**, *6*, 4369.
[66] F. Schuth, B. Bogdanovic, M. Felderhoff, *Chem. Commun.* **2004**, 2249.
[67] a) H. Gunaydin, K. N. Houk, V. Ozoliņš, *Proc. Natl. Acad. Sci. USA* **2008**, *105*, 3673; b) G. K. P. Dathar, D. S. Mainardi, *J. Phys. Chem. C* **2010**, *114*, 8026.
[68] G. Sandrock, K. Gross, G. Thomas, *J. Alloys Compd.* **2002**, *339*, 299.
[69] E. G. Maksimov, O. A. Pankratov, *Phys. Usp.* **1975**, *18*, 481.
[70] a) G. Schaumann, J. Völki, G. Alefeld, *Phys. Status Solidi B* **1970**, *42*, 401; b) R. L. Corey, T. M. Ivancic, D. T. Shane, E. A. Carl, R. C. Bowman, J. M. Bellosta von Colbe, M. Dornheim, R. Bormann, J. Huot, R. Zidan, A. C. Stowe, M. S. Conradi, *J. Phys. Chem. C* **2008**, *112*, 19784.
[71] O. Palumbo, R. Cantelli, A. Paolone, C. M. Jensen, S. S. Srinivasan, *J. Alloys Compd.* **2005**, *404–406*, 748.
[72] R. Hempelmann, *J. Less-Common Met.* **1984**, *101*, 69.
[73] S. Hao, D. S. Sholl, *Appl. Phys. Lett.* **2008**, *93*, 251901.
[74] D. G. Hunt, D. K. Ross, *J. Less-Common Met.* **1976**, *49*, 169.
[75] J. Bergsma, J. A. Goedkoop, *Physica* **1960**, *26*, 744.
[76] E. Wicke, H. Brodowsky, H. Züchner, in *Hydrogen in Metals II: Application-Oriented Properties* (Eds: G. Alefeld, J. Völkl), Springer, Berlin **1978**, pp. 73–155.
[77] T. L. Hill, *An Introduction to Statistical Thermodynamics*, Dover Publication, Inc., New York **1986**.
[78] D. W. Taylor, *Phys. Rev. B* **1980**, *21*, 5096.
[79] E. Wimmer, W. Wolf, J. Sticht, P. Saxe, C. B. Geller, R. Najafabadi, G. A. Young, *Phys. Rev. B* **2008**, *77*, 134305.
[80] C. Wagner, *Acta Metall.* **1971**, *19*, 843.
[81] a) O. J. Kleppa, P. Dantzer, M. E. Melnichak, *J. Chem. Phys.* **1974**, *61*, 4048; b) R. Johansson, R. Ahuja, O. Eriksson, B. Hjörvarsson, R. H. Scheicher, *Sci. Rep.* **2015**, *5*, 10301.
[82] a) V. V. Sumin, H. Wipf, B. Coluzzi, A. Biscarini, R. Campanella, G. Mazzolai, F. M. Mazzolai, *J. Alloys Compd.* **2001**, *316*, 189; b) A. Blomqvist, G. K. Pálsson, C. M. Araújo, R. Ahuja, B. Hjörvarsson, *Phys. Rev. Lett.* **2010**, *105*, 185901.
[83] A. Driessen, P. Sanger, H. Hemmes, R. Griessen, *J. Phys.: Condens. Matter* **1990**, *2*, 9797.
[84] Y.-L. Liu, Y. Zhang, G. N. Luo, G.-H. Lu, *J. Nucl. Mater.* **2009**, *390–391*, 1032.
[85] G. M. Evgenii, O. A. Pankratov, *Phys. Usp.* **1975**, *18*, 481.
[86] R. Khoda-Bakhsh, D. K. Ross, *J. Phys. F: Met. Phys.* **1982**, *12*, 15.
[87] V. A. Somenkov, *Ber. Bunsen-Ges. Phys. Chem.* **1972**, *76*, 733.
[88] L. R. Lichty, J. W. Han, R. Ibanez-Meier, D. R. Torgeson, R. G. Barnes, E. F. W. Seymour, C. A. Sholl, *Phys. Rev. B* **1989**, *39*, 2012.
[89] I. S. Anderson, J. J. Rush, T. Udovic, J. M. Rowe, *Phys. Rev. Lett.* **1986**, *57*, 2822.
[90] O. Blaschko, G. Krexner, L. Pintschovius, P. Vajda, J. N. Daou, *Phys. Rev. B* **1988**, *38*, 9612.
[91] V. Koteski, J. Belosevic-Cavor, K. Batalovic, J. Radakovic, A. Umicevic, *RSC Adv.* **2015**, *5*, 34894.
[92] J. Zhang, H. Qu, S. Yan, G. Wu, X. F. Yu, P. Peng, *J. Alloys Compd.* **2017**, *694*, 687.
[93] a) J. L. Souquet, *Annu. Rev. Mater. Sci.* **1981**, *11*, 211; b) K. Funke, *Solid State Ionics* **1986**, *18–19*, 183.
[94] R. Kirchheim, T. Mütschele, W. Kieninger, H. Gleiter, R. Birringer, T. D. Koblé, *Mater. Sci. Eng.* **1988**, *99*, 457.
[95] a) K. J. Gross, S. Guthrie, S. Takara, G. Thomas, *J. Alloys Compd.* **2000**, *297*, 270; b) W. Lohstroh, M. Fichtner, *Phys. Rev. B* **2007**, *75*, 184106.
[96] P. Martelli, A. Remhof, A. Borgschulte, P. Mauron, D. Wallacher, E. Kemner, M. Russina, F. Pendolino, A. Züttel, *J. Phys. Chem. A* **2010**, *114*, 10117.
[97] C. S. Sunandana, P. S. Kumar, *Bull. Mater. Sci.* **2004**, *27*, 1.
[98] a) R. P. Buck, *Sens. Actuators* **1981**, *1*, 137; b) J. B. Goodenough, *Annu. Rev. Mater. Res.* **2003**, *33*, 91.
[99] T. Mezaki, Y. Kuronuma, I. Oikawa, A. Kamegawa, H. Takamura, *Inorg. Chem.* **2016**, *55*, 10484.
[100] J. C. Bachman, S. Muy, A. Grimaud, H.-H. Chang, N. Pour, S. F. Lux, O. Paschos, F. Maglia, S. Lupart, P. Lamp, L. Giordano, Y. Shao-Horn, *Chem. Rev.* **2016**, *116*, 140.
[101] a) S. Hoshino, *Solid State Ionics* **1991**, *48*, 179; b) C. M. Araújo, A. Blomqvist, R. H. Scheicher, P. Chen, R. Ahuja, *Phys. Rev. B* **2009**, *79*, 172101.
[102] A. Borgschulte, A. Jain, A. J. Ramirez-Cuesta, P. Martelli, A. Remhof, O. Friedrichs, R. Gremaud, A. Züttel, *Faraday Discuss.* **2011**, *151*, 213.
[103] a) K. Jimura, S. Hayashi, *J. Phys. Chem. C* **2012**, *116*, 4883; b) A. V. Skripov, A. V. Soloninin, O. A. Babanova, R. V. Skoryunov, *J. Alloys Compd.* **2015**, *645*, S428; c) A. V. Skripov, A. V. Soloninin,

M. B. Ley, T. R. Jensen, Y. Filinchuk, *J. Phys. Chem. C* **2013**, *117*, 14965.
[104] R. L. Corey, D. T. Shane, R. C. Bowman, M. S. Conradi, *J. Phys. Chem. C* **2008**, *112*, 18706.
[105] a) M. Matsuo, Y. Nakamori, S.-I. Orimo, H. Maekawa, H. Takamura, *Appl. Phys. Lett.* **2007**, *91*, 224103; b) A. V. Soloninin, A. V. Skripov, A. L. Buzlukov, A. P. Stepanov, *J. Solid State Chem.* **2009**, *182*, 2357.
[106] N. Verdal, T. J. Udovic, J. J. Rush, H. Wu, A. V. Skripov, *J. Phys. Chem. C* **2013**, *117*, 12010.
[107] a) W. Li, G. Wu, Z. Xiong, Y. P. Feng, P. Chen, *Phys. Chem. Chem. Phys.* **2012**, *14*, 1596; b) L. Q. He, H. J. Lin, H. F. Li, Y. Filinchuk, J. J. Zhang, Y. Liu, M. Y. Yang, Y. Hou, Y. H. Deng, H. W. Li, H. Y. Shao, L. P. Wang, Z. G. Lu, *J. Power Sources* **2018**, *396*, 574; c) S. Kim, N. Toyama, H. Oguchi, T. Sato, S. Takagi, T. Ikeshoji, S. I. Orimo, *Chem. Mater.* **2018**, *30*, 386; d) H. Wang, H. J. Cao, W. J. Zhang, J. Chen, H. Wu, C. Pistidda, X. H. Ju, W. Zhou, G. T. Wu, M. Etter, T. Klassen, M. Dornheim, P. Chen, *Chem. - Eur. J.* **2018**, *24*, 1342; e) Z. P. Yao, S. Kim, K. Michel, Y. S. Zhang, M. Aykol, C. Wolverton, *Phys. Rev. Mater.* **2018**, *2*, 065402; f) R. Mohtadi, S.-I. Orimo, *Nat. Rev. Mater.* **2017**, *2*, 16091.
[108] M. Matsuo, S.-I. Orimo, *Adv. Energy Mater.* **2011**, *1*, 161.
[109] M. Matsuo, A. Remhof, P. Martelli, R. Caputo, M. Ernst, Y. Miura, T. Sato, H. Oguchi, H. Maekawa, H. Takamura, A. Borgschulte, A. Züttel, S.-I. Orimo, *J. Am. Chem. Soc.* **2009**, *131*, 16389.
[110] a) A. Holt, E. C. Edgar, J. B. Firth, *Z. Phys. Chem.* **1913**, *82U*, 513; b) E. Wicke, J. Blaurock, *J. Less-Common Met.* **1987**, *130*, 351.
[111] a) H. Inui, T. Yamamoto, M. Hirota, M. Yamaguchi, *J. Alloys Compd.* **2002**, *330–332*, 117; b) J. M. Joubert, M. Latroche, R. Černý, A. Percheron-Guégan, K. Yvon, *J. Alloys Compd.* **2002**, *330–332*, 208.
[112] J. J. Vajo, S. L. Skeith, F. Mertens, *J. Phys. Chem. B* **2005**, *109*, 3719.
[113] J. F. Mao, X. B. Yu, Z. P. Guo, H. K. Liu, Z. Wu, J. Ni, *J. Alloys Compd.* **2009**, *479*, 619.
[114] R. M. van Essen, K. H. J. Buschow, *Mater. Res. Bull.* **1980**, *15*, 1149.
[115] T. B. Flanagan, *Interstitial Intermetallic Alloys*, Vol. *281*, Springer, Netherlands **1994**.
[116] a) C. Zlotea, M. Latroche, *Colloids Surf. A* **2013**, *439*, 117; b) A. Pundt, *Adv. Eng. Mater.* **2004**, *6*, 11.
[117] A. Kianvash, I. R. Harris, *J. Mater. Sci.* **1985**, *20*, 682.
[118] a) S.-I. Orimo, Y. Nakamori, J. R. Eliseo, A. Züttel, C. M. Jensen, *Chem. Rev.* **2007**, *107*, 4111; b) B. Sakintuna, F. Lamari-Darkrim, M. Hirscher, *Int. J. Hydrogen Energy* **2007**, *32*, 1121.
[119] J. J. Reilly Jr., R. H. Wiswall Jr., *Inorg. Chem.* **1967**, *6*, 2220.
[120] A. Andreasen, M. Sørensen, R. Burkarl, B. Møller, A. Molenbroek, A. S. Pedersen, J. W. Andreasen, M. M. Nielsen, T. R. Jensen, *J. Alloys Compd.* **2005**, *404–406*, 323.
[121] S. Bouaricha, J. P. Dodelet, D. Guay, J. Huot, S. Boily, R. Schulz, *J. Alloys Compd.* **2000**, *297*, 282.
[122] J. R. Ares, K. F. Aguey-Zinsou, F. Leardini, I. J. Ferrer, J. F. Fernandez, Z. X. Guo, C. Sanchez, *J. Phys. Chem. C* **2009**, *113*, 6845.
[123] J. Yang, S. Hirano, *Adv. Mater.* **2009**, *21*, 3023.
[124] M. Fichtner, O. Fuhr, O. Kircher, *J. Alloys Compd.* **2003**, *356–357*, 418.
[125] S. Yamaguchi, H. Miyaoka, T. Ichikawa, Y. Kojima, *Int. J. Hydrogen Energy* **2017**, *42*, 5213.
[126] a) Y. Nakamori, G. Kitahara, S. Orimo, *J. Power Sources* **2004**, *138*, 309; b) Y. Sun, C. Shen, Q. Lai, W. Liu, D.-W. Wang, K.-F. Aguey-Zinsou, *Energy Storage Mater.* **2018**, *10*, 168.
[127] A. Züttel, P. Wenger, S. Rentsch, P. Sudan, P. Mauron, C. Emmenegger, *J. Power Sources* **2003**, *118*, 1.
[128] T. Graham, *J. Chem. Soc.* **1869**, *22*, 419.
[129] A. Kagawa, E. Ono, T. Kusakabe, Y. Sakamoto, *J. Less-Common Met.* **1991**, *172-174*, 64.
[130] T. Nambu, H. Ezaki, M. Takagi, H. Yukawa, M. Morinaga, *J. Alloys Compd.* **2002**, *330-332*, 318.
[131] S. Bowerman Biays, C. A. Wulff, B. Flanagan Ted, *Z. Phys. Chem.* **1979**, *116*, 197.
[132] a) A. R. Miedema, P. F. de Châtel, F. R. de Boer, *Cohesion in Alloys—Fundamentals of a Semi-Empirical Model. Physica B+C* **1980**, *100*, 1; b) M. Dornheim, in *Thermodynamics—Interaction Studies—Solids, Liquids and Gases* (Ed: J. C. Moreno-Pirajan), InTech, Rijeka **2011**.
[133] R. Griessen, T. Riesterer, in *Hydrogen in Intermetallic Compounds I*, Springer, Berlin **1988**, pp. 219–284.
[134] A. Djellouli, K. Benyelloul, H. Aourag, S. Bekhechi, A. Adjadj, Y. Bouhadda, O. ElKedim, *Int. J. Hydrogen Energy* **2018**, *43*, 19111.
[135] a) M. H. Mintz, Z. Hadari, *J. Appl. Phys.* **1981**, *52*, 463; b) F. A. Kuijpers, H. H. van Mal, *J. Less-Common Met.* **1971**, *23*, 395.
[136] J. J. Reilly Jr., R. H. Wiswall Jr., *Inorg. Chem.* **1968**, *7*, 2254.
[137] a) N. Terashita, K. Kobayashi, T. Sasai, E. Akiba, *J. Alloys Compd.* **2001**, *327*, 275; b) N. Hanada, S.-I. Orimo, H. Fujii, *J. Alloys Compd.* **2003**, *356–357*, 429.
[138] H. H. Van Mal, K. H. J. Buschow, F. A. Kuijpers, *J. Less-Common Met.* **1973**, *32*, 289.
[139] T. Gamo, Y. Moriwaki, N. Yanagihara, T. Yamashita, T. Iwaki, *Int. J. Hydrogen Energy* **1985**, *10*, 39.
[140] a) W. G. Moffat, *The Handbook of Binary Phase Diagrams*, General Electric Company, Corporate Research and Development, Shenecdaty, NY **1977**; b) T. B. Massalski, *Binary Alloy Phase Diagrams*, ASM International, **1990**.
[141] a) Z. Q. Zhou, H. Y. Zhang, D. Tang, in *6th World Hydrogen Energy Conference, Vol. Hydrogen Energy Progress VI* (Eds: T. N. Veziroğlu, N. Getoff, P. Weinzierl), Pergamon Press, Vienna, Austria **1986**; b) G. D. Sandrock, *Proc. 12th Intersociety Energy Conversion Engineering Conference*, American Nuclear Society, **1977**, pp. 951–958.
[142] W. A. Oates, T. B. Flanagan, *Mater. Res. Bull.* **1984**, *19*, 1397.
[143] J. C. Achard, A. Percheron-Guégan, H. Diaz, in *2nd International Congress on Hydrogen in Metals*, Pergamon, Paris, France **1977**.
[144] C. Lartigue, A. Percheron-Guégan, J. C. Achard, F. Tasset, *J. Less-Common Met.* **1980**, *75*, 23.
[145] J. Lamloumi, A. Percheron-Guegan, J. C. Achard, G. Jehanno, D. Givord, *J. Phys.* **1984**, *45*, 1643.
[146] J. Chen, S. X. Dou, H. K. Liu, *J. Power Sources* **1996**, *63*, 267.
[147] G. Inden, *Z. Metallkd.* **1975**, *66*, 648.
[148] J. S. Benjamin, *Metall. Trans.* **1970**, *1*, 2943.
[149] a) E. Ivanov, I. Konstanchuk, A. Stepanov, V. Boldyrev, *J. Less-Common Met.* **1987**, *131*, 25; b) M. Y. Song, E. Ivanov, B. Darriet, M. Pezat, P. Hagenmuller, *J. Less-Common Met.* **1987**, *131*, 71; c) A. Stepanov, E. Ivanov, I. Konstanchuk, V. Boldyrev, *J. Less-Common Met.* **1987**, *131*, 89.
[150] L. Zaluski, A. Zaluska, J. O. Ström-Olsen, *J. Alloys Compd.* **1995**, *217*, 245.
[151] a) A. Zaluska, L. Zaluski, J. O. Ström–Olsen, *J. Alloys Compd.* **1999**, *288*, 217; b) L. Zaluski, A. Zaluska, J. O. Ström-Olsen, *J. Alloys Compd.* **1997**, *253–254*, 70.
[152] J. Huot, D. Ravnsbæk, J. Zhang, F. Cuevas, M. Latroche, T. R. Jensen, *Prog. Mater. Sci.* **2013**, *58*, 30.
[153] G. Gorrasi, A. Sorrentino, *Green Chem.* **2015**, *17*, 2610.
[154] G. Kaupp, *CrystEngComm* **2009**, *11*, 388.
[155] F. Cuevas, D. Korablov, M. Latroche, *Phys. Chem. Chem. Phys.* **2012**, *14*, 1200.
[156] F. Delogu, G. Gorrasi, A. Sorrentino, *Prog. Mater. Sci.* **2017**, *86*, 75.
[157] a) N. Z. A. Khafidz, Z. Yaakob, K. L. Lim, S. N. Timmiati, *Int. J. Hydrogen Energy* **2016**, *41*, 13131; b) G. Friedlmeier, M. Groll, *J. Alloys Compd.* **1997**, *253–254*, 550.

[158] T. P. Yadav, R. M. Yadav, D. P. Singh, *Nanosci. Nanotechnol.* **2012**, *2*, 22.
[159] C. Vasilius-Oprea, F. Dan, *Macromolecular Mechanochemistry: Polymer Mechanochemistry*, Vol. *1*, Cambridge International Science Publishing Ltd, Cambridge, UK **2006**.
[160] a) C. F. Burmeister, A. Kwade, *Chem. Soc. Rev.* **2013**, *42*, 7660; b) B. K. Mishra, *Int. J. Miner. Process.* **2003**, *71*, 73; c) B. K. Mishra, *Int. J. Miner. Process.* **2003**, *71*, 95; d) T. H. Courtney, D. Maurice, *Scr. Mater.* **1996**, *34*, 5; e) E. J. Kreuzer, *Math. Modell.* **1987**, *8*, 37; f) R. Venugopal, R. K. Rajamani, *Powder Technol.* **2001**, *115*, 157.
[161] I. Colombo, G. Grassi, M. Grassi, *J. Pharm. Sci.* **2009**, *98*, 3961.
[162] C. Suryanarayana, N. Al-Aqeeli, *Prog. Mater. Sci.* **2013**, *58*, 383.
[163] a) I. Bonadies, M. Avella, R. Avolio, C. Carfagna, G. Gentile, B. Immirzi, M. E. Errico, *Polym. Test.* **2012**, *31*, 176; b) R. Avolio, I. Bonadies, D. Capitani, M. E. Errico, G. Gentile, M. Avella, *Carbohydr. Polym.* **2012**, *87*, 265.
[164] a) C. C. Koch, J. D. Whittenberger, *Intermetallics* **1996**, *4*, 339; b) B. S. Murty, S. Ranganathan, *Int. Mater. Rev.* **1998**, *43*, 101.
[165] J. Joardar, S. K. Pabi, B. S. Murty, *Scr. Mater.* **2004**, *50*, 1199.
[166] a) A. Tonejc, M. Stubicar, A. M. Tonejc, K. Kosanović, B. Subotić, I. Smit, *J. Mater. Sci. Lett.* **1994**, *13*, 519; b) A. Tonejc, A. M. Tonejc, D. Bagović, C. Kosanović, *Mater. Sci. Eng., A* **1994**, *181–182*, 1227.
[167] D. B. Witkin, E. J. Lavernia, *Prog. Mater. Sci.* **2006**, *51*, 1.
[168] J. R. Ares Fernandez, F. Aguey-Zinsou, M. Elsaesser, X. Z. Ma, M. Dornheim, T. Klassen, R. Bormann, *Int. J. Hydrogen Energy* **2007**, *32*, 1033.
[169] J. R. Ares, K. F. Aguey-Zinsou, T. Klassen, R. Bormann, *J. Alloys Compd.* **2007**, *434–435*, 729.
[170] C. Suryanarayana, G.-H. Chen, F. H. Froes, *Scr. Metall. Mater.* **1992**, *26*, 1727.
[171] a) J. H. Weber, in *TMS Fall Meeting* (Eds: A. H. Clauer, J. J. deBarbadillo), Warrendale, Pa.: Minerals, Metals & Materials Society, Indianapolis, Indiana **1990**; b) H. Imamura, N. Sakasai, Y. Kajii, *J. Alloys Compd.* **1996**, *232*, 218; c) H. Imamura, N. Sakasai, T. Fujinaga, *J. Alloys Compd.* **1997**, *253–254*, 34; d) M. A. Lillo-Rodenas, Z. X. Guo, K. F. Aguey-Zinsou, D. Cazorla-Amoros, A. Linares-Solano, *Carbon* **2008**, *46*, 126–137; e) M. A. Lillo-Rodenas, K. F. Aguey-Zinsou, D. Cazorla-Amoros, A. Linares-Solano, Z. X. Guo, *J. Phys. Chem. C* **2008**, *112*, 5984.
[172] O. Friedrichs, J. C. Sánchez-López, C. López-Cartes, M. Dornheim, T. Klassen, R. Bormann, A. Fernández, *Appl. Surf. Sci.* **2006**, *252*, 2334.
[173] a) H. Imamura, M. Kusuhara, S. Minami, M. Matsumoto, K. Masanari, Y. Sakata, K. Itoh, T. Fukunaga, *Acta Mater.* **2003**, *51*, 6407; b) H. Fujii, S. Orimo, *Phys. B* **2003**, *328*, 77.
[174] a) K. F. Aguey-Zinsou, J. R. Ares Fernandez, T. Klassen, R. Bormann, *Mater. Res. Bull.* **2006**, *41*, 1118; b) J. R. Ares-Fernández, K. F. Aguey-Zinsou, *Catalysts* **2012**, *2*, 330.
[175] a) M. S. El-Eskandarany, K. Sumiyama, K. Aoki, K. Suzuki, *J. Mater. Res.* **1992**, *7*, 888; b) K. Sikdar, S. Chakravarty, D. Roy, R. O. Scattergood, C. C. Koch, *J. Alloys Compd.* **2017**, *717*, 219; c) C. C. Koch, K. M. Youssef, R. O. Scattergood, K. L. Murty, *Adv. Eng. Mater.* **2005**, *7*, 787.
[176] a) J. Huot, J. F. Pelletier, G. Liang, M. Sutton, R. Schulz, *J. Alloys Compd.* **2002**, *330–332*, 727; b) J. Huot, M. L. Tremblay, R. Schulz, *J. Alloys Compd.* **2003**, *356–357*, 603; c) J. Huot, G. Liang, R. Schulz, *Appl. Phys. A: Mater. Sci. Process.* **2001**, *72*, 187.
[177] B. Bogdanović, M. Schwickardi, *J. Alloys Compd.* **1997**, *253–254*, 1.
[178] a) G. Barkhordarian, T. Klassen, R. Bormann, *J. Alloys Compd.* **2004**, *364*, 242; b) G. Liang, J. Huot, S. Boily, R. Schulz, *J. Alloys Compd.* **2000**, *305*, 239.
[179] C. Zhu, S. Hosokai, I. Matsumoto, T. Akiyama, *Cryst. Growth Des.* **2010**, *10*, 5123.
[180] a) S. Barcelo, M. Rogers, C. P. Grigoropoulos, S. S. Mao, *Int. J. Hydrogen Energy* **2010**, *35*, 7232; b) H. Fujii, K. Higuchi, K. Yamamoto, H. Kajioka, S. Orimo, K. Toiyama, *Mater. Trans.* **2002**, *43*, 2721; c) J. Qu, Y. Liu, G. Xin, J. Zheng, X. Li, *Dalton Trans.* **2014**, *43*, 5908.
[181] a) E. J. Setijadi, C. Boyer, K.-F. Aguey-Zinsou, *Phys. Chem. Chem. Phys.* **2012**, *14*, 11386; b) P. E. de Jongh, R. W. Wagemans, T. M. Eggenhuisen, B. S. Dauvillier, P. B. Radstake, J. D. Meeldijk, J. W. Geus, K. P. de Jong, *Chem. Mater.* **2007**, *19*, 6052; c) C. Zlotea, C. Chevalier-César, E. Léonel, E. Leroy, F. Cuevas, P. Dibandjo, C. Vix-Guterl, T. Martens, M. Latroche, *Faraday Discuss.* **2011**, *151*, 117.
[182] a) W. Liu, K.-F. Aguey-Zinsou, *J. Mater. Chem. A* **2014**, *2*, 9718; b) S. B. Kalidindi, B. R. Jagirdar, *Inorg. Chem.* **2009**, *48*, 4524.
[183] C. Shen, K.-F. Aguey-Zinsou, *Energies* **2016**, *9*, 1073.
[184] a) J. Huot, *Metals* **2012**, *2*, 22; b) K. Edalati, E. Akiba, Z. Horita, *Sci. Technol. Adv. Mater.* **2018**, *19*, 185.
[185] C. Suryanarayana, C. C. Koch, *Hyperfine Interact.* **2000**, *130*, 5.
[186] Q. Lai, T. Wang, Y. Sun, K. F. Aguey-Zinsou, *Adv. Mater. Technol.* **2018**, *3*, 1700298.
[187] E. Hellstern, H. J. Fecht, C. Garland, W. L. Johnson, *Mater. Res. Soc.* **1989**, *132*, 137.
[188] R. A. Varin, C. Chiu, *J. Alloys Compd.* **2005**, *397*, 276.
[189] a) J. Huot, D. B. Ravnsbaek, J. Zhang, F. Cuevas, M. Latroche, T. R. Jensen, *Prog. Mater. Sci.* **2013**, *58*, 30; b) C. Mottillo, T. Friscic, *Molecules* **2017**, *22*, 144.
[190] S. Li, K. Wang, L. Sun, Z. Wang, *Scripta Metall Mater* **1992**, *27*, 437.
[191] a) F. A. Mohamed, *Acta Mater.* **2003**, *51*, 4107; b) F. A. Mohamed, Y. Xun, *Mater. Sci. Eng., A* **2003**, *354*, 133.
[192] C. C. Koch, *Nanostruct. Mater.* **1997**, *9*, 13.
[193] A. R. Yavari, *Mater. Trans., JIM* **1995**, *36*, 228.
[194] A. A. Rostislav, *Phys.-Usp.* **2007**, *50*, 691.
[195] a) A. Oudriss, J. Creus, J. Bouhattate, E. Conforto, C. Berziou, C. Savall, X. Feaugas, *Acta Mater.* **2012**, *60*, 6814; b) T. Mütschele, R. Kirchheim, *Scr. Metall.* **1987**, *21*, 135; c) S.-M. Lee, J.-Y. Lee, *Metall. Trans. A* **1986**, *17*, 181.
[196] H. G. Schimmel, M. R. Johnson, G. J. Kearley, A. J. Ramirez-Cuesta, J. Huot, F. M. Mulder, *J. Alloys Compd.* **2005**, *393*, 1.
[197] a) H. J. Fecht, *Acta Metall. Mater.* **1990**, *38*, 1927; b) H. J. Fecht, *Phys. Rev. Lett.* **1990**, *65*, 610.
[198] a) K.-F. Aguey-Zinsou, J. A. Fernandez, T. Klassen, R. Bormann, *Mater. Res. Bull.* **2006**, *41*, 1118; b) M. Dornheim, N. Eigen, G. Barkhordarian, T. Klassen, R. Bormann, *Adv. Eng. Mater.* **2006**, *8*, 377; c) M. Dornheim, S. Doppiu, G. Barkhordarian, U. Boesenberg, T. Klassen, O. Gutfleisch, R. Bormann, *Scr. Mater.* **2007**, *56*, 841; d) B. Paik, A. Walton, V. Mann, D. Book, I. Jones, I. Harris, *Int. J. Hydrogen Energy* **2010**, *35*, 9012.
[199] O. Friedrichs, T. Klassen, J. C. Sánchez-López, R. Bormann, A. Fernández, *Scr. Mater.* **2006**, *54*, 1293.
[200] B. Zahiri, M. Danaie, X. Tan, B. S. Amirkhiz, G. A. Botton, D. Mitlin, *J. Phys. Chem. C* **2012**, *116*, 3188.
[201] J. Lu, Y. J. Choi, Z. Z. Fang, H. Y. Sohn, E. Rönnebro, *J. Am. Chem. Soc.* **2009**, *131*, 15843.
[202] a) O. Friedrichs, F. Aguey-Zinsou, J. R. A. Fernández, J. C. Sánchez-López, A. Justo, T. Klassen, R. Bormann, A. Fernández, *Acta Mater.* **2006**, *54*, 105; b) O. Friedrichs, A. F. Camacho, J. C. S. López, T. Klassen, R. Bormann, *EMPA Activities*, **2006**, pp. 70–71; c) O. Friedrichs, J. C. Sánchez-López, C. López-Cartes, T. Klassen, R. Bormann, A. Fernández, *J. Phys. Chem. B* **2006**, *110*, 7845.
[203] K. Lu, *Mater. Sci. Eng., R* **1996**, *16*, 161.
[204] M. Danaie, D. Mitlin, *J. Alloys Compd.* **2009**, *476*, 590.
[205] a) H. Gleiter, *Prog. Mater. Sci.* **1989**, *33*, 223; b) S. R. Phillpot, D. Wolf, H. Gleiter, *J. Appl. Phys.* **1995**, *78*, 847.
[206] a) R. W. Siegel, *Materials Interfaces: Atomic Level Structure and Properties*, Chapman & Hall, London, UK **1992**; b) Z. Horita,

D. J. Smith, M. Furukawa, M. Nemoto, R. Z. Valiev, T. G. Langdon, *J. Mater. Res.* **1996**, *11*, 1880.

[207] a) S. D. House, J. J. Vajo, C. Ren, A. A. Rockett, I. M. Robertson, *Acta Mater.* **2015**, *86*, 55; b) P. Larsson, C. M. Araújo, J. A. Larsson, P. Jena, R. Ahuja, *Proc. Natl. Acad. Sci. USA* **2008**, *105*, 8227.

[208] a) M. Y. Song, J.-L. Bobet, B. Darriet, *J. Alloys Compd.* **2002**, *340*, 256; b) W. Oelerich, T. Klassen, R. Bormann, *J. Alloys Compd.* **2001**, *315*, 237; c) K. F. Aguey-Zinsou, T. Nicolaisen, J. R. Ares Fernandez, T. Klassen, R. Bormann, *J. Alloys Compd.* **2007**, *434–435*, 738.

[209] a) L. Guoxian, W. Erde, F. Shoushi, *J. Alloys Compd.* **1995**, *223*, 111; b) M. Terzieva, M. Khrussanova, P. Peshev, *J. Alloys Compd.* **1998**, *267*, 235; c) C. Zhou, Z. Z. Fang, C. Ren, J. Li, J. Lu, *J. Phys. Chem. C* **2013**, *117*, 12973.

[210] a) M. Ponthieu, F. Cuevas, J. F. Fernández, L. Laversenne, F. Porcher, M. Latroche, *J. Phys. Chem. C* **2013**, *117*, 18851; b) M. Porcu, A. K. Petford-Long, J. M. Sykes, *J. Alloys Compd.* **2008**, *453*, 341.

[211] H. G. Schimmel, J. Huot, L. C. Chapon, F. D. Tichelaar, F. M. Mulder, *J. Am. Chem. Soc.* **2005**, *127*, 14348.

[212] a) B. Bogdanović, M. Felderhoff, G. Streukens, *J. Serb. Chem. Soc.* **2009**, *74*, 183; b) P. Wang, X. D. Kang, H. M. Cheng, *J. Phys. Chem. B* **2005**, *109*, 20131; c) C. P. Baldé, A. M. J. van der Eerden, H. A. Stil, F. M. F. de Groot, K. P. de Jong, J. H. Bitter, *J. Alloys Compd.* **2007**, *446–447*, 232; d) C. M. Andrei, J. C. Walmsley, H. W. Brinks, R. Holmestad, S. S. Srinivasan, C. M. Jensen, B. C. Hauback, *Appl. Phys. A* **2005**, *80*, 709.

[213] a) E. Raju, C. G. Aneesh, M. Joydev, V. Manvendra, S. Pratibha, *Mater. Res. Express* **2014**, *1*, 046502; b) B. Bogdanović, M. Felderhoff, A. Pommerin, F. Schueth, N. Spielkamp, *Adv. Mater.* **2006**, *18*, 1198; c) D. Sun, T. Kiyobayashi, H. T. Takeshita, N. Kuriyama, C. M. Jensen, *J. Alloys Compd.* **2002**, *337*, L8; d) R. H. Scheicher, S. Li, C. M. Araujo, A. Blomqvist, R. Ahuja, P. Jena, *Nanotechnology* **2011**, *22*, 335401; e) Z. Qian, M. S. L. Hudson, H. Raghubanshi, R. H. Scheicher, B. Pathak, C. M. Araújo, A. Blomqvist, B. Johansson, O. N. Srivastava, R. Ahuja, *J. Phys. Chem. C* **2012**, *116*, 10861.

[214] A. Leon, O. Kircher, J. Rothe, M. Fichtner, *J. Phys. Chem. B* **2004**, *108*, 16372.

[215] A. Léon, D. Schild, M. Fichtner, *J. Alloys Compd.* **2005**, *404–406*, 766.

[216] C. P. Balde, H. A. Stil, A. M. van der Eerden, K. P. de Jong, J. H. Bitter, *J. Phys. Chem. C* **2007**, *111*, 2797.

[217] C. Weidenthaler, A. Pommerin, M. Felderhoff, B. Bogdanović, F. Schüth, *Phys. Chem. Chem. Phys.* **2003**, *5*, 5149.

[218] C. M. Araújo, R. Ahuja, J. M. Osorio Guillén, P. Jena, *Appl. Phys. Lett.* **2005**, *86*, 251913.

[219] a) I. P. Jain, C. Lal, A. Jain, *Int. J. Hydrogen Energy* **2010**, *35*, 5133; b) T. Hongo, K. Edalati, M. Arita, J. Matsuda, E. Akiba, Z. Horita, *Acta Mater.* **2015**, *92*, 46.

[220] K. Aoki, A. Memezawa, T. Masumoto, *J. Mater. Res.* **1993**, *8*, 307.

[221] a) H. Leng, T. Ichikawa, S. Hino, N. Hanada, S. Isobe, H. Fujii, *J. Power Sources* **2006**, *156*, 166; b) Y. Kojima, K. Tange, S. Hino, S. Isobe, M. Tsubota, K. Nakamura, M. Nakatake, H. Miyaoka, H. Yamamoto, T. Ichikawa, *J. Mater. Res.* **2009**, *24*, 2185; c) T. Ichikawa, N. Hanada, S. Isobe, H. Leng, H. Fujii, *J. Phys. Chem. B* **2004**, *108*, 7887.

[222] T. Ichikawa, H. Leng, S. Isobe, N. Hanada, H. Fujii, *J. Power Sources* **2006**, *159*, 126.

[223] Y. Song, Z. Guo, *Phys. Rev. B* **2006**, *74*, 195120.

[224] P. Chen, Z. Xiong, G. Wu, Y. Liu, J. Hu, W. Luo, *Scr. Mater.* **2007**, *56*, 817.

[225] a) E. Rönnebro, E. H. Majzoub, *J. Phys. Chem. B* **2006**, *110*, 25686; b) J. Graetz, Y. Lee, J. Reilly, S. Park, T. Vogt, *Phys. Rev. B* **2005**, *71*, 184115; c) J. Zhang, M.-A. Pilette, F. Cuevas, T. Charpentier, F. Mauri, M. Latroche, *J. Phys. Chem. C* **2009**, *113*, 21242.

[226] M. Mamatha, B. Bogdanović, M. Felderhoff, A. Pommerin, W. Schmidt, F. Schüth, C. Weidenthaler, *J. Alloys Compd.* **2006**, *407*, 78.

[227] a) A. Remhof, Y. Yan, O. Friedrichs, J. Kim, P. Mauron, A. Borgschulte, D. Wallacher, A. Buchsteiner, A. Hoser, K. Oh, in *Journal of Physics: Conference Series*, Vol. *340*, IOP Publishing, **2012**, p. 012111; b) S. W. Linehan, A. A. Chin, N. T. Allen, R. Butterick, N. T. Kendall, I. L. Klawiter, F. J. Lipiecki, D. M. Millar, D. C. Molzahn, S. J. November, *Low-Cost Precursors to Novel Hydrogen Storage Materials*, Rohm and Haas Company, Philadelphia, PA **2010**.

[228] O. Friedrichs, A. Remhof, A. Borgschulte, F. Buchter, S. Orimo, A. Züttel, *Phys. Chem. Chem. Phys.* **2010**, *12*, 10919.

[229] D. Ravnsbæk, Y. Filinchuk, Y. Cerenius, H. J. Jakobsen, F. Besenbacher, J. Skibsted, T. R. Jensen, *Angew. Chem.* **2009**, *121*, 6787.

[230] R. Černý, P. Schouwink, Y. Sadikin, K. Stare, L. u. Smrčok, B. Richter, T. R. Jensen, *Inorg. Chem.* **2013**, *52*, 9941.

[231] a) R. Liu, D. Book, *Int. J. Hydrogen Energy* **2014**, *39*, 2194; b) M. Sharma, E. Didelot, A. Spyratou, L. M. Lawson Daku, R. Černý, H. Hagemann, *Inorg. Chem.* **2016**, *55*, 7090; c) G. L. Soloveichik, M. Andrus, Y. Gao, J. C. Zhao, S. Kniajanski, *Int. J. Hydrogen Energy* **2009**, *34*, 2144.

[232] T. Noritake, M. Aoki, S. Towata, A. Ninomiya, Y. Nakamori, S. Orimo, *Appl. Phys. A* **2006**, *83*, 277.

[233] Y. S. Chua, G. Wu, Z. Xiong, P. Chen, *J. Solid State Chem.* **2010**, *183*, 2040.

[234] a) H. Wu, W. Zhou, F. E. Pinkerton, M. S. Meyer, Q. Yao, S. Gadipelli, T. J. Udovic, T. Yildirim, J. J. Rush, *Chem. Commun.* **2011**, *47*, 4102; b) Y. S. Chua, H. Wu, W. Zhou, T. J. Udovic, G. Wu, Z. Xiong, M. W. Wong, P. Chen, *Inorg. Chem.* **2012**, *51*, 1599; c) F. Leardini, J. R. Ares, J. Bodega, M. J. Valero-Pedraza, M. A. Bañares, J. F. Fernández, C. Sánchez, *J. Phys. Chem. C* **2012**, *116*, 24430.

[235] a) N. Biliškov, A. Borgschulte, K. Užarević, I. Halasz, S. Lukin, S. Milošević, I. Milanović, J. G. Novaković, *Chem. - Eur. J.* **2017**, *23*, 16274; b) H. Wu, W. Zhou, Q. Yao, S. Gadipelli, T. Udovic, T. Yildirim, J. J. Rush, F. E. Pinkerton, M. S. Meyer, *Chem. Commun.* **2011**, *47*, 4102; c) Y. S. Chua, W. Li, G. Wu, Z. Xiong, P. Chen, *Chem. Mater.* **2012**, *24*, 3574; d) H. Chu, S. Qiu, L. Sun, F. Xu, in *Advanced Materials for Renewable Hydrogen Production, Storage and Utilization*, InTech, **2015**; e) K. T. Møller, M. Jørgensen, J. G. Andreasen, J. Skibsted, Z. Łodziana, Y. Filinchuk, T. R. Jensen, *Int. J. Hydrogen Energy* **2018**, *43*, 311.

[236] Z. Xiong, C. K. Yong, G. Wu, P. Chen, W. Shaw, A. Karkamkar, T. Autrey, M. O. Jones, S. R. Johnson, P. P. Edwards, *Nat. Mater.* **2008**, *7*, 138.

[237] K. J. Fijalkowski, R. V. Genova, Y. Filinchuk, A. Budzianowski, M. Derzsi, T. Jaroń, P. J. Leszczyński, W. Grochala, *Dalton Trans.* **2011**, *40*, 4407.

[238] T. Hügle, M. F. Kühnel, D. Lentz, *J. Am. Chem. Soc.* **2009**, *131*, 7444.

[239] a) R. Moury, U. B. Demirci, V. Ban, Y. Filinchuk, T. Ichikawa, L. Zeng, K. Goshome, P. Miele, *Chem. Mater.* **2014**, *26*, 3249; b) R. Moury, U. B. Demirci, T. Ichikawa, Y. Filinchuk, R. Chiriac, A. van der Lee, P. Miele, *ChemSusChem* **2013**, *6*, 667; c) Y. S. Chua, Q. Pei, X. Ju, W. Zhou, T. J. Udovic, G. Wu, Z. Xiong, P. Chen, H. Wu, *J. Phys. Chem. C* **2014**, *118*, 11244; d) S. Ould-Amara, D. Granier, R. Chiriac, F. Toche, P. Yot, U. Demirci, *Materials* **2017**, *10*, 750.

[240] W. Li, R. H. Scheicher, C. M. Araújo, G. Wu, A. Blomqvist, C. Wu, R. Ahuja, Y. P. Feng, P. Chen, *J. Phys. Chem. C* **2010**, *114*, 19089.

[241] R. B. Schwarz, W. L. Johnson, *Phys. Rev. Lett.* **1983**, *51*, 415.

[242] P. Wang, A. M. Wang, B. Z. Ding, Z. Q. Hu, *J. Alloys Compd.* **2002**, *334*, 243.

[243] U. Bösenberg, D. B. Ravnsbæk, H. Hagemann, V. D'Anna, C. B. Minella, C. Pistidda, W. Van Beek, T. R. Jensen, R. d. Bormann, M. Dornheim, *J. Phys. Chem. C* **2010**, *114*, 15212.
[244] X. Xiao, Z. Liu, S. Saremi-Yarahmadi, D. H. Gregory, *Phys. Chem. Chem. Phys.* **2016**, *18*, 10492.
[245] K. Aguey-Zinsou, S. Chaoqi, *J. Mater. Chem. A* **2017**, *5*, 8644.
[246] a) G. Liang, R. Schulz, *J. Mater. Sci.* **2003**, *38*, 1179; b) A. R. Yavari, P. J. Desré, T. Benameur, *Phys. Rev. Lett.* **1992**, *68*, 2235.
[247] G. X. Liang, R. Schulz, *J. Metastable Nanocryst. Mater.* **2002**, *12*, 93.
[248] G. Liang, *J. Alloys Compd.* **2004**, *370*, 123.
[249] C. X. Shang, M. Bououdina, Y. Song, Z. X. Guo, *Int. J. Hydrogen Energy* **2004**, *29*, 73.
[250] a) M. Scott, *J. Mater. Sci.* **1975**, *10*, 269; b) A. Inoue, T. Masumoto, *Mater. Sci. Eng., A* **1993**, *173*, 1.
[251] E. J. Lavernia, T. S. Srivatsan, *J. Mater. Sci.* **2010**, *45*, 287.
[252] a) K. Edalati, J. Matsuda, H. Iwaoka, S. Toh, E. Akiba, Z. Horita, *Int. J. Hydrogen Energy* **2013**, *38*, 4622; b) Y. Kusadome, K. Ikeda, Y. Nakamori, S. Orimo, Z. Horita, *Scr. Mater.* **2007**, *57*, 751.
[253] L. Zaluski, P. Tessier, D. H. Ryan, C. B. Doner, A. Zaluska, J. O. Ström-Olsen, M. L. Trudeau, R. Schulz, *J. Mater. Res.* **1993**, *8*, 3059.
[254] J. Graetz, *ISRN Mater. Sci.* **2012**, *2012*, 1.
[255] L. Wang, A. Rawal, K.-F. Aguey-Zinsou, *Chem. Eng. Sci.* **2019**, *194*, 64.
[256] L. Wang, A. Rawal, M. Z. Quadir, K.-F. Aguey-Zinsou, *Int. J. Hydrogen Energy* **2017**, *42*, 14144.
[257] A. J. Maeland, L. E. Tanner, G. G. Libowitz, *J. Less-Common Met.* **1980**, *74*, 279.
[258] A. Santoro, A. Maeland, J. J. Rush, *Acta Crystallogr., Sect. B: Struct. Crystallogr. Cryst. Chem.* **1978**, *34*, 3059.
[259] K. Samwer, *J. Less-Common Met.* **1987**, *131*, 210.
[260] K. Aoki, X. G. Li, T. Masumoto, *Acta Metall. Mater.* **1992**, *40*, 1717.
[261] J. J. Vajo, F. Mertens, C. C. Ahn, R. C. Bowman, B. Fultz, *J. Phys. Chem. B* **2004**, *108*, 13977.
[262] a) G. Barkhordarian, T. R. Jensen, S. Doppiu, U. Bösenberg, A. Borgschulte, R. Gremaud, Y. Cerenius, M. Dornheim, T. Klassen, R. Bormann, *J. Phys. Chem. C* **2008**, *112*, 2743; b) G. Barkhordarian, T. Klassen, M. Dornheim, R. Bormann, *J. Alloys Compd.* **2007**, *440*, L18.
[263] J. Rumble, *CRC Handbook of Chemistry and Physics*, 98th ed., CRC Press LLC, **2017**.
[264] M. Van Schilfgaarde, W. A. Harrison, *J. Phys. Chem. Solids* **1985**, *46*, 1093.
[265] E. Nishibori, M. Takata, M. Sakata, H. Tanaka, T. Muranaka, J. Akimitsu, *J. Phys. Soc. Jpn.* **2001**, *70*, 2252.
[266] a) T. E. Price, D. M. Grant, V. Legrand, G. S. Walker, *Int. J. Hydrogen Energy* **2010**, *35*, 4154; b) G. S. Walker, D. M. Grant, T. C. Price, X. Yu, V. Legrand, *J. Power Sources* **2009**, *194*, 1128; c) X. Yu, D. Grant, G. Walker, *Chem. Commun.* **2006**, 3906.
[267] F. E. Pinkerton, M. S. Meyer, G. P. Meisner, M. P. Balogh, J. J. Vajo, *J. Phys. Chem. C* **2007**, *111*, 12881.
[268] U. Bösenberg, J. W. Kim, D. Gosslar, N. Eigen, T. R. Jensen, J. M. Bellosta Von Colbe, Y. Zhou, M. Dahms, D. H. Kim, R. Günther, Y. W. Cho, K. H. Oh, T. Klasseng, R. Bormanna, M. Dornheim, *Acta Mater.* **2010**, *58*, 3381.
[269] D. T. Shane, R. C. Bowman Jr., M. S. Conradi, *J. Phys. Chem. C* **2009**, *113*, 5039.
[270] S. Kato, A. Borgschulte, M. Bielmann, A. Zuttel, *Phys. Chem. Chem. Phys.* **2012**, *14*, 8360.
[271] J. Li, A. Oudriss, A. Metsue, J. Bouhattate, X. Feaugas, *Sci. Rep.* **2017**, *7*, 45041.
[272] P. Mauron, F. Buchter, O. Friedrichs, A. Remhof, M. Bielmann, C. N. Zwicky, A. Züttel, *J. Phys. Chem. B* **2008**, *112*, 906.
[273] R. Gosalawit-Utke, C. Milanese, T. K. Nielsen, F. Karimi, I. Saldan, K. Pranzas, T. R. Jensen, A. Marini, T. Klassen, M. Dornheim, *Int. J. Hydrogen Energy* **2013**, *38*, 1932.
[274] F. Pendolino, P. Mauron, A. Borgschulte, A. Züttel, *J. Phys. Chem. C* **2009**, *113*, 17231.
[275] a) U. Bösenberg, S. Doppiu, L. Mosegaard, G. Barkhordarian, N. Eigen, A. Borgschulte, T. R. Jensen, Y. Cerenius, O. Gutfleisch, T. Klassen, *Acta Mater.* **2007**, *55*, 3951; b) H.-Q. Kou, X.-Z. Xiao, L.-X. Chen, S.-Q. Li, Q.-D. Wang, *Trans. Nonferrous Met. Soc. China* **2011**, *21*, 1040.
[276] E. Deprez, A. Justo, T. C. Rojas, C. López-Cartés, C. B. Minella, U. Bösenberg, M. Dornheim, R. Bormann, A. Fernández, *Acta Mater.* **2010**, *58*, 5683.
[277] C. Li, P. Peng, D. Zhou, L. Wan, *Int. J. Hydrogen Energy* **2011**, *36*, 14512.
[278] Y. Nakamori, K. Miwa, A. Ninomiya, H. Li, N. Ohba, S.-i. Towata, A. Züttel, S.-I. Orimo, *Phys. Rev. B* **2006**, *74*, 045126.
[279] a) C. Kim, S.-J. Hwang, R. C. Bowman Jr., J. W. Reiter, J. A. Zan, J. G. Kulleck, H. Kabbour, E. Majzoub, V. Ozolins, *J. Phys. Chem. C* **2009**, *113*, 9956; b) H. Hagemann, M. Longhini, J. W. Kaminski, T. A. Wesolowski, R. Cerny, N. Penin, M. H. Sørby, B. C. Hauback, G. Severa, C. M. Jensen, *J. Phys. Chem. A* **2008**, *112*, 7551; c) R. Cerny, G. Severa, D. B. Ravnsbæk, Y. Filinchuk, V. D'Anna, H. Hagemann, D. r. Haase, C. M. Jensen, T. R. Jensen, *J. Phys. Chem. C* **2010**, *114*, 1357; d) M. Chong, E. Callini, A. Borgschulte, A. Züttel, C. M. Jensen, *RSC Adv.* **2014**, *4*, 63933.
[280] a) H.-S. Lee, Y.-S. Lee, J.-Y. Suh, M. Kim, J.-S. Yu, Y. W. Cho, *J. Phys. Chem. C* **2011**, *115*, 20027; b) P. Javadian, T. R. Jensen, *Int. J. Hydrogen Energy* **2014**, *39*, 9871.
[281] Z. Zhao-Karger, R. Witter, E. G. Bardají, D. Wang, D. Cossement, M. Fichtner, *Energy Procedia* **2012**, *29*, 731.
[282] J. Lu, Z. Z. Fang, H. Y. Sohn, *Inorg. Chem.* **2006**, *45*, 8749.
[283] P. Chen, Z. Xiong, J. Luo, J. Lin, K. L. Tan, *Nature* **2002**, *420*, 302.
[284] P. Chen, Z. Xiong, J. Luo, J. Lin, K. L. Tan, *J. Phys. Chem. B* **2003**, *107*, 10967.
[285] Y. H. Hu, E. Ruckenstein, *J. Phys. Chem. A* **2003**, *107*, 9737.
[286] Y. Chen, C.-Z. Wu, P. Wang, H.-M. Cheng, *Int. J. Hydrogen Energy* **2006**, *31*, 1236.
[287] a) Z. Xiong, J. Hu, G. Wu, P. Chen, W. Luo, K. Gross, J. Wang, *J. Alloys Compd.* **2005**, *398*, 235; b) Z. Xiong, G. Wu, J. Hu, P. Chen, W. Luo, J. Wang, *J. Alloys Compd.* **2006**, *417*, 190; c) Y. Nakamori, G. Kitahara, A. Ninomiya, M. Aoki, T. Noritake, S.-I. Towata, S.-I. Orimo, *Mater. Trans.* **2005**, *46*, 2093; d) J. Wang, T. Liu, G. Wu, W. Li, Y. Liu, C. M. Araújo, R. H. Scheicher, A. Blomqvist, R. Ahuja, Z. Xiong, *Angew. Chem., Int. Ed.* **2009**, *48*, 5828; e) C. M. Araújo, R. H. Scheicher, R. Ahuja, *Appl. Phys. Lett.* **2008**, *92*, 021907.
[288] a) M. Aoki, K. Miwa, T. Noritake, G. Kitahara, Y. Nakamori, S. Orimo, S. Towata, *Appl. Phys. A* **2005**, *80*, 1409; b) F. E. Pinkerton, G. P. Meisner, M. S. Meyer, M. P. Balogh, M. D. Kundrat, *J. Phys. Chem. B* **2005**, *109*, 6.
[289] G. P. Meisner, M. L. Scullin, M. P. Balogh, F. E. Pinkerton, M. S. Meyer, *J. Phys. Chem. B* **2006**, *110*, 4186.
[290] a) M. Somer, S. Acar, C. Koz, I. Kokal, P. Hoehn, R. Cardoso-Gil, U. Aydemir, L. Akselrud, *J. Alloys Compd.* **2010**, *491*, 98; b) Y. Bai, L.-L. Zhao, Y. Wang, X. Liu, F. Wu, C. Wu, *Int. J. Hydrogen Energy* **2014**, *39*, 13576; c) A. V. Soloninin, O. A. Babanova, E. Y. Medvedev, A. V. Skripov, M. Matsuo, S.-I. Orimo, *J. Phys. Chem. C* **2014**, *118*, 14805.
[291] X. Yu, Y. Guo, D. Sun, Z. Yang, A. Ranjbar, Z. Guo, H. Liu, S. Dou, *J. Phys. Chem. C* **2010**, *114*, 4733.
[292] H. Chu, Z. Xiong, G. Wu, J. Guo, T. He, P. Chen, *Dalton Trans.* **2010**, *39*, 10585.
[293] L. Liu, G. Wu, W. Chen, Z. Xiong, T. He, P. Chen, *Int. J. Hydrogen Energy* **2015**, *40*, 429.

[294] a) Y. Nakamori, A. Ninomiya, G. Kitahara, M. Aoki, T. Noritake, K. Miwa, Y. Kojima, S. I. Orimo, *J. Power Sources* **2006**, *155*, 447; b) Z. Xiong, G. Wu, J. Hu, P. Chen, *J. Power Sources* **2006**, *159*, 167; c) J. Lu, Z. Z. Fang, *J. Phys. Chem. B* **2005**, *109*, 20830.

[295] J.-W. Jang, J.-H. Shim, Y. W. Cho, B.-J. Lee, *J. Alloys Compd.* **2006**, *420*, 286.

[296] a) L. Zaluski, A. Zaluska, J. Ström-Olsen, *J. Alloys Compd.* **1999**, *290*, 71; b) V. P. Balema, V. K. Pecharsky, K. W. Dennis, *J. Alloys Compd.* **2000**, *313*, 69.

[297] Y. Kojima, M. Matsumoto, Y. Kawai, T. Haga, N. Ohba, K. Miwa, S.-i. Towata, Y. Nakamori, S.-I. Orimo, *J. Phys. Chem. B* **2006**, *110*, 9632.

[298] G. Wolf, J. Baumann, F. Baitalow, F. Hoffmann, *Thermochim. Acta* **2000**, *343*, 19.

[299] a) A. Gutowska, L. Li, Y. Shin, C. M. Wang, X. S. Li, J. C. Linehan, R. S. Smith, B. D. Kay, B. Schmid, W. Shaw, *Angew. Chem., Int. Ed.* **2005**, *44*, 3578; b) M. J. Valero-Pedraza, V. Gascón, M. A. Carreón, F. Leardini, J. R. Ares, Á. Martín, M. Sánchez-Sánchez, M. A. Bañares, *Microporous Mesoporous Mater.* **2016**, *226*, 454.

[300] A. Feaver, S. Sepehri, P. Shamberger, A. Stowe, T. Autrey, G. Cao, *J. Phys. Chem. B* **2007**, *111*, 7469.

[301] a) S. Gadipelli, J. Ford, W. Zhou, H. Wu, T. J. Udovic, T. Yildirim, *Chem. - Eur. J.* **2011**, *17*, 6043; b) G. Srinivas, J. Ford, W. Zhou, T. Yildirim, *Int. J. Hydrogen Energy* **2012**, *37*, 3633; c) G. Srinivas, W. Travis, J. Ford, H. Wu, Z.-X. Guo, T. Yildirim, *J. Mater. Chem. A* **2013**, *1*, 4167.

[302] C. Salameh, G. Moussa, A. Bruma, G. Fantozzi, S. Malo, P. Miele, U. B. Demirci, S. Bernard, *Energy Technol.* **2018**, *6*, 570.

[303] L. Zhang, G. Xia, Y. Ge, C. Wang, Z. Guo, X. Li, X. Yu, *J. Mater. Chem. A* **2015**, *3*, 20494.

[304] a) A. B. E. Zirngiebl, *W. Ger. Pat.* **1959**, *70*, 148; b) O. Kravchenko, S. Kravchenko, *Zh. Obshch. Khim.* **1989**, *59*, 1935; c) V. N. Konoplev, T. A. Silina, *Zh. Neorg. Khim.* **1985**, *30*, 1125.

[305] Y. Guo, Y. Jiang, G. Xia, X. Yu, *Chem. Commun.* **2012**, *48*, 4408.

[306] a) S. R. Johnson, W. I. F. David, D. M. Royse, M. Sommariva, C. Y. Tang, F. Fabbiani, M. O. Jones, P. P. Edwards, *Chem. - Asian J.* **2009**, *4*, 849; b) Y. Guo, G. Xia, Y. Zhu, L. Gao, X. Yu, *Chem. Commun.* **2010**, *46*, 2599; c) M. Ramzan, F. Silvearv, S. Lebègue, R. Ahuja, *J. Phys. Chem. C* **2011**, *115*, 20036; d) Z. Tang, Y. Tan, Q. Gu, X. Yu, *J. Mater. Chem.* **2012**, *22*, 5312.

[307] a) X. Chen, F. Yuan, Y. Tan, Z. Tang, X. Yu, *J. Phys. Chem. C* **2012**, *116*, 21162; b) H. Chu, G. Wu, Z. Xiong, J. Guo, T. He, P. Chen, *Chem. Mater.* **2010**, *22*, 6021.

[308] W. Sun, X. Chen, Q. Gu, K. S. Wallwork, Y. Tan, Z. Tang, X. Yu, *Chem. - Eur. J.* **2012**, *18*, 6825.

[309] a) S. Zhou, X. Zhang, T. Li, N. Wang, H. Chen, T. Zhang, H. Yu, H. Niu, D. Liu, *Int. J. Hydrogen Energy* **2014**, *39*, 13628; b) M. Konarova, A. Tanksale, J. Norberto Beltramini, G. Qing Lu, *Nano Energy* **2013**, *2*, 98; c) Z. Zhao-Karger, J. Hu, A. Roth, D. Wang, C. Kubel, W. Lohstroh, M. Fichtner, *Chem. Commun.* **2010**, *46*, 8353; d) Y. S. Au, M. Ponthieu, R. van Zwienen, C. Zlotea, F. Cuevas, K. P. de Jong, P. E. de Jongh, *J. Mater. Chem. A* **2013**, *1*, 9983; e) W. Liu, K.-F. Aguey-Zinsou, *Int. J. Hydrogen Energy* **2016**, *41*, 1679; f) L. Wang, M. Z. Quadir, K.-F. Aguey-Zinsou, *Int. J. Hydrogen Energy* **2016**, *41*, 18088; g) W. Liu, K.-F. Aguey-Zinsou, *Int. J. Hydrogen Energy* **2016**, *41*, 14429; h) C. Zlotea, F. Cuevas, V. Paul-Boncour, E. Leroy, P. Dibandjo, R. Gadiou, C. Vix-Guterl, M. Latroche, *J. Am. Chem. Soc.* **2010**, *132*, 7720; i) X. Liu, D. Peaslee, C. Z. Jost, T. F. Baumann, E. H. Majzoub, *Chem. Mater.* **2011**, *23*, 1331; j) A. F. Gross, J. J. Vajo, S. L. Van Atta, G. L. Olson, *J. Phys. Chem. C* **2008**, *112*, 5651; k) Z.-Z. Fang, X.-D. Kang, P. Wang, *Int. J. Hydrogen Energy* **2010**, *35*, 8247; l) Z. Fang, P. Wang, T. Rufford, X. Kang, G. Lu, H. Cheng, *Acta Mater.* **2008**, *56*, 6257; m) Z.-Z. Fang, X.-D. Kang, P. Wang, H.-M. Cheng, *J. Phys. Chem. C* **2008**, *112*, 17023; n) S. Cahen, J.-B. Eymery, R. Janot, J.-M. Tarascon, *J. Power Sources* **2009**, *189*, 902; o) Y. Zhang, W.-S. Zhang, A.-Q. Wang, L.-X. Sun, M.-Q. Fan, H.-L. Chu, J.-C. Sun, T. Zhang, *Int. J. Hydrogen Energy* **2007**, *32*, 3976; p) C. P. Baldé, B. P. C. Hereijgers, J. H. Bitter, K. P. de Jong, *Angew. Chem., Int. Ed.* **2006**, *45*, 3501; q) C. P. Baldé, B. P. C. Hereijgers, J. H. Bitter, K. P. d. Jong, *J. Am. Chem. Soc.* **2008**, *130*, 6761; r) P. A. Berseth, A. G. Harter, R. Zidan, A. Blomqvist, C. M. Araújo, R. H. Scheicher, R. Ahuja, P. Jena, *Nano Lett.* **2009**, *9*, 1501; s) J. Gao, P. Adelhelm, M. H. W. Verkuijlen, C. Rongeat, M. Herrich, P. J. M. van Bentum, O. Gutfleisch, A. P. M. Kentgens, K. P. de Jong, P. E. de Jongh, *J. Phys. Chem. C* **2010**, *114*, 4675; t) M. S. Leo Hudson, H. Raghubanshi, D. Pukazhselvan, O. N. Srivastava, *Int. J. Hydrogen Energy* **2010**, *35*, 2083; u) T. K. Nielsen, P. Javadian, M. Polanski, F. Besenbacher, J. Bystrzycki, T. R. Jensen, *J. Phys. Chem. C* **2012**, *116*, 21046; v) R. D. Stephens, A. F. Gross, S. L. Van Atta, J. J. Vajo, F. E. Pinkerton, *Nanotechnology* **2009**, *20*, 204018.

[310] Y. Jia, C. Sun, S. Shen, J. Zou, S. S. Mao, X. Yao, *Renewable Sustainable Energy Rev.* **2015**, *44*, 289.

[311] a) K.-J. Jeon, H. R. Moon, A. M. Ruminski, B. Jiang, C. Kisielowski, R. Bardhan, J. J. Urban, *Nat. Mater.* **2011**, *10*, 286; b) L. H. Rude, T. K. Nielsen, D. B. Ravnsbæk, U. Bösenberg, M. B. Ley, B. Richter, L. M. Arnbjerg, M. Dornheim, Y. Filinchuk, F. Besenbacher, *Phys. Status Solidi A* **2011**, *208*, 1754.

[312] a) C. Zlotea, Y. Oumellal, S. J. Hwang, C. M. Ghimbeu, P. E. De Jongh, M. Latroche, *J. Phys. Chem. C* **2015**, *119*, 18091; b) P. Ngene, P. Adelhelm, A. M. Beale, K. P. de Jong, P. E. de Jongh, *J. Phys. Chem. C* **2010**, *114*, 6163.

[313] a) Q. Lai, M. Christian, K.-F. Aguey-Zinsou, *Int. J. Hydrogen Energy* **2014**, *39*, 9339; b) Q. Lai, K.-F. Aguey-Zinsou, *Sustainable Energy Fuels* **2017**, *1*, 1308.

[314] a) L. Wang, K.-F. Aguey-Zinsou, *Inorganics* **2017**, *5*, 38; b) M. Christian, K.-F. Aguey-Zinsou, *Nanoscale* **2010**, *2*, 2587.

[315] L. Ouyang, Z. Cao, H. Wang, R. Hu, M. Zhu, *J. Alloys Compd.* **2017**, *691*, 422.

[316] M. Fichtner, *Nanotechnology* **2009**, *20*, 204009.

[317] G. O. Piloyan, N. S. Bortnikov, N. M. Boeva, *J. Mod. Phys.* **2013**, *4*, 16.

[318] a) T. Frolov, Y. Mishin, *Phys. Rev. B* **2009**, *79*, 045430; b) Q. Zhao, Y. Liu, E. W. Abel, *J. Colloid Interface Sci.* **2004**, *280*, 174; c) L. Sandoval, C. Reina, J. Marian, *Sci. Rep.* **2015**, *5*, 17251.

[319] H. Omid, H. Delavari H, H. R. Madaah Hosseini, *J. Phys. Chem. C* **2011**, *115*, 17310.

[320] a) A. Pan, T. Kar, A. K. Rakshit, S. P. Moulik, *J. Phys. Chem. B* **2016**, *120*, 10531; b) L.-J. Chen, S.-Y. Lin, C.-C. Huang, *J. Phys. Chem. B* **1998**, *102*, 4350; c) A. Cooper, C. M. Johnson, J. H. Lakey, M. Nöllmann, *Biophys. Chem.* **2001**, *93*, 215; d) R. Lumry, S. Rajender, *Biopolymers* **1970**, *9*, 1125.

[321] a) E. B. Starikov, B. Nordén, *J. Phys. Chem. B* **2007**, *111*, 14431; b) K. Sharp, *Protein Sci.* **2001**, *10*, 661.

[322] K. C. Kim, B. Dai, J. K. Johnson, D. S. Sholl, *Nanotechnology* **2009**, *20*, 204001.

[323] a) S. Cheung, W.-Q. Deng, A. C. van Duin, W. A. Goddard, *J. Phys. Chem. A* **2005**, *109*, 851; b) J.-C. Crivello, B. Dam, R. Denys, M. Dornheim, D. Grant, J. Huot, T. R. Jensen, P. de Jongh, M. Latroche, C. Milanese, D. Milčius, G. S. Walker, C. J. Webb, C. Zlotea, V. A. Yartys, *Appl. Phys. A* **2016**, *122*, 97; c) R. W. P. Wagemans, J. H. van Lenthe, P. E. de Jongh, A. J. van Dillen, K. P. de Jong, *J. Am. Chem. Soc.* **2005**, *127*, 16675; d) Z. Wu, M. D. Allendorf, J. C. Grossman, *J. Am. Chem. Soc.* **2009**, *131*, 13918.

[324] Y. Liu, J. Zou, X. Zeng, X. Wu, H. Tian, W. Ding, J. Wang, A. Walter, *Int. J. Hydrogen Energy* **2013**, *38*, 5302.

[325] M. Yamauchi, R. Ikeda, H. Kitagawa, M. Takata, *J. Phys. Chem. C* **2008**, *112*, 3294.

[326] a) W. Liu, K. F. Aguey-Zinsou, *J. Mater. Chem. A* **2014**, *2*, 9718; b) M. Paskevicius, D. A. Sheppard, C. E. Buckley, *J. Am. Chem. Soc.* **2010**, *132*, 5077.
[327] W. Luo, W. Hu, *Phys. B* **2013**, *425*, 90.
[328] W. H. Qi, *Phys. B* **2005**, *368*, 46.
[329] a) P. E. De Jongh, P. Adelhelm, *ChemSusChem* **2010**, *3*, 1332; b) T. K. Nielsen, F. Besenbacher, T. R. Jensen, *Nanoscale* **2011**, *3*, 2086.
[330] Q. Lai, C. Milanese, K.-F. Aguey-Zinsou, *ACS Appl. Energy Mater.* **2018**, *1*, 421.
[331] J. J. Vajo, *Curr. Opin. Solid State Mater. Sci.* **2011**, *15*, 52.
[332] a) T. Mueller, G. Ceder, *ACS Nano* **2010**, *4*, 5647; b) E. H. Majzoub, F. Zhou, V. Ozolins, *J. Phys. Chem. C* **2011**, *115*, 2636.
[333] X. Liu, D. Peaslee, C. Z. Jost, E. H. Majzoub, *J. Phys. Chem. C* **2010**, *114*, 14036.
[334] M. L. Christian, K.-F. Aguey-Zinsou, *ACS Nano* **2012**, *6*, 7739.
[335] a) J. F. Perez-Benito, M. Mulero-Raichs, *J. Phys. Chem. A* **2016**, *120*, 7598; b) A. Pan, T. Biswas, A. K. Rakshit, S. P. Moulik, *J. Phys. Chem. B* **2015**, *119*, 15876.
[336] a) R. R. Krug, *Ind. Eng. Chem. Fundam.* **1980**, *19*, 50; b) E. B. Starikov, *Chem. Phys. Lett.* **2013**, *564*, 88.
[337] a) C. Piguet, *Dalton Trans.* **2011**, *40*, 8059; b) D. De Marco, A. Giannetto, W. Linert, *Thermochim. Acta* **1996**, *286*, 387.
[338] a) C. Langhammer, V. P. Zhdanov, I. Zorić, B. Kasemo, *Phys. Rev. Lett.* **2010**, *104*, 135502; b) X. Yao, Z. H. Zhu, H. M. Cheng, G. Q. Lu, *J. Mater. Res.* **2008**, *23*, 336.
[339] P. Ngene, R. van den Berg, M. H. W. Verkuijlen, K. P. de Jong, P. E. de Jongh, *Energy Environ. Sci.* **2011**, *4*, 4108.
[340] E. J. Setijadi, C. Boyer, K.-F. Aguey-Zinsou, *Int. J. Hydrogen Energy* **2013**, *38*, 5746.
[341] a) S.-H. Jhi, Y.-K. Kwon, *Phys. Rev. B* **2004**, *69*, 245407; b) S. A. Shevlin, Z. X. Guo, *Chem. Soc. Rev.* **2009**, *38*, 211.
[342] R. B. Getman, Y.-S. Bae, C. E. Wilmer, R. Q. Snurr, *Chem. Rev.* **2012**, *112*, 703.
[343] J. L. G. Hector, J. F. Herbst, *J. Phys.: Condens. Matter* **2008**, *20*, 064229.
[344] S. Baroni, S. de Gironcoli, A. Dal Corso, P. Giannozzi, *Rev. Mod. Phys.* **2001**, *73*, 515.
[345] D. Alfè, *Comput. Phys. Commun.* **2009**, *180*, 2622.
[346] C. Cazorla, J. Boronat, *Rev. Mod. Phys.* **2017**, *89*, 035003.
[347] S. A. Shevlin, C. Cazorla, Z. X. Guo, *J. Phys. Chem. C* **2012**, *116*, 13488.
[348] J. P. Soulié, G. Renaudin, R. Černý, K. Yvon, *J. Alloys Compd.* **2002**, *346*, 200.
[349] A. Tekin, R. Caputo, A. Züttel, *Phys. Rev. Lett.* **2010**, *104*, 215501.
[350] T. Yildirim, S. Ciraci, *Phys. Rev. Lett.* **2005**, *94*, 175501.
[351] P. Hänggi, P. Talkner, M. Borkovec, *Rev. Mod. Phys.* **1990**, *62*, 251.
[352] G. Henkelman, B. P. Uberuaga, H. Jónsson, *J. Chem. Phys.* **2000**, *113*, 9901.
[353] a) A. C. T. van Duin, S. Dasgupta, F. Lorant, W. A. Goddard, *J. Phys. Chem. A* **2001**, *105*, 9396; b) D. W. M. Hofmann, L. Kuleshova, B. D'Aguanno, *Chem. Phys. Lett.* **2007**, *448*, 138.
[354] a) C. Cazorla, *Coord. Chem. Rev.* **2015**, *300*, 142; b) E. F. George, *J. Phys.: Condens. Matter* **2002**, *14*, R453.
[355] W. Kohn, L. J. Sham, *Phys. Rev.* **1965**, *140*, A1133.
[356] D. M. Ceperley, B. J. Alder, *Phys. Rev. Lett.* **1980**, *45*, 566.
[357] S. Grimme, J. Antony, S. Ehrlich, H. Krieg, *J. Chem. Phys.* **2010**, *132*, 154104.
[358] A. Tkatchenko, M. Scheffler, *Phys. Rev. Lett.* **2009**, *102*, 073005.
[359] M. Dion, H. Rydberg, E. Schröder, D. C. Langreth, B. I. Lundqvist, *Phys. Rev. Lett.* **2004**, *92*, 246401.
[360] J. F. Dobson, T. Gould, *J. Phys.: Condens. Matter* **2012**, *24*, 073201.
[361] C. Cazorla, S. A. Shevlin, *Dalton Trans.* **2013**, *42*, 4670.
[362] a) M. Bajdich, F. A. Reboredo, P. R. C. Kent, *Phys. Rev. B* **2010**, *82*, 081405; b) J. Cha, S. Lim, C. H. Choi, M.-H. Cha, N. Park, *Phys. Rev. Lett.* **2009**, *103*, 216102.
[363] H. Tanaka, H. Kanoh, M. Yudasaka, S. Iijima, K. Kaneko, *J. Am. Chem. Soc.* **2005**, *127*, 7511.
[364] P. Kowalczyk, A. P. Terzyk, P. A. Gauden, S. Furmaniak, K. Kaneko, T. F. Miller, *J. Phys. Chem. Lett.* **2015**, *6*, 3367.
[365] C. Zhang, M. Dyer, A. Alavi, *J. Phys. Chem. B* **2005**, *109*, 22089.
[366] J. Behler, *Int. J. Quantum Chem.* **2015**, *115*, 1032.
[367] M. O. J. Jäger, E. V. Morooka, F. Federici Canova, L. Himanen, A. S. Foster, *npj Comput. Mater.* **2018**, *4*, 37.
[368] J. R. Hattrick-Simpers, K. Choudhary, C. Corgnale, *Mol. Syst. Des. Eng.* **2018**, *3*, 509.
[369] A. W. Thornton, C. M. Simon, J. Kim, O. Kwon, K. S. Deeg, K. Konstas, S. J. Pas, M. R. Hill, D. A. Winkler, M. Haranczyk, B. Smit, *Chem. Mater.* **2017**, *29*, 2844.
[370] a) M. Ley, M. Meggouh, R. Moury, K. Peinecke, M. Felderhoff, *Materials* **2015**, *8*, 5891; b) U. Demirci, *Energy Technol.* **2018**, *6*, 470; c) S. S. Muir, X. D. Yao, *Int. J. Hydrogen Energy* **2011**, *36*, 5983; d) H. L. Jiang, S. K. Singh, J. M. Yan, X. B. Zhang, Q. Xu, *ChemSusChem* **2010**, *3*, 541.
[371] E. Keskin, B. Coşkuner Filiz, S. Kılıç Depren, A. Kantürk Figen, *Int. J. Hydrogen Energy* **2018**, *43*, 20354.
[372] a) S. C. Amendola, S. L. Sharp-Goldman, M. S. Janjua, N. C. Spencer, M. T. Kelly, P. J. Petillo, M. Binder, *Int. J. Hydrogen Energy* **2000**, *25*, 969; b) S. C. Amendola, S. L. Sharp-Goldman, M. S. Janjua, M. T. Kelly, P. J. Petillo, M. Binder, *J. Power Sources* **2000**, *85*, 186.
[373] a) U. B. Demirci, *Energy Technol.* **2018**, *6*, 470; b) R. Chamoun, U. B. Demirci, P. Miele, *Energy Technol.* **2015**, *3*, 100.
[374] Y. Kojima, K.-i. Suzuki, K. Fukumoto, Y. Kawai, M. Kimbara, H. Nakanishi, S. Matsumoto, *J. Power Sources* **2004**, *125*, 22.
[375] B. S. Richardson, J. F. Birdwell, F. G. Pin, J. F. Jansen, R. F. Lind, *J. Power Sources* **2005**, *145*, 21.
[376] a) S.-C. Li, F.-C. Wang, *Int. J. Hydrogen Energy* **2016**, *41*, 3038; b) F.-C. Wang, W.-H. Fang, *Int. J. Hydrogen Energy* **2017**, *42*, 10376.
[377] B. G. Gang, S. Kwon, *Int. J. Hydrogen Energy* **2018**, *43*, 6331.
[378] a) K. Kim, T. Kim, K. Lee, S. Kwon, *J. Power Sources* **2011**, *196*, 9069; b) T. Kim, S. Kwon, *Int. J. Hydrogen Energy* **2012**, *37*, 615.
[379] E. S. Jung, H. Kim, S. Kwon, T. H. Oh, *Int. J. Green Energy* **2018**, *15*, 385.
[380] B. G. Gang, S. Kwon, *Int. J. Hydrogen Energy* **2018**, *43*, 9787.
[381] a) D. Gervasio, S. Tasic, F. Zenhausern, *J. Power Sources* **2005**, *149*, 15; b) S. Galli, M. De Francesco, G. Monteleone, R. Oronzio, A. Pozio, *Int. J. Hydrogen Energy* **2010**, *35*, 7344; c) T. Kim, *Int. J. Hydrogen Energy* **2011**, *36*, 1404.
[382] J. Lee, T. Kim, *Acta Astronaut.* **2014**, *101*, 165.
[383] T. H. Oh, *Energy Convers. Manage.* **2018**, *176*, 349.
[384] M. Rivarolo, O. Improta, L. Magistri, M. Panizza, A. Barbucci, *Int. J. Hydrogen Energy* **2018**, *43*, 1606.
[385] N. Lapeña-Rey, J. A. Blanco, E. Ferreyra, J. L. Lemus, S. Pereira, E. Serrot, *Int. J. Hydrogen Energy* **2017**, *42*, 6926.
[386] *Fuel Cells Bull.* **2007**, *2007*, 6.
[387] H. J. Kim, K.-J. Shin, H.-J. Kim, M. K. Han, H. Kim, Y.-G. Shul, K. T. Jung, *Int. J. Hydrogen Energy* **2010**, *35*, 12239.
[388] E. Petit, P. Miele, U. B. Demirci, *ChemSusChem* **2016**, *9*, 1777.
[389] J. Kim, T. Kim, *Appl. Energy* **2015**, *160*, 945.
[390] P. Brack, S. E. Dann, K. G. U. Wijayantha, *Energy Sci. Eng.* **2015**, *3*, 174.
[391] J. Andrieux, L. Laversenne, O. Krol, R. Chiriac, Z. Bouajila, R. Tenu, J. J. Counioux, C. Goutaudier, *Int. J. Hydrogen Energy* **2012**, *37*, 5798.
[392] a) Y. Kojima, T. Haga, *Int. J. Hydrogen Energy* **2003**, *28*, 989; b) C. Lang, Y. Jia, J. Liu, H. Wang, L. Ouyang, M. Zhu, X. Yao, *Int. J. Hydrogen Energy* **2017**, *42*, 13127.
[393] L. Z. Ouyang, H. Zhong, Z. M. Li, Z. J. Cao, H. Wang, J. W. Liu, X. K. Zhu, M. Zhu, *J. Power Sources* **2014**, *269*, 768.
[394] Ç. Çakanyıldırım, M. Gürü, *Renewable Energy* **2010**, *35*, 1895.

[395] a) B. H. Liu, Z. P. Li, J. K. Zhu, N. Morigasaki, S. Suda, *Energy Fuels* **2007**, *21*, 1707; b) B. H. Liu, Z. P. Li, N. Morigasaki, S. Suda, *Energy Fuels* **2008**, *22*, 1894.
[396] A. M. Beaird, P. Li, H. S. Marsh, W. A. Al-Saidi, J. K. Johnson, M. A. Matthews, C. T. Williams, *Ind. Eng. Chem. Res.* **2011**, *50*, 7746.
[397] W. Chen, L. Z. Ouyang, J. W. Liu, X. D. Yao, H. Wang, Z. W. Liu, M. Zhu, *J. Power Sources* **2017**, *359*, 400.
[398] a) H. Zhong, L. Ouyang, J. Liu, C. Peng, X. Zhu, W. Zhu, F. Fang, M. Zhu, *J. Power Sources* **2018**, *390*, 71; b) H. Zhong, L. Z. Ouyang, J. S. Ye, J. W. Liu, H. Wang, X. D. Yao, M. Zhu, *Energy Storage Mater.* **2017**, *7*, 222.
[399] a) C.-H. Liu, B.-H. Chen, *Materials* **2015**, *8*, 3456; b) L. Ouyang, W. Chen, J. Liu, M. Felderhoff, H. Wang, M. Zhu, *Adv. Energy Mater.* **2017**, *7*, 1700299; c) L. Ouyang, H. Zhong, H.-W. Li, M. Zhu, *Inorganics* **2018**, *6*, 10; d) İ. Ar, Ö. U. Güler, M. Gürü, *Int. J. Hydrogen Energy* **2018**, *43*, 20214.
[400] T. Kemmitt, G. J. Gainsford, *Int. J. Hydrogen Energy* **2009**, *34*, 5726.
[401] U. B. Demirci, *Turk. J. Chem.* **2018**, *42*, 193.
[402] A. E. Sanli, İ. Kayacan, B. Z. Uysal, M. L. Aksu, *J. Power Sources* **2010**, *195*, 2604.
[403] M. Monteverde, L. Magistri, *Int. J. Hydrogen Energy* **2012**, *37*, 5452.
[404] M. Chandra, Q. Xu, *J. Power Sources* **2007**, *168*, 135.
[405] G. Moussa, R. Moury, U. B. Demirci, P. Miele, *Int. J. Hydrogen Energy* **2013**, *38*, 7888.
[406] J.-F. Petit, P. Miele, U. B. Demirci, *Int. J. Hydrogen Energy* **2016**, *41*, 15462.
[407] O. T. Summerscales, J. C. Gordon, *Dalton Trans.* **2013**, *42*, 10075.
[408] T. Q. Hua, R. K. Ahluwalia, *Int. J. Hydrogen Energy* **2012**, *37*, 14382.
[409] B. L. Davis, D. A. Dixon, E. B. Garner, J. C. Gordon, M. H. Matus, B. Scott, F. H. Stephens, *Angew. Chem., Int. Ed.* **2009**, *48*, 6812.
[410] A. D. Sutton, A. K. Burrell, D. A. Dixon, E. B. Garner, J. C. Gordon, T. Nakagawa, K. C. Ott, J. P. Robinson, M. Vasiliu, *Science* **2011**, *331*, 1426.
[411] a) G. Moussa, U. B. Demirci, S. Malo, S. Bernard, P. Miele, *J. Mater. Chem. A* **2014**, *2*, 7717; b) Z. Tang, Y. Tan, X. Chen, X. Yu, *Chem. Commun.* **2012**, *48*, 9296.
[412] S. Hausdorf, F. Baitalow, G. Wolf, F. O. R. L. Mertens, *Int. J. Hydrogen Energy* **2008**, *33*, 608.
[413] C. Reller, F. Mertens, *ChemPlusChem* **2018**, *83*, 1013.
[414] P. Muthukumar, A. Singhal, G. K. Bansal, *Int. J. Hydrogen Energy* **2012**, *37*, 14351.
[415] K. J. Kim, B. Montoya, A. Razani, K. H. Lee, *Int. J. Hydrogen Energy* **2001**, *26*, 609.
[416] a) A. Jemni, S. B. Nasrallah, *Int. J. Hydrogen Energy* **1995**, *20*, 881; b) Z. Guo, H. J. Sung, *Int. J. Heat Mass Transfer* **1999**, *42*, 379; c) F. Laurencelle, J. Goyette, *Int. J. Hydrogen Energy* **2007**, *32*, 2957; d) B. J. Hardy, D. L. Anton, *Int. J. Hydrogen Energy* **2009**, *34*, 2992.
[417] a) F. Askri, A. Jemni, S. Ben Nasrallah, *Int. J. Hydrogen Energy* **2003**, *28*, 537; b) E. Bershadsky, Y. Josephy, M. Ron, *J. Less-Common Met.* **1989**, *153*, 65; c) M. Ron, D. Gruen, M. Mendelsohn, I. Sheft, *J. Less-Common Met.* **1980**, *74*, 445; d) A. R. Sánchez, H. P. Klein, M. Groll, *Int. J. Hydrogen Energy* **2003**, *28*, 515.
[418] F. S. Yang, G. X. Wang, Z. X. Zhang, X. Y. Meng, V. Rudolph, *Int. J. Hydrogen Energy* **2010**, *35*, 3832.
[419] a) I. Sheft, D. M. Gruen, G. J. Lamich, *J. Less-Common Met.* **1980**, *74*, 401; b) F. Laurencelle, Z. Dehouche, F. Morin, J. Goyette, *J. Alloys Compd.* **2009**, *475*, 810.
[420] R. C. Bowman Jr., *J. Alloys Compd.* **2003**, *356–357*, 789.
[421] M. Botzung, S. Chaudourne, O. Gillia, C. Perret, M. Latroche, A. Percheron-Guegan, P. Marty, *Int. J. Hydrogen Energy* **2008**, *33*, 98.
[422] H. Choi, A. F. Mills, *Int. J. Heat Mass Transfer* **1990**, *33*, 1281.
[423] a) L. Zu, S. Koussios, A. Beukers, *Int. J. Hydrogen Energy* **2012**, *37*, 14343; b) L. Zu, D. Zhang, Y. Xu, D. Xiao, *Int. J. Hydrogen Energy* **2012**, *37*, 1027.
[424] G. A. Lozano, J. M. Bellosta von Colbe, T. Klassen, M. Dornheim, *Int. J. Hydrogen Energy* **2014**, *39*, 18952.
[425] S. Vyazovkin, A. K. Burnham, J. M. Criado, L. A. Pérez-Maqueda, C. Popescu, N. Sbirrazzuoli, *Thermochim. Acta* **2011**, *520*, 1.
[426] a) M. Bhouri, J. Goyette, B. J. Hardy, D. L. Anton, *Int. J. Hydrogen Energy* **2011**, *36*, 621; b) M. Bhouri, J. Goyette, B. J. Hardy, D. L. Anton, *Int. J. Hydrogen Energy* **2012**, *37*, 1551.
[427] C. Na Ranong, M. Höhne, J. Franzen, J. Hapke, G. Fieg, M. Dornheim, N. Eigen, J. M. Bellosta von Colbe, O. Metz, *Chem. Eng. Technol.* **2009**, *32*, 1154.
[428] B. J. Hardy, D. L. Anton, *Int. J. Hydrogen Energy* **2009**, *34*, 2269.
[429] M. Raju, S. Kumar, *Int. J. Hydrogen Energy* **2011**, *36*, 1578.
[430] a) G. A. Lozano, C. N. Ranong, J. M. Bellosta von Colbe, R. Bormann, J. Hapke, G. Fieg, T. Klassen, M. Dornheim, *Int. J. Hydrogen Energy* **2012**, *37*, 2825; b) T. A. Johnson, M. P. Kanouff, D. E. Dedrick, G. H. Evans, S. W. Jorgensen, *Int. J. Hydrogen Energy* **2012**, *37*, 2835.
[431] J. Nam, J. Ko, H. Ju, *Appl. Energy* **2012**, *89*, 164.
[432] a) S. Srinivasa Murthy, *J. Heat Transfer* **2012**, *134*, 031020; b) Y. Ishido, M. Kawamura, S. Ono, *Int. J. Hydrogen Energy* **1982**, *7*, 173; c) E. Suissa, I. Jacob, Z. Hadari, *J. Less-Common Met.* **1984**, *104*, 287; d) S. Da-Wen, D. Song-Jiu, *J. Less-Common Met.* **1990**, *160*, 387; e) S. Suda, N. Kobayashi, K. Yoshida, *Int. J. Hydrogen Energy* **1981**, *6*, 521.
[433] a) A. Kempf, W. R. B. Martin, *Phys.-Usp.* **1986**, *11*, 107; b) J. Kapischke, J. Hapke, *Exp. Therm. Fluid Sci.* **1998**, *17*, 347.
[434] a) B. Delhomme, P. De Rango, P. Marty, M. Bacia, B. Zawilski, C. Raufast, S. Miraglia, D. Fruchart, *Int. J. Hydrogen Energy* **2012**, *37*, 9103; b) H. Bjurstrom, Y. Komazaki, S. Suda, *J. Less-Common Met.* **1987**, *131*, 225; c) A. Kumar Phate, M. Prakash Maiya, S. S. Murthy, *Int. J. Hydrogen Energy* **2007**, *32*, 1969; d) S. G. Lee, H. H. Lee, K. Y. Lee, J. Y. Lee, *J. Alloys Compd.* **1996**, *235*, 84.
[435] a) J. G. Park, K. J. Jang, P. S. Lee, J. Y. Lee, *Int. J. Hydrogen Energy* **2001**, *26*, 701; b) A. Isselhorst, M. Groll, *J. Alloys Compd.* **1995**, *231*, 888; c) D. Mori, N. Kobayashi, T. Shinozawa, T. Matsunaga, H. Kubo, K. Toh, M. Tsuzuki, *J. Jpn. Inst. Met.* **2005**, *69*, 308.
[436] S. Garrier, B. Delhomme, P. De Rango, P. Marty, D. Fruchart, S. Miraglia, *Int. J. Hydrogen Energy* **2013**, *38*, 9766.
[437] a) *Fuel Cells Bull.* **2016**, *2016*, 6; b) *Fuel Cells Bull.* **2015**, *2015*, 1.
[438] a) M. Jehan, D. Fruchart, *J. Alloys Compd.* **2013**, *580*, S343; b) *Fuel Cells Bull.* **2015**, *2015*, 13.
[439] K. H. Young, J. Nei, *Materials* **2013**, *6*, 4574.
[440] a) C. Wadell, S. Syrenova, C. Langhammer, *ACS Nano* **2014**, *8*, 11925; b) M. M. H. Bhuiya, A. Kumar, K. J. Kim, *Int. J. Hydrogen Energy* **2015**, *40*, 2231.
[441] M. V. Lototskyy, V. A. Yartys, B. G. Pollet, R. C. Bowman, *Int. J. Hydrogen Energy* **2014**, *39*, 5818.
[442] a) I. Kunce, M. Polanski, J. Bystrzycki, *Int. J. Hydrogen Energy* **2014**, *39*, 9904; b) M. Sahlberg, D. Karlsson, C. Zlotea, U. Jansson, *Sci. Rep.* **2016**, *6*, 36770.
[443] J. Wang, H.-W. Li, P. Chen, *MRS Bull.* **2013**, *38*, 480.
[444] J.-R. Ares, R. Nevshupa, E. Muñoz-Cortés, C. Sánchez, F. Leardini, I.-J. Ferrer, V. Minh Huy Tran, F. Aguey-Zinsou, J.-F. Fernández, *ChemPhysChem* **2019**, *20*, 1.
[445] J. Jepsen, *Technical and Economic Evaluation of Hydrogen Storage Systems Based on Light Metal Hydrides*, Germany, **2014**.
[446] V. C. Y. Kong, F. R. Foulkes, D. W. Kirk, J. T. Hinatsu, *Int. J. Hydrogen Energy* **1999**, *24*, 665.
[447] B. Bogdanović, G. Sandrock, *MRS Bull.* **2002**, *27*, 712.
[448] H. Schlesinger, H. C. Brown, *J. Am. Chem. Soc.* **1940**, *62*, 3429.

[449] K. Miwa, M. Aoki, T. Noritake, N. Ohba, Y. Nakamori, S.-I. Towata, A. Züttel, S.-I. Orimo, *Phys. Rev. B* **2006**, *74*, 155122.
[450] A. Züttel, S. Rentsch, P. Fischer, P. Wenger, P. Sudan, P. Mauron, C. Emmenegger, *J. Alloys Compd.* **2003**, *356–357*, 515.
[451] W. D. Davis, L. Mason, G. Stegeman, *J. Am. Chem. Soc.* **1949**, *71*, 2775.
[452] N. Webbook.
[453] K. Miwa, N. Ohba, S.-i. Towata, Y. Nakamori, S.-I. Orimo, *Phys. Rev. B* **2004**, *69*, 245120.
[454] B. Laversenne, L. Bonnetot, B. Bonnetot, *Entropy* **2005**, *184*, 183.
[455] O. Knacke, O. Kubaschewski, K. Hesselmann, Springer, Berlin **1991**.
[456] T. Matsunaga, F. Buchter, P. Mauron, M. Bielman, Y. Nakamori, S. Orimo, N. Ohba, K. Miwa, S. Towata, A. Züttel, *J. Alloys Compd.* **2008**, *459*, 583.
[457] H.-W. Li, K. Kikuchi, Y. Nakamori, N. Ohba, K. Miwa, S. Towata, S. Orimo, *Acta Mater.* **2008**, *56*, 1342.
[458] J. Mao, Z. Guo, C. K. Poh, A. Ranjbar, Y. Guo, X. Yu, H. Liu, *J. Alloys Compd.* **2010**, *500*, 200.
[459] H. Schlesinger, R. T. Sanderson, A. Burg, *J. Am. Chem. Soc.* **1940**, *62*, 3421.
[460] D. Pukazhselvan, V. Kumar, S. Singh, *Nano Energy* **2012**, *1*, 566.
[461] F. H. Stephens, V. Pons, R. T. Baker, *Dalton Trans.* **2007**, *25*, 2613.
[462] B. Bonnetot, G. Chahine, P. Claudy, M. Diot, J. M. Letoffe, *The J. Chem. Thermodyn.* **1980**, *12*, 249.
[463] M. Arroyo y de Dompablo, G. Ceder, *Z. Anorg. Allg. Chem.* **2005**, *631*, 1982.
[464] S. Hino, T. Ichikawa, Y. Kojima, *J. Chem. Thermodyn.* **2010**, *42*, 140.
[465] L. H. Jepsen, P. Wang, G. Wu, Z. Xiong, F. Besenbacher, P. Chen, T. R. Jensen, *Phys. Chem. Chem. Phys.* **2016**, *18*, 25257.
[466] H. Imamura, K. Masanari, M. Kusuhara, H. Katsumoto, T. Sumi, Y. Sakata, *J. Alloys Compd.* **2005**, *386*, 211.
[467] Y. Chen, J. Williams, *J. Alloys Compd.* **1995**, *217*, 181.
[468] S. Doppiu, L. Schultz, O. Gutfleisch, *J. Alloys Compd.* **2007**, *427*, 204.
[469] A. Zaluska, L. Zaluski, J. Ström-Olsen, *J. Alloys Compd.* **1999**, *289*, 197.
[470] M. Ponthieu, M. Calizzi, L. Pasquini, J. Fernández, F. Cuevas, *Int. J. Hydrogen Energy* **2014**, *39*, 9918.
[471] F. Hosseini-Gourajoubi, M. Pourabdoli, D. Uner, S. Raygan, *Adv. Powder Technol.* **2015**, *26*, 448.
[472] V. Fuster, G. Urretavizcaya, F. J. Castro, *J. Alloys Compd.* **2009**, *481*, 673.
[473] M.-H. Grosjean, L. Roué, *J. Alloys Compd.* **2006**, *416*, 296.
[474] D. Mirabile Gattia, G. Gizer, A. Montone, *Int. J. Hydrogen Energy* **2014**, *39*, 9924.
[475] D. A. Small, G. R. MacKay, R. A. Dunlap, *J. Alloys Compd.* **1999**, *284*, 312.
[476] H. Shao, M. Felderhoff, F. Schüth, *Int. J. Hydrogen Energy* **2011**, *36*, 10828.
[477] K. Prashanth, *Mater. Manuf. Processes* **2010**, *25*, 974.
[478] S.-I. Orimo, F. Kimmerle, G. Majer, *Phys. Rev. B* **2001**, *63*, 094307.
[479] S. Orimo, H. Fujii, T. Yoshino, *J. Alloys Compd.* **1995**, *217*, 287.
[480] M. S. El-Eskandarany, H. Ahmed, K. Sumiyama, K. Suzuki, *J. Alloys Compd.* **1995**, *218*, 36.
[481] K. Aoki, A. Memezawa, T. Masumoto, *J. Mater. Res.* **1994**, *9*, 39.
[482] H. Fujii, S. Munehiro, K. Fujii, S. Orimo, *J. Alloys Compd.* **2002**, *330–332*, 747.
[483] J. Huot, H. Hayakawa, E. Akiba, *J. Alloys Compd.* **1997**, *248*, 164.
[484] J. Huot, S. Boily, E. Akiba, R. Schulz, *J. Alloys Compd.* **1998**, *280*, 306.
[485] J. Chen, H. Takeshita, D. Chartouni, N. Kuriyama, T. Sakai, *J. Mater. Sci.* **2001**, *36*, 5829.
[486] M. G. Verón, A. M. Condó, F. C. Gennari, *Int. J. Hydrogen Energy* **2013**, *38*, 973.
[487] X. Liu, Y. Zhu, L. Li, *J. Alloys Compd.* **2008**, *455*, 197.
[488] J. Huot, E. Akiba, T. Takada, *J. Alloys Compd.* **1995**, *231*, 815.
[489] J. Zhang, F. Cuevas, W. Zaïdi, J.-P. Bonnet, L. Aymard, J.-L. Bobet, M. Latroche, *J. Phys. Chem. C* **2011**, *115*, 4971.
[490] S. Orimo, H. Fujii, K. Ikeda, *Acta Mater.* **1997**, *45*, 331.
[491] W. Kalisvaart, H. Wondergem, F. Bakker, P. Notten, *J. Mater. Res.* **2007**, *22*, 1640.
[492] L. Lu, Y. F. Zhang, *J. Alloys Compd.* **1999**, *290*, 279.
[493] K. Ninez, M. Junaidi, H. Purwaningsih, *Int. J. Mechan. Prod. Eng.* **2014**, *2*, 26.
[494] B. Srinivasarao, C. Suryanarayana, K. Oh-ishi, K. Hono, *Mater. Sci. Eng., A* **2009**, *518*, 100.
[495] W. Lee, S. Kwun, *J. Alloys Compd.* **1996**, *240*, 193.
[496] J. Keskinen, A. Pogany, J. Rubin, P. Ruuskanen, *Mater. Sci. Eng., A* **1995**, *196*, 205.
[497] Q. Zhang, H. Enoki, E. Akiba, *J. Alloys Compd.* **2007**, *427*, 153.
[498] C. Fan, X. Ju, C. Wan, *Int. J. Hydrogen Energy* **2010**, *35*, 8044.
[499] H. Gu, Y. Zhu, L. Li, *Int. J. Hydrogen Energy* **2008**, *33*, 2970.
[500] X. D. Li, O. Elkedim, M. Nowak, M. Jurczyk, *Int. J. Hydrogen Energy* **2014**, *39*, 9735.
[501] Y. Kojima, Y. Kawai, T. Haga, M. Matsumoto, A. Koiwai, *J. Alloys Compd.* **2007**, *441*, 189.
[502] M. Mamatha, C. Weidenthaler, A. Pommerin, M. Felderhoff, F. Schüth, *J. Alloys Compd.* **2006**, *416*, 303.
[503] J. M. Bellosta von Colbe, M. Felderhoff, B. Bogdanović, F. Schüth, C. Weidenthaler, *Chem. Commun.* **2005**, 4732.
[504] N. Eigen, M. Kunowsky, T. Klassen, R. Bormann, *J. Alloys Compd.* **2007**, *430*, 350.
[505] X. Xiao, K. Yu, X. Fan, Z. Wu, X. Wang, C. Chen, Q. Wang, L. Chen, *Int. J. Hydrogen Energy* **2011**, *36*, 539.
[506] J. Huot, S. Boily, V. Güther, R. Schulz, *J. Alloys Compd.* **1999**, *283*, 304.
[507] H. Morioka, K. Kakizaki, S.-C. Chung, A. Yamada, *J. Alloys Compd.* **2003**, *353*, 310.
[508] A. Bhatnagar, S. K. Pandey, R. R. Shahi, M. S. L. Hudson, M. Shaz, O. Srivastava, *Cryst. Res. Technol.* **2013**, *48*, 520.
[509] R. A. Varin, C. Chiu, T. Czujko, Z. Wronski, *J. Alloys Compd.* **2007**, *439*, 302.
[510] V. Iosub, T. Matsunaga, K. Tange, M. Ishikiriyama, *Int. J. Hydrogen Energy* **2009**, *34*, 906.
[511] Y. Kim, E.-K. Lee, J.-H. Shim, Y. W. Cho, K. B. Yoon, *J. Alloys Compd.* **2006**, *422*, 283.
[512] Y. Liu, Y. Pang, X. Zhang, Y. Zhou, M. Gao, H. Pan, *Int. J. Hydrogen Energy* **2012**, *37*, 18148.
[513] C. Li, X. Xiao, P. Ge, J. Xue, S. Li, H. Ge, L. Chen, *Int. J. Hydrogen Energy* **2012**, *37*, 936.
[514] Z. P. Li, B. H. Liu, N. Morigasaki, S. Suda, *J. Alloys Compd.* **2003**, *354*, 243.
[515] Z. P. Li, N. Morigazaki, B. H. Liu, S. Suda, *J. Alloys Compd.* **2003**, *349*, 232.
[516] H. W. Li, K. Kikuchi, Y. Nakamori, K. Miwa, S. Towata, S. Orimo, *Scr. Mater.* **2007**, *57*, 679.
[517] E. Jeon, Y. Cho, *J. Alloys Compd.* **2006**, *422*, 273.
[518] R. Liu, D. Reed, D. Book, *J. Alloys Compd.* **2012**, *515*, 32.
[519] R. Černý, N. Penin, V. D'Anna, H. Hagemann, E. Durand, J. Růžička, *Acta Mater.* **2011**, *59*, 5171.
[520] H. Leng, T. Ichikawa, S. Isobe, S. Hino, N. Hanada, H. Fujii, *J. Alloys Compd.* **2005**, *404–406*, 443.
[521] S. Hino, T. Ichikawa, H. Leng, H. Fujii, *J. Alloys Compd.* **2005**, *398*, 62.
[522] Z. Xiong, G. Wu, J. Hu, P. Chen, *J. Alloys Compd.* **2007**, *441*, 152.
[523] J. Hu, G. Wu, Y. Liu, Z. Xiong, P. Chen, K. Murata, K. Sakata, G. Wolf, *J. Phys. Chem. B* **2006**, *110*, 14688.
[524] H. Wu, *J. Am. Chem. Soc.* **2008**, *130*, 6515.

[525] J. Hu, Y. Liu, G. Wu, Z. Xiong, P. Chen, *J. Phys. Chem. C* **2007**, *111*, 18439.
[526] X. Kang, Z. Fang, L. Kong, H. Cheng, X. Yao, G. Lu, P. Wang, *Adv. Mater.* **2008**, *20*, 2756.
[527] H. Wu, W. Zhou, T. Yildirim, *J. Am. Chem. Soc.* **2008**, *130*, 14834.
[528] D. Tabor, *Proc. Phys. Soc. Sect. B* **1954**, *67*, 249.
[529] D. Tabor, *The Hardness of Metals*, Oxford University Press, **2000**.
[530] L. Peña-Parás, J. Taha-Tijerina, L. Garza, D. Maldonado-Cortés, R. Michalczewski, C. Lapray, *Wear* **2015**, *332–333*, 1256.
[531] L. O'Bannon, *Dictionary of Ceramic Science and Engineering*, Springer Science & Business Media, **2012**.
[532] G. V. Samsonov, *Handbook of the Physicochemical Properties of the Elements*, Springer Science & Business Media, **2012**.
[533] a) M. Lotoskyy, R. Denys, V. A. Yartys, J. Eriksen, J. Goh, S. N. Nyamsi, C. Sita, F. Cummings, *J. Mater. Chem. A* **2018**, *6*, 10740; b) F. C. Cowlard, J. C. Lewis, *J. Mater. Sci.* **1967**, *2*, 507.
[534] T. Hryniewicz, K. Rokosz, S. Gaiaschi, P. Chapon, R. Rokicki, D. Matysek, *Mater. Lett.* **2018**, *218*, 299.
[535] A. Patah, A. Takasaki, J. S. Szmyd, *Int. J. Hydrogen Energy* **2009**, *34*, 3032.
[536] T. Sadhasivam, K. Gurunathan, *Adv. Sci.* **2014**, *6*, 1.
[537] M. E. Fleet, C. M. De Almeida, N. Angeli, *Canadian Mineral.* **2002**, *40*, 341.
[538] M. Khaghani-Dehaghani, R. Ebrahimi-Kahrizsangi, N. Setoudeh, B. Nasiri-Tabrizi, *Int. J. Refract. Met. Hard Mater.* **2011**, *29*, 244.
[539] M. Lototskyy, M. W. Davids, J. M. Sibanyoni, J. Goh, B. G. Pollet, *J. Alloys Compd.* **2015**, *645*, S454.
[540] M. H. Tavakoli, T. A. Abasi, E. H. Ali, *Cryst. Res. Technol.* **2013**, *48*, 130.
[541] N. Yasuda, T. Tsuchiya, N. Okinaka, T. Akiyama, *Int. J. Hydrogen Energy* **2012**, *37*, 9706.
[542] K. Suganuma, T. Fujita, N. Suzuki, K. Niihara, *J. Mater. Sci. Lett.* **1990**, *9*, 633.
[543] D. Chartouni, F. Meli, A. Züttel, K. Gross, L. Schlapbach, *J. Alloys Compd.* **1996**, *241*, 160.
[544] M. S. Yahya, M. Ismail, *Int. J. Hydrogen Energy* **2018**, *43*, 6244.
[545] R. L. Smith, J. W. Miser, **1963**.
[546] V. Shukla, A. Bhatnagar, S. K. Pandey, R. R. Shahi, T. P. Yadav, M. A. Shaz, O. N. Srivastava, *Int. J. Hydrogen Energy* **2015**, *40*, 12294.
[547] F. P. Bowden, T. Hughes, *Proc. R. Soc. London, Ser. A* **1937**, *160*, 575.
[548] K. Yada, T. Tanji, I. Sunagawa, *Phys. Chem. Miner.* **1981**, *7*, 47.
[549] D. L. Whitney, M. Broz, R. F. Cook, *Am. Mineral.* **2007**, *92*, 281.
[550] M. Mungole, K. Rai, R. Balasubramaniam, K. Singh, *Int. J. Hydrogen Energy* **1992**, *17*, 607.
[551] J. M. Bellosta von Colbe, O. Metz, G. A. Lozano, P. K. Pranzas, H. W. Schmitz, F. Beckmann, A. Schreyer, T. Klassen, M. Dornheim, *Int. J. Hydrogen Energy* **2012**, *37*, 2807.
[552] I. Utz, M. Linder, N. Schmidt, J. J. Hu, M. Fichtner, A. Wörner, *Int. J. Hydrogen Energy* **2012**, *37*, 7645.
[553] R. Urbanczyk, S. Peil, D. Bathen, C. Heßke, J. Burfeind, K. Hauschild, M. Felderhoff, F. Schüth, *Fuel Cells* **2011**, *11*, 911.
[554] R. Urbanczyk, K. Peinecke, M. Felderhoff, K. Hauschild, W. Kersten, S. Peil, D. Bathen, *Int. J. Hydrogen Energy* **2014**, *39*, 17118.
[555] R. Urbanczyk, K. Peinecke, M. Meggouh, M. Felderhoff, S. Peil, D. Bathen, *J. Power Sources* **2015**, *324, 589*.
[556] J. M. Bellosta von Colbe, G. Lozano, O. Metz, T. Bücherl, R. Bormann, T. Klassen, M. Dornheim, *Int. J. Hydrogen Energy* **2015**, *40*, 2984.
[557] M.-Y. Yan, F. Sun, X.-P. Liu, J.-H. Ye, S.-M. Wang, L.-J. Jiang, *J. Alloys Compd.* **2015**, *628*, 63.
[558] I. Bürger, C. Luetto, M. Linder, *Int. J. Hydrogen Energy* **2014**, *39*, 7346.
[559] A. Chibani, C. Bougriou, *Int. J. Hydrogen Energy* **2017**, *42*, 23035.
[560] K. Komiya, M. Daigoro, M. Shinpei, H. Norihiko, Y. Kousei, W. Shintaro, T. Keiji, K. Hidehito, M. Mituo, M. Seiichiro, T. Makoto, *High-Pressure Hydrogen-Absorbing Alloy Tank for Fuel Cell Vehicles*, SAE International, **2010**.
[561] D. Mori, N. Haraikawa, T. Shinozawa, T. Matsunaga, K. Toh, K. Fujita, *Trans. Jpn. Soc. Mech. Eng. Ser. B* **2007**, *73*, 1236.
[562] P. Thongtan, P. Dansirima, S. Thiangviriya, N. Thaweelap, A. Suthummapiwat, P. Plerdsranoy, R. Utke, *Int. J. Hydrogen Energy* **2018**, *43*, 12260.
[563] S. Garrier, A. Chaise, P. de Rango, P. Marty, B. Delhomme, D. Fruchart, S. Miraglia, *Int. J. Hydrogen Energy* **2011**, *36*, 9719.
[564] Y. Chen, C. A. C. Sequeira, C. Chen, X. Wang, Q. Wang, *Int. J. Hydrogen Energy* **2003**, *28*, 329.
[565] L. K. Heung, T. Motyka, W. A. Summers, *Proc. of Hypothesis IV*, CRC Press, Boca Raton **2001**, pp. 336–340.
[566] S. A. Alabbadi, *Energy Procedia* **2012**, *29*, 12.
[567] M. Baricco, M. Bang, M. Fichtner, B. Hauback, M. Linder, C. Luetto, P. Moretto, M. Sgroi, *J. Power Sources* **2017**, *342*, 853.
[568] T. Ogawa, M. Takeuchi, Y. Kajikawa, *Sustainability* **2018**, *10*, 478.
[569] A. A. Akhil, G. Huff, A. B. Currier, B. C. Kaun, D. M. Rastler, S. B. Chen, A. L. Cotter, D. T. Bradshaw, W. D. Gauntlett, *Electricity Storage Handbook in Collaboration with NRECA*, Sandia National Laboratories, Albuquerque, New Mexico and Livermore, California **2013**.
[570] U. S. Department of Energy, *DOE Technical Targets for Onboard Hydrogen Storage for Light-Duty Vehicles*, Office of Energy Efficiency & Renewable Energy, **2012**.
[571] J. Maier, W. Münch, *Z. Anorg. Allg. Chem.* **2000**, *626*, 264.
[572] X. Fan, X. Xiao, J. Shao, L. Zhang, S. Li, H. Ge, Q. Wang, L. Chen, *Nano Energy* **2013**, *2*, 995.